550

THE JOHN CRERAR LIBRARY
NOV 1 1961

THE GEOLOGICAL SOCIETY OF AMERICA

BULLETIN

PUBLISHED BY THE SOCIETY

OCTOBER 1961

Council

PRESIDENT

THOMAS B. NOLAN, *Washington, D. C.*

VICE-PRESIDENT

M. KING HUBBERT, *Houston, Texas*

SECRETARY

FREDERICK BETZ, JR., 419 *West* 117 *Street, New York* 27, *N. Y.*

TREASURER

J. EDWARD HOFFMEISTER, *Rochester, N. Y.*

COUNCILORS

1960–1961 HOLLIS D. HEDBERG (PAST PRESIDENT) *Princeton, N. J.*

1959–1961

JOHN C. FRYE	ROBERT P. SHARP	CHARLES F. PARK, JR.	E. F. OSBORN
Urbana, Ill.	*Pasadena, Calif.*	*Stanford, Calif.*	*University Park, Pa.*

1960–1962

NORMAN D. NEWELL	VINCENT C. KELLEY	GEORGE P. WOOLLARD	HAROLD L. JAMES
New York, N. Y.	*Albuquerque, N. M.*	*Madison, Wis.*	*Menlo Park, Calif.*

1961–1963

EDUARDO J. GUZMAN	J. M. HARRISON	E. B. ECKEL	CARL TOLMAN
Mexico City, Mex.	*Ottawa, Ontario*	*Denver, Colo.*	*St. Louis, Mo.*

COMMITTEE ON PUBLICATIONS

WILLIAM C. KRUMBEIN, *Chairman*
E. N. GODDARD
J. E. ARMSTRONG

Conferees
FREDERICK BETZ, JR., *Secretary*
AGNES CREAGH, *Managing Editor*

EDITORIAL STAFF

AGNES CREAGH
Managing Editor

BARBARA ANNE FLYNN
Assistant Editor

UNSORTED

The Geological Society of America Bulletin

Volume 72 October 1961 Number 10

CONTENTS

Classification and a scheme for the identification of layer silicates . . . . . *Charlotte M. Warshaw and Rustum Roy* 1455–1492

Devitrification of natural glass . . . . . *Royal R. Marshall* 1493–1520

Granitic formations in the east-central Sierra Nevada near Bishop, California . . . . . *Paul C. Bateman* 1521–1538

Local evidence of Pleistocene to Recent orogeny in the Argentine Andes. . . . . *Walden P. Pratt* 1539–1550

Ages of batholithic intrusions of northern and central Chile. *Carlos Ruiz, Luis Aguirre, José Corvalán, H. J. Rose, Jr., Kenneth Segerstrom, and T. W. Stern* . . 1551–1560

SHORT NOTES

Wind striations in northern Alberta and Saskatchewan, Canada . . . . . *L. P. Tremblay* 1561–1564

Is the Tinaquillo, Venezuela, "pseudogabbro" metamorphic or magmatic? . . . . . *T. P. Thayer and C. E. Brown* 1565–1570

Is the Tinaquillo, Venezuela, "pseudogabbro" metamorphic or magmatic?—A reply . . . . . *D. B. MacKenzie* 1571–1574

Ice-grain structure and crystal orientation in an ice lens from Leda clay . . . . *E. Penner* 1575–1578

Rate of slope erosion in the White Mountains, California . . . . . *Val LaMarche* 1579–1580

Role of fluid pressure in overthrust faulting: A discussion. . . . . *Walter L. Moore* 1581–1586

Role of fluid pressure in mechanics of overthrust faulting: A reply to discussion by Walter L. Moore . . . . . *M. King Hubbert and William W. Rubey* 1587–1594

ANNOUNCEMENTS . . . . . P 21–P 22

Subscriptions $15.00 per year. Printing Office: Burlington, Vt. Second-class postage paid at Burlington, Vermont. Published monthly.

Communications regarding publications should be addressed to The Geological Society of America, Dr. Frederick Betz, Jr., Secretary, 419 West 117 Street, New York 27, N. Y.

Please give notice of change of address 4 weeks in advance. Claims for nonreceipt of the Bulletin of a given month must be sent to the Secretary of the Society before the end of the second succeeding month.

PAPERS IN PRESS FOR FORTHCOMING ISSUES

THEORY OF FOLDING OF STRATIFIED VISCOELASTIC MEDIA AND ITS IMPLICATIONS IN TECTONICS AND OROGENESIS. M. A. Biot

EXPERIMENTAL VERIFICATION OF THE THEORY OF FOLDING OF STRATIFIED VISCOELASTIC MEDIA. M. A. Biot, H. Odé, and W. L. Roever

PALEOECOLOGY OF AN EARLY OLIGOCENE BIOTA. R. L. Konizeski

BRECCIA PIPE NEAR CAMERON, ARIZONA. Jonathan Barrington and Paul F. Kerr

ORIGIN OF PENNSYLVANIAN UNDERCLAY AND RELATED SEAT ROCKS. John W. Huddle and Sam H. Patterson

STOCHASTIC VARIABLES OF GEOLOGIC SEARCH AND DECISION. Bahngrell W. Brown

TECTONIC MAP OF MEXICO

Compiled by Zoltan de Cserna. Scale 1:2,500,000. In full color
Price, $5.50
Special price to Fellows and Members of GSA, $4.00

TREATISE ON INVERTEBRATE PALEONTOLOGY

PART Q: ARTHROPODA 3 (OSTRACODES). 468 pages
Price, $11.50
Special price to Fellows and Members of GSA, $8.50

MEMOIR IN PRESS

85. X-RAY POWDER DATA FOR THE ORE MINERALS: THE PEACOCK ATLAS. L. G. Berry and R. M. Thompson
Price, $8.25
Special price to Fellows and Members of GSA, $6.00

REVIEW VOLUME IN ENGINEERING GEOLOGY IN PRESS

Volume 1. Thomas Fluhr and R. F. Legget, *Editors.*

Contains eight papers covering fields of engineering seismology, petrography applied to portland-cement concrete, sand and gravel, photo analysis and interpretation in engineering geology, engineering aspects of sediment transport, engineering geology of radioactive waste material, rock bolting, recent U.S.S.R. publications in selected fields of engineering soil science.
Price, $7.00
Pre-publication price (until November 1, 1961), $6.00
Special price to Fellows and Members of GSA, $5.00

NEW CODE OF STRATIGRAPHIC NOMENCLATURE

Authors of papers to be submitted to GSA for publication are requested to follow the usage for stratigraphic nomenclature recommended in the new Code of Stratigraphic Nomenclature (See May 1961 issue of the Bulletin of the American Association of Petroleum Geologists).

CHARLOTTE M. WARSHAW
RUSTUM ROY
Dept. Geophysics and Geochemistry, Pennsylvania State University, University Park, Pa.

Classification and a Scheme for the Identification of Layer Silicates

Abstract: The classification for the layer silicates (including most of the clay minerals) proposed here is based on structural studies of numerous investigators on natural materials. In many instances, however, the limits of chemical composition have been determined by research on synthetic layer silicates.

The layer lattice silicates can be subdivided by the successive application of three criteria: (1) height of fundamental repeat unit or "thickness of layer"; (2) gross composition, whether dioctahedral or trioctahedral, and ionic content of layers; (3) stacking sequence of layers and degree of orderliness of stacking.

The relationship between compositional and structural divisions is clearly indicated in compositional diagrams. These show that some structurally similar families may be widely separated in composition (kaolinite and septechlorite), whereas others —*e.g.*, phengites (micas) and beidellites—are not far apart with respect to bulk composition.

A scheme of successive operations that will permit the identification of layer lattice silicates singly or in simple mixtures is outlined, particularly for the nonspecialist. The essential apparatus includes only that for powder X-ray diffraction and a small laboratory furnace.

CONTENTS

Introduction 1456
Acknowledgments 1456
Classification of the layer silicates 1456
Definition and introduction 1456
Fundamental structural scheme common to layer silicates 1457
Composition of the layer silicates 1458
Polymorphism, polytypism, heteropolytypism, and homopolytypism 1461
Detailed description of mineral families 1462
Two-layer (1:1) silicates 1462
Three-layer (2:1) silicates: Pyrophyllite-talc . 1465
Three-layer (2:1) silicates : Expanded 2:1 minerals 1465
Three-layer (2:1) silicates : Micas 1470
Three-layer (2:1) silicates : Mixed-layer minerals (heteropolytypes) 1472
General discussion 1472
Illite and glauconite 1472
"Long-spacing" clay minerals 1473
Four-layer silicates : Chlorites 1474
Heteropolytypes of 3-layer and 4-layer silicates 1475
Scheme for identification of the clay minerals . . 1476
Methods used 1476
Sample preparation 1476
X-ray diffraction techniques 1476
Normal conditions 1476
Glycol or glycerol adsorption 1476
Controlled humidity 1477
Dry-heat treatments 1477
Other techniques 1477
Identification scheme 1478
Identification of 7 Å minerals 1478
Identification of 9.3 Å minerals 1481
Identification of 10–11 Å minerals 1481
Identification of 12–15 Å minerals 1481
Identification of long-spacing minerals 1483
Identification of minerals in mixtures 1483
References cited 1486
Appendix. Changes in X-ray diffraction patterns effected by heat treatments of layer silicates 1491

Figure
1. Silica, or tetrahedral, layer, viewed from above 1458
2. Gibbsite, or octahedral, layer, viewed from above 1458
3. Combinations of octahedral and tetrahedral layers 1459
4. Diagrammatic (100)* projections of septechlorite (a) and normal chlorite (b) of clinochlore composition. 1460
5. Diagrammatic (100)* projections of 2:1 layer silicates. 1460
6. Diagram showing compositions of aluminum, magnesium, and iron layer silicates containing no alkalies. 1462
7. Diagram showing compositions of the aluminum, magnesium, and iron 2:1 layer silicates. 1463
8. Examples of polytypism. 1465
9. Diagrams illustrating the variation in compositions of the micas 1471

Table
1. Principal groups of layer silicates 1464
2. Two-layer (1:1) silicates 1466
3. Three-layer (2:1) silicates—expanded 2:1 minerals 1468

Geological Society of America Bulletin, v. 72, p. 1455–1492, 9 figs., October 1961

4. Three-layer (2:1) silicates—micas. 1469
5. Chemical relationships among some of the dioctahedral 2:1 layer silicates 1473
6. Four-layer silicates—chlorites 1474
7. Identification scheme for layer silicates . . . 1477
8. Identification of minerals of 7 Å group . . . 1479
9. Identification of minerals of 10–11 Å group . 1480
10. Identification of minerals of 12–15 Å group . 1482
11. Identification of clay mineral mixtures with basal reflections at 10–11 Å and either 12–15 Å or 7 Å. 1484
12. Identification of clay mineral mixtures with basal reflections at both 7 Å and 12–15 Å 1485

INTRODUCTION

The scientific study of the clays was initiated many decades ago because of their importance, especially in ceramics and agriculture. The colloid chemistry of clays, which has been actively investigated for the past 70–80 years, has been supplemented only in the past few decades by the intensive study of the crystal chemistry of clay minerals. Although earlier research yielded much practical information on the properties of clay materials, it was very markedly hampered—when compared to the study of other mineral assemblages—by the extremely fine-grained nature of the clays. The petrographic microscope was of limited use in the recognition and identification of the phases. With the advent of X-ray diffraction methods in the late 1920's and early 1930's, the correct outlines of the classification and identification of clay minerals were drawn by such men as Pauling, Gruner, Ross, Hendricks, Hofmann, and Kerr, and the post World War II popularization of the X-ray diffractometer was the key factor in the rapid expansion of the systematic study of this mineral family.

Clay mineralogy is an important branch of geology, because these minerals are the principal constituents of many fine-grained sediments, schists, weathering products of all types of rocks, and hydrothermal deposits. Moreover, these minerals are now used in many industries other than the ceramics industry.

The present article attempts to summarize the knowledge of the classification of the layer silicates, including most of the clay minerals, and to present a workable "scheme" for their laboratory identification by nonspecialists. Necessarily the presentation of a simplified general view of both these aspects results in the sacrificing of some accuracy of detail.

ACKNOWLEDGMENTS

During the past decade at the Pennsylvania State University, active clay mineralogical work has been in progress in several departments. Much of the material presented here has been presented in class lectures. Especial mention must be made of our colleagues Profs. E. C. Henry, T. F. Bates, and G. W. Brindley who have helped formulate many of the ideas by suggestion or even by disagreement. The responsibility for the opinions expressed is, of course, that of the authors.

We thank the organizations that donated samples of natural clays for use in our studies, as noted in the Appendix. Our knowledge of the properties of synthetic clay minerals has been obtained with the help of many graduate students in the Department of Geophysics and Geochemistry at Pennsylvania State University. Most of the recent work carried out with synthetic clays in the Departments of Geophysics and Geochemistry and of Ceramic Technology has been supported by American Petroleum Institute Project 55.

Correlation of the data and preparation of this manuscript was supported by a grant from The Petroleum Research Fund administered by the American Chemical Society. Grateful acknowledgment is hereby made to the donors of said fund.

CLASSIFICATION OF THE LAYER SILICATES

Definition and Introduction

The clay minerals are hydrous layer lattice silicates. Classically the term "clay" has included the connotation of small particle size ($<2\mu$), but in our present state of knowledge this is not a reasonable basis for definition of a mineral family. It is not logical to define clay minerals on the basis of size or to limit clay minerals to clay-grade material, since many layer silicates that are usually macroscopic also occur in submicroscopic particles. Thus micas, chlorites, and vermiculites, which frequently occur as microscopic crystals, are not separated from minerals such as kaolinite and montmorillonite in the classification of the hydrous layer silicates.

Mineral-classification schemes have been based on chemical composition, atomic structure, and properties such as expansion and morphology. The earliest classification of clays was compositional; later ones have tended to overemphasize the minutiae of structural de-

tail while neglecting gross variations of chemistry. The attempt is made here to keep a proper balance between composition and structure as the two basic properties for a classification scheme.

Classification immediately leads to the problem of nomenclature. The principles that have guided us in this area include the following:

(1) As Fleischer (1951) has pointed out, a logical redefinition of many terms is needed rather than the coining of a new terminology. This is attempted wherever possible.

(2) We have been more concerned with a logical and consistent scheme than with historical details of the precedence of one name over another. In this paper some of the older, "more established" terms are redefined and used rather than those proposed by the Clay Minerals Group (British) Subcommittee on Nomenclature of Clay Minerals (Brown, 1955).

No attempt is made to review in detail the history of classification of the clay minerals. Mackenzie (1959) has reviewed the various classifications proposed in the past decade.

The basic advance in the crystal chemistry of the layer silicates came about through the work of Pauling (1930) on the general structural features of these minerals. The detailed features, which serve as a basis for classification, have been thoroughly described in several books and articles on crystal chemistry and clay mineralogy (*e.g.*, Brindley, 1951; Grim, 1953; Brindley and MacEwan, 1953; Mackenzie, 1957).

Fundamental Structural Scheme Common to Layer Silicates

The fundamental structural units in layer silicates are silica layers and brucite (or gibbsite) layers. The former consist of Si–O tetrahedra connected at three corners in the same plane so that a two-dimensional network of hexagonal rings is obtained. The fourth, unjoined oxygen corners all point in the same direction. The silica, or tetrahedral, layer is shown in Figure 1. The brucite or gibbsite layers consist of hydroxyl ions in two planes, above and below a plane of magnesium or aluminum ions which are octahedrally co-ordinated by the hydroxyls. The difference between the brucite and gibbsite layers lies in the fact that in the former all the octahedral cation positions are filled, whereas in the latter only two-thirds of these positions are filled. A gibbsite layer is shown in Figure 2. The dimensions of the hexagonal units are essentially the same as those of the tetrahedral layer. Nearly all the clay minerals can be generated by very simple combinations of these two units. These two layers are combined in such a way that the unlinked oxygens of the tetrahedra replace two-thirds of the hydroxyls in one plane of the octahedral layer. The remaining hydroxyls in this plane assume positions at the centers of the hexagons formed by the oxygens of the tetrahedra, as shown in Figure 3a. The combination of one of each type of layer is shown in Figure 3b and c. Examination of the unit cell outlined in Figure 3b shows that a unit cell of a silica sheet plus a gibbsite layer contains the following ions in sequential layers: 6 oxygens, 4 silicons, 4 oxygens plus 2 hydroxyls, 4 aluminums, 6 hydroxyls (Fig. 3c).

The layer lattice silicates are subdivided on the basis of three criteria, two basically structural and one basically compositional: (1) the type of combination of the tetrahedral silica layers with the brucite or gibbsite layers, 1 tetrahedral:1 octahedral or 2 tetrahedral:1 octahedral; (2) the cation content of the octahedral layer, either 2 cations per half unit cell (dioctahedral) or 3 cations per half unit cell (trioctahedral); (3) the manner and perfection of stacking of the fundamental unit (2:1 or 1:1) packets upon each other.

As shown in Table 1, the use of the first criterion divides the clay minerals into the three main groups.[1] Figures 4 and 5 illustrate the combinations of layers in these groups.

The simplest combination of one octahedral layer and one tetrahedral layer yields the so-called "kaolinite-septechlorite" group, which is also aptly described by the term "1:1 clay mineral group." It is also referred to as the "7 Å group" from the fact that 7 Å is approximately the thickness of the combined layers, and this corresponds to the largest spacing observed on the X-ray diffraction pattern. The units of this group are illustrated in Figures 3b, 3c, and 4a.

Next is the "talc-mica-montmorillonite"

[1] There is a fourth group of clay minerals, including sepiolite and palygorskite or attapulgite, which will not be discussed in this paper since the structural units are chains (or ribbons) rather than layers (Bradley, 1940; Nagy and Bradley, 1955). However, these hydrated magnesium silicates have been included in the identification scheme since they are occasionally encountered in soils (desert type), sediments (alkaline lacustrine), and alteration products of mafic rocks (especially serpentine and amphibolites). The genesis and stability of these minerals are discussed by Mumpton and Roy (1958).

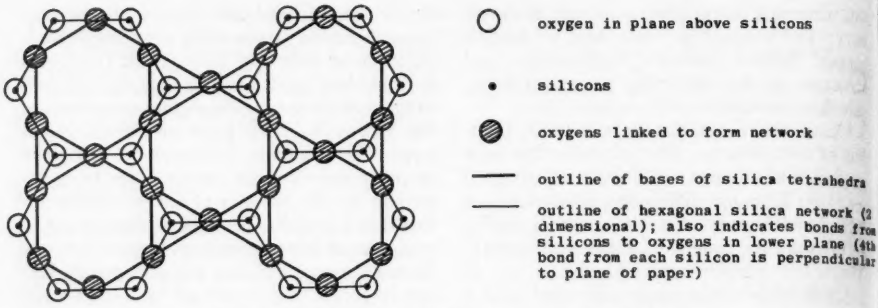
oxygen in plane above silicons
silicons
oxygens linked to form network
outline of bases of silica tetrahedra
outline of hexagonal silica network (2 dimensional); also indicates bonds from silicons to oxygens in lower plane (4th bond from each silicon is perpendicular to plane of paper)

Figure 1. Silica, or tetrahedral, layer, viewed from above

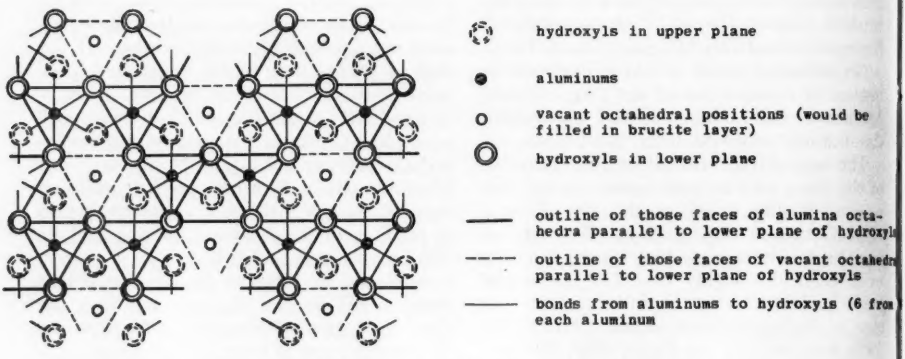
hydroxyls in upper plane
aluminums
vacant octahedral positions (would be filled in brucite layer)
hydroxyls in lower plane
outline of those faces of alumina octahedra parallel to lower plane of hydroxyls
outline of those faces of vacant octahedra parallel to lower plane of hydroxyls
bonds from aluminums to hydroxyls (6 from each aluminum

Figure 2. Gibbsite, or octahedral, layer, viewed from above

group, which is also referred to as the "2:1" or the "10 Å" group, the former in reference to the fact that there are two tetrahedral layers for each octahedral layer in the unit. The "10 Å", as before, refers to the height of such a 2:1 combination (Fig. 5).

The chlorites, or "14 Å" group, consist of a regularly alternating sequence of 2:1, or talc, units and complete brucite layers. The sequence of sheets is therefore (2:1) (1) (2:1) (1) (Fig. 4b).

Also shown in Table 1 is the application of the second classification criterion to divide each of the three main groups into dioctahedral and trioctahedral portions.

Some of the mixed-layer clay minerals (heteropolytypes) consist of combinations of fundamental units of more than one main group.

Composition of the Layer Silicates

The simplicity of the compositional relationships among and within the main families of the clay minerals can be shown in a ternary compositional diagram having as apices SiO_2, $R^{2+}O$, and $R^{3+}{}_2O_3$ (Figs. 6, 7). The minerals and families plotted on Figure 6 contain no alkalies, and the anhydrous compositions are plotted on a ternary diagram that is actually the anhydrous base of the tetrahedron with H_2O as the fourth apex. In the plotting of Figure 7, both water and alkali oxides were subtracted from the mineral compositions so that this diagram actually represents the composition planes of both the micas and the expanded 2:1 minerals in the anhydrous tetrahedron R_2O-RO-R_2O_3-SiO_2. Talc and pyrophyllite also are shown in Figure 7. The crossed

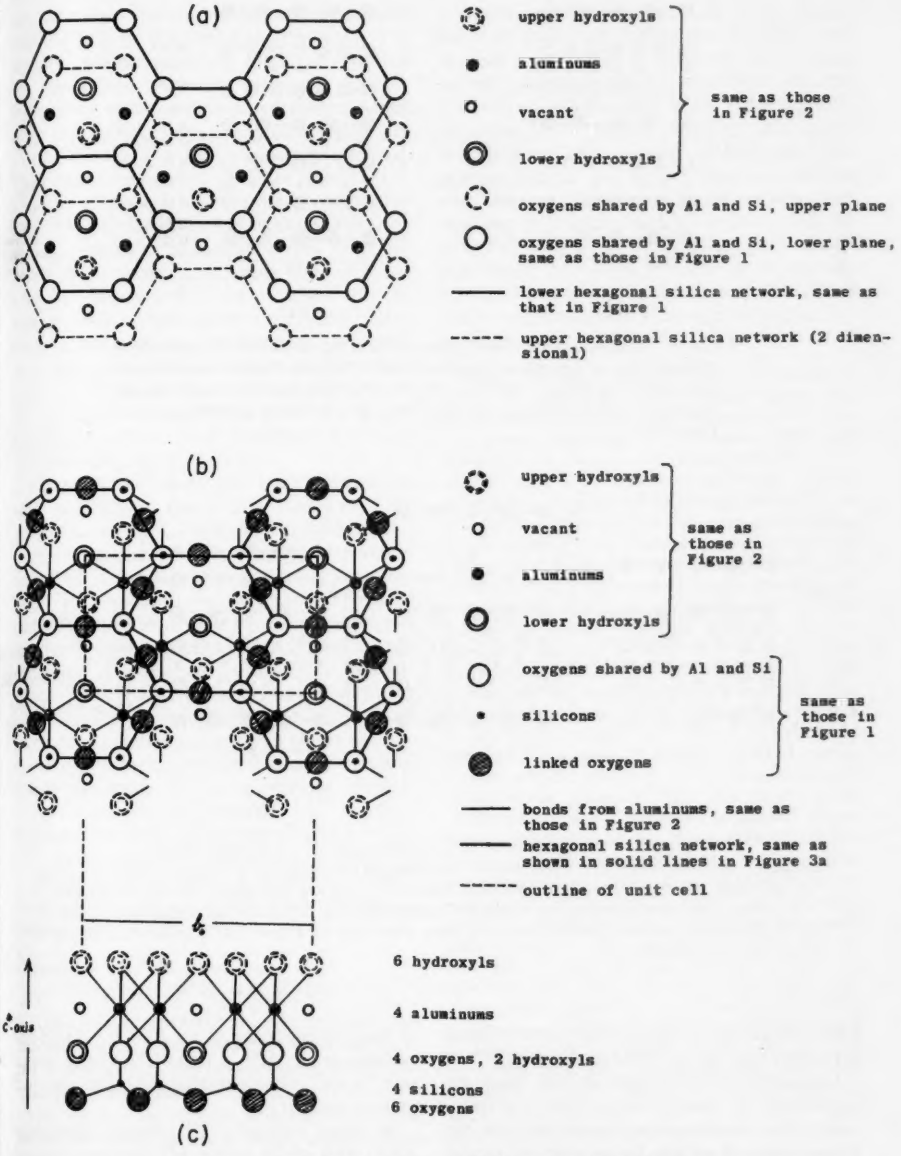

Figure 3. Combinations of octahedral and tetrahedral layers
a. Octahedral layer when part of a 2:1 mineral, for example pyrophyllite or muscovite
b. Combined tetrahedral and octahedral layers, 1:1, (001) projection (The diagram shows no distortion, and the unit cell is monoclinic rather than triclinic like kaolinite.)
c. (100)* projection of unit cell shown in 3b

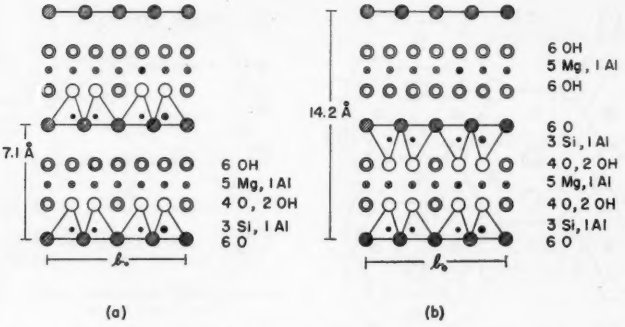

Figure 4. Diagrammatic (100)* projections of septechlorite (a) and normal chlorite (b) of clinochlore composition. Compare Figure 4a with the dioctahedral analogue shown in Figure 3c. The exact locations of the aluminum ions shown in the octahedral and tetrahedral layers are not significant.

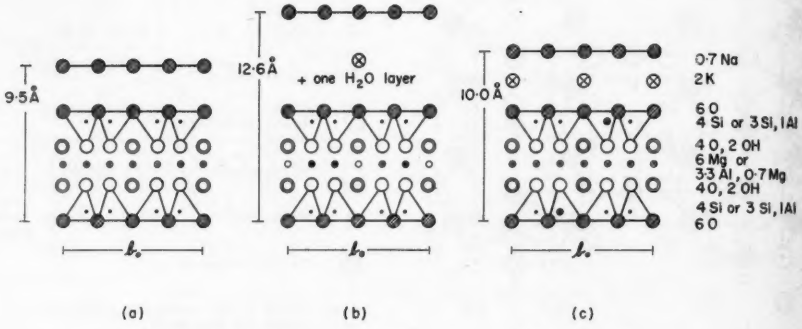

Figure 5. Diagrammatic (100)* projections of 2:1 layer silicates
(a) talc, (b) montmorillonite, (c) phlogopite. Variations in the thickness of unit layers (not thickness of unit cells, which may contain more than one unit layer) are indicated. The exact locations of the substituting ions shown in the octahedral and tetrahedral layers are not significant. This style of diagrammatic presentation is patterned after that used by Pabst (1955) in his description of the 1-layer mica structure.

lines indicate the extent of solid solution found experimentally by hydrothermal synthesis.

Compositional variations in the clays are controlled by simple crystal-chemical principles. The simplest substitutions involve the replacement of an ion by another of similar ionic radius but identical charge—*e.g.*, Fe^{2+} replacing Mg^{2+}. However, many more interesting combinations are possible by "balanced substitution" in the various positions in the layer lattice. Thus a very common substitution is Mg^{2+} (in 6-fold co-ordination) + Si^{4+} (4-fold) being replaced by Al^{3+} (in 6-fold co-ordination) + Al^{3+} (4-fold). The charge lost in one "layer" is compensated for by an identical gain in another.

In micas, expanded 2:1 minerals, and chlorites, with three types of positions, several combinations are possible. Silicon is commonly replaced by aluminum or ferric iron, and the ions commonly substituting for one another in the octahedral layer are aluminum, magnesium, ferrous and ferric ion, and lithium. Hydroxyl ions are replaced by fluorine or chlorine ions,

but these substitutions do not require accompanying substitutions in other positions. The ions that may occur in the interlayer position are commonly potassium, sodium, calcium, magnesium, aluminum, and hydronium. Many other cations have been nearly completely substituted for these by cation exchange methods. The elements that occur as minor or trace constituents in the layer silicates will be mentioned later. A number of these have been substituted in larger amounts in synthetic clay minerals. Much of the theory concerning ionic substitution has been verified by synthesis of the various layer silicates under controlled conditions of composition, temperature, and pressure. Such restrictions on the variations place quite strict limitation on the compositions of clay minerals and provide a guide on the acceptability of "structural formulae" arrived at by rationalization of analyses.

Figures 6 and 7 show that the various structural families are also clearly represented by compositional ones. Thus, the trioctahedral and dioctahedral 1:1 families (Fig. 6) are widely separated. The presence of separate 2:1 families (Fig. 7) is also clearly shown, although here the compositional tendency to merge into one another is also apparent. With regard to the expanded 2:1 minerals, considerable idealization is involved in the representation of the compositional variation as straight lines. Both work on synthetics and analyses of natural material suggest much greater latitude in compositional variation, reflecting various possible combinations of structural "defects". Figure 7 indicates that probable substitution of Fe^{3+} for Al^{3+} is not the only idealization involved in representing muscovite as $KAl_2Si_3AlO_{10}(OH)_2$ since there is solid solution toward both phengite and phlogopite.

Polymorphism, Polytypism, Heteropolytypism, and Homopolytypism

The application of the third criterion in the classification of layer silicates, the manner and perfection of stacking, permits more subtle distinctions among the clay minerals.

The "layers" in all layer silicates are held together by forces that are weak, compared to intralayer forces. This property is responsible for the fact that the layers in a particular mineral may be stacked slightly differently. Because each individual layer has fairly high symmetry, a number of different translations and rotations are possible. Thus a variety of regular, as well as random, stacking sequences is found among these minerals. Layer lattice minerals consisting of the same kinds of units stacked in a variety of ways are often called polymorphs, while those consisting of different types of units have been called "mixed-layer" minerals. Both "mixed layering" and polymorphism of layer silicates are examples of a general feature of layer structures termed "polytypism". This refers to any variations in stacking, either structural or compositional; the latter is designated heteropolytypism. Common usage by others prompts us to use the term "mixed-layer" in this paper. The entire subject of polytypism is treated in greater detail below.

Where the same chemical entity or compound occurs in two structurally different forms, the phenomenon is known as polymorphism. Polytypism, a term introduced by Baumhauer (1915) and developed by Strock and Brophy (1955), is a special case. The structural differences among polymorphs may be of unlimited simplicity or complexity. They may involve a complete change in the primary co-ordination, as for instance in GeO_2, which changes from a 6-co-ordinated rutile structure to a 4-co-ordinated quartz structure, or a mere straightening of bonds, such as in the low quartz–high quartz transition. The cases of polymorphism that can be referred to as polytypism are those in which the only structural change[2] involved is the manner in which identical two-dimensional sheets are stacked. The classic examples of polytypism are ZnS, SiC, and the clay minerals. Identical layers made up of closely packed spheres may be stacked according to two simple arrangements, called hexagonal close packing and cubic close packing. The hexagonal close-packed lattice corresponds to the repetition sequence ABABAB. This is the case for wurtzite, and such sequences are named by the number of layers involved in the repeat unit (in this case 2) and by the symmetry of the resulting structure (in this case hexagonal, abbreviated H). Thus wurtzite is called the 2H polytype of ZnS. If the stacking sequence is ABCABCABC, one generates a three-layer cubic close-packed structure, corresponding to cubic sphalerite, or ZnS-3C. There is an infinite number of combinations of hexagonal and cubic packing sometimes with very long repeat distances. Thus 3C, 20H, and 594R samples have been identified in SiC, SiO_2, or ZnS. Quite analogous to these polytypes are muscovite-1M or chlorite-6H, corresponding to 1-layer monoclinic and 6-layer hexagonal phases respectively.

In these cases the two-dimensional units are all essentially identical. In the clay minerals one en-

[2] This represents, of course, a minor approximation, since, when stacking sequences are changed, the position of ions within the layers may be slightly altered.

counters a phenomenon very similar to polytypism but one that involves two (or, theoretically, more) types of layers. Instead of only mica layers, one can conceive of a mixed stack of mica layers and water layers, or of mica layers and chlorite layers. This phenomenon has variously been referred to as "interstratification," "interlayering," "mixed layering," etc. Because of its close connection with polytypism, we have called this phenomenon "heteropolytypism"; the polytypism encountered in ZnS or in pure muscovite would be more narrowly defined as "homopolytypism." Heteropolytypism then is the phenomenon encountered in the stacking of two (or more) types of two-dimensional sheets in such a way or on such an intimate scale as to alter the X-ray unit cell from those of the separate phases. A mixed-layer clay may be referred to as a heteropolytype, giving the ratio of the component layers an index of the amount of randomness (and symmetry if ever available). Thus we may have a (3 mica:2 chlorite)$_r$ heteropolytype or, on the other hand, a 1 mica:1 chlorite. The subscript r for random should be reserved for randomness of stacking in the c direction—*i.e.*, the failure to preserve a proper sequence of layers. The subscript d for disorder, for example, kaolinite$_d$ or mica$_d$ or muscovite-1M$_d$, should be reserved for the failure to "register" each successive sheet properly on top of the preceding one, with respect to the alignment of the a–b planes above each other. The characterization of polytypes is illustrated in Figure 8.

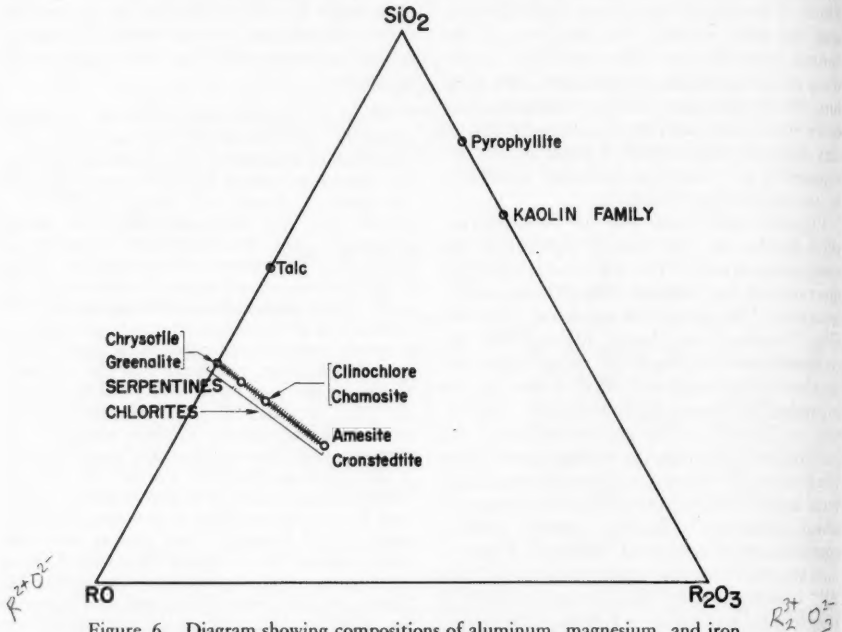

Figure 6. Diagram showing compositions of aluminum, magnesium, and iron layer silicates containing no alkalies. Diagram shows projection of hydrous phases onto anhydrous base.

DETAILED DESCRIPTION OF MINERAL FAMILIES

Two-Layer (1:1) Silicates

The names of the minerals within this group (Table 2) are well established, and designations by polytype need not be used although differences in stacking may be the principal distinction among them. Nevertheless, a logical system of nomenclature depending on polytypes is given for comparison with other groups of clay minerals to be described later. A similar system has been proposed by Mackenzie (1959). The nomenclature situation is discussed in the footnotes, where references to detailed structure studies are also given. The two-layer silicates are clearly divided into the kaolinite (dioctahedral) and septechlorite (trioctahedral) families.

The dioctahedral minerals are all pure hydrous aluminum silicates. It is not likely that

the minor amounts of other constituents found in samples of these minerals, particularly kaolinite$_d$, are incorporated in the kaolinite structure. In the synthesis of kaolinite it has not been possible to substitute even ferric iron or gallium for aluminum, or germanium for silicon in amounts recognizable by changes of X-ray properties. Kaolinite is the only member of this family that has so far been reproducibly synthesized by hydrothermal methods (Roy and Osborn, 1954).

the trioctahedral 7 Å minerals containing appreciable amounts of aluminum and/or iron are related by a simple polymorphic transformation to chlorites, the 14 Å minerals, as shown in Figure 4. Many of them are macroscopically and microscopically similar to the chlorites. The "septe," of course, refers to the 7 Å basal spacing.

Other than in the minor (tri- *vs.* dioctahedral) difference in structure, the septechlorites differ markedly from the kaolinite minerals

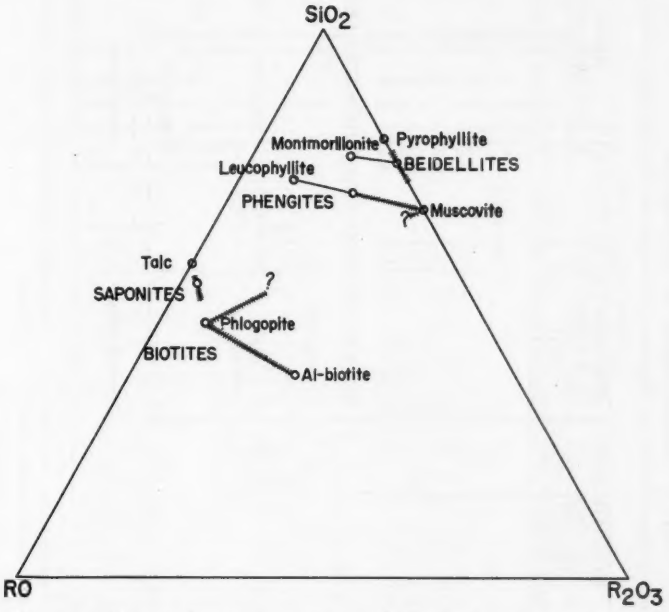

Figure 7. Diagram showing compositions of the aluminum, magnesium, and iron 2:1 layer silicates. Diagram represents projection of mica and montmorillonite composition planes onto anhydrous, alkali-free base.

The trioctahredral 1:1 minerals are called septechlorites rather than serpentines, since the latter cannot logically be used for the whole group. The term "serpentine" is used by geologists and petrologists for the greenish minerals (fibrous, splintery, or massive, but not micaceous) occurring in altered ultrabasic rocks or for the altered rock itself. The serpentines are magnesium septechlorites containing only minor amounts of aluminum and negligible iron; they may be nickeliferous. The term "septechlorite" was proposed by Nelson and Roy (1954), who noted that the inclusion of "chlorite" in the group name is desirable since with respect to variations in composition. Whereas the latter show no ionic substitutions, extensive solid solution occurs among the septechlorites. In addition to the simple ion-for-ion replacement, the solid solution is of the specific type illustrated by the simultaneous entry of Al^{3+} for Mg^{2+} in the octahedral and Al^{3+} for Si^{4+} in the tetrahedral layer. In the natural minerals, magnesium, nickel, manganese, ferrous and ferric iron, chromium, and aluminum are found in the octahedral positions, and aluminum and ferric iron may substitute for as much as half the silicon. A systematic study of the ionic substitutions in serpentines

TABLE 1. PRINCIPAL GROUPS OF LAYER SILICATES

Groups	2-layer = 1:1 = 7 Å		3-layer = 2:1 = 10 Å						4-layer = 14 Å
	KAOLIN-SEPTECHLORITE (For details *see* Table 2)		PYROPHYLLITE-TALC		EXPANDED 2:1 MINERALS (For details *see* Table 3)		MICA (For details *see* Table 4)		CHLORITE (For details *see* Table 6)
	dioct.	trioct.	dioct.	trioct.	dioct.	trioct.	dioct.	trioct.	trioct.
Mineral or mineral families*	Kaolinite Dickite Nacrite Halloysite Endellite	Chrysotile (SERPENTINES)	Pyrophyllite	Talc	Montmorillonite nontronite	Hectorite Stevensite	Celadonite	Polylithionite	
increasing tetrahedral substitution	SEPTECHLORITES				BEIDELLITES dioct. vermiculites	SAPONITES VERMICULITES	PHENGITES Muscovite Margarite	LEPIDOLITES Phlogopite BIOTITES	CHLORITES
Common heteropolytypes					mixed layers		mixed layers		

* Family names are in capital letters; names of minerals that have close to idealized end-member compositions are written with initial capitals. This convention used in Tables 2–4 also. See Tables 2–6 for more details, especially composition, and for relationships of less common layer silicates to those given above.

made by Roy and Roy (1954) also demonstrated complete substitution of germanium for silicon in the magnesium and nickel compounds.

Much research has been carried out on the structures of the natural and the synthetic septechlorites. A number of papers on serpentines have been presented by Whittaker and by Zussman. A joint paper (1956) reviews the structural studies on serpentines and proposes that three main types exist: chrysotile, lizardite, and antigorite. There are three forms of the first, clino-, ortho-, and parachrysotile. In a later paper (1958) they give a useful criticism of some other papers on the subject. The polytypism of the synthetic serpentines has been found by Gillery (1959a) to be related to composition. When aluminum is introduced into the serpentines, the platy varieties obtained are 1-layer and/or 6-layer orthohexagonal varieties. The former is equivalent to lizardite, while the latter has now also been found in nature (Zussman and Brindley, 1957).

Three-Layer (2:1) Silicates: Pyrophyllite-Talc

Only three minerals fall into this group; no polytypic variations have been found. Pyrophyllite, the dioctahedral mineral, is a pure hydrous aluminum silicate. A small amount of substitution of aluminum in talc, the trioctahedral magnesium mineral, has been found (Stemple and Brindley, 1960). Minnesotaite is the ferrous iron analogue of talc (Gruner, 1944).

Three-Layer (2:1) Silicates: Expanded 2:1 Minerals

These minerals are intermediate in structural scheme between the pyrophyllite-talc minerals and the micas (Fig. 5). This concept is well known as the Hofmann-Endell-Wilm-Marshall-Hendricks structure of montmorillonite, which also includes the hypothesis that these minerals

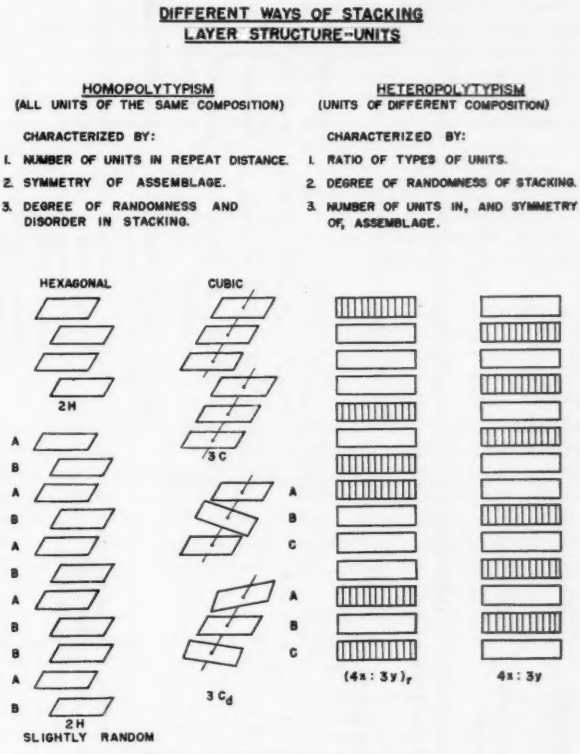

Figure 8. Examples of polytypism

TABLE 2. TWO-LAYER (1:1) SILICATES

Dioctahedral—KAOLINITE MINERALS			Trioctahedral—SEPTECHLORITES[13]			
Composition and name	Polytype			Composition (idealized)	Name	Polytype
$Al_4Si_4O_{10}(OH)_8$			SERPENTINES	$Mg_6Si_4O_{10}(OH)_8$	Chrysotile[6,7]	3 2-layer types
Nacrite[1]	6-layer monoclinic	(kaolinite-6M)			antigorite[6]	1-layer monoclinic (with a large a_0)
Dickite[2]	2-layer monoclinic	(kaolinite-2M)			lizardite[6]	1-layer orthohexagonal
Kaolinite[3]	1-layer triclinic	(kaolinite-1T)		$Mg_{5.5}Al_{0.5}Si_{3.5}Al_{0.5}O_{10}(OH)_8$		1-layer orthohexagonal
Kaolinite$_d$[4]	1-layer (monoclinic?) *b* axis disordered	(kaolinite$_d$)		$Mg_{5.0}Al_{1.0}Si_{3.0}Al_{1.0}O_{10}(OH)_8$	Clinochlore[7]	1- and 6-layer
Halloysite[5]	1-layer *a* and *b* disordered	(kaolin$_d$)		$Mg_{4.0}Al_{2.0}Si_{2.0}Al_{2.0}O_{10}(OH)_8$	Amesite[7,8]	6-layer orthohexagonal
$Al_4Si_4O_{10}(OH)_8 \cdot 4H_2O$				$Fe_6Si_4O_{10}(OH)_8$	Greenalite[9]	
Endellite[5]	1-layer $+ H_2O$ (d_{001} = ca. 10 A)			$Fe''_{4.0}Fe'''_{2.0}Si_{2.0}Fe_{2.0}0_{10}(OH)_8$	Cronstedtite[10]	
				$Fe''_{5.0}Al\ \ Si_3\ \ Al\ \ O_{10}(OH)_8$	chamosite[11]	
				$(Ni,Mg)_6Si_4O_{10}(OH)_8$ (variable)	garnierite[12] (Ni-serpentine)	
				$Mn_5\ \ Al\ \ Si_3\ \ Al\ \ O_{10}(OH)_8$	bementite (and grovesite)	

Note: Family names are in capital letters; names of minerals which have close to idealized end-member compositions are written with initial capitals; others vary in composition between certain limiting end members.

[1] Hendricks (1939a)

[2] Newnham and Brindley (1956)

[3] Brindley and Robinson (1946a). Name "kaolinite T" proposed by Holdridge and Vaughan *in* Mackenzie (1957)

[4] Called "fireclay" in structural study by Brindley and Robinson (1946b). Name "kaolinite pM" proposed by Holdridge and Vaughan in Mackenzie (1957); "ψM-kaolinite" proposed by Mackenzie" (1959). The subscript "*d*" used in this classification signifies a disordered mineral. This subscript has been used by one of the authors in previous publications (*e.g.*, Hill and Roy, 1958).

[5] The relation between structure and tubular morphology has been discussed by Bates, Hildebrand, and Swineford (1950). The nomenclature above agrees with the proposals of Faust (1955).

[6] Whittaker and Zussman (1956)

[7] Gillery (1959a)

[8] Brindley, Oughton, and Youell (1951)

[9] Gruner (1936)

[10] Hendricks (1939b)

[11] Brindley and Youell (1953); the name "berthierine" is preferred by the Clay Minerals Group Subcommittee on Nomenclature (Brown, 1955).

[12] Noll and Kircher (1952)

[13] Prefix "septe" may be added to names of septechlorites, *e.g.* septeclinochlore, only if it should be desirable to differentiate between these minerals and the normal chlorites.

have a two-dimensional lattice with no order in the stacking of layers. The expanded minerals, unlike the other 2:1 layer silicates, include loosely bound cations and layers of water between the silicate sheets. The water can be partially or completely replaced by polar organic molecules. Because the amount and thickness of water and organic compounds in the interlayer position may vary, the spacing of the first basal X-ray diffraction maximum of these minerals is also variable. Moreover, many of these minerals, especially those from bentonite deposits, form complexes with much larger amounts of water than would occupy interlayer space in an oriented manner. Such clay–water complexes exhibit the remarkable properties that have long been the subject of investigation for many colloid chemists and electrochemists.

The physical swelling of these minerals, although of great importance, is not a basis for their classification; however, the variability in basal spacing is the property all expanded 2:1 layer silicates share, and this separates them from the other 2:1 layer silicates in the crystallochemical classification used in this paper. Thus the expanded 2:1 layer silicates are those three-layer silicates with less than two-thirds of the possible interlayer cation population and with reversibly variable basal spacings. The number of interlayer cations is commonly, but not invariably, approximately one-third that found in the micas. These cations under natural conditions are sodium, calcium, magnesium, and aluminum and/or hydrogen or hydronium. Others may be substituted for these in the laboratory.

Although these minerals have variable basal spacings, expansion of this spacing to 17–18 Å with organic liquids is not a part of the definition. This does not occur with most vermiculites, which are included in this group. Also, the two-dimensional structural character of the expanded 2:1 minerals is not stressed, because many of them, particularly the trioctahedral ones, show *hkl* reflections, demonstrating considerable order of stacking.

The expanded (or expandable) 2:1 layer silicates are listed in Table 3. The interlayer cations have been omitted from the formulae, because they may be varied by simple cation exchange. The table is split into portions both horizontally and vertically; several families exist within this important group of clay minerals. Montmorillonite, hectorite, and stevensite show less variation in composition than do the other minerals in this group, because only minor amounts of substitution occur in the tetrahedral layer. Montmorillonite is the most common of these three minerals. Minerals having both octahedral and tetrahedral substitution fall into three families: beidellite, saponite, and vermiculite.

It is generally agreed that the minerals in the upper portion of Table 3 should be grouped together, and Ross (1960) has included all of them except beidellite in his revised classification of this group. Because they can be distinguished from the vermiculites, which have larger amounts of tetrahedral substitution, by heat treatment and/or by treatment with ethylene glycol, it is convenient to have a subgroup name for the upper portion of Table 3. "Montmorillonite" is used as a group name by most American clay mineralogists, whereas "smectite" has been proposed by the Nomenclature Subcommittee of the Clay Minerals Group (British) with some justification (Brown, 1955).

The montmorillonite group includes all the 2:1 minerals that can be expanded with ethylene glycol to about 17 Å. In theory we believe that vermiculites should properly not be separated from the montmorillonite-type minerals since the properties probably are continuously variable from saponites to vermiculites. However, because of their high tetrahedral charge (and their usually coarse particle size), vermiculites have been classified as a separate subgroup of the expandable 2:1 layer silicates on the basis of the distinctive criterion of failure to expand to 17 Å with ethylene glycol at room temperature (particularly when magnesium is the interlayer cation; Walker, 1958).

The question of the relationship between vermiculites and Mg-saponites has been treated by Roy and Romo (1957) and by Walker (1957; 1958). The variations in composition and properties of vermiculites have been correlated with genesis by Weaver (1958). The dioctahedral vermiculites, which are all fine-grained clay minerals, have been described (although not always given this name) by Brown (1953), Hathaway (1955), Rich and Obenshain (1955), and van der Marel (1954), among others, and are common in soils.

The term "beidellite" was originally used for a natural expanded 2:1 mineral believed to be an aluminum-rich variety with predominantly tetrahedral charge. Since the type mineral has been found to be impure, the term is no longer acceptable to Ross (1960) and

[18] Prefix "septe" may be added to names of septechlorites, *e.g.* septeclinochlore, only if it should be desirable to differentiate between these minerals and the normal chlorites.

[19] This subscript has been used in this classification signifies a disordered mineral. This subscript has been used by one of the authors in previous publications (*e.g.*, Hill and Roy, 1958).

[20] The relation between structure and tubular morphology has been discussed

TABLE 3. THREE-LAYER (2:1) SILICATES—EXPANDED 2:1 MINERALS

	Dioctahedral			Trioctahedral	
	Name	Formula of 2:1 Layer*	Seat of charge	Name	Formula of 2:1 Layer*
MONTMORILLONITE GROUP	Montmorillonite[1,3]	$Al_{2-x}Mg_xSi_4O_{10}(OH)_2$	octahedral only (essentially)	Hectorite[3]	$Mg_{3-x}Li_xSi_4O_{10}(OH)_2$
			x > y, y near 0	Stevensite[1,3,6]	$Mg_{3-x}\square_xSi_{4-y}\square_yO_{10}(OH)_2$
			octahedral dominant x > y	SAPONITE[1,3]	$Mg_{3-x}Al_xSi_{4-y}Al_yO_{10}(OH)_2$
				pimelite[2,3]	$Ni_{3-x}Al_xSi_{4-y}Al_yO_{10}(OH)_2$
	(BEIDELLITE)			sauconite[2,3]	$Zn_{3-x}Al_xSi_{4-y}Al_yO_{10}(OH)_2$
	nontronite[4]	$(Fe,Al)_2Si_{4-y}Al_yO_{10}(OH)_2$	tetrahedral dominant y > x	medmontite	$Cu_{3-x}Al_xSi_{4-y}Al_yO_{10}(OH)_2$
	volchonskoite[2]	$(Al,Cr)_2Si_{4-y}Al_yO_{10}(OH)_2$			
	(synthetic) beidellite[1,3]	$Al_2Si_{4-y}Al_yO_{10}(OH)_2$	tetrahedral only y < 0.5	(synthetic)[1,3] saponite	$Mg_3Si_{4-y}Al_yO_{10}(OH)_2$
	dioctahedral vermiculite[5]	$(Al,Fe)_{2-x}Mg_xSi_{4-y}Al_yO_{10}(OH)_2$	tetrahedral dominant y near 1	VERMICULITE	$Mg_{3-x}Fe_xSi_{4-y}Al_yO_{10}(OH)_2$

* Idealized; interlayer cations omitted because variable

Note: Family names are in capital letters; names of minerals that have close to idealized end-member compositions are written with initial capitals; others vary in composition between certain limiting end members.

[1] The expandable 2:1 silicates in the system MgO-Al_2O_3-SiO_2-H_2O (Roy and Roy, 1955) have been synthesized many times. An example of the systematic studies on variation of properties with composition is that of Koizumi and Roy (1959). The natural minerals of the montmorillonite group have been described in detail by Ross and Hendricks (1945)

[2] Synthesis reported by Roy and Sand (1956)

[3] Synthesis reported by Mumpton and Roy (1956)

[4] Synthesis reported by Ewell and Insley (1935)

[5] Properties of natural material described by, *e.g.*, Brown (1953), Hathaway (1955)

[6] Detailed mineralogical study of stevensite made by Faust, Hathaway, and Millot (1959)

TABLE 4. THREE-LAYER (2:1) SILICATES—MICAS

and Roy (1959). The natural minerals of the montmorillonite group have been

Millot (1959)

TABLE 4. THREE-LAYER (2:1) SILICATES—MICAS

Dioctahedral		Number of silicons Seat of charge	Trioctahedral	
Name	Formula (idealized)*		Name	Formula (idealized)*
Leucophyllite[1]	$KAlMgSi_4O_{10}(OH)_2$	tetrasilicic octahedral only	Taeniolite[1]	$KMg_2LiSi_4O_{10}(OH)_2$
Celadonite[2]	$K(Fe,Al)(Mg,Fe)Si_4O_{10}(OH)_2$		Polylithionite[1]	$KAl_2Li_2Si_4O_{10}(OH)_2$
PHENGITE[3]	$K(Al,Fe)_{2-x}(Mg,Fe)_xSi_{3+x}Al_{1-x}O_{10}(OH)_2$	octahedral and tetrahedral	LEPIDOLITE[4]	$KAl_{\frac{2-x}{2}}Li_{\frac{3+x}{2}}Si_{3+x}Al_{1-x}O_{10}(OH)_2$
roscoelite[3]	$K(Al,V)_{2-x}(Mg,Fe)_xSi_{3+x}Al_{1-x}O_{10}(OH)_2$			
fuchsite[3]	$K(Al,Cr)_{2-x}(Mg,Fe)_xSi_{3+x}Al_{1-x}O_{10}(OH)_2$			
Muscovite	$KAl_2Si_3AlO_{10}(OH)_2$	trisilicic tetrahedral only	Phlogopite[5]	$KMg_3Si_3AlO_{10}(OH)_2$
Paragonite	$NaAl_2Si_3AlO_{10}(OH)_2$		Annite[6]	$KFe_3Si_3AlO_{10}(OH)_2$
			Manganophyllite[5]	$K(Mg,Mn)_3Si_3AlO_{10}(OH)_2$
		octahedral and tetrahedral	BIOTITE[5]	$K(Mg,Fe)_{2+x}(Fe,Al)_{2-x}Si_{2+x}(Al,Fe)_{2-x}O_{10}(OH)_2$
			siderophyllite[6]	$KFe''_{2+x}Al_{1-x}Si_{2+x}Al_{2-x}O_{10}(OH)_2$
			lepidomelane[6]	$KFe''_{2+x}Fe'''_{1-x}Si_{2+x}Al_{2-x}O_{10}(OH)_2$
		disilicic octahedral and tetrahedral	Al-biotite[8]	$KMg_2AlSi_2Al_2O_{10}(OH)_2$
Brittle Micas				
Margarite[1]	$CaAl_2Si_2Al_2O_{10}(OH)_2$	tetrahedral only	Seybertite[1]	$CaMg_3Si_2Al_2O_{10}(OH)_2$
		monosilicic	Xanthophyllite[7]	$CaMg_{2.2}Al_{0.8}Si_{1.2}Al_{2.8}O_{10}(OH)_2$

*$x < 1$

Note: Family names are in capital letters; names of minerals that have close to idealized end-member compositions are written with initial capitals; others vary in composition between certain limiting end members.

[1] Schaller (1950)
[2] Hendricks and Ross (1941)
[3] Foster (1956)
[4] Levinson (1953)
[5] Levinson and Heinrich (1954)
[6] Foster (1957)
[7] Forman (1951)
[8] Crowley, M.S., 1959, Ph.D. Thesis, Pa. State Univ.

others. However, an aluminum-rich montmorillonite can easily be synthesized (Roy and Osborn, 1954), and the name "beidellite" as originally defined can be applied to this material. Moreover, Greene-Kelly (1955) cites evidence for the existence of pure natural beidellite.

Since all the 2:1 minerals with variable basal spacings, including vermiculites, have been included in one group, one might believe that "swelling chlorite" should also be included in this group. "Swelling chlorite" was first described by Stephen and MacEwan (1950). In a later paper on unusual chloritic clay minerals (Stephen and MacEwan, 1951) they compare this "swelling chlorite" and a chlorite-montmorillonite mixed-layer mineral (later named "corrensite") with the chlorite-like material synthesized by Caillère and Hénin (1949). The term "swelling chlorite" thus came to include all these chloritic minerals. Caillère, Hénin, and Esquevin (1954) perpetuated this idea and included some iron-rich chlorites that can be transformed to "montmorillonite" by acid treatment. They used the terms "swelling chlorite" and "pseudo chlorite" interchangeably for all these chlorite-like minerals. The latter was a better choice since not all of them exhibit swelling. "Pseudo-chlorite" is given preference by Caillère and Hénin (Mackenzie, 1957, Ch. VIII). Roy and Romo (1957) have used the term "pseudo-chlorite" for a chlorite-like material developed from vermiculite by hydrothermal treatment. Because of this confusion, it seems advisable to avoid both terms. Depending on their properties, these minerals may be described as vermiculite, saponites with interlayer complex, corrensite, or chlorite.

All the expanded 2:1 minerals except vermiculite can be synthesized readily under hydrothermal conditions. References for the hydrothermal syntheses are given in Table 3. Substitutions are possible in the dioctahedral minerals because the resulting layer charges can be balanced by the interlayer cations, in contrast to the situation with pyrophyllite and kaolinite. Systematic studies of the variation in properties of expanded 2:1 layer silicates with types and amounts of substitution have been made by Koizumi and Roy (1959), Gillery (1959b), Karšulin and Stubičan (1954), and Ames and Sand (1958). The investigation made by Koizumi and Roy showed that the amounts of substitution in "montmorillonoids" are variable and that corresponding variations in cation exchange capacity are obtained.

Experimental evidence indicates that the solid solution between synthetic dioctahedral and trioctahedral expanded 2:1 minerals is incomplete (Mumpton and Roy, 1956); this agrees with observations on natural minerals (Foster, 1951). In addition to minerals of the compositions in Table 3, a gallium variety has been prepared (Roy and Roy, 1954, p. 965).

Three-Layer (2:1) Silicates: Micas

The structural unit of the micas consists of two tetrahedral layers with a layer of octahedrally co-ordinated cations between them and with a layer of large cations (the interlayer cations) bonding this 2:1 unit to the next. There is one interlayer cation per formula unit (two per unit cell of a single-layer polytype). The interlayer positive charge is balanced by substitutions of ions of smaller charge for some of those in the octahedral layer or tetrahedral layer or both. The bonding between sheets is much stronger in the micas than in the other clay minerals since the interlayer cations fill all possible positions and are not hydrated.

Thus, for the most part, there is order in the "registration" of stacking of the fundamental unit layers. A limited variety of sequences of stacking is possible because of the hexagonal nature of the unit layer. The polytypism (polymorphism) observed in the micas was first described by Hendricks and Jefferson (1939). More recently this subject has been treated theoretically by Smith and Yoder (1956) who illustrate very clearly how the fundamental layers in the various polytypes are related by translation and/or rotation through 0 to 360° in multiples of 60°. The polytype formed appears to bear some relation to composition. Thus, "pure" muscovite is commonly the 2M (two-layer monoclinic) polytype, whereas phlogopite and celadonite are commonly the 1M (one-layer monoclinic) polytype. Crowley (Crowley, M. S., 1959, Ph.D. Thesis, Pa. State Univ., p. 18) has shown a similar effect in synthetic phases, where the 3T polytype of muscovite forms when much Mg^{2+} is admitted in solid solution. Polytypism, both with and without some disorder, is found among the fine-grained (clay-grade) micas as well as among the macrocrystalline varieties.

The classification of the micas is based primarily on composition. They are grouped according to whether they are dioctahedral or trioctahedral, as is also done with the other layer silicates. The older separation of micas into heptaphyllites and octaphyllites (Winchell, 1925, p. 427–428) is the same manner of grouping—heptaphyllites are dioctahedral and octaphyllites trioctahedral, the "hepta" and "octa" referring to the total number of cations in the mica "formula."

Micas are also categorized according to the number of silicon ions in the tetrahedral positions; thus they may be tetrasilicic, tri-

silicic, disilicic, or monosilicic. Both types of grouping are used in Table 4. The minerals included here show large variations in composition. Many more varieties of mica have been named, but they have the same types of cationic substitution as shown here. The name sericite has not been included, since it merely implies the fine-grained nature of a mica.

In Table 4 a dioctahedral family, which includes many natural micas, is given the name PHENGITE. Foster (1956) has shown that phengites are micas intermediate in the dioctahedral tetrasilicic-trisilicic series. The term "high-silica sericites" (Schaller, 1950) has frequently been used for these micas; however, as stated above, there are grave objections to the term "sericite." (*See also* Yoder and Eugster, 1955, p. 255.) We have generalized the formula of PHENGITE to show the common substitutions encountered. Muscovite and Leucophyllite refer to the trisilicic and tetrasilicic micas containing no iron. The relation of various common mineral names to the general scheme is shown: thus, fuchsite is a chromian phengite usually close to the trisilicic end and hence in some cases properly referred to as a chromian muscovite; Celadonite is the iron-bearing analoque of Leucophyllite.

Just as the term PHENGITE encompasses a group of micas falling between trisilicic and tetrasilicic end members, the exactly analogous term BIOTITE encompasses some that are between trisilicic and disilicic. The difference between BIOTITE and Phlogopite, which is the trisilicic end member, is not in the iron content but in the fact that biotites have more tetrahedral substitution of $Al^{3+} + Fe^{3+}$ for Si^{4+} than does phlogopite. Annite is used for the pure ferrous analogue of phlogopite, following Yoder and Eugster (1954, p. 179), since the end member is known only in the laboratory. The compositional relationships among the micas can also be visualized by reference to Figure 9, on which the variations are shown on a three-dimensional plot.

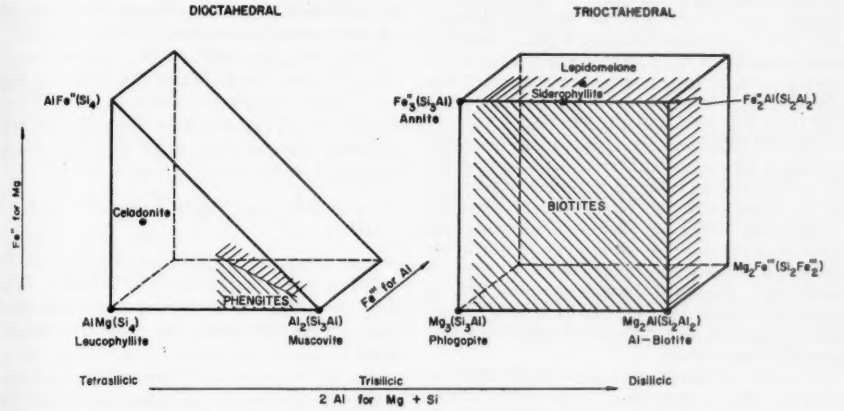

Figure 9. Diagrams illustrating the variation in compositions of the micas. The octahedral and tetrahedral cations are indicated. The phengite and biotite families are shown as volumes, the boundaries of which are not sharply defined. The solid circles indicate "idealized" end-member compositions on corners, edges, or faces of the dioctahedral wedge or trioctahedral cube.

LEPIDOLITE, the other family name, includes many lithium micas intermediate between tri- and tetrasilicic with Taeniolite and Polylithionite representing tetrasilicic end members. Levinson (1953) claims to have found some lepidolites intermediate between trioctahedral and dioctahedral mica; Crowley (Crowley, M. S., 1959, Ph. D. Thesis, Pa. State Univ., p. 34) presents experimental evidence for similar partial solubility between muscovite and phlogopite.

Appreciable amounts of fluorine and some chlorine substitute for hydroxyl ions in natural micas; the former frequently predominates over hydroxyl in phlogopite and lepidolite.

Fluoro-micas in which complete substitution takes place are synthesized readily. They form the basis for the synthetic mica of commerce, and because of this interest an enormous volume of work has been done in the field of the crystal chemistry of the synthetic micas (Eitel *et al.*, 1953; 1954, p. 874–876; Noda, 1955). To some extent synthetic micas may be "tailor-made" to have certain desirable properties.

A variety of cations are found in the structures of natural micas. In addition to those shown in Table 4, are Rb and Cs in the interlayer positions and Ti in the octahedral layer. A large variety of substitutions has been demonstrated also in the synthetic micas including hydroxyl micas. Additional elements incorporated in the synthetic micas are Tl, Sr, Co, Ni, Cu, Be, B, and Ga.

The crystallochemical classification of micas, described above, is both systematic and useful. They may also be classified according to polytype as has been done by Taboadela and Ferrandis (Mackenzie, 1957), but such a classification is of limited practical use. It seems more logical to use polytypic designations as modifiers of the mica name, *e.g.*, muscovite-1M and muscovite-2M. In some instances the polytype may be known but not the composition, and the mineral might be called mica-3T, for example.

A number of investigators have sought relationships between composition and polytype with some measure of success. Levinson (1953; 1955; Levinson and Heinrich, 1954) has examined by X-ray diffraction a large number of natural micas for which chemical analyses were available. Yoder and Eugster (1954; 1955) have studied both natural and synthetic micas; Crowley (Crowley, M. S., 1959, Ph.D. Thesis, Pa. State Univ.) has studied synthetic micas. Much useful information on polytypism has been obtained from the investigation of natural micas, but the problem may be solved unequivocally only by the examination of micas synthesized under controlled conditions of composition, temperature, and pressure. It is still not clear whether there is a thermodynamically stable *p-t* region for more than one polytype in any layer silicate.

Three-Layer (2:1) Silicates: Mixed-Layer Minerals (Heteropolytypes)

General discussion. Many of the mixed-layer clay minerals consist of 2:1 layers, usually expandable layers plus mica units. Most of the 2:1 clay minerals formed and maintained at relatively low temperatures and pressures are mixtures of expandable and nonexpandable layers (Weaver, 1956). There has been a considerable discussion about whether such mixtures should be given mineral names. (*See*, for example, Yoder and Eugster, 1955, p. 252–254.) In the sense of classical mineralogy they are not minerals; however, these materials do exhibit limits of composition and structure and are too common to be lightly dismissed as "mixtures." Thus, it is of considerable practical use to name and classify them, while understanding in what manner they differ from the classical concept of minerals. They are indeed on the borderline between single phases and two phases. The mixing is on such an intimate scale (in one direction) that the primary tool of solid-state chemistry, X-ray diffraction, can detect interaction between the two phases.

Illite and glauconite. The random mixed-layer 2:1 dioctahedral minerals, including illite and glauconite, are compared in Table 5 with the micas and expanded 2:1 minerals. The bulk chemical compositions of all of these may be expressed by the same general formula:

$$X_{1-x+y}(Al,Fe''')_{2-y}(Mg,Fe'')_{y}Si_{3+x}Al_{1-x}O_{10}(OH)_2$$

where X signifies interlayer cations, and the value of x may range between 0 and 1. Thus, only tetrasilicic and trisilicic micas and those intermediate between the two are included here.

For all the micas, x is practically equal to y, since the interlayer positions are filled. The ratio x/y is large for the completely expandable minerals: x/y for montmorillonite = 1/0.3, for beidellite = 0.7/0. The clay minerals to which the name "K bentonite" has been applied are intermediate; some have a majority of mica layers, and others a majority of expandable layers. They are considered to be typical random mixed-layer minerals.

Glauconite and illite, on the other hand, consist predominantly of mica layers and only a small percentage of expandable layers and are not commonly considered mixed-layer minerals. The term "illite" is, in fact, commonly used only for those poorly crystallized, fine-grained minerals that are difficult to distinguish from micas. Glauconite differs from illite in having larger amounts of Fe''' than Al in the octahedral layer. It appears that glauconites are generally nearer the tetrasilicic end of the series, and illites are generally nearer the trisilicic end of the series.

The composition of hydromuscovite can be expressed as a mica-type formula only if some of the water present is calculated as H_3O^+ and considered to be in the interlayer position (Brown and Norrish, 1952), and then $x = y$.

However, the properties of hydromuscovites indicate that they, like K bentonites, consist of mica layers randomly interstratified with significant amounts of expandable layers (Warshaw, 1960).

There are no mineralogical differences between some K bentonites and some illites, *e.g.* the illite from Ballater, Scotland (Mackenzie, Walker, and Hart, 1949). Classification of the so-called K bentonites thus depends on genesis, which is not a good practice but serves a useful purpose at present.

There are other random mixed-layer minerals with compositions similar to that of K bentonite. They have been given a variety of names and are described by Cole and Hosking and by Taboadela and Ferrandis in the book edited by Mackenzie (1957).

The trioctahedral analogue of illite (Walker, 1950) is not common and is not a stable mineral among low-temperature mineral assemblages. Hydrobiotites, on the other hand, are fairly common, and Walker (Brindley, 1951, p. 212–215) has shown that they are related to both biotite and vermiculite and may well represent the intermediate stage of the transformation of one into the other.

"Long-spacing" clay minerals. Regular mixed-layer minerals have X-ray diffraction peaks at low angles and are so-called "long-spacing" minerals. The value of this basal spacing gives some indication of what units are combined in the mixed-layer mineral. Although the regular mixed-layer minerals do yield diffraction peaks at low angles, the presence of these low-angle maxima (d = 24–30 Å) alone does not necessarily mean that the mixture has a regular sequence, as has been explained by Bradley (Weaver, 1956, p. 217–219).

The following "long-spacing" minerals have been described as having a regular stacking arrangement of layers. Rectorite (Bradley, 1950) consists of alternating pyrophyllite and vermiculite units. A similar mineral, allevardite, has been described by Brindley (1956) as consisting of double mica layers separated by layers of water molecules. Several other unusual "long-spacing" dioctahedral minerals have been found in the hydrothermal clay deposits of Japan and are described by Sudo (1959; Sudo and Hayashi, 1956). A regularly alternating sequence of illite (mica) and montmorillonite has been described by Heystek (1954). Because of the types of units involved, this mineral has more in common with the random mixed-layer minerals found in soils and sediments than do the other regular mixed-layer minerals mentioned above.

TABLE 5. CHEMICAL RELATIONSHIPS AMONG SOME OF THE DIOCTAHEDRAL 2:1 LAYER SILICATES
All have the general composition: $X_{1-x+y}(Al,Fe''')_{2-y}(Mg,Fe'')_ySi_{3+x}Al_{1-x}O_{10}(OH)_2$*

	$x = y$		$x > y$		$x >> y$
Range of values of x	X = K[1]	X = K + H_3O[2]	X = K		X = Na,Ca
1	Celadonite[1] $Fe''' > Al$				Montmorillonite[6]
.7–1	↑ Phengite[1]		Glauconite[1,3] $Fe''' > Al$	K bentonite[5]	Beidellite[6,7] y–0
.3–.6	↓		Illite[4]		
0	Muscovite[1]	Hydromuscovite[2]			
	←	Increasing x/y value		→	

*Expresses composition, not necessarily structural formula
[1] Foster (1956)
[2] Brown and Norrish (1952)
[3] Warshaw, C. M. (1957, Ph.D. Thesis, Pa. State Univ.); Burst (1958)
[4] Taboadela and Ferrandis (Mackenzie, 1957, Ch. VI)
[5] Cole and Hosking (Mackenzie, 1957, Ch. X). Name in common usage, retention in a revised classification is open to question.
[6] Foster (1954)
[7] Roy and Osborn (1954)

TABLE 6. FOUR-LAYER SILICATES—CHLORITES[1]

Magnesium—Aluminum—Iron Chlorites[2]

Idealized formula	Septechlorites		Normal chlorites			
	$R'' = Mg, R''' = Al$	$R'' = Fe'', R''' = Fe''', Al$	$R'' = Mg, R''' = Al$	Increasing Fe'' and $Fe'''\rightarrow$		Oxidized Fe
				(orthochlorites)		(leptochlorites)
$R''_6Si_4O_{10}(OH)_8$	Chrysotile	Greenalite				
	Antigorite			Diabantite		Delessite
	Lizardite		Penninite			
$R''_5R'''Si_3R''O_{10}(OH)_8$	Clinochlore[3]	Chamosite[3]	Clinochlore	Pycnochlorite	Brunsvigite	Chamosite
			Sheridanite	Prochlorite	Daphnite	
				Ripidolite		
			Corundophyllite		Pseudo-thuringite	Thuringite
$R''_4R'''_2Si_2R'''_2O_{10}(OH)_8$	Amesite	Cronstedtite	Amesite			

[1] Based on studies of Nelson and Roy (1954; 1958) and Hey (1954)

[2] Schuchardite is a nickeliferous normal chlorite, and grovesite is a manganese chlorite which may be either the 7 Å or 14 Å polymorph. In kämmererite, the chromian chlorite, this element substitutes for aluminum only in octahedral positions (DeVries and Roy, 1958).

[3] Prefix "septe" may be added to names of septechlorites, *e.g.*, septeclinochlore, if it should be desirable to differentiate between these minerals and the normal chlorites.

Four-Layer Silicates: Chlorites

In chlorites the fundamental unit layer consists of a talc layer (2:1, three-layer unit) plus a complete brucite layer. These minerals are usually trioctahedral.[3] Chlorites differ from biotite in that a brucite layer rather than interlayer potassium is between the 2:1 or talc units. They differ from saponite and vermiculite in that a complete brucite layer rather than a less densely populated layer of hydrated magnesium ions is present in the interlayer. Another difference among these minerals is that greater amounts of substitution occur in both the tetrahedral and brucite layers of chlorite, resulting in stronger electrostatic attraction in the chlorites than in saponite and vermiculite. Normal chlorites have a stable 14 Å basal spacing, whereas the basal spacing of saponite and vermiculite, which is near 14 Å, is variable with some mild treatments such as low-temperature dehydration, hydration, or glycolation. So-called "swelling chlorites" have been discussed in the section on expanded 2:1 layer silicates.

It has already been mentioned that the compositions that yield true 14 Å chlorites also can occur both in nature and in the laboratory in a form with the 1:1 structure. These have been called septechlorites. Nelson and Roy (1954) have demonstrated a polymorphic relationship between the 7 Å and 14 Å minerals; the former is the low-temperature form. The principal structural difference between the two is that in the normal chlorites alternate layers of silica tetrahedra are pointed in opposite directions, while in the septechlorites all tetrahedra point in the same direction (Fig. 4). A mineral that may be intermediate between the two has been described by Brindley and Gillery (1954).

There is a large variety of chlorites because of the wide range of possible ionic substitutions. Many names have been used although, because of extensive solid solution, there are no sharp boundaries between varieties. A recent effort to systematize the classification of the chlorites is that of Hey (1954), while the work of Nelson and Roy (1958) on synthetic chlorites provides significant new data toward systematization of the chlorites. The relationships among the normal chlorites and also the relationships between them and the septechlorites are shown in Table 6, which is based on these studies.

A striking feature of this classification is that the septechlorites commonly have relatively little substitution of aluminum for silicon, whereas the normal chlorites have more than 10 per cent tetrahedral substitution, balanced by substitutions in the brucite layer or in both octahedral layers. Attempts to synthesize a normal chlorite with the composition of chrysotile have not been successful (Nelson and Roy, 1958). Apparently a normal chlorite can form only when the talc and brucite units are oppositely charged with a certain minimum charge.

The normal chlorites have been divided into orthochlorites and leptochlorites, the latter apparently an oxidized variation of the former since they contain larger amounts of ferric iron and less structural water. In other words, chlorites containing large amounts of ferrous iron may be oxidized without any change in structure if the oxidation is accompanied by dehydration (Brindley and Youell, 1953), as in other hydroxyl compounds of metals in a low oxidation state. Essentially all that is involved is the removal of protons.

The chlorites show polytypism as well as polymorphism. The polytypism of the septechlorites has been discussed; that of the normal chlorites has been investigated by Brindley, Oughton, and Robinson (1950) and by Steinfink (1958a; 1958b). Steinfink has discussed the deviations from the "ideal" structure and the anisotropy of the distribution of substituting ions.

Heteropolytypes of 3-Layer and 4-Layer Silicates

In view of the crystallochemical similarities between chlorites and the trioctrahedral three-layer minerals, indicated in the preceding section, it is not surprising that units of these minerals are found intimately interstratified. In fact, it is difficult to find vermiculite that does not contain some interstratified chlorite layers or admixed chlorite. The interstratified three- and four-layer minerals show more tendency toward regular sequences than do the mixed-layer 2:1 minerals.

A variety of mixed-layer mineral (heteropolytype) recently found to be relatively common in sediments consists of chlorite and an expanded 2:1 mineral. The latter has been called vermiculite by some and montmorillonite or "swelling chlorite" by others. It is an

[3] The occurrence of dioctahedral chlorite in soils was reported by J. E. Brydon, J. S. Clark, and Vincent Osborne at the 8th National Clay Conference in Norman, Oklahoma, October 14, 1959. Sudo has reported a mixed-layer mineral containing dioctahedral chlorite units (Sudo and Hayashi, 1956).

expandable, magnesium-rich, trioctahedral 2:1 layer silicate. Most samples of this mixed-layer mineral show at least a small basal X-ray diffraction peak at 24–30 Å. The variations in basal spacings with various treatments indicate that the basal spacings of the expandable but not the chlorite layers are affected by these treatments.

Samples of this mineral varying somewhat in relative amounts of the two layers and in the degree of regularity of stacking have been described by Honeyborne (1951), Stephen and MacEwan (1951), Lippmann (1954), Earley, Brindley, McVeagh, and Vanden Heuvel (1956), Early and Milne (1956), Heystek (1956), and Bradley and Weaver (1956). This mineral, consisting of a regular 1:1 growth of chlorite and expanded layers, has been named "corrensite" by Lippmann. A dioctahedral analogue of corrensite has been described by Sudo and Hayashi (1956).

SCHEME FOR IDENTIFICATION OF THE CLAY MINERALS

Methods Used

Since the foregoing classification of the clays has been based on both structure and composition of the phases, methods to determine these two properties naturally dominate the scheme for identification. With the widespread use of X-ray diffraction in mineralogical laboratories, it is no longer unusual to specify the use of X-ray methods as indispensable in the identification of clays. The compositional part of the characterization is less easily accomplished. Wet (or instrumental) chemical analyses at certain stages of the scheme are very desirable but often impractical. Here also, X-ray diffraction may be quite useful, since in some families of clay minerals changes in the spacings and intensities of the diffraction peaks have been correlated with variation in chemical composition. X-ray diffraction may also be used as a substitute for chemical analysis in a "secondary" manner. By utilizing certain known thermal reactions (performed easily in a simple laboratory furnace) or simple chemical treatment, and analyzing the phase composition of the products by X-rays, one can estimate the composition of the clay. Thus the absolutely required pieces of apparatus for operating the following scheme are: (1) X-ray diffraction apparatus, (2) a simple laboratory furnace for temperatures to 1100°C, with ±25° control. Definitely of secondary importance in this scheme are differential thermal analysis (DTA), electron microscopy, and infra-red spectroscopy.

Sample Preparation

The clay minerals must be separated from any coarser material. The rock should be disaggregated with as little grinding as possible. Wet grinding in a blender is recommended if more drastic treatment is required. Suspensions should be prepared with as little chemical treatment as possible. Methods of disaggregation and of clay suspension are described by Krumbein and Pettijohn (1938, Ch. 3).

Centrifugation or supercentrifugation is the quickest and safest means of removing the clay from the suspension.

Other methods include allowing the clay to settle and decanting the supernatant liquid. The suspension may be concentrated by evaporation (below boiling temperature when done under atmospheric pressure). If the concentrated clay is to be analyzed immediately, it need not be dried; otherwise, drying should be carried out at room temperature, or at least well below 100°C.

A method by which a clay fraction is concentrated and prepared for X-ray and further examination at the same time was developed by Kinter and Diamond (1956). The material is deposited by centrifugation as thin oriented films on porous tiles.

X-Ray Diffraction Techniques

Normal conditions. A knowledge of the basal spacings of clay minerals is required to assign them to the principal groups. For this purpose samples with preferred orientation parallel to the basal plane are best. Samples to be used with an X-ray diffractometer are prepared by allowing a thick aqueous suspension of the well-dispersed clay to dry on a glass slide.

The spacing of the 060 reflection frequently needs to be determined to distinguish dioctahedral from trioctahedral clay minerals, and *hkl* reflections are required to differentiate polytypes. These sets of reflections are obtained from samples with random orientation. On the diffractometer this is achieved by using a glass slide with a well into which the dry clay powder is placed in such a manner that preferred basal orientation is avoided. Film techniques have a decided advantage in this respect. In these techniques the sample may be prepared in spherical or rod shapes (spindle or filled capillary) or as a wedge.

Glycol or glycerol adsorption. Some clay minerals are differentiated on the basis of whether they adsorb ethylene glycol or glycerol with resultant changes in the basal spacings. Ethylene glycol is easier to use because its viscosity and boiling point are lower than those

of glycerol. The latter expands most montmorillonite-type minerals to 17.7 Å, and the former to a somewhat lower value.

The following method of preparing oriented, glycolated clay samples on glass slides is the surest one for general use. The sample is mixed on the glass slide with a slight excess of glycol and allowed to "dry" overnight at room temperature or at a slightly elevated temperature until it looks "dry."

Other methods that may be used are: (1) Small drops of glycol may be placed around the edges of a dry oriented clay sample prepared from a water suspension. Enough glycol should be used gradually to saturate the sample. The addition of enough glycol all at once will usually disturb the orientation. (2) An oriented clay slide may be exposed to glycol vapor for at least an hour (Brunton, 1955).

Controlled humidity. An alternate method of determining expandability of a clay mineral consists of X-raying the slide preparation while it is in contact with air of nearly 100 per cent relative humidity. Some of the many advantages of this method over glycol-adsorption have been discussed by Milne and Warshaw (1956). The only disadvantage is that the standard X-ray equipment must be modified (*e.g.*, as shown by Milne and Warshaw), but this can usually be done readily. With this apparatus specimens may also be X-rayed with dried air passing over them or in contact with air of controlled variable humidity.

Dry-heat treatments. A furnace for use with X-ray diffractometers may be quite useful in clay mineralogical studies but is not necessary for the purposes of identification. To distinguish clay samples on the basis of heat treatments, they may be heated in any furnace, cooled in a desiccator, and then subjected to X-ray diffraction analysis. In a few instances rehydration takes place rapidly, but this can be prevented, especially if controlled-humidity apparatus is available on the X-ray machine.

The changes that occur on heating the various clay minerals are summarized in the Appendix, which also illustrates the importance of particle size, crystallinity, and composition.

The best method of observing changes in the intensities and spacings of the X-ray reflections is to use the same slide preparation that was used to analyze the sample prior to heat treatment. The slide, or porous tile (Kinter and Diamond, 1956), may be heated to successively higher temperatures.

TABLE 7. IDENTIFICATION SCHEME FOR LAYER SILICATES

Oriented sample	X-ray sample and measure basal reflections	7 Å group	*See* Table 8
		9.3 Å minerals	*See* text
		10–11 Å group	*See* Table 9
		12–15 Å group	*See* Table 10
		long spacing clay minerals	*See* text
		mixtures of groups	*See* Tables 11 and 12

When ordinary glass slides are used, the upper limit to which they may be heated (about 600°C.) depends not only on the tendency of the glass to soften and warp or to crack on removal from the furnace but also on the fact that clays containing alkalies or alkaline earths may react with the glass. Vycor slides have been used for temperatures up to 800°C (Hathaway, 1955).

Other Techniques

Methods other than X-ray diffraction analysis have been used successfully, but less effectively, to identify clay minerals. Although they have not been given in the identification scheme proposed here, methods such as differential thermal analysis, thermogravimetric analysis, electron microscopy, and infra-red absorption are useful in the detailed structural studies of clay minerals. Electron microscopy is particularly useful in distinguishing halloysite (tubes) from kaolinite (plates), but even large amounts of kaolinite in a mixture of the two may be overlooked (Brindley and Comer, 1956). There appears to be some evidence (Stubičan and Roy, 1959; Tuddenham and Lyon, 1959) that infra-red spectroscopy may soon be developed to the point where the ionic content of a layer may be determined from the absorption pattern. However, to keep the scheme as generally

applicable as possible, the minimum number of instrumental methods are utilized.

The petrographic microscope is, of course, of considerable use in the study and identification of the coarser-grained layer silicates and may in some instances be the principal tool in their study.

Identification Scheme

An identification scheme for the clay minerals is given in Tables 7–12. In order to facilitate identification by X-ray diffraction, it is recommended that patterns of "standard" clay minerals, and of the minerals commonly associated with them, be available for comparison.

The groups into which the layer silicates may be divided on the basis of X-ray diffraction analysis are not quite the same as given in the crystallochemical classification. This is essentially because some of the minerals—*e.g.*, expanded 2:1 minerals and endellite—contain variable amounts of interlayer water.

A complete identification of a clay mineral is simple with the schemes presented if minerals of only one group are present. Moreover, one may have an idea of what minerals are likely to be present or absent in different types of rocks. (Some data on the occurrence of clay minerals are given by Grim, 1953; an excellent summary of the "clay petrology of sediments" is given by Weaver, 1959.)

Mixtures of groups present difficulties. It may not be possible to obtain complete identification of each mineral because of the uncertainties involved in chemical analyses of mixtures or because of possible reactions between the mineral phases during heating tests. With a mixture, attempts should always be made to fractionate the clay sample, usually by sedimentation, but also by other density and magnetic methods. By the examination of several fractions, it may be possible to determine which X-ray diffraction peaks in a complex pattern are related.

There is considerable difficulty in identifying a minor constituent when its diffraction pattern is almost masked by the reflections from the major constituents. However, clay minerals tend to approach "equilibrium" with their environment because of their fine-grained character; thus the assemblages are more likely to be simple than complex. This is particularly true in metamorphic rocks and hydrothermal deposits. It is also true to some extent in sediments that have undergone extensive reactions during cementation. Thus the 7 Å mineral in magnesium-rich rocks is more likely to be a septechlorite than a kaolinite mineral, whether the rock be an altered ultrabasic, a dolomitized sediment, or a mafic igneous rock in an intermediate stage of weathering. The most complicated assemblages are found in sediments derived from more than one type of source area, in which weathering had not been extensive. Such a sediment might appear to be intermediate between graywacke and arkose. Even here, the problem is less complicated if mineralogical studies are made of the coarse-grained minerals and if petrographic examination is carried out with a view to determining the relationships between the clay minerals and the other silicates. Clues to the type of clay minerals probably present in a sediment may be obtained from petrographic studies that reveal, among other things, the extent of alteration of feldspars and the presence of various rock fragments which may contain certain types of clay minerals.

Identification of 7 Å Minerals

The scheme for the 7 Å group of minerals is given in Table 8. The separation into the two families is based on the 060 spacing. A further check may be made by heating the samples at 1000°–1100°C for 1–2 hours. This method may also be used to differentiate the members of the septechlorite family. Color is also indicative of the family when the minerals are pure; the kaolinite minerals are white, whereas the septechlorites are pale shades of green except for bementite, which is honey-colored.

The well-crystallized minerals of this group may be distinguished on the basis of the powder X-ray diffraction patterns. For determining whether a serpentine is a particular one or a mixture of the three principal varieties, reference should be made to the X-ray studies of Whittaker and Zussman (1956). Moreover, a fair amount of information on the serpentines may be obtained by electron diffraction and microscopy.

The means of distinguishing the well-crystallized kaolinite minerals have been described by Brindley (1951, p. 49–50). Since nacrite is rather rare, only the distinction between kaolinite and dickite is important. Patterns for these minerals are given by Brindley (1951) and by Grim (1953). Kaolinite$_d$ generally gives a pattern with fewer distinct lines than does well-ordered kaolinite, and its diffractometer traces show an asymmetric 02 band with sharp head at 4.45 Å and fading away toward higher

TABLE 8. IDENTIFICATION OF MINERALS OF 7 Å GROUP

TABLE 8. IDENTIFICATION OF MINERALS OF 7 Å GROUP

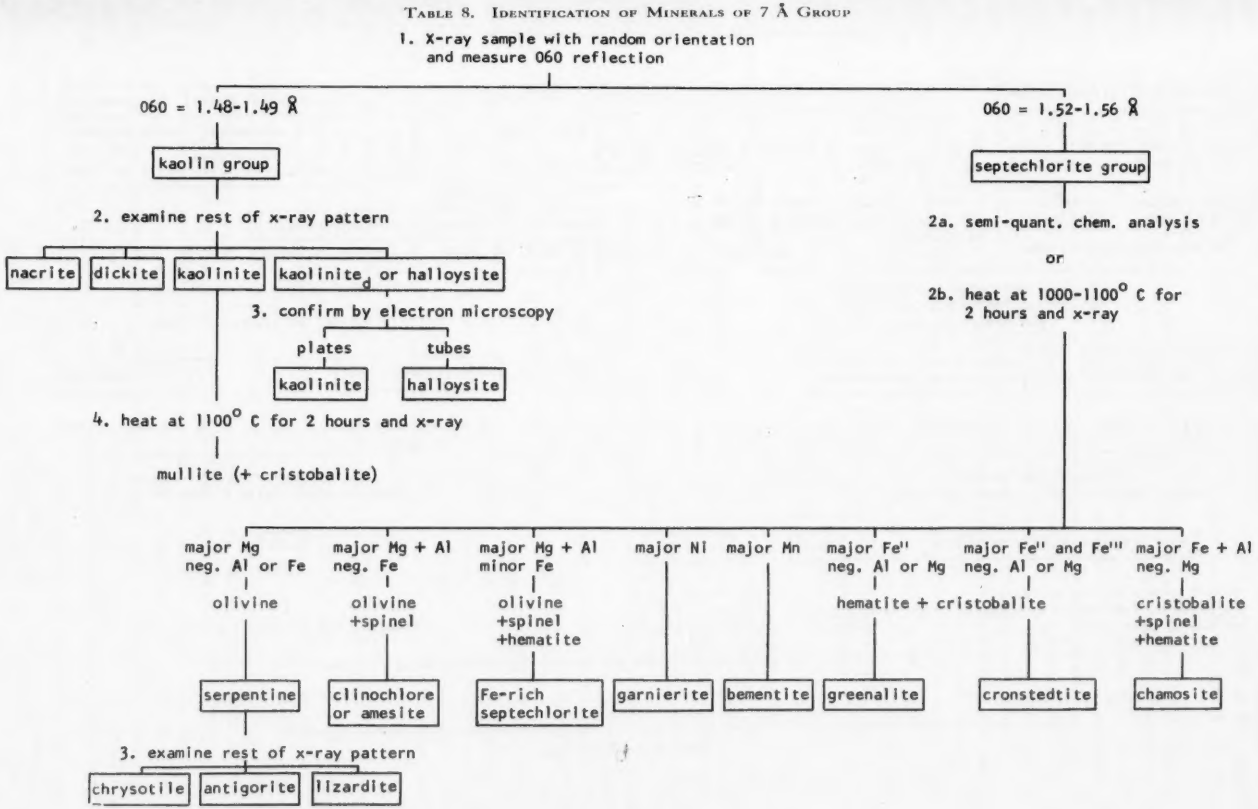

TABLE 9. IDENTIFICATION OF MINERALS OF 10–11 Å GROUP

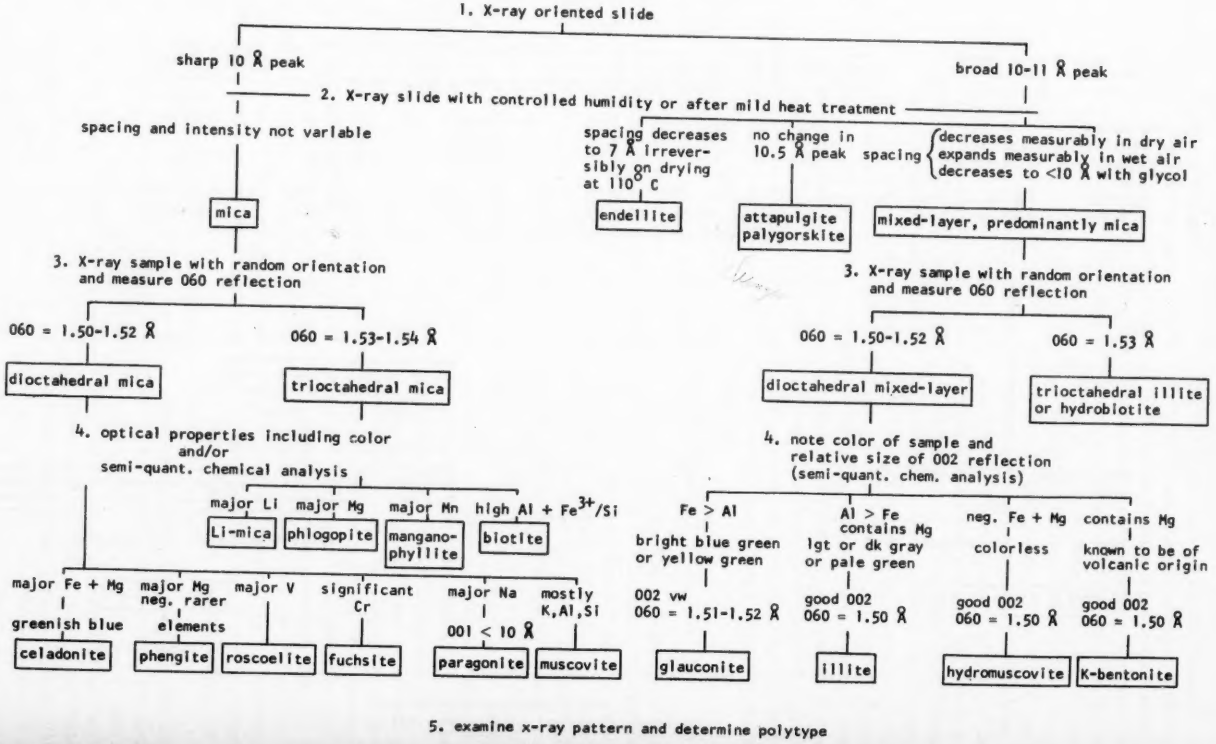

angles. Well-ordered kaolinite, on the other hand, shows little or no band in this region, and the reflections at 4.17 and 4.12 Å are resolved. Halloysite patterns are similar to those of kaolinite$_d$, but its basal reflections are distinctly broader, and the 02 band is usually more intense than the basal reflections.

Mixtures of kaolinite and septechlorite minerals are encountered only in sediments. The septechlorite is frequently an iron-rich variety, and both minerals are characterized by disorder. That both dioctahedral and trioctahedral minerals are present is determined by the presence of two 06 reflections. In some instances, the 002 reflections may be resolved by slow scanning on a diffractometer, also indicating the presence of the two 7 Å minerals. If it is suspected that both kaolinite$_d$ and a septechlorite are present even though no resolution of peaks is observed, further tests may be made, as described in the scheme for mixtures.

Identification of 9.3 Å Minerals

Pyrophyllite, talc, and minnesotaite are readily distinguished on the basis of their 060 (1.49, 1.54, 1.57 A, respectively) reflections among others. Minnesotaite is easily distinguished because of its high iron content. The identifications should be verified by examination of the whole X-ray pattern, since these minerals might be confused, on the basis of the (001) spacing alone, with some platy zeolites.

Identification of 10–11 Å Minerals

The scheme for the 10–11 A group of minerals is given in Table 9, which shows that they may be readily separated into micas, mixed layers, endellite, and attapulgite (palygorskite) on the basis of the variability of the 10 Å reflection with hydration state. Further separation is based on the 060 spacings.

The micas pose no problems, especially when coarse-grained. Some careful chemical work may be necessary to distinguish some of the fine-grained dioctahedral micas.

Glauconites and illites are not easily distinguished from micas, but the distinction can be made if the X-ray diffractometer traces are obtained with a slow scanning speed under a variety of humidity conditions or with and without ethylene glycol. Hydromuscovites and K bentonites, on the other hand, usually contain significant amounts of interstratified expandable layers, which are readily detectable. Some detailed X-ray diffraction work is usually necessary to complete the identification of mixed-layer clay minerals. Examples of the procedures that may be used in the identification of these minerals are given by Weaver (1956).

The dioctahedral minerals of this group occur very much more abundantly in clay-grade material. This is true also for the 1:1 minerals and the expanded 2:1 minerals. Evidence shows that under weathering conditions trioctahedral layer silicates are less stable than are dioctahedral ones. Thus, muscovite is the most persistent mica and may occur as detrital grains in sediments that contain no other detrital grains except quartz and certain heavy minerals. Moreover, the clays formed by degradation are ultimately all dioctahedral; the common soil minerals are kaolinite, montmorillonite and beidellite-type expanding clay, illite, and "dioctahedral vermiculite." Trioctahedral illite, hydrobiotite, and vermiculite are unstable minerals found only in weathering products representing early stages of weathering of mafic rocks. Aggradation processes that have yielded some of the better crystallized clay minerals in fine-grained sediments and altered pyroclastic rocks also generally produce dioctahedral minerals. However, some trioctahedral layer silicates (*e.g.*, chlorite, corrensite, hectorite) may be formed by aggradation processes under special environmental conditions or by "diagenesis" or low-grade metamorphism.

If the presence of either hydrobiotite or trioctahedral illite is suspected in a sample, it is well to compare its properties with those described by Walker for hydrobiotite (Brindley, 1951, p. 212–215) and trioctahedral illite (Walker, 1950).

Identification of 12–15 Å Minerals

The scheme for the 12–15 Å group of minerals is given in Table 10, in which the first separation has as its basis the behavior of these minerals with ethylene glycol. The mixed-layer minerals have nonintegral orders of basal reflections, both before and after glycol treatment. (*See* Weaver, 1956, for more detail.) Further distinctions are made as a result of heat treatments at relatively low temperatures. If it should be desirable to know more about a montmorillonite-type mineral (smectite[4]) than

[4] As mentioned earlier, "smectite" is the name proposed by British clay mineralogists (Brown, 1955) for the montmorillonite group. For brevity, this term is used in Tables 10–12 instead of the longer term "montmorillonite-type mineral" which is the approved one.

TABLE 10. IDENTIFICATION OF MINERALS OF 12–15 Å GROUP

1a. X-ray oriented slide
1b. X-ray oriented slide after treatment with ethylene glycol (preferably after saturation of clay mineral with Mg++)
1c. compare X-ray patterns
little or no change in 14 Å peak, no 17 Å peak
no change in 12 Å peak, no 17 Å peak
new peak at 17 Å
new peak at 15-16 Å
chlorite, vermiculite
sepiolite
smectite
mixed-layer, predominantly smectite
see text for more detail
2. heat slide 1a at 350-400° C for 12-15 hrs and x-ray again (preventing rehydration)
2. heat slide 1a at 250° C for 12-15 hours and x-ray again (preventing rehydration)
little or no change
decrease in intensity and spacing of 001 to 12 Å
replacement of sharp 14 Å peak by broad band at 9 Å
decrease in spacing of 001 to 9.7-10.0 Å
decrease in spacing of 001 to 12-13 Å
chlorite
dioctahedral vermiculite
vermiculite
non-complexed smectite
organic-complexed smectite
3. confirm this distinction by heating further at 550° C
3. X-ray sample with random orientation and measure 060 reflection
increase in intensity of 14 Å peak
no 14 Å peak, just broad band at 10-11 Å
060 = 1.49-1.52 Å
060 = 1.53-1.54 Å
dioctahedral smectite
trioctahedral smectite
4. semi-quant. chem. analysis
only Al + Si
Mg
Fe
Cr
only Mg + Si
Li
Al
neg. rarer elements
Zn
Ni
Cu
beidellite
montmorillonite
nontronite
volchonskoite
stevensite
hectorite
saponite
sauconite
pimelite
medmontite

merely whether it is a di- or trioctahedral, then chemical analysis may be necessary.

The identification of vermiculite frequently presents some problems because of the variable behavior of this mineral (Weaver, 1958; Walker, 1957, 1958).

The usual methods do not distinguish between montmorillonite and beidellite in sediments and soils. It may be possible to distinguish these minerals by a technique such as that proposed by Greene-Kelly (1955), which involves saturating the minerals with lithium and then heating them to determine whether the substitutions are in the octahedral or tetrahedral layer. Infra-red techniques may also be useful in this respect (Stubičan and Roy, 1959).

Identification of Long-Spacing Minerals

Corrensite (Table 12) appears to be the only relatively common long-spacing mineral. It is characterized by a weak reflection with a spacing of 29 Å and a strong 14.5 Å reflection. These spacings are changed by dehydration or glycolation; glycolation yields a change of the low-angle reflection to 31 Å. The identity may be confirmed by heat treatment, as indicated in the Appendix.

Rectorite and allevardite have 25 Å reflections, which are shifted to 26.5 Å with ethylene glycol (Bradley, 1950; Brindley, 1956).

A mineral with strong reflections at 25.8 and 12.4 Å may be comparable to the long-spacing mineral described by Heystek (1954).

Long-spacing minerals that have not yet been adequately described may also be found. They should be compared with those described by Sudo (1959), especially if the occurrence appears to be hydrothermal.

Identification of Minerals in Mixtures

For mixtures of clay minerals of the different groups, the identification of the specific minerals may not be possible to the extent shown in Tables 8–10. A scheme for identification of minerals in mixtures is presented in Tables 11 and 12.

The 10–11 Å group offers the least difficulty in mixtures. Regardless of the complexity of the mixture, well-crystallized micas can be differentiated from mixed-layer minerals unless the latter are present in far greater amounts. The type of mica may be obvious from petrographic examination, but it may not be possible to determine the variety of a fine-grained mica in a fine-grained rock; if the mica is dioctahedral but the sample contains some magnesium, it is not possible to state positively whether the mica is phengite or muscovite. If the amount of mica is too small to determine whether it is dioctahedral or trioctahedral, it can only be designated "mica." Nor would it be possible to determine the polytype in this instance. A relationship similar to that between phengite and muscovite exists between illite and hydromuscovite, and the difficulties are comparable. However, the latter usually is found in altered felsic igneous rocks of simple mineralogy containing little or no magnesium. Glauconite, although very finely crystallized, occurs in sand-sized grains that are aggregates of fine crystals.

It is no more difficult to identify the various 12–15 Å minerals when mixed with 10–11 A and/or 7 Å groups than it is to identify them in mixtures of minerals within the group.

The kaolinite and septechlorite minerals are the most difficult to differentiate in mixtures since neither varies in spacing with humidity or glycol treatment. To produce changes in the intensities or spacings of the basal reflections, one must heat the 1:1 clay minerals to temperatures at which thermal transformations occur. It is not possible to specify the heat treatment required for any one sample, since the extent of changes produced in kaolinite and in both septechlorites and normal chlorites depends on many variables—*e.g.*, particle size, duration of treatment, chemical composition (Nelson and Roy, 1954). Nevertheless, heat treatments should be tried for identification of kaolinite or septechlorite that cannot be distinguished by X-ray diffraction analysis of the unheated samples. Septechlorites frequently develop a rather broad reflection at 13–14 Å when heated to about 500°C, whereas kaolinite does not. However, the absence of this peak does not necessarily mean that a septechlorite (*e.g.*, chamosite) is not present; if a septechlorite is suspected, acid treatments should be tried. Strong (∽2N), hot acid may be used because kaolinite is much more resistant to acid attack than are chlorites. Dickite may also give a peak near 14 Å after heat treatment (Hill, 1955), but, since dickite crystals are usually larger than those of kaolinite or septechlorite, the presence of dickite may be determined by optical methods. A short high-temperature heat treatment (1–2 hours, 1000°–1100°C) may be used to confirm the presence of kaolinite minerals in a mixture containing any variety of chlorite, since mullite is formed from the kaolinite minerals at high temperatures. How-

TABLE 11. IDENTIFICATION OF CLAY MINERAL MIXTURES WITH BASAL REFLECTIONS AT 10–11 Å AND EITHER 12–15 Å OR 7 Å

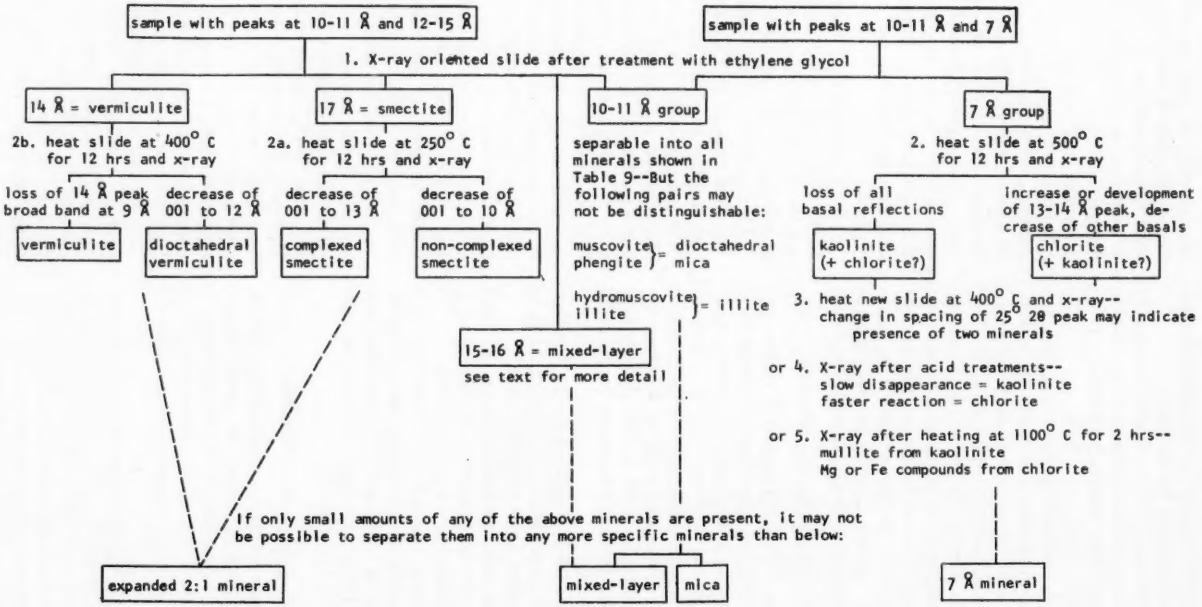
sample with peaks at 10-11 Å and 12-15 Å
sample with peaks at 10-11 Å and 7 Å
1. X-ray oriented slide after treatment with ethylene glycol
14 Å = vermiculite
17 Å = smectite
10-11 Å group
7 Å group
2b. heat slide at 400° C for 12 hrs and x-ray
2a. heat slide at 250° C for 12 hrs and x-ray
separable into all minerals shown in Table 9--But the following pairs may not be distinguishable:
2. heat slide at 500° C for 12 hrs and x-ray
loss of 14 Å peak broad band at 9 Å
decrease of 001 to 12 Å
decrease of 001 to 13 Å
decrease of 001 to 10 Å
loss of all basal reflections
increase or development of 13-14 Å peak, decrease of other basals
vermiculite
dioctahedral vermiculite
complexed smectite
non-complexed smectite
muscovite, phengite = dioctahedral mica
kaolinite (+ chlorite?)
chlorite (+ kaolinite?)
hydromuscovite, illite = illite
3. heat new slide at 400° C and x-ray--change in spacing of 25° 2θ peak may indicate presence of two minerals
15-16 Å = mixed-layer
see text for more detail
or 4. X-ray after acid treatments--slow disappearance = kaolinite faster reaction = chlorite
or 5. X-ray after heating at 1100° C for 2 hrs--mullite from kaolinite Mg or Fe compounds from chlorite
If only small amounts of any of the above minerals are present, it may not be possible to separate them into any more specific minerals than below:
expanded 2:1 mineral
mixed-layer
mica
7 Å mineral

TABLE 12. IDENTIFICATION OF CLAY MINERAL MIXTURES WITH BASAL REFLECTIONS AT BOTH 7 Å AND 12–15 Å

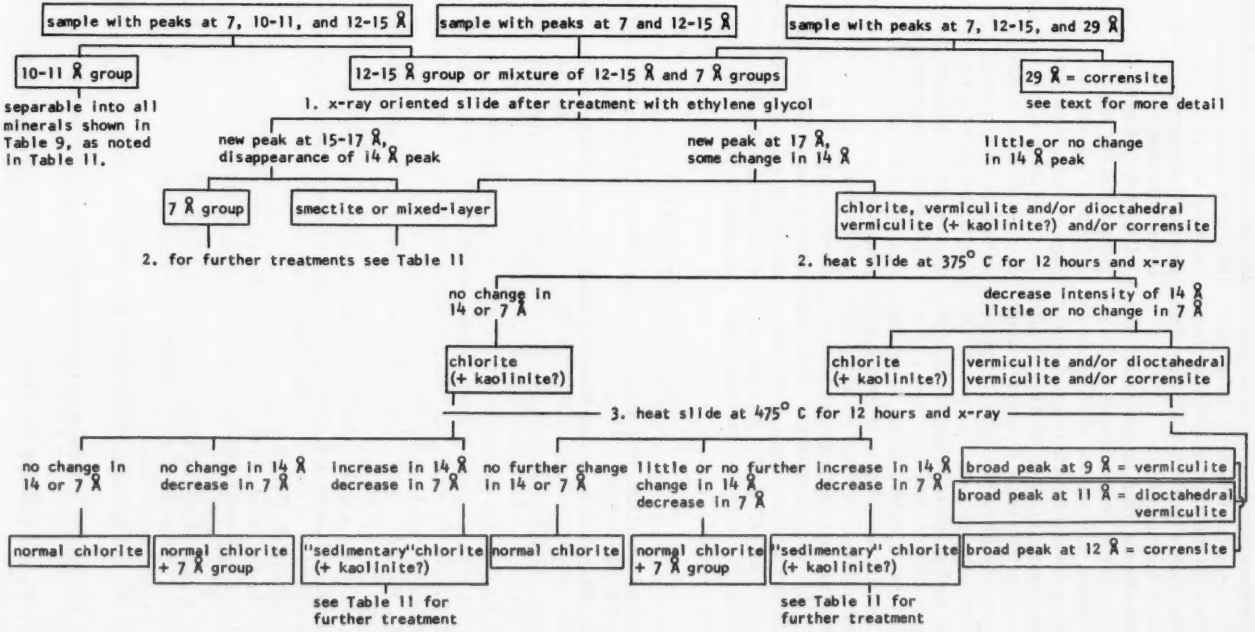
sample with peaks at 7, 10-11, and 12-15 Å
sample with peaks at 7 and 12-15 Å
sample with peaks at 7, 12-15, and 29 Å
10-11 Å group
separable into all minerals shown in Table 9, as noted in Table 11.
12-15 Å group or mixture of 12-15 Å and 7 Å groups
29 Å = corrensite
see text for more detail
1. x-ray oriented slide after treatment with ethylene glycol
new peak at 15-17 Å, disappearance of 14 Å peak
new peak at 17 Å, some change in 14 Å
little or no change in 14 Å peak
7 Å group
smectite or mixed-layer
chlorite, vermiculite and/or dioctahedral vermiculite (+ kaolinite?) and/or corrensite
2. for further treatments see Table 11
2. heat slide at 375° C for 12 hours and x-ray
no change in 14 or 7 Å
decrease intensity of 14 Å little or no change in 7 Å
chlorite (+ kaolinite?)
chlorite (+ kaolinite?)
vermiculite and/or dioctahedral vermiculite and/or corrensite
3. heat slide at 475° C for 12 hours and x-ray
no change in 14 or 7 Å
no change in 14 Å decrease in 7 Å
increase in 14 Å decrease in 7 Å
no further change in 14 or 7 Å
little or no further change in 14 Å decrease in 7 Å
increase in 14 Å decrease in 7 Å
broad peak at 9 Å = vermiculite
broad peak at 11 Å = dioctahedral vermiculite
normal chlorite
normal chlorite + 7 Å group
"sedimentary" chlorite (+ kaolinite?)
normal chlorite
normal chlorite + 7 Å group
"sedimentary" chlorite (+ kaolinite?)
broad peak at 12 Å = corrensite
see Table 11 for further treatment
see Table 11 for further treatment

ever, the temperature should not be greater than 1100°C since the mullite is not an equilibrium phase in mixtures containing magnesium and eventually reacts with the other components to form cordierite.

It is unfortunate that kaolinite and the septechlorites should be so difficult to distinguish in mixtures, since many of the conclusions regarding environment have been based on the presence or absence of these minerals. Moreover, some of the minerals in these groups commonly occur together, especially in young marine or brackish sediments. This may be due to the fact that kaolinite is one of the most resistant clay minerals and may persist in an environment where septechlorites, rather than kaolinite, may form. This same resistance may be used to advantage, however, in distinguishing these minerals by acid treatment.

Green pellets in sediments that look like glauconite frequently have basal X-ray reflections only at 7 and 3.5 Å. These consist of a variety of chlorite rather than kaolinite. Some samples show also the 14 Å reflection characteristic of a normal chlorite, but it has a low intensity relative to that of the 7 Å peak essentially because of a large amount of iron in the structure.

If a major amount of a normal chlorite is present, it is not possible to determine by X-ray diffraction whether any septechlorite is also present, but optical methods may be of some use. The relative intensities of the basal reflections in such a mixture are not reliable criteria for determining a mixture since the relative intensities of the reflections of a normal chlorite itself depend on chemical composition.

The scheme presented in Tables 11 and 12 may not yield a positive identification of all the minerals present in a mixture but probably will yield useful results in all instances where the minerals are fairly well crystallized and/or coarse-grained. The troubles occasionally encountered are due to fine particle size, poor crystallinity, or the presence of significant amounts of iron.

REFERENCES CITED

Ames, L. L., and Sand, L. B., 1958, Factors effecting the maximum hydrothermal stability in montmorillonites: Am. Mineralogist, v. 43, p. 641–648

Bates, T. F., Hildebrand, F. A., and Swineford, Ada, 1950, Morphology and structure of endellite and halloysite: Am. Mineralogist, v. 35, p. 463–484

Baumhauer, H., 1915, Über die verschiedenen Modifikationen des Carborundums und die Erscheinung der Polytypie: Zeitschr. Krist., Band 55, p. 249–259

Bradley, W. F., 1940, The structural scheme of attapulgite: Am. Mineralogist, v. 25, p. 405–410

—— 1950, The alternating layer sequence of rectorite: Am. Mineralogist, v. 35, p. 590–595

Bradley, W. F., and Weaver, C. E., 1956, A regularly interstratified chlorite-vermiculite clay mineral: Am. Mineralogist, v. 41, p. 497–504

Brindley, G. W., *Editor,* 1951, X-ray identification and crystal structure of clay minerals: London, Mineralog. Soc., 345 p.

—— 1956, Allevardite, a swelling double-layer mica mineral: Am. Mineralogist, v. 41, p. 91–103

Brindley, G. W., and Comer, J. J., 1956, The structure and morphology of a kaolin clay from Les Eyzies (France), p. 61–66 *in* Swineford, Ada, *Editor,* Clays and clay minerals: Natl. Acad. Sci.–Natl. Research Council Pub. 456, 444 p.

Brindley, G. W., and Gillery, F. H., 1954, A mixed-layer kaolin-chlorite structure, p. 349–353 *in* Swineford, Ada, and Plummer, Norman, *Editors,* Clays and clay minerals: Natl. Acad. Sci.–Natl. Research Council Pub. 327, 498 p.

Brindley, G. W., and MacEwan, D. M. C., 1953, Structural aspects of the mineralogy of clays and related silicates, p. 15–59 *in* Green, A. T., and Stewart, G. H., *Editors,* Ceramics—a symposium: Stoke-on-Trent, British Ceramic Society, 877 p.

Brindley, G. W., and Robinson, Keith, 1946a, The structure of kaolinite: Mineralog. Mag., v. 27, p. 242–253

—— 1946b, Randomness in the structures of kaolinitic clay minerals: Faraday Soc. Trans., v. 42B, p. 198–205

Brindley, G. W., and Youell, R. F., 1953, Ferrous chamosite and ferric chamosite: Mineralog. Mag., v. 30, p. 57–70

Brindley, G. W., Oughton, B. M., and Robinson, Keith, 1950, Polymorphism of the chlorites. I. Ordered structures: Acta Crystallographica, v. 3, p. 408–416

Brindley, G. W., Oughton, B. M., and Youell, R. F., 1951, The crystal structure of amesite and its thermal decomposition: Acta Crystallographica, v. 4, p. 552–557

Brown, George, 1953, The dioctahedral analogue of vermiculite: Clay Minerals Bull., v. 2, p. 64–70

—— 1955, Report of the Clay Minerals Group Subcommittee on Nomenclature of Clay Minerals: Clay Minerals Bull., v. 2, p. 294–302

Brown, George, and Norrish, Keith, 1952, Hydrous micas: Mineralog. Mag., v. 29, p. 929–932

Brunton, George, 1955, Vapor pressure glycolation of oriented clay minerals: Am. Mineralogist, v. 40, p. 124–126

Burst, J. F., 1958, Mineral heterogeneity in glauconite pellets: Am. Mineralogist, v. 43, p. 481–497

Caillère, S., and Hénin, S., 1949, Experimental formation of chlorites from montmorillonite: Mineralog. Mag., v. 28, p. 612–620

Caillère, S., Hénin S., and Esquevin, J., 1954, Transformation expérimentale de chlorite en montmorillonite: Clay Minerals Bull., v. 2, p. 166–170

DeVries, R. C., and Roy, Rustum, 1958, The influence of ionic substitution on the stability of micas and chlorites: Econ. Geology, v. 53, p. 958–965

Earley, J. W., and Milne, I. H., 1956, Regularly interstratified montmorillonite-chlorite in basalt, p. 381–384 *in* Swineford, Ada, *Editor*, Clays and Clay minerals: Natl. Acad. Sci.–Natl. Research Council Pub. 456, 444 p.

Earley, J. W., Brindley, G. W., McVeagh, W. J., and Vanden Heuvel, R. C., 1956, A regularly interstratified montmorillonite-chlorite: Am. Mineralogist, v. 41, p. 258–267

Eitel, Wilhelm, 1954, The physical chemistry of the silicates: Chicago, Univ. Chicago Press, 1592 p.

Eitel, Wilhelm, Hatch, R. A., and Denny, M. V., 1953, Synthetic mica investigations: II, Role of fluorides in mica batch reactions: Jour. Am. Ceram. Soc., v. 36, p. 341–348

Ewell, R. H., and Insley, Herbert, 1935, Hydrothermal synthesis of kaolinite, dickite, beidellite, and nontronite: Jour. Research Natl. Bur. Standards, v. 15, p. 173–186

Faust, G. T., 1955, The endellite-halloysite nomenclature: Am. Mineralogist, v. 40, p. 1110–1118

Faust, G. T., Hathaway, J. C., and Millot, Georges, 1959, A restudy of stevensite and allied minerals: Am. Mineralogist, v. 44, p. 342–370

Fleischer, Michael, 1951, Ten years of new mineral names: Am. Mineralogist, v. 36, p. 630–631

Forman, S. A., 1951, Xanthophyllite: Am. Mineralogist, v. 36, p. 450–457

Foster, M. D., 1951, The importance of exchangeable magnesium and cation-exchange capacity in the study of montmorillonitic clays: Am. Mineralogist, v. 36, p. 717–730

—— 1954, The relation between "illite," beidellite, and montmorillonite, p. 386–397 *in* Swineford, Ada, and Plummer, Norman, *Editors*, Clays and Clay minerals: Natl. Acad. Sci.–Natl. Research Council Pub. 327, 498 p.

—— 1956, Correlation of dioctahedral potassium micas on the basis of their charge relations: U. S. Geol. Survey Bull. 1036-D, p. 57–67

—— 1957, Interpretation of the compositions of trioctahedral micas (Abstract): Geol. Soc. America Bull., v. 68, p. 1729

Gillery, F. H., 1959a, X-ray study of synthetic Mg-Al serpentines and chlorites: Am. Mineralogist, v. 44, p. 143–152

—— 1959b, Adsorption-desorption characteristics of synthetic montmorillonoids in humid atmospheres: Am. Mineralogist, v. 44, p. 806–818

Greene-Kelly, R., 1955, Dehydration of the montmorillonite minerals: Mineralog. Mag., v. 30, p. 604–615

Grim, R. E., 1953, Clay mineralogy: New York, McGraw-Hill Book Co., Inc., 384 p.

Gruner, J. W., 1936, The structure and chemical composition of greenalite: Am. Mineralogist, v. 21, p. 449–455

—— 1944, Composition and structure of minnesotaite, a common iron silicate in iron formations: Am. Mineralogist, v. 29, p. 363–372

Hathaway, J. C., 1955, Studies of some vermiculite-type clay minerals, p. 74–86, *in* Milligan, W. O., *Editor*, Clays and clay minerals: Natl. Acad. Sci.–Natl. Research Council Pub. 395, 573 p.

Hendricks, S. B., 1939a; The crystal structure of nacrite, $Al_2O_3 \cdot 2SiO_2 \cdot 2H_2O$, and polymorphism of the kaolin minerals: Zeitschr. Krist., B. 100, p. 509–518

—— 1939b, Random structures of layer minerals as illustrated by cronstedite ($2FeO \cdot Fe_2O_3 \cdot SiO_2 \cdot 2H_2O$). Possible iron content of kaolin: Am. Mineralogist, v. 24, p. 529–539

Hendricks, S. B., and Jefferson, M. E., 1939, Polymorphism of the micas: Am. Mineralogist, v. 24, p. 729–771

Hendricks, S. B., and Ross, C. S., 1941, Chemical composition and genesis of glauconite and celadonite: Am. Mineralogist, v. 26, p. 683–708

Hey, M. H., 1954, A new review of the chlorites: Mineralog. Mag., v. 30, p. 277–292

Heystek, H., 1954, An occurrence of a regular mixed-layer clay-mineral: Mineralog. Mag., v. 30, p. 400–408

—— 1956, Vermiculite as a member in mixed-layer minerals, p. 429–434 *in* Swineford, Ada, *Editor*, Clays and clay minerals: Natl. Acad. Sci.–Natl. Research Council Pub. 456, 444 p.

Hill, R. D., 1955, 14 Å spacings in kaolin minerals: Acta Crystallographica, v. 8, p. 120

Hill, V. G., and Roy, Rustum, 1958, Silica structure studies: V, The variable inversion in cristobalite: Am. Ceram. Soc. Jour., v. 41, p. 532–537

Honeyborne, D. B., 1951, The clay minerals in the Keuper marl: Clay Minerals Bull., v. 1., p. 150–157

Karšulin, Miroslav, and Stubičan, Vladimir, 1954, Über die Struktur und die Eigenschaften synthetischer Montmorillonite: Monatsh. Chemie, B. 85, p. 343–358

Kinter, E. B., and Diamond, Sidney, 1956, A new method for preparation and treatment of oriented-aggregate specimens of soil clays for X-ray diffraction analysis: Soil Sci., v. 81, p. 111–120

Koizumi, Mitsue, and Roy, Rustum, 1959, Synthetic montmorillonoids with variable exchange capacity: Am. Mineralogist, v. 44, p. 788–805

Krumbein, W. C., and Pettijohn, E. J., 1938, Manual of sedimentary petrography: New York, D. Appleton-Century Co., Inc., 549 p.

Levinson, A. A., 1953, Studies in the mica group; relationship between polymorphism and composition in the muscovite-lepidolite series: Am. Mineralogist, v. 38, p. 88–107

—— 1955, Studies in the mica group: polymorphism among illites and hydrous micas: Am. Mineralogist, v. 40, p. 41–49

Levinson, A. A., and Heinrich, E. W., 1954, Studies in the mica group; single crystal data on phlogopites, biotites and manganophyllites: Am. Mineralogist, v. 39, p. 937–945

Lippmann, Friedrich, 1954, Über einen Keuperton von Zaisersweiher bei Maulbronn: Heidel. Beitr. Mineralogie Petrographie, B. 4, p. 130–134

Mackenzie, R. C., *Editor*, 1957, The differential thermal investigation of clays: London, Mineralog. Soc., 456 p.

Mackenzie, R. C., 1959, The classification and nomenclature of clay minerals: Clay Minerals Bull., v. 4, p. 52–66

Mackenzie, R. C., Walker, G. F., and Hart, R., 1949, Illite occurring in decomposed granite at Ballater, Aberdeenshire: Mineralog. Mag., v. 28, p. 704–713

Marel, H. W. vander, 1954, Potassium fixation in Dutch soils: mineralogical analyses: Soil Sci., v. 78, p. 163–179

Milne, I. H., and Warshaw, C. M., 1956, Methods of preparation and control of clay mineral specimens in X-ray diffraction analysis, p. 22–30, *in* Swineford, Ada, *Editor*, Clays and clay minerals: Natl. Acad. Sci.–Natl. Research Council Pub. 456, 444 p.

Mumpton, F. A., and Roy, Rustum, 1956, The influence of ionic substitution on the hydrothermal stability of montmorillonoids, p. 337–339, *in* Swineford, Ada, *Editor*, Clays and clay minerals: Natl. Acad. Sci.–Natl. Research Council Pub. 456, 444 p.

—— 1958, New data on sepiolite and attapulgite, p. 136–143, *in* Swineford, Ada, *Editor*, Clays and clay minerals: Natl. Acad. Sci.–Natl. Research Council Pub. 566, 360 p.

Nagy, Bartholomew, and Bradley, W. F., 1955, The structural scheme of sepiolite: Am. Mineralogist, v. 40, p. 885–892

Nelson, B. W., and Roy, Rustum, 1954, New data on the composition and identification of chlorites, p. 335–348, *in* Swineford, Ada, and Plummer, Norman, *Editors*, Clays and clay minerals: Natl. Acad. Sci.–Natl. Research Council Pub. 327, 498 p.

—— 1958, Synthesis of chlorites and their structural and chemical constitution: Am. Mineralogist, v. 43, p. 707–725

Newnham, R. E., and Brindley, G. W., 1956, The crystal structure of dickite: Acta Crystallographica, v. 9, p. 759–764

Noda, Tokiti, 1955, Synthetic mica research in Japan: Am. Ceram. Soc. Jour., v. 38, 147–152

Noll, W., and Kircher, H., 1952, Syntheses des Garnierites: Naturw., Jahrg. 39, Heft 10, p. 233–234

Pabst, Adolf, 1955, Redescription of the single layer structure of the micas: Am. Mineralogist, v. 40, p. 967–974

Pauling, Linus, 1930, The structure of the micas and related minerals: Natl. Acad. Sci. Proc., v. 16, p. 123–129

Rich, C. I., and Obenshain, S. S., 1955, Chemical and clay mineral properties of a red-yellow podzolic soil derived from muscovite schist: Soil Sci. Soc. America Proc., v. 19, p. 334–339

Ross, C. S., 1960, Review of the relationships in the montmorillonite group of clay minerals, p. 225–229, *in* Swineford, Ada, *Editor*, Clays and clay minerals, proceedings of the Seventh National Conference: London, Pergamon Press, 369 p.

Ross, C. S., and Hendricks, S. B., 1945, Minerals of the montmorillonite group, their origin and relation to soils and clays: U.S. Geol. Survey Prof. Paper 205-B, p. 23–79

Roy, D. M., and Roy, Rustum, 1954, An experimental study of the formation and properties of synthetic serpentines and related layer silicate minerals: Am. Mineralogist, v. 39, p. 957–975

—— 1955, Synthesis and stability of minerals in the system MgO–Al_2O_3–SiO_2–H_2O: Am. Mineralogist, v. 40, p. 147–178

Roy, Rustum, and Osborn, E. F., 1954, The system Al_2O_3–SiO_2–H_2O: Am. Mineralogist, v. 39, p. 853–885

Roy, Rustum, and Romo, L. A., 1957, Weathering studies. 1. New data on vermiculite: Jour. Geology, v. 65, p. 603–610

Roy, Rustum, and Sand, L. B., 1956, A note on some properties of synthetic montmorillonites: Am. Mineralogist, v. 41, p. 505–509

Schaller, W. T., 1950, An interpretation of the composition of high-silica sericites: Mineralog. Mag., v. 29, p. 405–415

Smith, J. V., and Yoder, H. S., 1956, Experimental and theoretical studies of the mica polymorphs: Mineralog. Mag., v. 31, p. 209–235

Steinfink, Hugo, 1958a, The crystal structure of chlorite. I. A monoclinic polymorph: Acta Crystallographica, v. 11, p. 191–195

—— 1958b, The crystal structure of chlorite. II. A triclinic polymorph: Acta Crystallographica, v. 11, p. 195–198

Stemple, Irene S., and Brindley, G. W., 1960, A structural study of talc and talc-tremolite relations: Am. Ceram. Soc. Jour., v. 43, p. 34–42

Stephen, I., and MacEwan, D. M. C., 1950, Swelling chlorite: Géotechnique, v. 2, p. 82–83

—— 1951, Some chloritic clay minerals of unusual type: Clay Minerals Bull., v. 1, 157–162

Strock, L. W., and Brophy, V. A., 1955, Synthetic zinc sulfide polytype crystals: Am. Mineralogist, v. 40, p. 94–106

Stubičan, Vladimir, and Roy, Rustum, 1959, Isomophous substitution and infra-red spectra of clay minerals (Abstract): Geol. Soc. America Bull., v. 70, p. 1682

Sudo, Toshio, 1959, Mineralogical study on clays of Japan: Tokyo, Maruzen Co., Ltd., 328 p.

Sudo, Toshio, and Hayashi, Hisato, 1956, Types of mixed-layer minerals from Japan, p. 389–412, *in* Swineford, Ada, *Editor*, Clays and clay minerals: Natl. Acad. Sci.–Natl. Research Council Pub. No. 456, 444 p.

Tuddenham, W. M., and Lyon, R. J. P., 1959, Relation of infrared spectra and chemical analysis for some chlorites and related minerals: Anal. Chemistry, v. 31, p. 377–380

Walker, G. F., 1950, Trioctahedral minerals in the soil-clays of northeast Scotland: Mineralog. Mag., v. 29, p. 72–84

—— 1957, On the differentiation of vermiculites and smectites in clays: Clay Minerals Bull., v. 3, p. 154–163

—— 1958, Reactions of expanding-lattice clay minerals with glycerol and ethylene glycol: Clay Minerals Bull., v. 3, p. 302–313

Warshaw, C. M., 1960, Experimental studies of illite, p. 303–316 *in* Swineford, Ada, *Editor*, Clays and clay minerals, proceedings of the Seventh National Conference: London, Pergamon Press, 369 p.

Warshaw, C. M., Rosenberg, P. E., and Roy, Rustum, 1960, Changes effected in layer silicates by heating below 550°C: Clay Minerals Bull., v. 4, p. 113–126

Weaver, C. E., 1956, The distribution and identification of mixed-layer clays in sedimentary rocks: Am. Mineralogist, v. 41, p. 202–221

Weaver, C. E., 1958, The effects and geologic significance of potassium "fixation" by expandable clay minerals derived from muscovite, biotite, chlorite and volcanic material: Am. Mineralogist, v. 43, p. 839–861

—— 1959, The clay petrology of sediments, p. 154–187 *in* Swineford, Ada, *Editor*, Clays and clay minerals, proceedings of the Sixth National Conference: London, Pergamon Press, 411 p.

Whittaker, E. J. W., and Zussman, J., 1956, The characterization of serpentine minerals by X-ray diffraction: Mineralog. Mag., v. 31, p. 107–126

—— 1958, The characterization of serpentine minerals: Am. Mineralogist, v. 43, p. 917–920

Winchell, A. N., 1925, Studies in the mica group—Part II: Am. Jour. Sci., v. 209, p. 415–430

Yoder, H. S., and Eugster, H. P., 1954, Phlogopite synthesis and stability range: Geochim. et Cosmochim. Acta, v. 6, p. 157–185

—— 1955, Synthetic and natural muscovites: Geochim. et Cosmochim. Acta, v. 8, p. 225–280

Zussman, J., and Brindley, G. W., 1957, Serpentines with 6-layer orthohexagonal cells: Am. Mineralogist, v. 42, p. 666–670

Manuscript Received by the Secretary of the Society, March 1, 1960
Contribution No. 59-40, College of Mineral Industries, The Pennsylvania State University, University Park, Pa.

Appendix. Changes in X-Ray Diffraction Patterns Effected by Heat Treatments of Layer Silicates[1]

APPENDIX. CHANGES IN X-RAY DIFFRACTION PATTERNS EFFECTED BY HEAT TREATMENTS OF LAYER SILICATES[1]

Mineral	270° C	400° C	450° C	475° C	500° C
Montmorillonite[2]	Decrease in intensity and spacing of 001 reflection from 12–15 Å to 9.8 Å				
Beidellite[3]					
Saponite[3]					
Illite[4]	Sharpening of 001 reflection and decrease in spacing from 10.1–10.5 Å to 10.0 Å				
Montmorillonite[4] (or beidellite?) in young sediments	Sharpening of 001 reflection and decrease in spacing from 14–15 Å to 10.0 Å				
Natural organic-complexed montmorillonite[4] (or beidellite?)	Partial decrease of 001 from 14Å to 12–13 Å	Sharpening of 001 reflection and decrease to 10.0 Å			
Natural organic-complexed montmorillonite (or beidellite?) (organic + trivalent?)[4]	Partial decrease of 001 from 14 Å to 13 Å	Partial decrease of 001 to 11 Å	Partial decrease of 001 to 10.3 Å		
Dioctahedral vermiculite[5]	Partial decrease of 001 from 14 Å to 13 Å	Partial decrease of 001 to 12 Å	Broadening of 001 reflection with decrease in spacing		Broadening of 001 reflection and decrease to 11 Å
Vermiculite	Sharp 14 Å peak gone, now broad band consisting of peaks at 12.6 and 10.8 Å	Sharp 14 Å peak gone, now broad band consisting of peaks at 10.2 Å and 8.7 Å, the former being the principal peak and the latter being more important at 475° C than at 400° C			Sharp 14 Å peak gone, now broad band consisting principally of 9.6 Å peak with slight 8.7 Å shoulder
Corrensite[6]	Low-angle peak (3° 2θ) and sharp 14 Å peak gone, now has small broad peaks at 12.3 Å and 8.1 Å, reflection with 4.8 Å spacing remains unchanged				Only one basal reflection at 12 Å, and this is more intense than when first developed at lower temperatures
Dioctahedral chlorite[7]	Decrease in intensity and spacing of 001 reflection from 14.3 Å to 13.8 Å	Decrease in intensity of 7 Å peak, no further decrease in 14 Å peak		Further decrease in 7 Å, slight increase in 13.8 Å peak (broad)	Only one basal reflection at 13.5 Å, and this has increased intensity

APPENDIX (*Continued*). CHANGES IN X-RAY DIFFRACTION PATTERNS EFFECTED BY HEAT TREATMENTS OF LAYER SILICATES[1]

Mineral	270°C	400°C	450°C	475°C	500°C
Sedimentary chlorite[4] (Fe-rich, green pellets)	Broadening and decrease in intensity of 7 Å peak (sample turns brown)	Amorphous?	Amorphous		
Synthetic kaolinite	No change	Some decrease in intensities of basal reflections	Basal peaks all gone		
Kaolinite$_d$[8]					
Sedimentary chlorite[6] (small 14 Å peak)	No change	Some decrease in intensities of 7 and 3.5 Å peaks	Large decrease in height and broadening of 7 and 3.5 Å peaks, slight increase in height and breadth of 14 Å peak		Only one basal reflection at 13.8 Å (originally at 14.2 Å), this has increased intensity
Kaolinite[8] (well crystallized)	No change		Large decrease in intensities of basal reflections		Basal peaks all gone
Septeclinochlore (synthetic)	No change		Slight decrease in intensities of basal reflections		Large decrease in intensities of basal reflections
Synthetic chrysotile	No change				Slight decrease in intensities of basal reflections
Muscovite (1M and 2M)	No change				Slight decrease in intensities of basal reflections
Clinochlore (natural and synthetic)	No change				Increase in intensity of 14Å peak, decrease in intensities of other basals (slightly higher temperature may be required to effect this change)

[1] This table is taken from a paper by Warshaw, Rosenberg, and Roy (1960) on the heat treatment of clay minerals

[2] Natural sample obtained from the Filtrol Corporation

[3] Synthetic

[4] Fractionated sample obtained from Gulf Research and Development Company

[5] Fractionated sample obtained from J. C. Hathaway, U. S. Geological Survey

[6] Sample obtained from Shell Development Company

[7] Fractionated sample obtained from L. G. Schultz, U. S. Geological Survey

[8] Sample obtained from G. W. Brindley, The Pennsylvania State University

ROYAL R. MARSHALL *Jet Propulsion Lab., California Institute of Technology, Pasadena, Calif.*

Devitrification of Natural Glass

Abstract: Many aspects of the history of natural glasses are related to the physicochemical properties of silicate melts. Glasses are thermodynamically unstable; with time and under a variety of conditions, they become crystalline. When little water is present, devitrification may be described in much the same terms as those which apply to the crystallization of silicate melts. The writer uses simple rate theory and the available experimental data to set an approximate lower limit to the time required for *thermal* reconstruction of natural glasses as a function of temperature. The time required for a glass at 300° C to become a felsite is estimated to be at least a million years, at 400° C, at least a few thousand years. The secular disappearance of strain birefringence in volcanic glasses at low temperatures indicates an intermediate stage in the process of devitrification.

Devitrification along fractures in most volcanic glasses, however, is dependent upon water. In a number of samples, the width of the layer *hydrothermally* reconstructed is moderate to vanishingly small. The geologic ages of these glasses indicate that the rate of devitrification at low temperature (around 20° C) is no more than about 4–5 μ in 100 million years. Hydrothermal reconstruction is very sensitive to temperature; the depth of devitrification generally varies substantially among macroscopically unaltered samples from a single flow. In the least devitrified specimens, the depth of devitrification seems to be related to the age of the flow.

Presumably, the diffusion of water controls the rate of hydrothermal reconstruction. The diffusion constant at 20° C is estimated to be 10^{-23} cm^2/sec, and pressure-bomb experiments indicate an activation energy of 30 kcal/mole. Time-temperature relationships are estimated for hydrothermal reconstruction. In contrast to thermal reconstruction, devitrification in the presence of water requires only a short time (within experimental range) at temperatures no more than about 300° C.

CONTENTS

Introduction and acknowledgments 1494
Distribution of volcanic glasses according to silica content 1495
Thermodynamic relationships 1496
Thermal reconstruction: kinetics of crystallization 1498
Crystal growth and temperature 1498
Nucleation 1498
Cooling history 1499
An equation for the rate of crystal growth . . 1500
Secondary changes 1502
Rates of thermal reconstruction at low temperatures 1502
Other secular changes 1503
Glass in meteorites 1503
Hydrothermal reconstruction 1506
Petrographic studies of volcanic glasses 1506
Perlites 1506
Completely devitrified perlites 1509
Tuffs 1509
Water and devitrification 1511
Mechanism 1511
Diffusion equations 1511
Hydrothermal experiments 1514
Time-temperature relationships for hydrothermal reconstruction 1514
Water content of perlites and pitchstones . 1516
Hydrothermal reconstruction of basaltic glasses 1517
Summary 1517
References cited 1518

Figure
1. Silica content of 159 volcanic glasses 1495
2. Change in the viscosity of glass with increase of temperature 1496
3. Schematic diagram showing variation of degree of order (or viscosity) with free energy for a glass at a temperature below the transformation range 1497
4. Rate of crystal growth in glasses as a function of temperature 1499
5. Size distribution of 101 belonites selected at random from a thin section of perlite from the Dublin Hills, Shoshone quadrangle, California 1500
6. Minimum time required for thermal reconstruction of natural glass plotted against temperature 1507
7. Depth of devitrification for glasses listed in Table 6 compared to geologic age 1509
8. Concentration of water in volcanic glass relative to depth from a saturated surface at about 20° C 1513
9. Time required for the hydrothermal reconstruction of perlite to a depth of 100 μ as a function of temperature 1515

Plate Facing
1. Thin section of pumiceous perlite from approximately 7 miles south of Big Pine, Inyo County, California 1508

Geological Society of America Bulletin, v. 72, p. 1493–1520, 9 figs., 2 pls., October 1961

Fractionated sample obtained from Gulf Research and Development Company

2. Thin sections of three perlites illustrating differences in degree of devitrification along fractures 1509

Table

1. Free energy differences for a few transformations 1498
2. Average lengths of crystallites in obsidian from Mono Crater, Mono County, California 1501
3. Rate parameters from devitrification studies on artificial glasses 1501
4. Additional values for the factor $Ae^{\Delta S^*/R}$ . . 1502
5. Activation energies of viscosities of some artificial glasses and melted rocks . . . 1502
6. Depth of devitrification in volcanic glasses of various ages 1504
7. Depth of devitrification in volcanic glasses of unknown ages 1508
8. Variation of depth of devitrification within single extrusive masses 1510
9. Devitrified films on glass shards in tuffs . . . 1512
10. Data from pressure-bomb experiments using pumiceous perlite fragments from Fish Springs, California 1516
11. Water analyses of perlites 1517

INTRODUCTION AND ACKNOWLEDGMENTS

Volcanic glass may form under pyroclastic conditions or in extrusions or shallow intrusions of magma. Magmas of nearly every composition have formed glasses. The principal requirement for glass formation is rapid chilling, but the chemical composition has a great influence in determining the physical state of a magma when it is quenched. The composition controls viscosity, which in turn limits crystallization.[1]

Nearly all known volcanic glasses are Miocene or younger. The Cretaceous welded tuff described by Barksdale (1951) is exceptional, as is a "partly devitrified perlite" of Ordovician age in Wales (Cantrill and Thomas, 1906, Pl. XXIV, fig. 2). The glassy origin of many Precambrian and Paleozoic rocks (Rutley, 1888; Williams, 1922) is now indicated only by the outlines of perlitic cracks, which have persisted in spite of devitrification, and by the presence of spherulites.

Parkinson (*in* Bonney and Parkinson, 1903) expressed the opinion that secondary crystallization in perlite begins by hydration of the glass along cracks. Königsberger and Müller (1906) found that pieces of obsidian were affected slightly by water at 320° C. They observed alteration on the surface and found that it increased in the presence of sodium bicarbonate. Other experimenters (Hauser and Reynolds, 1939; Norton, 1941) demonstrated that pulverized glass can be devitrified readily with water at temperatures as low as 300° C. These and other similar observations and suggestions have convinced most geologists that volcanic glasses are easily devitrified in the presence of water at temperatures not much greater than its boiling point.

Water acts on glasses by leaching cations and forming hydroxyl groups with silica (silanol). Dissolved material may be deposited in crystalline form, following transportation over distances ranging from millimeters to miles. (The secondary mineralization in the vicinity of volcanic rocks may occur largely through the dissolution of the surfaces of shards in tuffs.) An intermediate effect of chemical weathering or hydrothermal alteration is the leaching of certain constituents and the crystallization of the remaining glass *in situ*. In this case, kaolin or allophane may be formed (Sudo, 1951). Glass that has been hydrothermally (or thermally) reconstructed *in situ* with negligible loss of material is termed *devitrified*. In the limiting case of reorientation, the crystallizing particles move only very short distances (on the order of atomic dimensions).

Although there are many references to the occurrence and the petrography of volcanic glass, there has been little emphasis on the processes transforming volcanic glass to the holocrystalline state and even less emphasis on the rates of those processes. The author discusses first the kinetics of crystallization in the presence of only slight amounts ($\lesssim$1 per cent) of water[2] and extends them to natural glasses at low temperatures. Then, the author estimates the rate of hydrothermal reconstruction at low temperatures (around 20° C), on the basis of his study of thin sections of a variety of volcanic glasses. These glasses represent a number of localities widely differing in geologic age. The

[1] Hawkes (1930) has briefly reviewed some of the experimental work on silicate melts and has applied it to the physical classification of volcanic glass and to some aspects of its occurrence.

[2] Most volcanic glass contains at least a few tenths of a per cent of water. Even these small amounts greatly affect the properties of the rock. However, in the first discussion which follows, the amounts of water are assumed to be so small that their principal effect is to compensate for the lower viscosities of the artificial glasses to which the natural glasses are compared.

diffuse, irregular, devitrified layers along cracks in perlites and the data from some experiments with a pressure bomb permit estimation of the time-temperature relationships for this reconstruction.

The author gratefully acknowledges the encouragement and help of Prof. Ian Campbell (California Institute of Technology) and the careful preparation of the many thin sections by Mr. Rudolph von Huene (California Institute of Technology). The author also thanks Prof. R. H. Jahns (California Institute of Technology) and Prof. H. Ramberg (University of Chicago) for their helpful comments and Prof. George Kennedy (University of California, Los Angeles, California) for the loan of a pressure bomb. The writer greatly appreciates the assistance of the many persons who have contributed samples and information for this study.

DISTRIBUTION OF VOLCANIC GLASSES ACCORDING TO SILICA CONTENT

Volcanic glass constitutes only a small percentage by volume of all extrusive rock. The relative natural abundance may be reflected in the number of analyses made of these rocks.[3] Perhaps as much as 10 per cent of all extrusive rocks contain some glass or devitrified glass.

The effect of composition on primary crystallization is indicated by the common occurrence of high-silica glasses as compared to low-silica glasses: basic glasses occur usually as thin selvages and as scattered fragments of ash, rarely as thick glassy flows.

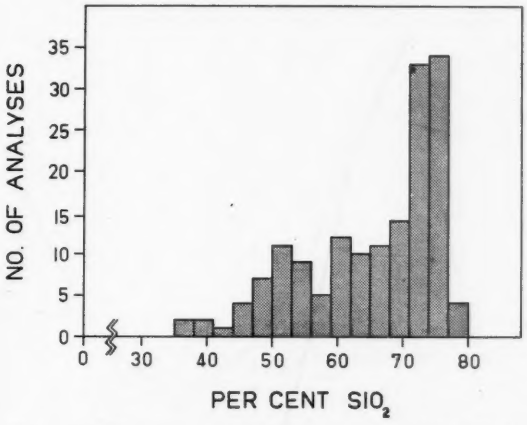

Figure 1. Silica content of 159 volcanic glasses (after Washington, 1917), including pitchstones, obsidians, perlites, marekanites, tholeiites, tachylites, palagonites, and rocks with the prefixes *vitro-* and *hyalo-*. Pumice, ash, scoria, and Pele's hair, and rocks such as limburgite which have a more or less glassy groundmass, were not included. Except where glass represented a significant part of the groundmass, it did not appear in the rock name, and there was no way to take it into account.

Elliott's (1956) analysis of the glassy portion of the Eskdalemuir tholeiite revealed 70 per cent silica compared to only 60 per cent for the rock as a whole. This rock is andesitic, but crystallization has fractionated a basaltic phase, leaving a siliceous interstitial glass—just as glassy rocks in general represent a high-silica fractionation. Vogt (1921) commented that in rocks with total SiO_2 content less than about 72 per cent, the glassy groundmass is more

[3] Analyses of volcanic glasses constitute about 4 per cent of the more than 2200 superior analyses of extrusive and shallow intrusive rocks made in the world from 1884 to 1913, as listed by Washington (1917). Nearly 28 per cent of all the analyses were made on rhyolitic rocks ($\geq$ 65 per cent SiO_2).

siliceous than the rest of the rock. George (1924) cited a number of examples and also indicated (his Fig. 3) the predominence of glasses with silica content in the range 70–75 per cent.

The relative abundance of glass of a particular composition is perhaps more clearly expressed in Figure 1. This is a histogram summarizing the silica content of 159 samples of glassy rocks given in Washington's (1917) compilation. In addition to the dominant peak at about 73 per cent silica, the graph has a distinct maximum at about 52 per cent corresponding to basaltic glasses. Rhyolitic glass seems to be about 3 times more abundant than basaltic or andesitic glass, as would be predicated in a general way from the properties of the magmas. If the sampling can be considered approximately random, the distribution in Figure 1 should be roughly proportional to the stability (in respect to thermal reconstruction) of glasses of various silica content. In the more than 2200 superior analyses of extrusive and shallow intrusive rocks that Washington (1917) listed, the ratio of basalts to rhyolites is very close to 2:1. Thus, the likelihood of formation of a glass from a rhyolitic melt compared to that from a basaltic melt may be roughly estimated as 6:1.

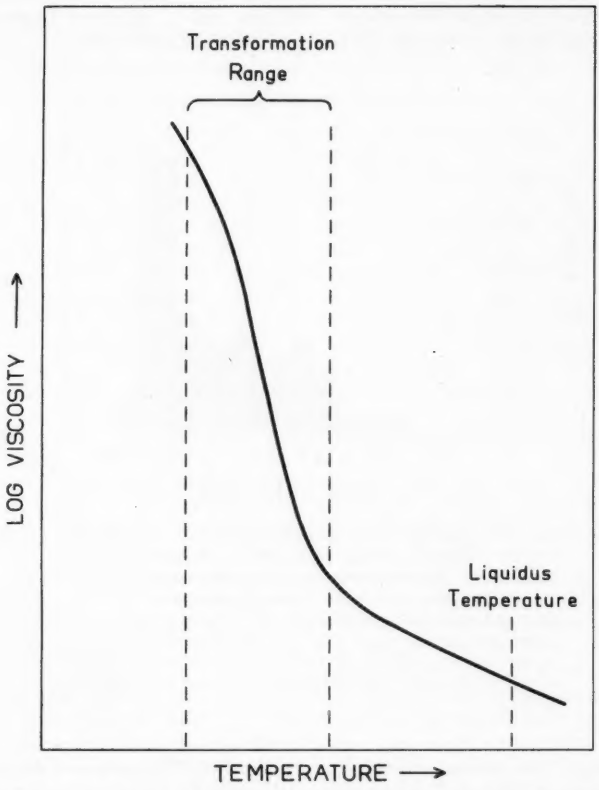

Figure 2. Change in the viscosity of glass with increase of temperature

THERMODYNAMIC RELATIONSHIPS

On the basis of thermodynamics, glass should change to a crystalline assemblage. Although the rate cannot be obtained from thermodynamics, its concepts are useful in understanding the kinetics of crystallization discussed later. The glassy state and the important

qualitative features of its transformation are described briefly hereafter.

Above the liquidus temperature (Fig. 2), the crystalline state is unstable. When the temperature is lowered below that point, the melt (in the absence of effective nucleation) is a supercooled liquid until the transformation range[4] is reached. At this stage, the viscosity increases rapidly over a limited temperature range (Fig. 2): it becomes very high compared to that of ordinary liquids, but the individual particles can still adjust (within experimental time) to the internal equilibrium characteristic of a supercooled liquid.

At still lower temperatures, rearrangement in the amorphous solid or glass is virtually impossible. At ordinary temperatures, say 25° C, most of the particles are frozen (except for thermal vibration) in the random distribution characteristic of a supercooled liquid at a temperature some hundreds of degrees higher. The glass has the free energy (ΔF) corresponding to the minimum free energy for the system at this higher temperature.

As the degree of order[5] of the system increases (Fig. 3), the particle configuration of the disordered liquid changes to that of an ordered (supercooled) liquid, *i.e.*, to the system of minimum free energy (ΔF_{min}) at the low temperature. High viscosity prevents the system from reaching this metastable equilibrium. However, some of the cations are in shallow potential wells, and when small amounts of energy become available, they move to more stable positions. Thus, some readjustment through thermal fluctuations is possible at low temperatures.[6] The approach of ΔF toward ΔF_{min} is evidenced by gradual changes in the

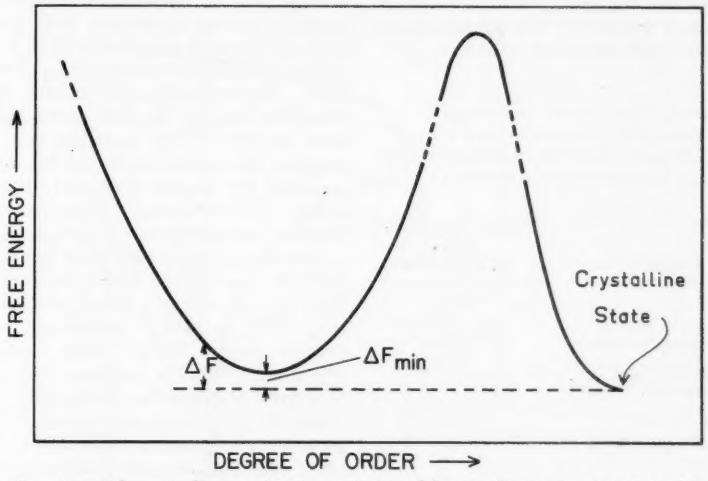

Figure 3. Schematic diagram showing variation of degree of order (or viscosity) with free energy for a glass at a temperature below the transformation range

[4] Condon (1954) gives a good review of the evidence establishing the transformation range. Jones and Simon (1949) carefully discuss this range and the thermodynamic state of glass.

[5] The degree of order is given by an ordering parameter, S. This parameter must be a monotonic function of the constraints which prevent relaxation of the system to complete thermal equilibrium. The latter is reached in the crystalline state. Viscosity is a constraint satisfying the preceding condition on S. The degree of ordering may be written as a function of the viscosity coefficient, η, thus: $S(\eta)$.

[6] Although complete thermal equilibrium is not reached, the system is still considered describable by a thermodynamic potential. However, parameters must be introduced in addition to such variables as pressure and temperature which suffice to describe states of equilibrium. The assumption is made that the usual definitions for pressure and temperature can be used for systems not too far from equilibrium.

properties of the glass. Weyl (*in* Smoluchowski, Mayer, and Weyl, 1951, p. 307 *ff.*) discussed slow shifts in the electrical conductivity and the index of refraction of glass which indicate such a reduction in the disorder of the glass.

A large amount of energy (indicated by the height of the off-scale peak on Figure 2) is required to change the glass from the supercooled-liquid state to the crystalline state, its lowest free-energy state. This energy involves that for the formation and the subsequent growth of nuclei. However, the following discussion is restricted to a consideration of the latter because crystallites already present in most glasses supply abundant nuclei.

Table 1. Free Energy Differences for a Few Transformations

Data from *Selected Values of Chemical Thermodynamic Properties*, U. S. National Bureau of Standards Circular 500 (1952)

Transformation	$\Delta F_{298\cdot16^\circ K}$ (kcal/mole)
Fused silica → quartz (low-temperature form)	−1.5
Boric anhydride (glass) → boric anhydride (crystal)	−2.6
Aragonite → calcite	−0.25

Free energy is generally considered the driving force for devitrification, but the ΔF's for glasses are no more than a few kilocalories. Table 1 gives two examples of the difference in free energy between the crystal and its respective glass, and the free energy difference between two polymorphs of calcium carbonate for comparison. M. J. Buerger (*in* Smoluchowski *et al.*, 1951, p. 205) considers the latter transformation to be reconstructive because the first-co-ordination bonds of the original structure must be broken, and the units must be reassembled. The transformation is extremely sluggish, but the tendency of aragonite to become calcite is apparent in the geologic record (A. Papst *in* Smoluchowski *et al.*, 1951, p. 211). The process requires considerable energy and is analogous to that for glass. Devitrification is also reconstructive: the strong Si-O bond may be considered as a first-co-ordination bond to be broken and reformed. A high activation energy of at least 50 kcal/mole is required for thermal reconstruction. Hydrothermal reconstruction, on the other hand, is devitrification catalyzed to a great extent by water; therefore, its rate is considerably more rapid.

THERMAL RECONSTRUCTION: KINETICS OF CRYSTALLIZATION

Crystal Growth and Temperature

Although volcanic glasses may be essentially holohyaline, they invariably contain crystallites. Primary crystallites, formed during solidification of magma, are generally flow-oriented and are commonly well developed, although they are usually too small for petrographic identification (Bonney and Parkinson, 1903). Devitrification of volcanic glass by heat alone involves the same atomic rearrangement as that in the crystallization of most magmas. The major distinction between these processes lies in the time and temperature factors. Devitrification is a metamorphic process which may proceed over a long period.

Numerous experiments have demonstrated that the rate of growth of crystals in silicate melts is constant at a given temperature, as long as the growth is unhindered by other crystals (Swift, 1947a; 1947b; Grauer and Hamilton, 1950). The rate depends on the kind of mineral as well as the temperature. Figure 4 illustrates the general dependence of rate of growth on temperature. The rate is negative above the liquidus temperature: crystals do not form, or they dissolve if already present. Below this temperature, the rate of growth increases to a maximum and then falls off exponentially. Rates too small to measure are reached within a few hundred degrees below the liquidus point. Any given positive rate of growth (except the maximum) occurs at both a high and a low temperature, but only the low-temperature side of the curve will be further emphasized.

Nucleation

Tammann (1914) demonstrated that the rate of nucleation is a function of temperature and is similar to that for the rate of growth. Thus, the number of crystal nuclei formed per unit of time passes through a maximum as the temperature is lowered from the liquidus point. Maximum nucleation occurs at a lower temperature than that for the maximum rate of growth, but the two curves overlap considerably.

The average crystal size depends on both

the rate of growth and the rate of nucleation, which, in turn, are determined by the cooling history. Large crystals of approximately equal size form only if low rates of cooling prevail at temperatures a little below the liquidus point (where the rate of growth is large but nucleation is negligible). Again, a stage may be reached in which much of the crystallization of a single mineral occurs at rather constant rates of both growth and nucleation. Then the end representing smaller crystals (corresponding to the formation of more nuclei below, rather than above, the temperature at which the maximum rate of nucleation occurs). The peak corresponds to the most probable length, which in this case is very close to the average length of the belonites.

Cooling History

With a constant rate of growth for any

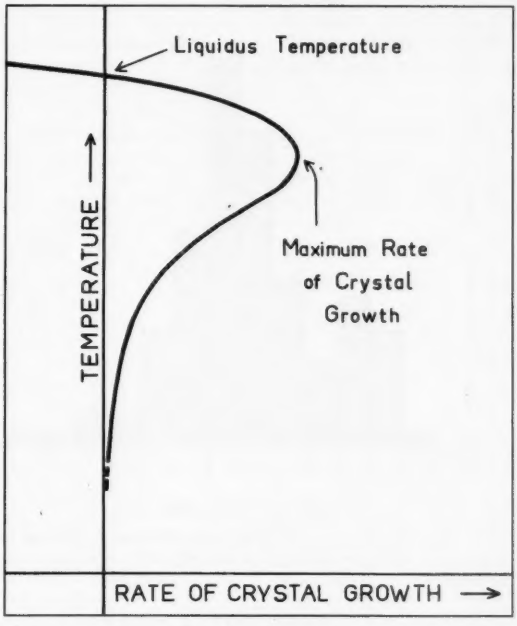

Figure 4. Rate of crystal growth in glasses as a function of temperature (after Swift, 1947a)

sizes of the crystals range uniformly from zero to a maximum. Winkler (1949) has carefully related the variations in average crystal size to the sequence of crystallization of several of the minerals of a tholeiite dike. A simple cooling history could be assumed in this example.

Similarly, the cooling of most volcanic glasses was probably a simple and continuous as well as rapid process. Figure 5, a histogram representing the size distribution of the belonites (of an unidentified mineral) in a perlite, has, therefore, nearly the same form as the curve for the rate of nucleation *versus* temperature. The histogram is slightly skewed toward the

temperature, the average length of crystallites of a particular mineral depends on the length of cooling. Three samples of obsidian from the Mono Craters, Mono County, California, illustrate the effects of slightly different cooling histories. Thin sections reveal in each case two sets of crystallites. One set consists of small, colorless, lath-shaped crystals (belonites), the other of yellow-green to yellow-brown lath-shaped crystals (microlites). Table 2 summarizes the average lengths of these distinct, but not further identified, minerals.

The ratio of the average lengths of the two crystallites is essentially constant in these

sections. This should be the case for two independent linear (in respect to time) rates of growth in the same environment providing that the ratio of the slopes of the rate-of-growth—temperature curves remains nearly constant.

An Equation for the Rate of Crystal Growth

It is interesting to speculate on the rates of crystal growth at temperatures below 700–800° C and on the maximum size possible at those rates during geologic time. Because it is impossible to vary the time factor over a wide enough range in controlled experiments on devitrification, one must extrapolate from experiments on crystallization at higher temperatures.

The rate of crystallization in silicate melts (Fig. 4) is considered to result from two opposing forces (Grauer and Hamilton, 1950): a driving force which increases as temperatures drop below the liquidus point, and a force which impedes crystallization and which is inversely proportional to the viscosity. This second force dominates crystallization below the temperature corresponding to the maximum rate of crystal growth. Because viscosity increases rapidly as the temperature falls, the linear rate of crystal growth, G, generally passes through its maximum within 100° C below the liquidus point. The following equation describes the change in rate of crystal growth below this maximum temperature:

$$G = Ae^{-\Delta F^*/RT} = Ae^{\Delta S^*/R}e^{-\Delta H^*/RT}. \quad \text{(Ia)}$$

The factor A from the theory of absolute reaction rates (Glasstone, Laidler, and Eyring, 1941, p. 14) is $\left(\frac{kT}{h}\right)d$. The term in parentheses (Boltzman's constant times the absolute temperature over Planck's constant) corresponds to the frequency of atomic vibration (about 10^{13}/sec at 20° C), and d is the average distance (about 10^{-8} cm) that atoms move in their reorganization. The term ΔF^* is the free-energy maximum (Fig. 3) necessary to form an activated state (indicated by the asterisk) that can either revert to the supercooled liquid or progress to the crystalline state. The symbols R and T represent the gas constant and the absolute temperature, respectively, and ΔH^* represents the correspond-

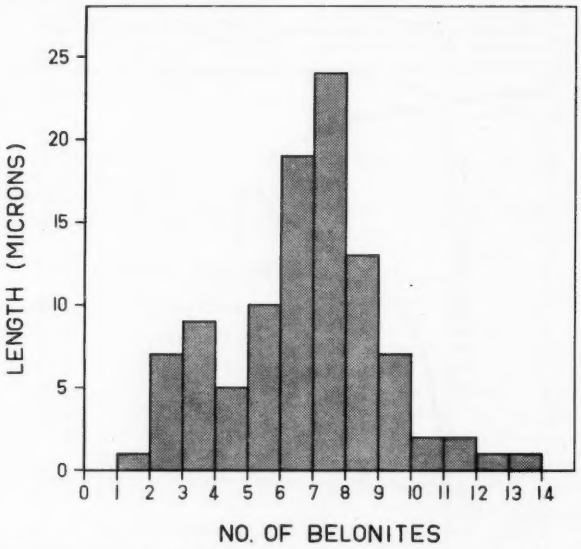

Figure 5. Size distribution of 101 belonites selected at random from a thin section of perlite from the Dublin Hills, Shoshone quadrangle, California

TABLE 2. AVERAGE LENGTHS OF CRYSTALLITES IN OBSIDIAN FROM MONO CRATER, MONO COUNTY, CALIFORNIA

Thin section*	Crystallite	Average length (μ)	Ratio of lengths
MB 11	microlite	130	9:1
	belonite	14	
MB 13a	microlite	80	7:1
	belonite	12	
MB 18	microlite	46	8:1
	belonite	6	

*In the collection of thin sections of the California Institute of Technology

gives the deduced values of ΔH^* and the factor $Ae^{\Delta S^*/R}$. Note that $Ae^{\Delta S^*/R}$ has been calculated from observed rates of crystal growth and the average value of ΔH^* (50 kcal/mole). The uncertainties in the calculation of individual activation energies from these data can be no more than a few kilocalories. The variation in values is considerably greater than this uncertainty, although there is no apparent systematic variation of ΔH^* with the composition. The average value is taken as representative but is assigned an uncertainty of twice the mean deviation.

Rutley (1886) completely devitrified an obsidian from Ascension Island by keeping it between 850° C and 1100° C for 701 hours. Crystals as long as about 30 μ (Rutley's Pl. 4, fig. 4) formed. A similar experiment failed to completely devitrify an obsidian from the Yellowstone district, Montana, although white crystalline pellets and specular hematite crystals formed (Rutley's Pl. 4). The size of the pellets indicates crystal lengths of about 500–1000 μ; the average size of the specular hematite crystals was about 50 μ. The rate of crystal growth in the obsidian from Ascension must have been no greater than 10^{-2} μ/hr. The obsidian from Yellowstone indicates greater rates, ranging up to about 1 μ/hr. If the average temperature in these experiments is taken as

TABLE 3. RATE PARAMETERS FROM DEVITRIFICATION STUDIES ON ARTIFICIAL GLASSES

Reference	Crystalline phase	ΔH^* (kcal/mole)	$Ae^{\Delta S^*/R}$† (μ/hr) $\times 10^{-11}$	SiO_2 (%)	Al_2O_3 (%)	CaO (%)	MgO (%)	Na_2O (%)
After Swift (1947a)	$Na_2Ca_3Si_6O_{16}$ (devitrite)	51	7.	69.	2.	12.	..	17.
After Swift (1947b)	$Na_2Ca_3Si_6O_{16}$ (devitrite)	54	4.	73.5	0.3	10.0	0.2	15.8
After Swift (1947b)	$Na_2Mg_2Si_6O_{15}$	57	0.8	73.5	0.2	0.3	9.9	15.9
After Swift (1947b)	$Na_2Ca_3Si_6O_{16}$ (devitrite)	35	11.	71.	..	12.	..	17.
After Swift (1947b)	$Na_2Ca_3Si_6O_{16}$ (devitrite)	56	5.	67.	4.	12.	..	17.
After Swift (1947b)	$CaSiO_3$ (wollastonite)	50	3.	63.	8.	12.	..	17.
After Grover and Hamilton (1950)	$Na_2Ca_3Si_6O_{16}$ (devitrite)	49	2.	70.	..	10.	..	20.
	AVERAGE	50 ± 10						

†Calculated from observed rates, using $\Delta H^* = 50$ kcal/mole

ing change in enthalpy for the activated complex. The product of the exponential entropy term, $e^{\Delta S^*/R}$, and A constitutes the pre-exponential factor in the usual Arrhenius function. The temperature dependence of this factor is negligible in the following estimation of its magnitude.

The writer has tested the usefulness of this equation by plotting the logarithm of crystallization rates in artificial glasses (Swift, 1947a; 1947b; Grauer and Hamilton, 1950) against the reciprocal of the absolute temperature. Reasonably linear graphs have been obtained from data on CaO-Na_2O glasses and their modifications with aluminum or magnesium. Table 3

950° C and ΔH^* is 50 kcal/mole, the values of $Ae^{\Delta S^*/R}$ range from $>10^7$ μ/hr to as much as 10^9 μ/hr. Values for $Ae^{\Delta S^*/R}$ in artificial glasses (Table 3) are generally larger, ranging up to 10^{12} μ/hr.

TABLE 4. ADDITIONAL VALUES FOR THE FACTOR $Ae^{\Delta S^*/R}$

Crystalline phase	$Ae^{\Delta S^*/R}$† (μ/hr) $\times 10^{-11}$	Reference
SiO_2 (cristobalite)	2.	Figure 1A
$Na_2Ca_3Si_6O_{16}$ (devitrite)	2.	Figure 1B
SiO_2 (cristobalite)	0.7	Figure 1B
$Na_2Ca_3Si_6O_{16}$ (devitrite)	1.	Figure 1C
SiO_2 (cristobalite)	0.4	Figure 1C
$Na_2Mg_2Si_6O_{15}$	0.2	Figure 1D
SiO_2 (cristobalite)	0.6	Figure 1D
$CaMgSi_2O_6$ (diopside)	0.07	Figure 1E
$Na_2Mg_2Si_6O_{15}$	0.2	Figure 1E
$Na_2Ca_3Si_6O_{16}$ (devitrite)	7.	Figure 2B
$CaSiO_3$ (wollastonite)	0.2	Figure 2C
$CaSiO_3$ (wollastonite)	0.4	Figure 2D
$Na_2Ca_3Si_6O_{16}$ (devitrite)	0.6	Figure 2D
Pyroxene crystals in basaltic glass	0.7	Volarovich and Leontieva (1948)

(Swift (1947b) — Figure 1A through Figure 2D)

† Calculated from observed rates, using $\Delta H^* = 50$ kcal/mole

The writer has calculated more values for $Ae^{\Delta S^*/R}$ from observed rates of crystal growth in artificial glasses and in a basaltic glass using the activation energy of 50 kcal/mole (Table 4). To summarize from Tables 3 and 4, values of $Ae^{\Delta S^*/R}$ for devitrite have the range 6–110 $\times 10^{10}$ μ/hr; for $Na_2Mg_2Si_6O_{16}$, 2–8 $\times 10^{10}$ μ/hr; for cristobalite, 4–20 $\times 10^{10}$ μ/hr; and for pyroxenes, 0.7–30 $\times 10^{10}$ μ/hr. A generized value of $Ae^{\Delta S^*/R}$ for the crystallization of minerals is about 10^{10} μ/hr; reasonable lower and upper limits, in spite of variations in the compositions of the glasses, are about 10^9 and 10^{11} μ/hr, respectively. Values for $Ae^{\Delta S^*/R}$ calculated from rates given by Kittle (1912) for a variety of minerals are well within this range.

From the generalized value for $Ae^{\Delta S^*/R}$, the value calculated for ΔS^* is about -10 to -20 cal/mole deg. This negative value indicates a low probability of achieving the activated state.

Secondary Changes

Rates of thermal reconstruction at low temperatures. For any given average crystal length (L) in a devitrified glass, the minimum time in millions of years estimated for devitrification at various temperatures is given by the following equation:

$$t = \frac{L}{10^{20} \exp(-50 \text{ kcal}/RT)}. \qquad \text{(Ib)}$$

The solid line in Figure 6 shows the plot of the logarithm of time *versus* temperature for $L = 10$ μ. This line represents only an upper limit for the rate of devitrification in most volcanic glasses. This limitation is due partly to the fact that the viscosities of volcanic glasses are generally higher than those of CaO-Na_2O glasses. If some water is present in the natural glass, it tends to compensate for differences in viscosity which are due to composition. The value of 50 kcal/mole (Table 3) is essentially the activation energy for the viscosity of the more fluid CaO-Na_2O glasses in the high-temperature range. In the transformation range, the activation energy of the viscosity of a CaO-Na_2O glass is even higher, between 2 to 3 times that for the same glass at higher temperatures (*cf.* Fig. 2). Table 5 gives activation energies for the viscosities of some artificial glasses and melted rocks.

TABLE 5. ACTIVATION ENERGIES OF VISCOSITIES OF SOME ARTIFICIAL GLASSES AND MELTED ROCKS

Glass	ΔH^* (kcal/mole)	Temperature range (°C)	Reference
CaO-Na_2O, artificial	49	900–1400	After H. R. Lillie (*in* Morey, 1954, p. 157)
	120	500– 700	
CaO-Na_2O, artificial	43	1100–1400	After M. P. Volarovich (*in* Eitel, 1954, p. 170)
Melted andesite	66	1100–1400	
Melted diorite	64	1250–1400	

The conclusions pertinent to devitrification may be summarized briefly. The activation energy for thermal reconstruction of natural glass seems to be no less than about 50 kcal/mole. Using this value in equation Ib, it follows that devitrification would be com-

pleted within 10^6 years at a temperature of 300° C, within 10^7 years at 275° C, and within 10^8 years at 250° C.[7] The time required at 25° C would be 10^{23} years. The activation energy for most natural glasses is probably closer to 100 kcal/mole. In this case, complete devitrification within 10^9 years requires a temperature of 750° C. At 25° C the time required is 10^{60} years.[8]

Other secular changes. Over a period of many years, thermal fluctuations at about room temperature may change the character of a glass appreciably. These secular changes (referred to in the preceding section on Thermodynamic Relationships) are generally indeterminate because the original values of the index of refraction, electrical conductivity, *etc.*, are unknown. However, strain birefringence may reveal secular change in volcanic glasses.

A large dome of pumiceous perlite of late Quaternary age, about 3 miles southwest of Fish Springs, Owens Valley, Big Pines quadrangle, California, is characterized by the striking strain birefringence shown in Figure 2 of Plate 1. A sample of this perlite kept for 3 months in water at 100° C did not lose this birefringence. However, other samples heated to 330° C did lose their birefringence, including those held under pressure in a bomb with excess water present throughout the annealing. Although the fracture of volcanic glass often results in small spheres (thus the description perlitic), the center of Figure 2 of Plate 1 shows a hexagon suggestive of the tension-formed cracks of the polygonal blocks of columnar basalt.

Similar strain patterns occur in a slightly perlitic glassy rock near Coso Hot Springs, Inyo County, California. This rock is also late Quaternary; it is probably less than 100,000 years old. A volcanic breccia from Yellowstone Park, Wyoming,[9] includes fragments of glassy rock. The clear glass is speckled with small crystallites. Some perlitic structure is present, but the cracks are not bounded by devitrified layers. However, strain birefringence is prominent, principally along the outer surfaces of the fragments.

Marekanite and perlite from the upper Tertiary or lower Quaternary deposits near Superior, Arizona, also show prominent strain patterns under crossed nicols. In the marekanite, birefringent bands radiate outward from enclosed crystallites. The lengths of the bands of light are proportional to the size of the crystallites, indicating that the birefringence results from differential contraction. Other notable strain patterns appearing in glass are reported in marekanites from near Okhotsh, Siberia, and in perlite from New Mexico (Ross and Smith, 1955, Pl. 2b). Older volcanic glasses show only slight, if any, such polarization, probably because of gradual relaxation of the strain through thermal reconstruction, involving the breaking and reforming of relatively few Si-O bonds.[10]

Glass in meteorites. The argon-potassium age determinations for meteorites range up to somewhat more than 4×10^9 years (Geiss and Hess, 1958). The ages found for the Holbrook and Richardton chondrites are 4.40×10^9 and 4.15×10^9 years, respectively. Glass has been observed in both these meteorites (Foote, 1912; Quirke, 1919), as well as in a number of others. Such glass is several billion years older than the oldest known terrestrial glass. The calculations in the preceding section indicate that if a glass remains at temperatures as high

[7] Eitel (1954, p. 572) reports the devitrification of an artificial glass over a period of several years at only 200° C. If $Ae^{\Delta S^*/R}$ were 1000 times greater (corresponding to a rapidly crystallizing phase) and the activation energy lower by 10 or 15 kcal/mole, then this unusually high rate of devitrification could be arrived at using equation Ib. Possibly water within the glass or water vapor on the surface was active in the process. In any case, such instances are unusual and presumably occur under circumstances rare for natural glasses which contain very little water.

[8] Richards (1936) derived an equation for the thermal relaxation time of molecules in supercooled liquids. He calculated that a time $> 10^{50}$ years would be required for relaxation of an ordinary laboratory glass at room temperature. The agreement between his value and the one given here is to be expected because both calculations are dominated by the extremely high value for viscosity.

[9] California Institute of Technology thin section T 588.

[10] Water may act indirectly or even directly to produce much of this birefringence, according to Irving Friedman and Robert L. Smith of the U. S. Geological Survey. In discussions with the writer they have emphasized the close relationship between the water content and the optical properties of these rocks (*See* Ross and Smith, 1955; Friedman and Smith, 1959). Their observations suggest that hydration of the surfaces of obsidian may occur within a geologically short time, although the diffusion of water into glass (as discussed later in this paper) seems to be much slower. Possibly surface diffusion along submicroscopic cracks and cation-exchange reactions are important in producing the optical effects which they observe.

TABLE 6. DEPTH OF DEVITRIFICATION IN VOLCANIC GLASSES OF VARIOUS AGES

(Perlites unless noted otherwise)

Thin section	Approximate depth of devitrification (μ)	Geologic age	Locality	Donor
RM 1a	3.	Late Tertiary or early Quaternary	Superior, Ariz., area	E. D. Wilson
RM 2	4.	Miocene (?)	W. of Magdalena, Socorro Co., N. Mex.	V. C. Kelley
RM 3	4.	Pliocene or late Miocene	Bear Canyon, Jemez Mtns., Sandoval Co., N. Mex.	
RM 4	2.	Pliocene or late Miocene	Agate claims, Jemez Mtns., Sandoval Co., N. Mex.	
RM 5 (pumiceous perlite)	0.	Pliocene or late Miocene	Peralta Canyon, Jemez Mtns., Sandoval Co., N. Mex.	
RM 6 (pumiceous perlite)	0.	Pliocene (?)	Great Lakes Carbon Co. mine near Socorro, N. Mex.	
RM 7	3.	Late Tertiary or early Quaternary	Superior, Ariz.	G. Burnham
RM 8	3.5			
RM 9	0.	Late Quaternary	Near Coso Hot Springs, Inyo Co., Calif.	P. St. Amand
RM 9a	0.			
RM 10	1.	Pliocene	Glass Tunnel, Peralta Canyon (Santa Clara #3 quad.), Sandoval Co., N. Mex.	C. S. Ross and R. L. Smith
RM 11 (fractured obsidian)	0.9	Pliocene	Top of Bear Head Peak (Santa Clara #3 quad.), Sandoval Co., N. Mex.	
RM 12	2.	Pliocene	Bland Canyon (Santa Clara #3 quad.), Sandoval Co., N. Mex.	
RM 13	2.	Pliocene	Related to RM 12, but from a separate dike; Bland Canyon (Santa Clara #3 quad.), Sandoval Co., N. Mex.	
RM 14	2.	Pliocene	From same outcrop as RM 13	
RM 15	0.	Pliocene	Media Dia Canyon, ½ mi. above junction with Cochiti Canyon (Santa Clara #3 quad.), Sandoval Co., N. Mex.	
RM 16 (fractured obsidian)	3.5	Pliocene	Bland Canyon, 2¼ mi. above Bland (Santa Clara #2 quad.), Sandoval Co., N. Mex.	
RM 17	2.	Pliocene	Borrego Spring (Jemez quad.), Sandoval Co., N. Mex.	
RM 18	1.5	Pliocene	Perlite prospect, 1¼ mi. SSE. of Bear Springs Peak (Jemez quad.), Sandoval Co., N. Mex.	
RM 19	2.	Pliocene	Road ½ mi. E. of Bear Springs perlite prospect (Jemez quad.), Sandoval Co., N. Mex.	
RM 22	2.	Older than late Pliocene	West boundary of Inspiration quad., Ariz.	N. P. Peterson
RM 23 (slightly fractured glass)	1.5	Eocene	Dooley Mt., southern Baker Co., Ore.	R. S. Mason
RM 24	1.5	Eocene	Lady Francis mine, Wasco Co., Ore.	
(82) 34–13–17	0.	Pleistocene	Evans Creek, Ochoco Reservoir quad., Ore.	A. C. Waters
T 949 (vitrophyre)	6.	Permian	*Ca.* 15 km N. of Bolzano, Italy	C. J. Blom

TABLE 6. *Continued*

Thin section	Approximate depth of devitrification (μ)	Geologic age	Locality	Donor
N 10	1.	Probably late Pliocene	Perlite Aggregates, Inc., quarry; *ca.* 5 mi. SE. of Saint Helena, Napa Co., Calif.	C. W. Chesterman
LF 9	2.	Late Miocene to early Pliocene	Foster's property, near N. end of Sugar Hill, northern Warner Range, Modoc Co., Calif.	
BR 21	0.	Late Quaternary	*Ca.* 7 mi. S. of Big Pine, Inyo Co., Calif.	
(49) 9–13–18	2.	Oligocene	Sec. 9, T. 13, R. 18, Ochoco Reservoir quad., Ore.	A. C. Waters
24–14–17	1.5	Oligocene	Polly Butte, Ochoco Reservoir quad., Ore.	
RM 50 (collapsed pumice with perlitic cracks)	1.	Oligocene	Eagle Rock, Eagle Rock quad., Ore.	
16–13–17 (welded tuff)	<1.	Oligocene	Green Mt., Ochoco Reservoir quad., Ore.	
RM 53 (pumiceous perlite)	0.	Late Pliocene	Sec. 6, T. 22 S., R. 39 E., M.D.M., Coso Range, Inyo Co., Calif.	C. W. Chesterman
RM 69	0.	Pliocene	SW¼NE¼ sec. 3, T. 24 S., R. 9 W., Millard Co., Utah	R. R. Coats
RM 72	0.	Pliocene (?)	NE¼NE¼ sec. 34, T. 8 N., R. 5 W., Napa Co., Calif.	
RM 74	<2.*	Eocene or Oligocene	SW¼ sec. 10, T. 19 N., R. 16 E., Sierra Co., Calif.	
RM 76	1.	Pliocene (?)	Sec. 9, T. 28 S., R. 63 E., Clark Co., Nev.	
RM 77	0.8	Pliocene (?)	Sec. 34, T. 22 N., R. 6 E., Shoshone quad., Inyo Co., Calif.	
RM 78	2.	Miocene	Saguache Co., Colo.	
RM 79	2.	Miocene	SE¼ sec. 36, T. 46 N., R. 2 E., Saguache Co., Colo.	
RM 80	3.	Middle Miocene or older	3 mi. NW. of Opal Mt., Opal Mt. quad., Calif.	T. McCulloh
RM 81 (volcanic breccia)	3.	Middle Miocene or older	2¼ mi. E. of Fremont Peak, Fremont Peak quad., Calif.	
RM 82 (vitrophyre)	2.	Younger than late Miocene; probably middle Pliocene	W. of Pickhandle Pass in NW Calico Mts., Lane quad., Calif.	
RM 86	0.9	Middle Miocene	Puddingstone Reservoir, San Jose Hills, Los Angeles Co., Calif.	G. Eaton
RM 88	2.	Late late Cretaceous	Wolf Creek, Mont.	J. D. Barksdale
H–6–49–B1	2.			
H–6–49–3	1.5			
H–6–49–2	1.5			
2 V 128–5	0.9	Late Pliocene	6–8 mi. N. of Cuddeback Lake (playa) in Lava Mts., NW. corner of San Bernardino Co., Calif.	G. I. Smith
63–67 (fractured pitchstone)	3.†	Eocene	Crum Canyon, Chelan Co., Wash.	M. T. Huntting
Mashel R.	3.–4.	Early Miocene or older	Mashel River area, Pierce Co., Wash.	
Dry Gulch	5.	Middle Eocene	Near Wenatchee, Chelan Co., Wash.	
Divide	2.	Early Miocene or older	White River area, Pierce Co., Wash.	

*No evidence of devitrification along borders of most of the cracks

†Devitrified layers as much as 10 μ thick along one major fracture

as 200° C for such long periods, thermal reconstruction will still not be complete.[11]

HYDROTHERMAL RECONSTRUCTION

Petrographic Studies of Volcanic Glasses

Perlites. Devitrification in perlites is characterized by irregular zones of crystallization along cracks and surfaces of vesicles and by enlargement of crystallites. Under crossed nicols, devitrification is often apparent as speckled, diffusely birefringent zones along the cracks; in wholly devitrified samples, small, irregular, interlocking birefringent areas may occur throughout the rock.

The writer examined thin sections of volcanic glasses with the petrographic microscope, generally at magnifications around 500×. Filar and stage micrometers were used to measure the distance to which devitrification had penetrated inward from the surfaces of the glass; this distance is termed the *depth of devitrification.* Table 6 gives the depths of detrification for 53 thin sections, representing about 46 localities. Generally, each value is the average of a number of measurements, and in many cases the devitrified layer is sufficiently uniform throughout the sample so that the mean deviation for 10 or 20 measurements is less than 25 per cent. The mean deviation is typically less than 50 per cent of the average value, but for highly devitrified glasses (depths of 5–15 μ) it may be slightly greater.

Figure 1 of Plate 2 shows the narrow, sharply defined cracks characteristic of young and unaltered perlite. Figures 2 and 3 of Plate 2 illustrate well-developed devitrified layers bordering the cracks. A secondary mineral up to several microns wide, occasionally with uniform extinction for tens of microns, may fill the cracks in perlites.

Additional volcanic glasses which were examined but which are of unknown ages are listed with their average depths of devitrification in Table 7. Probably none of these glasses is older than Miocene; the extent of devitrification confirms that illustrated by Table 6.

In Figure 7 the depth of devitrification (from Table 6) is plotted against the square root of the geologic age of the sample. The reason for using this scale will be apparent from the following section interpreting the role of water in the process of devitrification. Because of the great scatter, the measurements in themselves cannot justify the dependence of the depth of devitrification on the square root of age. They merely suggest a trend. The dashed line indicates that the rate of devitrification at ordinary temperatures can be no more than approximately 4 or 5 μ in 100 million years. Some of the best preserved older glasses which are only slightly devitrified indicate that the rate may be closer to only 2 or 3 μ per 100 million years. Some of the scattered points in Figure 7 probably represent short periods of exposure of the rocks to temperatures above 20° to 30° C. For example, the volcanic region of northern New Mexico (represented by thin sections RM 10 through RM 19 in Table 6) still abounds in hot springs. Hot water and (for surface samples) solar heating may bring about detectable devitrification rapidly.

Petrographic descriptions of perlites from a number of localities have been published recently by Anderson *et al.* (1956). The degree of devitrification they observed in samples from Saint Helena, California, Big Pine, California, Superior, Arizona, and Socorro, New Mexico, agrees with the measurements given here for thin sections N 10 (Table 6); BR 21 (Table 6) and RM 58 through 68 (Table 8, Section A); RM 1a, RM 7, and RM 8 (Table 6); and RM 6 (Table 6), respectively.

Samples were taken from several perlitic extrusive masses to determine variations in the extent of devitrification within individual flows. About 10 thin sections were prepared from samples representative of each locality; they are listed in Table 8 with the observed depths of detrification.

The Fish Springs perlite deposit (Table 8, section A) is a fine example of a young extrusion dome. Eleven of the 12 samples from this deposit (including thin section BR 21, Table 6)

[11] The presence of argon and the other gases in meterorites indicates that many of them have not been at elevated temperatures (except perhaps momentarily) since their formation. Measurement of the loss (through diffusion) of these gases is one of the most sensitive ways to estimate the mean temperatures to which meteorites have been exposed (Goles, Fish, and Anders, 1960). DuFresne and Anders (1961) draw interesting conclusions from the release of residual strain in fragments of glass from the Mighei carbonaceous chondrite. The age of this meteorite is probably close to that of other carbonaceous chondrites, which have been dated by the lead-lead method (R. R. Marshall, unpublished data) at about 4.6×10^9 years. If this is the case, the rate of annealing of strain is extremely slow at low temperatures.

show no effects of devitrification, although they show crystallites and well-developed flow lines. The exception (RM 68) is a sample from the periphery and near the base of the main body and evidently represents a rim from an earlier phase of the extrusion. In this sample, devitrification occurs to a depth of about 6 μ from the surfaces of vesicles and of some cracks. Many of the cracks, however, show no signs of devitrification except a narrow central filling.

The age of the Lordsburg (New Mexico) perlite deposit (Table 8, section F) is not well established. The minimum depth of devitrification appears to be between 1 and 1.5 μ. Some

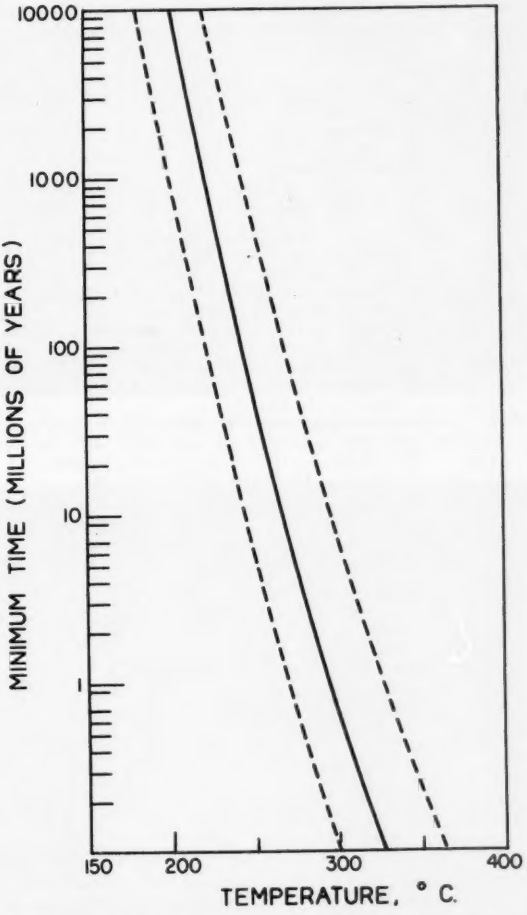

Figure 6. Minimum time required for thermal reconstruction of natural glass plotted against temperature. The curve of minimum time (solid line) was determined from equation Ib, using a crystal length of 10 μ. The dashed curves were plotted using pre-exponential factors 10 times higher (left) and 10 times lower (right); these curves also approximate the curves for activation energies 2.5 kcal/mole lower and higher, respectively.

specimens are considerably devitrified, and surfaces along the larger cracks are more deeply altered.

The most extensive deposit sampled is that in Black Canyon, northwest of Barstow, California. Samples RM 92 through RM 101 are from the eastern side of the hill, RM 102 through RM 106 are from the western side (Table 8, section D). Approximately half the samples have average depths of devitrification of about 1.5 μ. This extrusion is probably the oldest listed in Table 8.

The perlite deposit a few miles west of Shoshone, California, is pre-Quaternary and may be as young as Pliocene. The least altered samples (Table 8, section C) are devitrified to depths of less than about 1.5 μ. The general appearance of these thin sections suggests that the samples from Black Canyon are slightly more devitrified.

Dibblee and Gay (1952) discuss the perlite in Last Chance Canyon, California, and indicate that its age is Pliocene. In places the deposit appears to be macroscopically altered. Only in two thin sections (Pl. 2, fig. 1) are most of the cracks little altered (Table 8, section B). The cracks in the other samples are as deeply devitrified as older flows are. Probably much of the devitrification along these perlitic cracks depends on factors other than time—most likely on increased temperature.

All the samples from the Desolation Canyon area, Death Valley, California (Table 8, section E), are appreciably devitrified (Pl. 2, fig. 3). In the least altered specimen, devitrification extends to an average depth of about 2 μ;

TABLE 7. DEPTH OF DEVITRIFICATION IN VOLCANIC GLASSES OF UNKNOWN AGES
(Perlites unless noted otherwise)

Thin section	Approximate depth of devitrification (μ)	Locality	Donor
RM 21	3.	Lordsburg, New Mex.	M. Peters
RM 25 (pumiceous glass)	0.	U. S. Gypsum deposit, *ca.* 7 mi. N. of railroad, Grants, N. Mex.	"
RM 36	3.	From area S. of Beaverhead, N. Mex.	R. Weber
RM 37	2.	½ mi. W. of Lake Valley (sec. 29, T. 18 S., R. 7 W.), N. Mex.	R. Weber
RM 38*	2.–4.	McDonald Ranch area, *ca.* 16 mi. NW. of Gage (El Paso Perlite Co. deposit, SE¼ sec. 20, T. 22 S., R. 14 W.), Grant Co., N. Mex. Samples approximately ½ mi. apart	R. Weber
RM 39*	1.5		R. Weber
RM 40*	2.	McDonald Ranch area, *ca.* 16 mi. NW. of Gage (Cureton perlite; sec. 33–34, T. 21 S., R. 15 W.), Grant Co., N. Mex.	R. Weber
RM 41*	1.5		R. Weber
RM 42	2.	Morrow Ranch deposit, sec. 19, T. 22 S., R. 14 W., N. Mex.	R. Weber
RM 43	1.5	NW. of NE. sec. 19, T. 22 S., R. 14 W., N. Mex.	R. Weber
RM 44	2.	Center of sec. 12, T. 22 S., R. 15 W., N. Mex.	R. Weber
RM 55	2.	Van Cleve deposit near Las Vegas, Nev.	S. Gindoff
RM 57a	1.	Klondike deposit, just N. of highway between Ludlow and Amboy, Calif.	S. Gindoff
RM 57b (welded tuff)†	2.–3.		S. Gindoff
RM 70	1.5	Eccles deposit, Lincoln Co., Nev.	R. R. Coats
RM 71	2.	NW. ¼ sec. 35, T. 17 N., R. 18 W., Mojave Co., Ariz.	R. R. Coats
RM 73	1.5	Nathrop, Chaffee Co., Colo.	R. R. Coats
RM 75	1.	Sec. 22, T. 4 N., R. 65 E., Lincoln Co., Nev.	R. R. Coats
W 4	7.	Nathrop, Chaffee Co., Colo.	Calif. Inst. Tech. thin section collection
T 273 (green obsidian)	3.	4 mi. from head of Jawbone Canyon by Owens Valley Aqueduct, Calif.	Calif. Inst. Tech. thin section collection

* Probably late Tertiary
† Reddish-brown veining

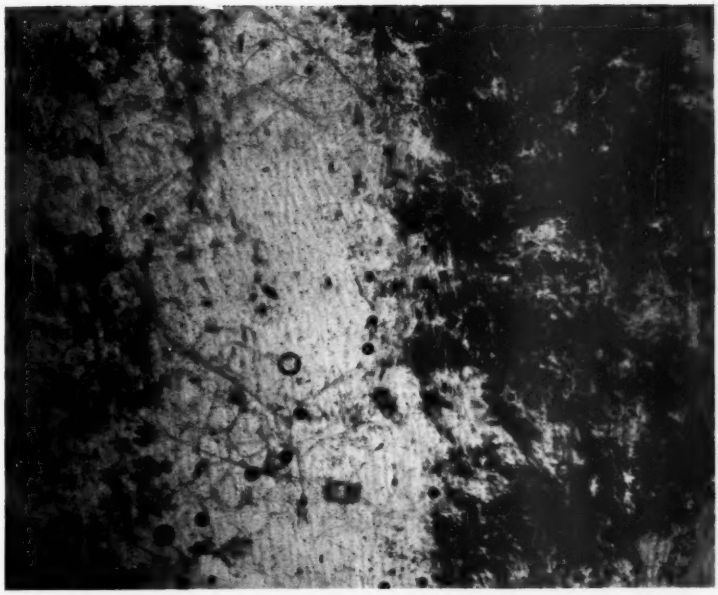

Figure 1. Narrow perlitic cracks showing no devitrification. (Ordinary light, magnification 24×. Dark rings are bubbles in mounting medium)

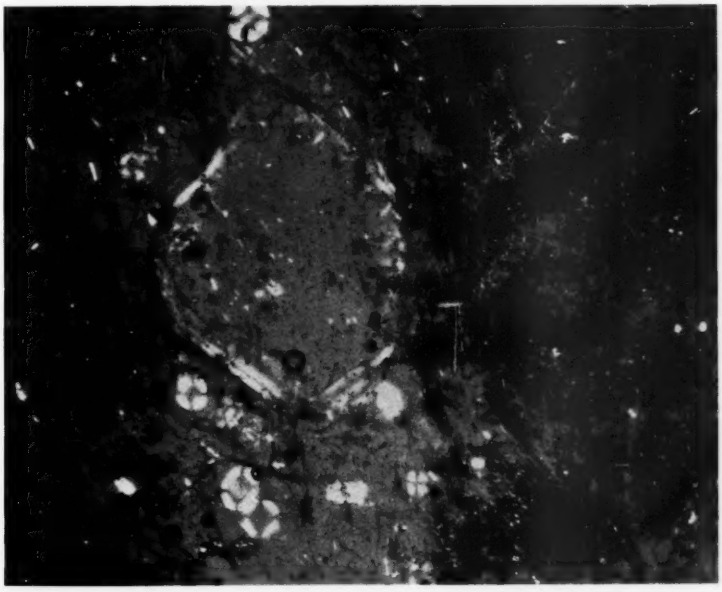

Figure 2. Same view as above with nicols crossed, showing prominent strain birefringence bordering the perlitic cracks

THIN SECTION OF PUMICEOUS PERLITE FROM APPROXIMATELY 7 MILES SOUTH OF BIG PINE, INYO COUNTY, CALIFORNIA

MARSHALL, PLATE 1

Geological Society of America Bulletin, volume 72

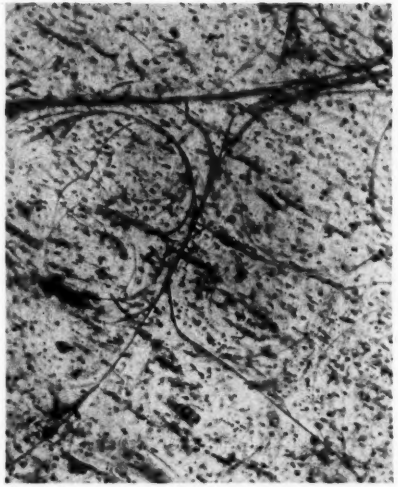

Figure 1. Pliocene perlite, Last Chance Canyon, Mojave Desert, California (thin section RM 128, Table 8, section B). Devitrified layers less than 1 μ thick; many small flow-oriented crystallites

Figure 2. Late Tertiary perlite, near Lordsburg, New Mexico (thin section RM 30, Table 8, section F). Single crack with appreciably devitrified borders

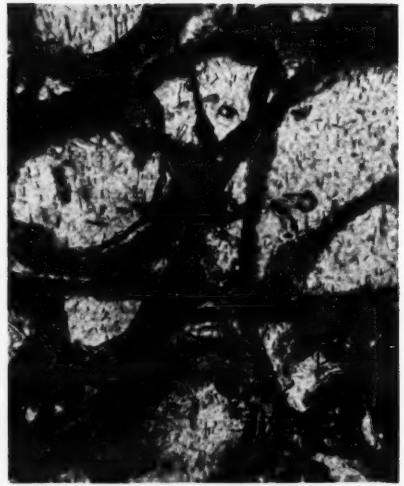

Figure 3. Miocene perlite, Desolation Canyon, Death Valley, California (thin section RM 123, Table 8, section E). Extensively devitrified along the cracks; belonites prominent in the glassy cores

THIN SECTIONS OF THREE PERLITES ILLUSTRATING DIFFERENCES IN DEGREE OF DEVITRIFICATION ALONG FRACTURES (MAGNIFICATION 81×)

according to the trend of Figure 7, this is in general agreement with the Miocene age of the perlite. Because these samples were collected as float, part of the devitrification could be due to exposure at the surface.

Surface temperatures in the desert may rise to well over 50° C on warm days. Because the rate of erosion may vary considerably from one area to another, secular effects within a flow would be most accurately estimated from samples taken from under several feet of cover

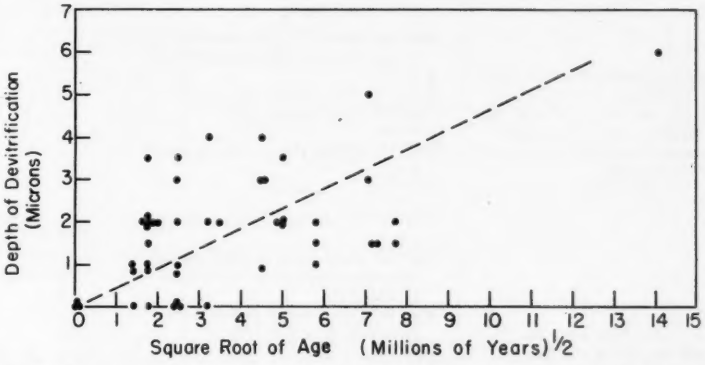

Figure 7. Depth of devitrification for glasses listed in Table 6 compared to geologic age. Dashed line indicates general trend of rate of devitrification

and from a number of widely separated points. Unfortunately, many of the samples examined in this study were not selected with this in mind.

Although many of the samples listed in Tables 6, 7, and 8 are from the surface, some of those from prospect pits also show considerable evidence of devitrification, particularly those from Last Chance Canyon (RM 126, RM 129, and RM 131, Table 8, section B) and that from the drift in Black Canyon (RM 105, Table 8, section D). Much of the variation in degree of devitrification must be due to local hydrothermal action rather than to solar heating. Variation of chemical composition could also be an important factor, but the composition of perlites is quite uniform. They are generally rhyolitic, but a few tend toward dacitic composition.

Completely devitrified perlites. Two completely devitrified perlites were examined. One occurs as opalized volcanic rock in the Mojave Desert about 5 miles north of Leadpipe Spring (about 10 miles northeast of Granite Wells, Searles Lake quadrangle), California. Prominent zones of devitrification extend from the fractures into the groundmass to a depth of approximately 4 μ. Many of the flow-oriented belonites are sharply outlined, but others have irregular margins with a margaritic appearance, owing to secondary enlargement. The groundmass, clear in normal light, appears under crossed nicols as a mosaic of irregular birefringent areas, some only a few microns across and others as large as 10–20 μ across. The products of primary and secondary crystallization remain clearly distinguishable in this sample.

Yellowish nonvitreous rock occurs with layers of unaltered perlite (RM 22, Table 6) along the west boundary of the Inspiration quadrangle, Arizona. The altered rock was perlite, but it has been completely devitrified. Under crossed nicols the fibrous alignment of colorless minerals normal to the perlitic cracks is clearly visible. Devitrification was directed inward from the surfaces along the cracks for lengths of about 100 μ. These closely associated extremes in the degree of alteration suggest that under certain conditions volcanic glasses are especially susceptible to attack under moderate and localized temperatures.

Tuffs. Some welded tuffs which are predominantly glassy have been included in the section on perlite. A few additional tuffs con-

TABLE 8. VARIATION OF DEPTH OF DEVITRIFICATION WITHIN SINGLE EXTRUSIVE MASSES

Locality	Sample*	Depth of devitrification (μ)
A. Fish Springs pumiceous perlite dome, *ca.* 7 mi. S. of Big Pine, Inyo Co., Calif. (late Quaternary)	Thin sections RM 58 through RM 60 (scattered samples from quarry at W. end of dome)	No signs of devitrification, but strain birefringence present
	Thin sections RM 61 through RM 67 (from active quarry at E. end of dome; *ca.* ¾ mi. E. of above exposure†)	No signs of devitrification, but strain birefringence present
	Average	*0.*
	Thin section RM 68 (perlite from base of deposit at E. end of dome, near mill; earlier phase of extrusion)	As much as 6 μ depth of devitrification along many cracks; strain birefringence present
B. Last Chance Canyon, Saltdale quad., Calif. (NW¼ sec. 9, SE¼ sec. 8, and NE¼ sec. 17, T. 29 S., R. 38 E.). Samples from prospect pits and scattered outcrops, from a belt nearly a mile long. (Pliocene)	RM 126 (pieces of perlite surrounded by altered rock; from prospect pit)	4.
	RM 127	2.–3.
	RM 128 (from weathered outcrop)	<1.
	RM 129 (from prospect pit)	3.
	RM 130	<1.
	RM 131 (perlite breccia from prospect pit)	5.
	Average	*2.6*
C. Flows in Dublin Hills a few mi. W. of Shoshone (SW¼ sec. 26, SE¼ sec. 27, NE¼ sec. 34, and NW¼ sec. 35, T. 22 N., R. 6 E.), Shoshone quad., Calif.** Samples scattered over an area of *ca.* ¼ sq. mi. (Probably late Miocene to Pliocene)	RM 107 (banded perlite from prospect pit)	<1.5
	RM 108 (large pieces of black perlitic vitrophyre in rhyolite, *ca.* 60 ft. S. of RM 107)	<1.5
	RM 109 (black perlite in flow breccia *ca.* 450 ft. S. of RM 108)	2.
	RM 110	6.
	RM 111	1.5
	RM 112	2.
	RM 113 (perlite with spherulites)	2.
	RM 114 (banded perlite)	2.
	RM 115	5.
	RM 116 (spherulitic perlite)	2.
	RM 117 (from prospect pit; sample next to altered zone 2–3 in. thick)	2. or <2.
	RM 118 (from prospect pit; one of the least altered samples in appearance)	1.
	RM 77 (Table 6)	0.8
	Average	*2.2*
D. Perlite deposits in Black Canyon, about 3 mi. NW. of Opal Mt., Searles Lake quad., Calif. Samples from large area, separated by distances up to a mile (middle Miocene or older)	RM 92 (perlite breccia)	<1.5
	RM 93 (perlite breccia)	4.
	RM 94	1.
	RM 95	2.
	RM 96 (perlite breccia)	5.
	RM 97	1.5
	RM 98	1.
	RM 99	8.
	RM 100	1.5
	RM 101	1.5
	RM 102 (from prospect pit)	1.5
	RM 103 (from prospect pit)	4.
	RM 104 (from prospect pit)	3.
	RM 105 (from end of drift 15 ft. long)	7.
	RM 80 (Table 6)	3.
	Average	*3.0*
	RM 106 (welded tuff from about 50 ft. W. of drift from which RM 105 came)	(Nearly completely devitrified)

TABLE 8. *Continued*

Locality	Sample*	Depth of devitrification (μ)
E. About 4 mi. SE. of Furnace Creek Inn, Death Valley (sec. 12, T. 26 N., R. 1 E., Furnace Creek quad.), Calif. Scattered samples from large dry wash (Miocene)	RM 121	5.
	RM 122	5.
	RM 123	12.
	RM 124	2.
	RM 125	8.
	Average	*6.4*
F. Lordsburg deposit, *ca.* 10 mi. S. of Lordsburg, N. Mex. Samples from prospect pits and scattered outcrops, generally at least 50 yds apart (late ? Tertiary)	RM 27 (from main pit)	1.5
	RM 28 (brown glass; from main pit, *ca.* 10 ft. away from RM 27)	1.†
	RM 29 (green glass; adjacent to RM 28 in main pit)	1.5
	RM 30	6.
	RM 31	1.5
	RM 32	3.
	RM 33	7.
	RM 34 (from small prospect pit)	4.
	RM 35 (from small prospect pit *ca.* 200 ft. from preceding pit)	2.
	RM 21 (Table 7)	3.
	Average	*3.1*

* Perlite unless noted otherwise
† Sampled through the courtesy of Mr. S. Gindoff, U. S. Mining Corp.
** Sampled through the courtesy of Mr. E. Grimshaw

taining shards of glass were examined; Table 9 compares the thickness of devitrified borders of the shards to the geologic ages of these samples. The variation of thickness of the devitrified layer with age in tuffs agrees quite well with the trend of the measurements for perlites (Fig. 7).

The thin zones of devitrified glass bordering the shards show up well under crossed nicols. Along some of these zones, extinction occurs uniformly for tens of microns. This probably represents one form of devitrification of the shard itself, although such extinction could indicate the deposition of a secondary mineral on the surface.

In welded tuffs, devitrification may have occurred on the surfaces of glass shards at high temperatures during compaction of the ash. Such effects would be difficult to distinguish from those due to the action of water at low temperatures. If the crystalline material could be identified, the presence of hydrated minerals would be significant.

Water and Devitrification

Mechanism. Many experiments indicate that water plays an important role in the low-temperature alteration of glass. The most probable mechanism is the breaking of the strong Si-O-Si bridges by the formation of two hydroxyl groups, each attached to one of the two silicon ions. The diffusion of water molecules and the formation of such hydroxyl groups can break enough cross links so that slight adjustments involving relatively little energy can orient silica tetrahedra. Crystallization also occurs as Si-O-Si bridges re-form; the water molecules moving along act as a catalyst. In the following sections, this mechanism is elaborated upon and used to interpret the observations regarding volcanic glasses and the results of pressure-bomb experiments.

Diffusion equations. Fick's law of diffusion, which refers to the change in concentration, C, of a substance at a particular point in space with the co-ordinate x, as a function of time, t, is:

$$\frac{\delta C}{\delta t} = D\frac{\delta^2 C}{\delta x^2}. \qquad \text{(II)}$$

In this form of the equation, the diffusion coefficient, D, is assumed to be independent of the concentration.

The solution (Barrer, 1951, p. 9, 12) of equation II for the case of diffusion into a semi-infinite solid from a plane surface is:

$$C = C_o\left[1 - \frac{2}{\sqrt{\pi}}\left\{\frac{x}{2\sqrt{Dt}} - \frac{x^3}{3\cdot 1!\,(2\sqrt{Dt})^3} + \frac{x^5}{5\cdot 2!\,(2\sqrt{Dt})^5} - \cdots\right\}\right] \quad \text{(IIIa)}$$

where C_o is the fixed concentration at the surface.

from the leaching of alkalis from artificial glasses (Lyle, 1943). In this application, x represents the amount of sodium dissolved from the glass during a certain length of time, t. The exponent of x must be adjusted to the data, but it is usually near 2. An exchange of sodium ions for protons occurs; the comparatively slow diffusion of sodium ions from the interior to the surface of the glass undoubtedly determines the rate of leaching. Because diffusion of entire water molecules is necessary in order to break the Si-O-Si cross linking, two

Table 9. Devitrified Films on Glass Shards in Tuffs

Sample	Approximate depth of devitrification (μ)	Geologic age	Locality	Donor
RM 90 (welded tuff*)	0.	Pleistocene	From old quarry, SE. corner of Round Valley, near Bishop, Calif.	R. Shreve
SO-3 (tuff)	0.	Pleistocene	From canyon near Fillmore, Fillmore quad. (sec. 28, T. 4 N., R. 20 W.), Calif.	G. Eaton
Capistrano (vitric tuff)	1.	No younger than early Pliocene	Along U.S. Hwy. 101 between Capistrano Beach and Mission San Juan Capistrano, Calif.	
TU (vitric tuff)	0.8	Middle or late Miocene	Just S. of Fascination Springs, San Gabriel Mts. (Sunland quad.), Los Angeles Co., Calif.	
Ttt (vitric tuff)	1.	Middle Miocene	Just E. of El Modeno, Orange Co., Calif.	
Peters Canyon Rd. (crystal vitric tuff)	1.	Early middle or late early Miocene	Along Peters Canyon Rd., due E. of Santa Ana, Calif.	
H-129 (volcanic ash)	1.	Oligocene (?)	Morrill Co., Nebr.	R. L. Miller
H-207 (tuffaceous Wasatch sandstone)	2.–3.	Eocene	Jackson Hole, Wyo.	

* Bishop tuff. *See* Putnam (1949).

One can compute D with less than 20 per cent error in the present application, using the following simplification of equation IIIa:

$$\sqrt{\pi}\left(1 - \frac{C}{C_o}\right) = \frac{x}{\sqrt{Dt}} - \frac{x^3}{12\,(\sqrt{Dt})^3}. \quad \text{(IIIb)}$$

The still simpler expression

$$\pi\left(1 - \frac{C}{C_o}\right)^2 Dt = x^2 \quad \text{(IIIc)}$$

may be used to calculate an approximate value of D.

Equation IIIc can also summarize the data

distinct mechanisms for hydration are possible: exchange and addition. Hydrothermal reconstruction must depend upon addition.

The diffusion of water into glass seems to be such a slow process that finite solids may be considered semi-infinite (the value of x is extremely small compared to the radius of curvature of perlite surfaces). However, the estimation of the diffusion constant for water in volcanic glasses depends upon the following important assumptions:

(1) Perlitic structure forms at essentially the same time at which the rock forms.

(2) Water is always present in the cracks.

(3) The diffusion constant is independent of C, and its variation among different glasses is negligible.

(4) Crystallization occurs in the glasses when the concentration of water molecules, diffusing inward, reaches a sufficiently high value.

Perlitic structure apparently develops as a result of the strain formed during the rapid cooling of silicate melts; strain birefringence characterizes many young perlites. Ground water or water from the atmosphere is probably absorbed by the numerous capillary openings. The energy of hydration for simple adsorption processes is characteristically low. King, Todd, and Kelly (1948) found that the energy of hydration for 65 per cent of the water of the perlite from Superior, Arizona, is no more than about 4 kcal/mole. The heat of chemisorption of liquid water on silica at 23° C is similarly low, 4.7 kcal/mole of water (Brunauer, Kantro, and Weise, 1956).

In addition, Ross and Smith (1955) found that perlites may be dehydrated relatively easily to a water content of about 0.3 per cent. They found that this limit is typical for obsidians and that the rate of change of the index of refraction for perlite is discontinuous at this point, becoming equal to that of obsidian with lower water content. Their studies indicate that generally no more than a few tenths of 1 per cent of the water in perlites is magmatic, the rest being secondary. Isotopic analyses of the water in perlites by Friedman and Smith (1959) support the contention that most of the water is not magmatic in origin. They found that the deuterium-hydrogen ratio is consistently lower for water in perlite than in the local ground water, indicating some isotopic fractionation.

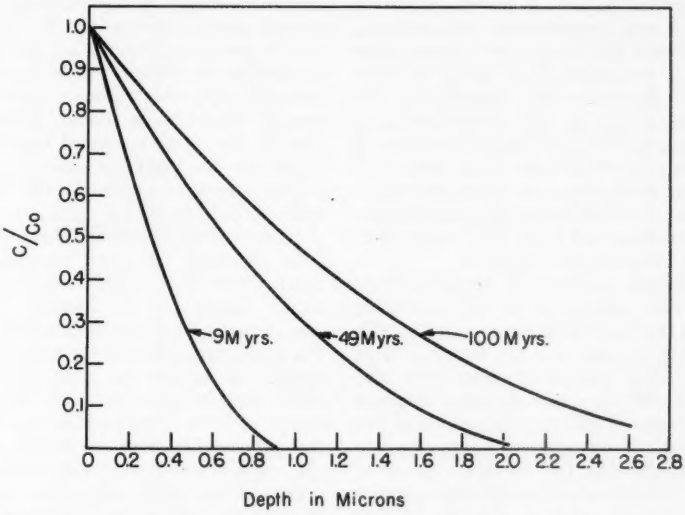

Figure 8. Concentration of water in volcanic glass relative to depth from a saturated surface at about 20° C

Presumably, most of the well-preserved glasses listed in Table 6 have remained at average temperatures of about 20° C since their formation. The rate of devitrification at that temperature may be estimated from Figure 7. Let x be the depth of devitrification in equation IIIb. The average value of x for two ages must be used to calculate the diffusion constant, D, and also the ratio of the concentration of water required for crystallization, C, to the fixed concentration at the surface of the glass, C_o. For depths of devitrification of 1 μ developed during 25 million years (m. y.) and 1.5 μ developed during 64 m. y., the value for D is 9×10^{-11} cm^2/m.y. and that for C/C_o is 0.25. If the rate of devitrification is high enough to produce 2 μ of crystallization during 25 m. y. and 4 μ during 64 m. y. (*See* dashed line, Fig. 7), then D would be 5×10^{-10} cm^2/m. y., and C/C_o would be 0.26. In

view of the smallness of the effects and the uncertainties in their measurement, this second set of average values is not significantly different from the first more conservative ones.[12]

The ratio of C to C_o as a function of depth in the glass, as calculated from equation IIIb using $D = 10^{-10}$ cm²/m. y., is shown in Figure 8 for the periods of 9, 49, and 100 m. y.

Hydrothermal experiments. Fragments from a sample of the pumiceous perlite from the Fish Springs deposit (RM 58, Table 8, section A) were placed in a pressure bomb with sufficient water to insure the presence of a liquid phase throughout the experiment. Table 10 summarizes the data from these experiments. The average depths of the dark alteration zones were measured with an estimated accuracy of 25 per cent. In several experiments the bomb leaked, and, in the absence of water, devitrification did not occur. However, the disappearance of strain birefringence in all the samples indicated that annealing had occurred.

The diffusion constant, D, calculated from equation IIIb with $C/C_o = 0.25$ and using data from the experiment on sample RM 850, is 18 cm²/m.y., and that for RM 853 is 11 cm²/m.y. These two experiments were performed at 330° C over two quite different lengths of time (Table 10); the agreement between these two values for the diffusion constant is satisfactory. The average constant at 330° C is 14 cm²/m.y. The diffusion constant at 260° C (calculated from the data for RM 854) is 4 cm²/m.y., and that at 20° C (estimated from the geological observations) is approximately 10^{-10} cm²/m.y.

With these three diffusion constants, the activation energy, E, for the diffusion process can be calculated from the following equation

$$D = D_o e^{-E/RT} \qquad \text{(IVa)}$$

to be 30 ± 5 kcal/mole.[13]

Another sample of perlite from the Fish Springs deposit which was kept for 2552 hours at 100° C in water at 1 atmosphere of pressure revealed no devitrification. Therefore, the diffusion constant at 100° C is less than 10^{-2} cm²/m.y.; this upper limit is in agreement with the activation energy calculated above.

The activation energy of 30 kcal/mole seems to be somewhat greater than that for the diffusion of sodium ions. Verhoogen (1952), for example, finds only 24 kcal/mole for the activation energy of the diffusion of sodium through quartz, compared to 32 kcal/mole for that of potassium through quartz. Activation energies for the diffusion of the large gas molecules (N_2, O_2, Ar) through fused silica are around 30 kcal/mole (Barrer, 1951, p. 126), close to the value estimated here for water. Values for the small gas molecules (He, Ne, H_2) are around 10 kcal/mole; the larger water molecule or hydroxyl ion should have a greater activation energy, more like that of potassium.

In discussing the $\alpha \rightarrow \beta$ transformation of quartz, Silverman (1956) suggests that the energy barrier for the formation of lattice imperfections in quartz is 32.2 kcal/mole. If this value corresponds to the energy needed to displace an oxygen ion to an interstitial position, then its agreement with the activation energy of 32 kcal/mole for K^{+1} in quartz and that presented here for the diffusion of molecular water in glass is more than satisfactory.

One of the most interesting comparisons between the diffusion constants estimated here and independent experiments may be deduced from equation IVa rewritten in terms of the theory of absolute reaction rates (Glasstone, Laidler, and Eyring, 1941, p. 524), thus:

$$D = \left(\frac{kT}{h}\right) d^2 e^{\Delta S^*/R} e^{-\Delta H^*/RT}. \qquad \text{(IVb)}$$

Assuming that a water molecule shifts a distance d of several Å, ΔS^* is about 5 cal/mole deg. This calculation is approximate because of the uncertainty in the value for the activation energy. However, ΔS^* in this case is comparable to the entropy of hydration in crystals, which is 5–10 cal/mole deg (Fyfe, Turner, and Verhoogen, 1958, p. 117); in particular, it is much more positive than the ΔS^* for thermal reconstruction.

Time-temperature relationships for hydrothermal reconstruction. In perlites, fracturing has occurred down to small cores of about 100-μ radius. One can calculate the lengths of time required for water to diffuse to the center of these cores with the diffusion con-

[12] Marshall (1954) reported an upper limit of 10^{-3} cm²/m. y. for the diffusion constant.

[13] Todd (1955) gives activation energies for the escape of water from various artificial glasses. The low concentrations of water in these glasses would be present as scattered hydroxyl groups. Outgassing of this water must be a more complicated process than the diffusion of individual water molecules as paired hydroxyl groups. Depending on the chemical composition of the glass, Todd's values for the activation energy range from 36 to more than 70 kcal/mole; these are significantly greater than the energy calculated here for the simple diffusion of water.

stant at various temperatures. Using an activation energy of 30 kcal/mole for the diffusion constant and $C/C_o = 0.25$, the time required for devitrification by hydrothermal reconstruction can be expressed as a function of the temperature, as Figure 9 shows. The selection of 100 μ as a typical depth of devitrification is consistent with the maximum lengths (20–100 μ) reported in this paper for optically continuous secondary crystalline material in completely devitrified perlite.

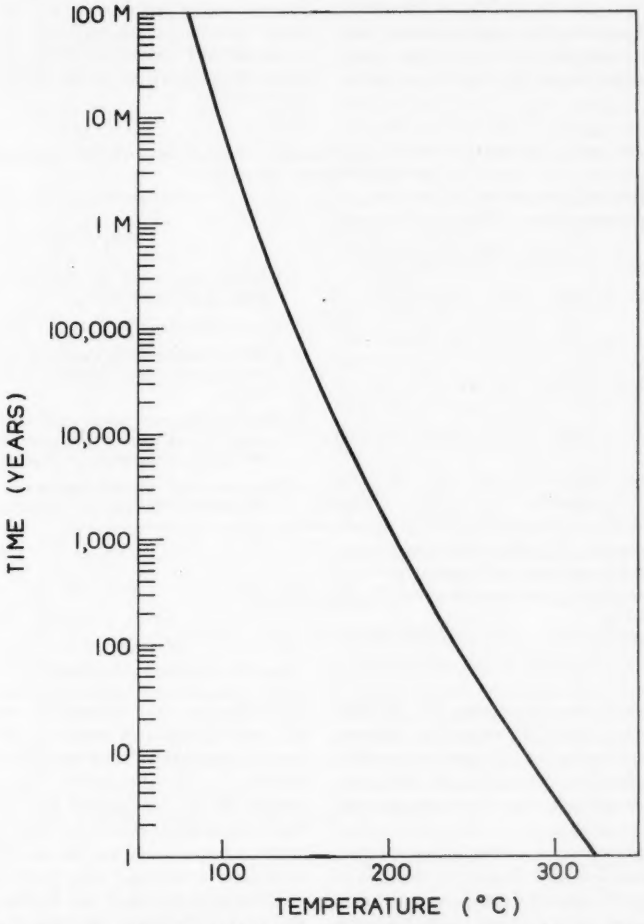

Figure 9. Time required for the hydrothermal reconstruction of perlite to a depth of 100 μ as a function of temperature

In obsidian from Obsidian Cliff, Yellowstone National Park, Wyoming,[14] vesicles are lined with devitrified zones 100–200 μ thick, forming lithophysae. Lithophysae (including those which are much larger than in the example given here) evidently develop through hydrothermal alteration of the walls of vesicles during the later stages of the cooling of glassy flows. Upon extrusion, the lava expels gases, including water vapor. The water that does not escape

[14] California Institute of Technology thin section T 493

before the lava becomes rigid attacks the walls of the vesicles as the temperature falls gradually through the last few hundred degrees.

Water content of perlites and pitchstones. Perlites typically contain 2–5 per cent water, a large amount for most volcanic glasses. In accounting for the devitrification bordering the cracks, it is reasonable to suppose that most of this water is present in or along the cracks. That such is the case is also indicated by the sample from Dry Gulch, Wenatchee, Washington, have large total water contents. These rocks combine the features of both perlites and pitchstones. The Lordsburg material, in particular, can be described as a perlitic pitchstone. Although the approximately 10 per cent water in pitchstones could very well be homogeneously distributed throughout the glass, the total amount seems to be too small to bring about devitrification. In the preceding section,

TABLE 10. DATA FROM PRESSURE-BOMB EXPERIMENTS, USING PUMICEOUS PERLITE FRAGMENTS FROM FISH SPRINGS, CALIFORNIA

Thin section	Temperature (°C)*	Pressure† (atm)	Time (hr)	Observations**
RM 850	330	130	98	Scattered dark-brown to black patches and zones; depth of alteration = 7 μ
RM 851	330	1††	533	No altered zones or patches
RM 852	330	1††	116	A few small scattered dark zones on one side of section; may be secondary effects. Depth of alteration <5 μ
RM 853	330	130	650	Extensive alteration; large yellow-brown areas, as well as many dark patches and zones like those in RM 850; depth of alteration = 14 μ
RM 854***	260	48	292	Extensive dark patches and zones like those in
	330	1††	2,550	850 and RM 853; depth of alteration = 6 μ

* Temperature held to within 15° C of these values
† Taken as the vapor pressure of water
** Strain birefringence not found in any of these heated samples
†† Bomb leaked
*** Bomb cooled but not opened before temperature was raised to 330° C

ease with which the water may be expelled from the rock. Other glasses with a resinous luster and a still higher water content are called pitchstones. Because the latter are often unfractured, it is unlikely that the water in them is secondary in origin.

The water contents of some of the volcanic glasses listed in Tables 6, 7, and 8 are listed in Table 11. Approximately 1-gm portions of perlite, which had been crushed in a diamond mortar but not sized, were heated for 2 hours at 105° C. The loss in weight is reported in the column headed H_2O^-. The water driven off from aliquots of the same samples in 1 hour at temperatures above 800° C was condensed in Penfield tubes and weighed to give the total H_2O content. The H_2O^+ is the total water less the H_2O^-.

Samples from Lordsburg, New Mexico (RM 28, RM 30, and RM 32 in Table 11), and the

devitrification was calculated to occur when the concentration of water in the perlite becomes equal to 0.25 of the effective concentration (C_o) at the surface. Because glass is metastable, it can absorb much more water than silicate melts dissolve at their high temperatures, or more than can be accommodated by crystalline structure. The hydration of silica surfaces indicates that the C_o for glass is 100 per cent. Therefore, devitrification seems to require the presence of approximately 25 per cent water, more than twice as much as that occurring in pitchstones. This is the amount necessary to break approximately one half of the Si-O-Si, Si-O-Al, and Al-O-Al cross linkages. Probably much of the water acts as a catalyst and is forced out when crystallization takes place. However, zeolites are commonly formed in the process of devitrification (Harris and Brindley, 1954), and most of the other

products are probably more or less hydrated.

The water content of perlites varies because the amount of water trapped in the magma upon quenching varies greatly, as does the extent of fracturing and the surface area available for adsorption. However, water could be gradually acquired to replenish that which diffuses inward from the surfaces and to hydrate the products of devitrification. The most loosely bound water content (H_2O^-, Table 11) of a perlite is generally greater for greater depths of devitrification (Tables 6, 8). Apparently, the crystalline phase along the fractures holds water very loosely. If the fractures in perlite are not completely sealed with secondary minerals, the older glasses, such as that from Dry Gulch, should have higher water contents. Even a sample of middle Tertiary age or older has a slightly greater total water content than one from the late Quaternary (*cf.* samples RM 81 and RM 58 in Table 11), although such small differences may well be due only to variations of the compositions of the magmas. Data reported by Allen (1946, Pl. 8A) indicate that under certain conditions perlite continues to pick up more water with time. His frequency distribution curve for a large number of water analyses of samples of an Eocene perlite is strikingly skewed to the side of higher water content. Most of his samples have total water contents close to 3.3 per cent (ranging from about 2.9 per cent to 3.7 per cent); the others, including those for a number of surface samples, range up to around 5 per cent.

TABLE 11. WATER ANALYSES* OF PERLITES

Sample† and age	H_2O^{-}** (%)	H_2O^{+} (%)	Temperature for H_2O^{+} release (°C)††
RM 58 (late Quaternary)	0.01	2.98	950
	0.03	3.01	
		2.97	
		3.00	
		3.19***	~960
RM 81 (Middle Miocene or older)	0.61	2.58	900
		2.97***	~960
RM 4 (Pliocene or late Miocene)	0.33	4.29	825
RM 28 (late? Tertiary)	1.10	7.03	825
RM 30 (late? Tertiary)	1.09	6.36	825
RM 32 (late? Tertiary)	0.52	6.04	825
Dry Gulch††† (middle Eocene)	1.86	5.62	900
	2.10	5.68***	~960

* By the Penfield method, unless noted otherwise

† Refer to description of corresponding thin sections in Tables 6 and 8.

** Sample held for 2 hours at 105° C

†† Sample held for 1 hour at this temperature

*** Ignition in platinum

††† Huntting (1949) found 5.6, 5.0, and 5.0 per cent H_2O^{+} in three samples from Dry Gulch. The H_2O^{-} was 0.6–0.7 per cent.

Hydrothermal reconstruction of basaltic glasses. Crystallization occurs in acidic glasses when the concentration of water is sufficient to break about one-fourth of the network-forming bonds (Si-O, Al-O). In basaltic glasses, there are fewer of these bonds. Assuming that in this case the same proportion must be broken, the amount of water (C) required for crystallization is only about 15 per cent. The diffusion constant for water in basaltic glass would not differ significantly from that in acidic glass; therefore, the time necessary for hydrothermal reconstruction of basaltic glasses, as derived from equation IIIc, must be about 20 per cent shorter than that for acidic glasses.

SUMMARY

Thermal reconstruction or crystallization of volcanic glasses in the presence of very small amounts of water is a very slow process at low temperatures. A high activation energy of at least 50 kcal/mole appears to control the process. Little devitrification can occur through this mechanism at temperatures below several hundred degrees centigrade even within the longest geologic (or meteoritic) time.

The temperatures necessary for thermal reconstruction occur on earth at present only at considerable depths or in areas with unusually high geothermal gradients. Volcanic glasses do occur in such areas; probably some of them are transformed through heat alone. Most volcanic glasses, however, must change through other processes involving water, particularly in those cases in which the surface area is relatively large compared to the volume.

In view of (1) the characteristically high water content of perlites, (2) the ease with which most of the water is removed or the fact

that most of the water is held in a way different from that of the small amounts characteristic of obsidians (Ross and Smith, 1955) and the large amounts characteristic of pitchstones, (3) the localization of secondary effects along the cracks, and (4) the alteration of glass by water at only a few hundred degrees, it may be concluded that perlites develop in the following way:[15]

A magma cools rapidly and its viscosity increases to the point where the rates of crystal growth are insignificant, and a glass forms. If subsequent cooling at still lower temperatures (in the annealing range) is also rapid, the strain at very low temperatures is enough to shatter the glass. Although part of the strain is removed in the shattering, perlitic structure may be initially accompanied by strain birefringence. Water is absorbed into the cracks of the glass from the ground or from the atmosphere, and in the following years material dissolved from the surfaces is reprecipitated in the cracks, possibly reducing the permeability of the perlite. Heating of the rock to no more than 100° or 200° C may produce a thin but readily observable devitrified layer along the surfaces of the cracks and may anneal out strain birefringence. The least devitrified samples from flows indicate a secular change from glass to crystallinity at temperatures around 20° C. The effect is slight; films only 2–5 μ thick form in 100 million years.

The surface devitrification of perlites can be interpreted in terms of the diffusion of water. Water can break the strong Si-O-Si bridge by forming hydroxyl groups, allowing small groups of atoms to relax thermally to form crystalline units. The diffusion coefficient is calculated to be approximately 10^{-10} cm^2/m.y. at 20° C. Hydrothermal alteration of perlite in a pressure bomb indicates that devitrification is very sensitive to temperature; its activation energy is estimated to be 30 kcal/mole. This value is about one-half that for thermal reconstruction; of greater significance in comparing the rates is the much more positive entropy of activation for hydrothermal reconstruction. The amount of water in perlites also seems to be related to the extent of devitrification and to geologic age.

Within a given time, devitrification of volcanic glass in the presence of water (hydrothermal reconstruction) occurs at temperatures at least 200° C lower than those necessary for thermal reconstruction. The ubiquity of water on the earth severely limits the existence of volcanic glasses and accounts for the absence of glass in old formations.

[15] The origin of perlite has also been discussed by Wilfley and Taylor (1953), Chesterman (1954), Ross and Smith (1955), and Friedman and Smith (1959).

REFERENCES CITED

Allen, J. E., 1946, Perlite deposits near the Deschutes River—Southern Wasco County, Oregon: Ore. Dept. Geol. and Min. Ind. Short Paper No. 16, 17 p.

Anderson, F. G., Selvig, W. A., Baur, G. S., Colbassani, P. J., and Bank, W., 1956, Composition of perlite: U. S. Bur. Mines Rept. of Inv. 5199, 13 p.

Barksdale, J. D., 1951, Cretaceous glassy welded tuffs—Lewis and Clark County, Montana: Am. Jour. Sci., v. 249, p. 439–443

Barrer, R. M., 1951, Diffusion in and through solids: corrected ed., Cambridge Univ. Press, 464 p.

Bonney, T. G., and Parkinson, J., 1903, On primary and secondary devitrification in glassy igneous rocks: Geol. Soc. London Quart. Jour., v. 59, p. 429–444

Brunauer, S., Kantro, D. L., and Weise, C. H., 1956, The surface energies of amorphous silica and hydrous amorphous silica: Canadian Jour. Chemistry, v. 34, p. 1483–1496

Cantrill, T. C., and Thomas, H. H., 1906, On the igneous and associated sedimentary rocks of Llangynog (Caermarithenshire): Geol. Soc. London Quart. Jour., v. 62, p. 223–250

Chesterman, C. W., 1954, Genesis of perlite (Abstract): Geol. Soc. America Bull., v. 65, p. 1336

Condon, E. U., 1954, Physics of the glassy state, II. The transformation region: Am. Jour. Physics, v. 22, p. 132–142

Dibblee, T. W., Jr., and Gay, T. E., Jr., 1952, Mineral deposits of Saltdale quadrangle: Calif. Div. Mines Bull. 160, 66 p.

DuFresne, E. R., and Anders, E., 1961, The record in the meteorites —V. A thermometer mineral in the Mighei carbonaceous chondrite: Geochim. Cosmochim. Acta, v. 23, p. 200–208

Eitel, W., 1954, The physical chemistry of the silicates: Chicago, Univ. Chicago Press, 1592 p.

Elliott, R. B., 1956, The Eskdalemuir tholeiite and its contribution to an understanding of tholeiite genesis: Mineralogical Mag., v. 31, p. 245–254

Foote, W. M., 1912, Preliminary note on the shower of meteoric stones near Holbrook, Navajo County, Arizona, July 19th, 1912, including a reference to the Perseid swarm of meteors visible from July 11th to August 22d: Am. Jour. Sci., 4th ser., v. 34, p. 437–456

Friedman, I., and Smith, R. L., 1959, The deuterium content of water in some volcanic glasses: Geochim. Cosmochim. Acta, v. 15, p. 218–228

Fyfe, W. S., Turner, F. J., and Verhoogen, J., 1958, Metamorphic reactions and metamorphic facies: Geol. Soc. America Mem. 73, 259 p.

Geiss, J., and Hess, D. C., 1958, Argon-potassium ages and the isotopic composition of argon from meteorites: Astrophys. Jour., v. 127, p. 224–236

George, W. O., 1924, The relation of the physical properties of natural glasses to their chemical composition: Jour. Geology, v. 32, p. 353–372

Glasstone, S., Laidler, K. J., and Eyring, H., 1941, The theory of rate processes: New York, McGraw-Hill Book Co., 611 p.

Goles, G. G., Fish, R. A., and Anders, E., 1960, The record in the meteorites —I. The former environment of stone meteorites as deduced from K^{40}-Ar^{40} ages: Geochim. Cosmochim. Acta, v. 19, p.177–195

Grauer, O. H., and Hamilton, E. H., 1950, An improved apparatus for the determination of liquidus temperatures and rates of crystal growth in glasses: Jour. Research U. S. Natl. Bur. Standards, v. 44, Research Paper RP2096, p. 495–502

Harris, P. G., and Brindley, G. W., 1954, Mordenite as an alteration product of a pitchstone glass: Am. Mineralogist, v. 39, p. 819–824

Hauser, E. A., and Reynolds, H. H., 1939, Alteration of glasses to montmorillonite: Am. Mineralogist, v. 24, p. 590–597

Hawkes, L., 1930, On rock glass, and the solid and liquid states: Geological Mag., v. 67, p. 17–24

Huntting, M. T., 1949, Perlite and other volcanic glass occurrences in Washington: Wash. Div. Mines and Geology, Rept. of Inv. No. 17, 77 p.

Jones, G. O., and Simon, F. E., 1949, What is a glass? : Endeavour, v. 8, p. 175–181

King, E. G., Todd, S. S., and Kelley, K. K., 1948, Perlite: thermal data and energy required for expansion: U. S. Bur. Mines Rept. of Inv. 4394, 15 p.

Kittle, E., 1912, Experimentelle Untersuchungen, über Kristallisation-geschwindigkeit und Kristallisationsvermögen von Silikaten: Zeitschr. f. anorg. Chem., v. 77, p. 335–364

Königsberger, J., and Müller, W. J., 1906, Versuche über die Bildung von Quarz und Silikaten: Centralbl. f. Mineral. Geol. u. Paläon., v. 339, p. 353–372

Lyle, A. K., 1943, Theoretical aspects of chemical attack of glasses by water: Am. Ceramic Soc. Jour., v. 26, p. 201–204

Marshall, R. R., 1954, Devitrification in perlite (Abstract): Geol. Soc. America Bull., v. 65, p. 1281–1282 (*reprinted in* Am. Mineralogist, 1955, v. 40, p. 325)

Morey, G. W., 1954, The properties of glass: 2d ed., New York, Reinhold Pub. Co., 591 p.

Norton, F. H., 1941, Hydrothermal formation of clay minerals in the laboratory, Part II: Am. Mineralogist, v. 26, p. 1–17

Putnam, W. C., 1949, Quaternary geology of the June Lake district, California: Geol. Soc. America Bull., v. 60, p. 1281–1302

Quirke, T. T., 1919, The Richardton meteorite: Jour. Geology, v. 27, p. 431–448

Richards, W. T., 1936, Remarks concerning the formation and crystallization of vitreous media: Jour. Chem. Phys., v. 4, p. 449–457

Ross, C. S., and Smith, R. L., 1955, Water and other volatiles in volcanic glasses: Am. Mineralogist, v. 40, p. 1071–1089

Rutley, F., 1886, Notes on alteration induced by heat in certain vitreous rocks: Royal Soc. London Proc., v. 40, p. 430–440

——1888, On perlitic felsites, probably of Archean age, from the flanks of the Herefordshire Beacon; and on the possible origin of some epidosites: Geol. Soc. London Quart. Jour., v. 44, p. 740–744

Silverman, S. M., 1956, Transformation of quartz: Jour. Chem. Phys., v. 25, p. 1081

Smoluchowski, R., Mayer, J. E., and Weyl, W. A., *Editors,* 1951, Phase transformations in solids: New York, John Wiley & Sons, Inc., 660 p.

Sudo, T., 1951, Minerals from pumiceous tuff in Japan: Science, v. 113, p. 266–267

Swift, H. R., 1947a, Some experiments on crystal growth and solution in glasses: Am. Ceramic Soc. Jour., v. 30, p. 165–169

—— 1947b, Effect of magnesia and alumina on rate of crystal growth in some soda-lime-silica glasses: Am. Ceramic Soc. Jour., v. 30, p. 170–174

Tammann, G., 1914, Ein Verfahren zur Erzwingung spontaner Kristallization: Zeit. f. anorg. Chem., v. 87, p. 248–252

Todd, J. B., 1955, Outgassing of glass: Jour. Applied Physics, v. 26, p. 1238–1243

Verhoogen, J., 1952, Ionic diffusion and electrical conductivity in quartz: Am. Mineralogist, v. 37, p. 637–655

Vogt, J. H. L., 1921, The physical chemistry of the crystallization and magmatic differentiation of igneous rocks: Jour. Geology, v. 29, p. 318–350

Volarovich, M. P., and Leontieva, A. A., 1948, Linear velocity of crystallization of rock melts as affected by pressure: Mineral. Abstracts, v. 10, p. 322 (Compte Rendues (Doklady) Acad. Sci. U. S. S. R., 1947, v. 55, p. 241–242)

Washington, H. S., 1917, Chemical analyses of igneous rocks: U. S. Geol. Survey Prof. Paper 99, 1201 p.

Wilfley, R. D., and Taylor, C. W., June, 1953, Perlite mining and processing—a new industry for the West: Eng. and Min. Jour., v. 151, no. 6, p. 80–83

Williams, H., 1922, The igneous rocks of the Capel Curig district (North Wales): Liverpool Geol. Soc. Proc., v. 13, p. 166–202

Winkler, H., 1949, Crystallization of basaltic magma as recorded by variation in crystal size in dikes: Mineralogical Mag., v. 28, p. 557–574

Manuscript Received by the Secretary of the Society, May 9, 1960

Publications of the Division of Geological Sciences, California Institute of Technology, Pasadena, California (Contribution No. 1008)

PAUL C. BATEMAN *U. S. Geological Survey, Menlo Park, Calif.*

Granitic Formations in the East-Central Sierra Nevada Near Bishop, California

Abstract: This report establishes lithologic units among the granitic rocks of the east-central Sierra Nevada near Bishop, California. In this area the Sierra Nevada batholith is composed chiefly of quartz-bearing plutonic rocks ranging in composition from quartz diorite to alaskite but includes scattered small masses of darker and older plutonic rocks and remnants of metamorphosed sedimentary and volcanic rocks. The granitic rocks are in discrete plutons, either in sharp contact with one another or separated by thin septa of metamorphic or mafic igneous rock or by late aplitic dikes. The granitic rocks are grouped into lithologic units on the basis of composition, texture, and intrusive relations. The units include six new formations, three informal units made up of the rocks in several plutons, and four informal units that include the rocks in single plutons. The new formations are the Inconsolable Granodiorite, Tinemaha Granodiorite, Wheeler Crest Quartz Monzonite, Round Valley Peak Granodiorite, Lamarck Granodiorite, and Tungsten Hills Quartz Monzonite.

CONTENTS

Introduction 1521
General geologic relations 1521
Cartographic groupings 1523
Compositional classification 1523
Analytic data 1524
Sequence of emplacement 1526
Age 1527
New formations 1528
Inconsolable Granodiorite 1528
Tinemaha Granodiorite 1529
Wheeler Crest Quartz Monzonite 1530
Round Valley Peak Granodiorite 1532
Lamarck Granodiorite 1532
Tungsten Hills Quartz Monzonite 1533
Informal units that include the rock in several plutons 1534
Informal units that include the rock in single plutons 1536
References cited 1537

Figure

1. Map of the bedrock geology in the east-central Sierra Nevada near Bishop, California . . 1522
2. System of classification of the granitic rocks of the Sierra Nevada near Bishop, California 1524
3. Plot of normative quartz, orthoclase, and plagioclase in the granitic rocks of the Sierra Nevada near Bishop, California . . 1527
4. Plot of modal averages of quartz, K feldspar, and plagioclase in different plutons of the Sierra Nevada near Bishop, California . . 1529
5. Diagram showing intrusive relations and probable age sequence of the granitic rocks of the Sierra Nevada near Bishop, California . . 1530

Table

1. Summary of chemical and spectrographic analyses of the granitic rocks of the Sierra Nevada near Bishop, California 1525
2. Norms of the granitic rocks of the Sierra Nevada near Bishop, California 1526
3. Averages of modal analyses for different plutons of the Sierra Nevada near Bishop, California 1528
4. Lead-alpha ages of the granitic rocks of the Sierra Nevada near Bishop, California . . 1531

INTRODUCTION

As part of a co-operative program of the U.S. Geological Survey with the California Division of Mines seven 15-minute quadrangles in the east-central Sierra Nevada have been mapped, and the mapping of several others is in progress. Several reports, chiefly ones dealing with the mineral deposits of the district, have been published, and others are being prepared for publication. In the reports published on this region the granitic rocks have been designated by informal names. The purpose of this report is to establish lithologic units and designate formation names for the more extensive or significant granitic rocks near Bishop, California.

GENERAL GEOLOGIC RELATIONS

The Sierra Nevada batholith in its east-central part is composed chiefly of granitic

Geological Society of America Bulletin, v. 72, p. 1521–1538, 5 figs., October 1961

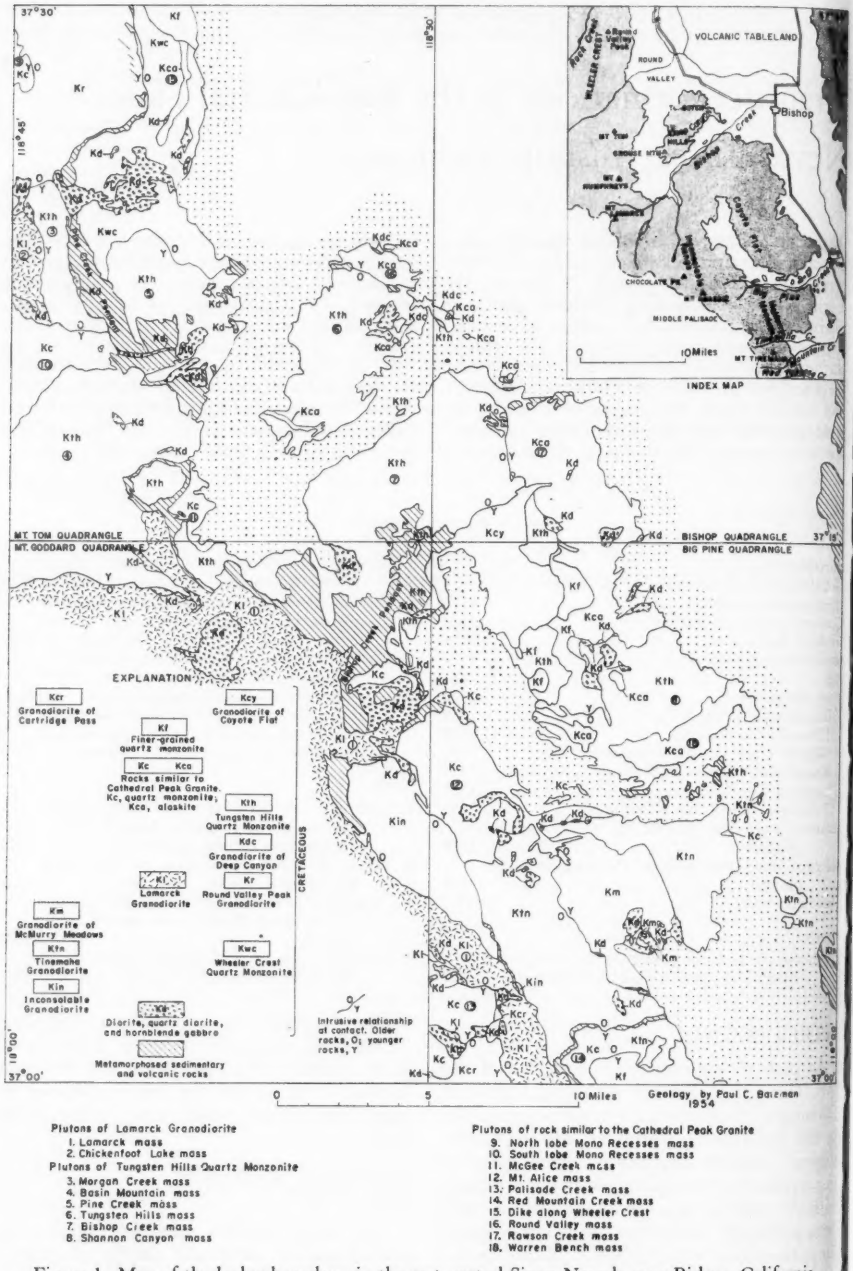
INDEX MAP
VOLCANIC TABLELAND
Bishop
10 Miles
MT. TOM QUADRANGLE
MT. GODDARD QUADRANGLE
BISHOP QUADRANGLE
BIG PINE QUADRANGLE
EXPLANATION
Granodiorite of Cartridge Pass
Granodiorite of Coyote Flat
Finer-grained quartz monzonite
Rocks similar to Cathedral Peak Granite. Kc, quartz monzonite; Kca, alaskite
Tungsten Hills Quartz Monzonite
Granodiorite of Deep Canyon
Lamarck Granodiorite
Round Valley Peak Granodiorite
Granodiorite of McMurry Meadows
Tinemaha Granodiorite
Wheeler Crest Quartz Monzonite
Inconsolable Granodiorite
Diorite, quartz diorite, and hornblende gabbro
Metamorphosed sedimentary and volcanic rocks
Intrusive relationship at contact. Older rocks, O; younger rocks, Y
CRETACEOUS
0 5 10 Miles
Geology by Paul C. Bateman 1954
Plutons of Lamarck Granodiorite
1. Lamarck mass
2. Chickenfoot Lake mass
Plutons of Tungsten Hills Quartz Monzonite
3. Morgan Creek mass
4. Basin Mountain mass
5. Pine Creek mass
6. Tungsten Hills mass
7. Bishop Creek mass
8. Shannon Canyon mass
Plutons of rock similar to the Cathedral Peak Granite
9. North lobe Mono Recesses mass
10. South lobe Mono Recesses mass
11. McGee Creek mass
12. Mt. Alice mass
13. Palisade Creek mass
14. Red Mountain Creek mass
15. Dike along Wheeler Crest
16. Round Valley mass
17. Rowson Creek mass
18. Warren Bench mass

Figure 1. Map of the bedrock geology in the east-central Sierra Nevada near Bishop, California

rocks ranging in composition from quartz diorite to alaskite but includes scattered smaller masses of darker and older plutonic rocks and remnants of metamorphosed sedimentary and volcanic rocks (Fig. 1). The granitic rocks are in discrete masses or plutons that are in sharp contact with one another or are separated by thin septa of metamorphic or mafic igneous rock or by late aplitic dikes that were intruded along contacts between plutons. Rocks in the compositional ranges of quartz monzonite and granodiorite predominate and are about equally abundant.

Individual plutons range from less than a square mile to 50 square miles or more in exposed area. The Lamarck pluton may underlie several hundred square miles. On the whole the batholith appears to consist of a few large plutons and many smaller ones.

CARTOGRAPHIC GROUPINGS

Where the granitic rocks of the Sierra Nevada have been mapped in detail, it has been found possible to distinguish lithologic units on the basis of composition, texture, and intrusive relations. Some lithologic units are of formational rank; others are informal units that include the rock in several plutons or the rock in single plutons. Where two or more plutons are assigned to the same formation, approximate temporal equivalence is assumed. Slight age differences between correlated plutons are considered allowable because the cooling period of an intrusion may be of considerable duration, and some lobes may be slightly older than others. Such age differences among intrusive masses assigned to the same formation are analogous to age differences in transgressive or regressive sedimentary formations.

Thirteen lithologic units of granitic rock have been distinguished in the area near Bishop, California; six are designated formations (the Inconsolable Granodiorite, Tinemaha Granodiorite, Wheeler Crest Quartz Monzonite, Round Valley Peak Granodiorite, Lamarck Granodiorite, and Tungsten Hills quartz monzonite). Each of the plutons assigned to the new formations has been named, and one chosen from each formation as the type mass or pluton. Should subsequent information such as re-evaluated field evidence, radiometric age determinations, or isotopic studies show that the type mass and another mass assigned to the same formation are not approximately of the same age, the type mass should retain the formational name, and the other mass should be assigned to another lithologic unit.

Three informal lithologic units include the rock in several plutons. "Diorite, quartz diorite, and hornblende gabbro" includes scattered small bodies of different composition and texture, but all older than the more felsic granitic rocks. "Finer-grained quartz monzonite" includes several plutons of compositionally and texturally similar rock for which compelling evidence of temporal equivalence is lacking. "Rocks similar to the Cathedral Peak granite" include bodies of quartz monzonite and alaskite similar in composition and in places similar in texture to the Cathedral Peak Granite of Yosemite (F. Calkins, *in* Matthes, 1930, p. 126–127). These rocks may actually be part of the Cathedral Peak Granite but are not continuous with the Cathedral Peak Granite in the Yosemite region, and approximate temporal equivalence has not been established.

The other four informal lithologic units refer to rocks in single plutons that have no known counterparts; no purpose would be served by adding new formational names to already overburdened lexicons for the rocks in these plutons. They include the granodiorite of McMurry Meadows, granodiorite of Deep Canyon, granodiorite of Coyote Flat, and granodiorite of Cartridge Pass.

COMPOSITIONAL CLASSIFICATION

The compositional classification used (Fig. 2) is modal and is similar to several published systems. The granitic rocks contain at least 10 per cent quartz. Boundaries between the fields of the different granitic rocks are in terms of the ratio of K feldspar (including perthite) to total feldspar as follows: quartz diorite, 0–10 per cent; granodiorite, 10–35 per cent; quartz monzonite, 35–65 per cent; granite, more than 65 per cent. Few Sierran rocks fall in the granite field as defined; however, many geologists class granitic rocks in which the modal plagioclase is albite (An_{0-10}) as granite even though the rocks plot in the quartz monzonite field as defined in this report. In the Bishop area, rocks in which the plagioclase is albite contain only a few per cent of mafic minerals and are called alaskite rather than granite.

Near the plagioclase corner of the diagram, quartz diorite passes into diorite where the quartz content is less than 10 per cent of the total content of the felsic minerals, or into hornblende gabbro where the anorthite content

of the plagioclase is more than 50 per cent. Most of the relatively small masses of older mafic rock are either hornblende gabbro or quartz diorite; some are dark granodiorite and a few are diorite.

The composition indicated by the names of the units is the average composition of the unit. Cathedral Peak granite (Knopf, 1918, p. 68) was used. The nine specimens analyzed by standard chemical methods were also analyzed by quantitative spectrographic means for minor elements. Table 1 summarizes the chemical and spectrographic analyses. C.I.P.W. norms are given in Table 2 and plotted in Figure 3.

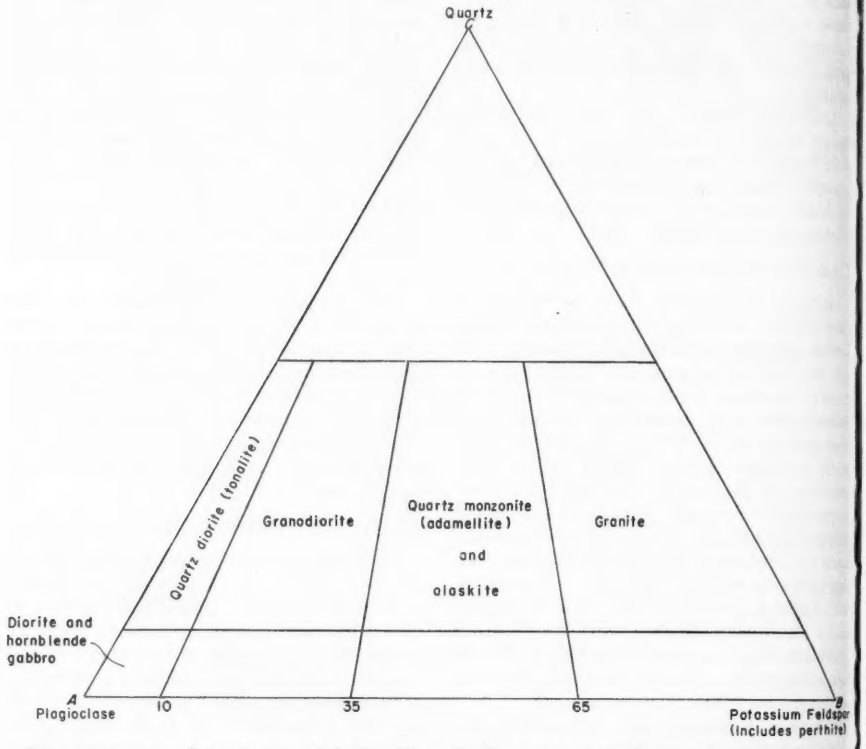

Figure 2. System of classification of the granitic rocks of the Sierra Nevada near Bishop, California

Many plutons, especially those designated granodiorite, are compositionally zoned and include two or more compositional variants.

ANALYTIC DATA

Two kinds of analytic data were obtained from the granitic rocks: limited chemical data and extensive modal data. Fourteen samples were analyzed chemically, nine by standard methods and five by the rapid method described by Shapiro and Brannock (1956). In addition, a partial analysis of a sample of alaskite from the Bishop area similar to that in the

The modes of about 300 samples of granitic rocks were determined using thin sections of standard size (averaging about 0.8 square inch) and a point counter of the type Chayes (1949) described. Thin sections of this size are not large enough to be individually representative of the coarser-grained rocks, but modal averages of many thin sections from a pluton or from two or more plutons are believed to be representative. These average modes are given in Table 3 and plotted in Figure 4.

In early 1960, recounting of the coarser-grained rocks was begun using rock slabs on

	Quartz diorite	Inconsolable Granodiorite	Tinemaha Granodiorite	Granodiorite of McMurry Meadows	Wheeler Crest Quartz Monzonite	Round Valley Peak Granodiorite	Lamarck Granodiorite	Tungsten Hills Quartz Monzonite Spec. 5	Tungsten Hills Quartz Monzonite Spec. 52	Rocks similar to Cathedral Peak Granite: Quartz Monzonite Spec. 4	Quartz Monzonite Spec. 12	Quartz Monzonite Spec. 23	Alaskite Spec. 37	Alaskite Spec. 46	Spec. K
	*	†	†	†	†	†	†	†	†	**	**	†	**	**	††
SiO_2	59.0	61.00	62.82	64.86	71.42	63.53	66.92	71.42	69.60	71.8	73.0	74.11	71.0	75.4	76.28
Al_2O_3	17.2	16.06	15.44	16.12	14.47	15.61	15.19	14.03	14.89	15.3	15.2	13.7	15.7	13.3	
Fe_2O_3	2.0	1.86	2.59	1.90	1.03	2.35	1.45	.89	1.07	1.0	.4	.60	.9	.3	
FeO	4.6	4.06	3.17	2.52	1.38	3.25	2.52	1.63	1.99	.65	.34	.88	.81	.74	
MgO	2.8	3.10	2.35	1.55	.78	2.54	1.74	.70	.91	.34	.16	.32	.39	.12	
CaO	6.2	5.46	5.04	3.80	2.86	4.58	3.79	1.91	2.70	1.8	1.1	1.29	1.6	.48	.47
Na_2O	3.3	3.45	3.15	3.44	3.44	3.31	3.16	2.86	3.18	3.8	3.8	3.44	3.8	4.1	4.72
K_2O	2.1	2.95	3.72	4.03	3.69	2.98	3.82	5.35	4.45	4.1	5.0	4.92	5.0	4.5	4.73
H_2O-	1.0	.05	.03	.06	.06	.04	.06	.08	.08	.48	.48	.12	.69	.46	
H_2O+		.58	.62	.51	.21	.61	.48	.35	.31			.18			
TiO_2	.82	.88	.64	.57	.25	.63	.47	.36	.42	.22	.09	.18	.22	.10	
CO_2	< .05	.00	.01	.00	.03	.03	.02	.02	.01	.08	.10	.01	.07	.11	
P_2O_5	.34	.25	.30	.23	.10	.23	.18	.09	.12	.05	.05	.06	.05	.01	
MnO	.14	.10	.11	.09	.08	.12	.08	.05	.07	.06	.06	.05	.04	.08	
BaO	..	..	..	..	..	..	..	..	..	..	..	..	..	..	
Total	100	99.80	99.99	99.81	99.80	99.81	99.88	99.74	99.80	100	100	99.89	100	100	
	Quantitative spectrographic analyses for minor element***														
B		.004	.001	0.	0.0	0.0	0.	0.0	0.			0.			
Ba		.1	.2	.2	.2	.2	.1	.1	.2			.1			
Co		.002	.002	.0009	.0004	.001	.001	.0005	.0005			.0001			
Cr		.004	.001	.001	.0003	.002	.001	.0006	.0005			.0003			
Cu		.002	.001	.001	.0003	.0009	.0006	.0004	.0008			.0002			
Ga		.002	.002	.001	.001	.002	.001	.001	.001			.001			
La		.006	.01	.009	.01	.009	.009	.008	.01			.005			
Nb		.002	.002	.002	.002	.002	.002	.002	.002			.001			
Ni		.003	.0008	.0004	.0001	.0007	.0005	.0003	.0002			.0001			
Pb		.002	.002	.002	.001	.002	.002	.002	.002			.002			
Sc		.001	.001	.0007	.001	.001	.001	.001	.001			.0007			
Sr		.1	.09	.06	.05	.09	.07	.03	.03			.04			
V		.01	.01	.007	.005	.009	.006	.004	.005			.001			
Y		.003	.005	.005	.003	.003	.004	.004	.005			.002			
Yb		.0003	.0004	.0003	.0002	.0002	.0002	.0003	.0004			.0001			
Zn		.01	0.	0.	.0	.01	0.	0.	0.			0.			
Zr		.01	.02	.02	.01	.01	.01	.05	.02			.03			

Looked for but not found: Ag, As, Au, Bi, Cd, Ge, In, Mo, Pt, Sb, Sn, Ta, Th, Tl, U, W. A trace of Be (less than 0.00005) was found in all samples.

*Rapid rock analysis. Analysts: H. F. Phillips, P. L. D. Elmore, and K. E. White

**Rapid rock analysis (Shapiro and Brannock, 1956). Analysts: P. L. D. Elmore, S. D. Botts, and M. D. Mack

†Standard rock analysis. Analyst: L. M. Kehl

***Analyst: P. R. Barnett

††Partial analysis reported by Knopf (1918, p. 68) of alaskite from Rawson canyon

TABLE 2. NORMS OF THE GRANITIC ROCKS OF THE SIERRA NEVADA NEAR BISHOP, CALIFORNIA

	Quartz diorite	Inconsolable Granodiorite	Tinemaha Granodiorite	Granodiorite of McMurry Meadows	Wheeler Crest Quartz Monzonite	Round Valley Peak Granodiorite	Lamarck Granodiorite	Tungsten Hills Quartz Monzonite Spec. 5	Tungsten Hills Quartz Monzonite Spec. 52	Rocks similar to Cathedral Peak Granite Quartz Monzonite Spec. 4	Rocks similar to Cathedral Peak Granite Quartz Monzonite Spec. 12	Rocks similar to Cathedral Peak Granite Quartz Monzonite Spec. 23	Rocks similar to Cathedral Peak Granite Quartz Monzonite Spec. 37	Rocks similar to Cathedral Peak Granite Alaskite Spec. 46	Rocks similar to Cathedral Peak Granite Alaskite Spec. K
Q	13.30	13.32	16.69	18.90	29.94	15.84	22.62	28.38	26.52	29.64	29.22	31.92	25.68	32.58	29.76
or	12.29	17.27	22.20	23.91	21.71	17.76	22.76	31.68	26.13	24.46	29.47	28.94	29.47	26.69	27.24
ab	27.84	29.32	26.71	28.82	28.85	32.42	26.72	24.11	26.72	31.96	31.96	28.85	31.96	34.58	39.82
an	25.95	19.46	16.68	16.68	13.35	16.13	15.84	9.46	12.51	8.90	5.56	6.40	8.06	2.50	2.50
di	2.51	4.73	5.16	.36	..	5.44	1.83	..	..						
hy	11.67	10.00	6.18	5.91	3.43	6.55	6.18	3.55	4.53	.90	.66	1.72	1.26	1.36	
mt	2.78	2.78	3.74	2.78	1.46	3.43	2.09	1.39	1.57	1.39	.70	.89	1.39	.46	
il	1.52	1.67	1.22	1.07	.47	1.21	.90	.65	.78	.46		.32	.46		
ap	.64	.64	.69	.62	.27	..	.35	..	.29						
c	..	..	..	..	..	..	..	.10	.31	1.33	1.53	.51	1.12	.71	
Total	98.50	99.19	99.27	99.05	99.48	98.78	99.29	99.32	99.36	99.04	99.10	99.55	99.40	98.88	

which K feldspar had been stained yellow and plagioclase light red to reddish brown by the method described by Bailey and Stevens (1960). In this procedure K feldspar is stained with sodium cobaltinitrate, and plagioclase is stained with rhodozonic acid which acts on previously introduced barium. The counting is done by projecting colored photographic transparencies of the stained slabs onto a grid of approximately 2000 dots. Counting slabs permits the use of samples several times larger than thin sections of ordinary size but has the disadvantage that only four constituents can be counted: quartz, K feldspar, plagioclase, and mafic minerals; biotite and hornblende cannot be counted separately.

Plots of modes made of slabs from individual plutons of Inconsolable Granodiorite, Tinemaha Granodiorite, Wheeler Crest Quartz Monzonite, Lamarck Granodiorite, Round Valley Peak Granodiorite, Tungsten Hills Quartz Monzonite, and rocks similar to Cathedral Peak Granite show less scatter than plots of modes made from thin sections cut from the same samples. The few average modes that have been calculated agree closely with the average modes made from thin sections, indicating that the data in Table 3 and Figure 4 are fairly reliable.

SEQUENCE OF EMPLACEMENT

The intrusive relations of as many of the granitic rocks as possible were established by observing the contact relations between pairs of intrusive masses in the field. The principal criteria used were aschistic dikes and apophyses, inclusions, truncated structures, and the presence or absence of characteristic marginal features. Mafic dikes, which James G. Moore (Oral communication, 1960) found useful in distinguishing between a predike series and a postdike series of granitic rocks in the adjoining Mt. Pinchot quadrangle, were not used in the Bishop area because the age relations there between mafic dikes and the granitic rocks are ambiguous. Not all the granitic rocks were found in contact with one another, and some contacts failed to yield diagnostic criteria. Contacts that provided no critical data include those where two intrusions meet along a smooth surface, those occupied by dikes or septa of metamorphic rock, and those obscured by weathering products and cover. Figure 5 shows the intrusive relations, based on the available data, and an interpretation of the sequence of intrusion.

AGE

E. S. Larsen, Jr., and associates (1958, Table 9, p. 52–53) determined the lead-alpha ages of eight samples from the Bishop area. The results are summarized in Table 4. The lead-alpha ages range from 88 to 116 million years and average 105 million years. The lead-alpha ages show little relation to observed intrusive relations. Larsen *et al.* (1952) believe that the error inherent in the lead-alpha method is about 10 per cent, and this is not accurate enough to permit comparing the age of one mass with another.

More recently, Evernden, Curtis, and Lipson (1957, p. 2121–2125) and Curtis, Evernden, and Lipson (1958, p. 7–9) have determined the ages of a suite of granitic rocks from Yosemite National Park by the potassium-argon method. The calculated ages of these rocks range from 76.9 to 95.3 million years and agree remarkably with the order of intrusion established in the field by F. Calkins (*in* Matthes, 1930, p. 120–129). The Cathedral Peak granite was determined to have an age of 83.7 million years; if masses in the Bishop area are correctly assigned to the Cathedral Peak this figure provides an index to the ages of the eastern Sierra rocks by the potassium-argon method.

The Cretaceous lasted from 135 to 70 million years ago according to Holmes' (1960) revision of his time scale and from 133 to 58 million years ago according to Curtis, Evernden, and Lipson (1958, p. 11). On these scales both the lead-alpha determinations of Bishop rocks and potassium-argon determinations of the Yosemite rocks fall close to the middle of the Cretaceous. Although many difficulties remain to

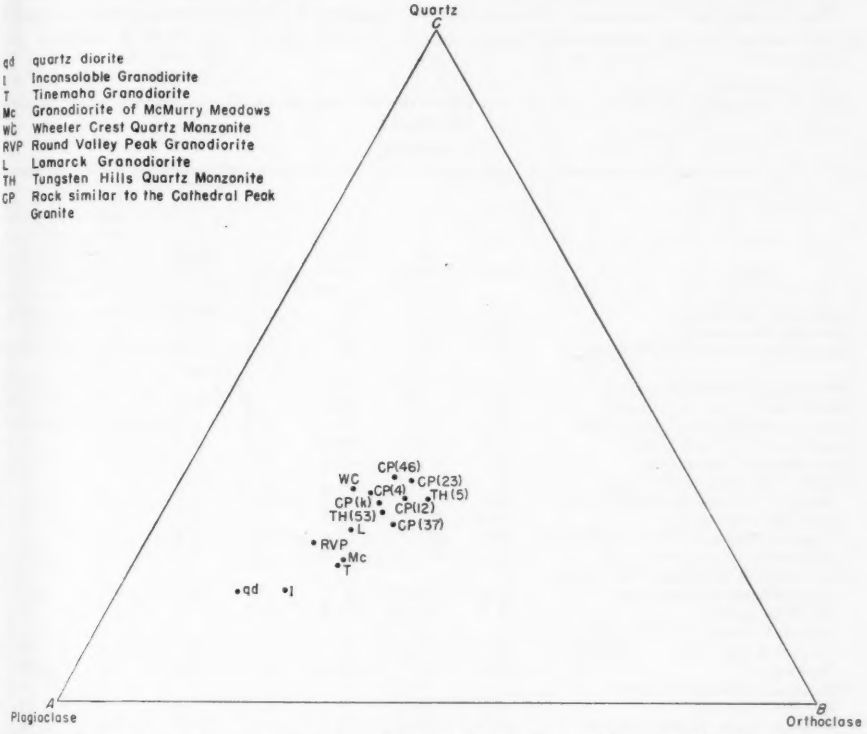

Figure 3. Plot of normative quartz, orthoclase, and plagioclase in the granitic rocks of the Sierra Nevada near Bishop, California

be worked out in integrating radiometric age with paleontologic age, it seems reasonable to assume a Cretaceous age for the granitic rocks of the east-central Sierra Nevada.

NEW FORMATIONS

Inconsolable Granodiorite

The Inconsolable Granodiorite (Cretaceous) is here named for the Inconsolable Range, its type locality. It is a medium-grained, medium-gray rock that crops out in the Sierra Nevada divide from Middle Palisade to Mt. Agassiz and extends northward in the Inconsolable Range to the latitude of Chocolate Peak (Fig. 1, inset). The spectacular cirques at the heads of the North and South forks of Big Pine Creek, still occupied by glaciers, are carved in this rock. The main mass of rock is elongate in a northwesterly direction and has an outcrop area of a little more than 12½ square miles. A second very small mass with an outcrop area of only about a tenth of a square mile is about half a mile south of the main mass. Some facies of the granodiorite are similar to rock in the Tungsten Hills classified as quartz diorite.

The Inconsolable Granodiorite is megascopically equigranular and medium-grained, with an average grain size of about 2 mm. It is distinctly finer-grained toward most margins. In over-all aspect the rock is medium to medium-dark gray; the relatively dark color results partly from a high average mafic mineral content of about 18 per cent and partly from a prevalent gray to grayish-red color of the feldspar. Many specimens, especially those from marginal parts, contain scattered small but conspicuous grains of moderate red to reddish-brown plagioclase. Plagioclase generally is about twice as abundant as quartz or K feldspar, which are equally abundant. Biotite is the predominant mafic mineral, followed by horn-

TABLE 3. AVERAGES OF MODAL ANALYSES FOR DIFFERENT PLUTONS OF THE SIERRA NEVADA NEAR BISHOP, CALIFORNIA

(In per cent)

Area	Quartz	K feldspar	Plagioclase	Biotite	Hornblende	Accessories and alteration products	Specific gravity
Inconsolable Granodiorite	16.5	14.0	50.5	10.4	*5.7	2.9	2.75
Tinemaha Granodiorite	19.2	24.5	42.3	4.6	*6.0	3.4	2.72
Granodiorite of McMurry Meadows	20.5	26.4	40.1	8.0	*3.1	1.6	2.70
Wheeler Crest Quartz Monzonite	24.6	25.4	38.6	12.0			2.65
Round Valley Peak Granodiorite	25.9	15.0	46.4	7.2	3.6	1.9	2.69
Lamarck Granodiorite Lamarck mass	24.2	21.6	44.4	6.5	2.7	1.4	2.69
Granodiorite of Deep Canyon	23.6	14.8	45.4	9.3	3.7	3.1	2.70
Granodiorite of Coyote Flat	22.1	12.8	47.9	8.7	4.7	3.9	2.71
Tungsten Hills Quartz Monzonite							
Morgan Creek and Pine Creek masses	31.4	29.0	33.0	4.8	3.9	1.4	2.62
Basin Mountain mass	27.2	22.5	40.2	5.9	1.4	2.7	2.65
Tungsten Hills and Bishop Creek masses	27.9	31.7	32.6	5.5	0.2	2.1	2.63
Shannon Canyon masses	28.5	31.6	32.8	4.0	0.1	2.9	2.62
Rocks similar to Cathedral Peak Granite							
Lobes of Mono Recesses mass	29.8	29.0	36.5	2.9	0.0	2.2	2.61
Mt. Alice mass	31.2	35.8	27.5	2.7	0.0	2.8	2.61
Palisade Creek and Red Mountain Creek masses	30.5	37.6	27.4	2.7	0.2	1.7	2.60
Alaskite	34.8	35.8	24.8	1.8	0.2	2.2	2.60
Finer-grained quartz monzonites							
Wheeler Crest mass	36.3	31.0	28.1	3.3	0.4	1.0	2.63
Freeman Creek, Shannon Canyon, and Sugarloaf masses	26.0	28.8	40.0	4.4	0.0	0.8	2.64
Taboose mass	35.7	28.4	31.4	3.6	0.0	0.8	2.62

*Includes augite

blende and augite. The texture in thin section is seriate, and the largest grains are plagioclase.

Primary foliation generally is recognizable and is especially conspicuous near the margins of the intrusive masses. Lenticular mafic inclusions oriented parallel with the foliation are abundant. Mafic dikes were observed only in the extreme north end.

granodiorite in the south half of the Big Pine quadrangle is approximately 32 square miles. Most of it is in an oval mass that is nearly bisected by the granodiorite of McMurry Meadows (Fig. 1). A smaller mass with an area of half a square mile lies south of Red Mountain Creek.

The Tinemaha Granodiorite appears very

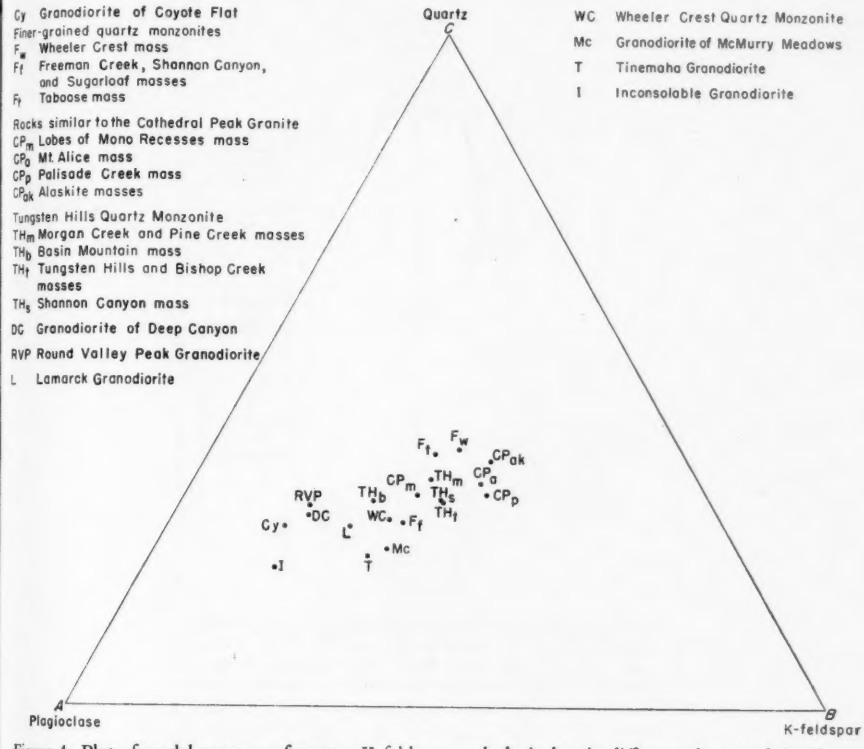

Figure 4. Plot of modal averages of quartz, K feldspar, and plagioclase in different plutons of the Sierra Nevada near Bishop, California

The Inconsolable Granodiorite is clearly intruded by the Lamarck Granodiorite and by quartz monzonite similar to the Cathedral Peak Granite, but its relations with the Tinemaha Granodiorite have not been determined.

Tinemaha Granodiorite

The Tinemaha Granodiorite (Cretaceous) is here named after Mt. Tinemaha; its type locality is in the cirques at the head of Tinemaha Creek (Fig. 1, inset). The outcrop area of the

nearly the same in all exposures: differences in texture and in color index do not materially affect the general appearance of the rock. Adjacent to the Inconsolable Granodiorite it is somewhat finer-textured than in most other places, but the difference in grain size is not great.

Commonly the granodiorite is porphyritic and contains subhedral to anhedral grains of perthite up to 1½ cm across; some specimens are equigranular or seriate. The groundmass is

hypidiomorphic-granular, and the grain size generally ranges from 2 to 4 mm. The content of mafic minerals averages about 14 per cent and ranges from 6 per cent to 25 per cent. The rock is unique among the granitic rocks of the Bishop district in that hornblende generally is more abundant than biotite. Much of the hornblende is in euhedral or subhedral prisms, whereas biotite is rarely euhedral.

The granodiorite contains numerous lenticular mafic inclusions, which with the biotite and hornblende crystals define a foliation. Steeply dipping mafic dikes, most of which strike N. 70° W., are abundant.

The Tinemaha Granodiorite is not known to intrude any other plutonic rock except small bodies of diorite, quartz diorite, and hornblende gabbro, and its intrusive relations with the Inconsolable Granodiorite have not been determined. It is intruded by the Lamarck Granodiorite, granodiorite of McMurry Meadows, and quartz monzonite similar to the Cathedral Peak Granite.

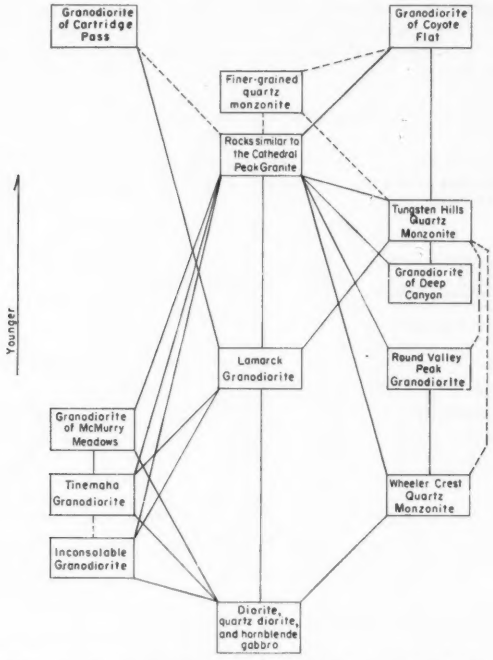

Figure 5. Diagram showing intrusive relations and probable age sequence of the granitic rocks of the Sierra Nevada near Bishop, California. Solid lines indicate observed relations; dashed lines indicate probable relations inferred from the map pattern or from inconclusive field observations.

Wheeler Crest Quartz Monzonite

The Wheeler Crest Quartz Monzonite (Cretaceous) is here named after Wheeler Crest. It is well exposed in the steep eastern face of Wheeler Crest (Fig. 1, inset) where it underlies a little more than 17 square miles. The rock can be examined readily on both sides of the entrance to Pine Creek canyon, and the exposures on the north side are considered the type locality.

Most of the quartz monzonite contains conspicuous phenocrysts of K feldspar, set in a

TABLE 4. LEAD-ALPHA AGES OF THE GRANITIC ROCKS OF THE SIERRA NEVADA NEAR BISHOP, CALIFORNIA
Data from Larsen *et al.* (1958)

Intrusive unit	Mass	Location	Probable order of emplacement	Mineral	Activity α/mg/hr	Lead ppm	Calculated age (10^6 years)
Quartz monzonite similar to Cathedral Peak Granite	Mt. Alice	Big Pine quad. SW¼ sec. 26, T. 9 S., R. 32 E. At end of Big Pine Creek Road	6	Zircon	618	26	105
Tungsten Hills Quartz Monzonite	Morgan Creek	Mt. Tom quad. West of surface workings of Pine Creek mine	5	Zircon	796	37	116
Tungsten Hills Quartz Monzonite	Bishop Creek	Mt. Goddard quad. NE¼ sec. 20, T. 8 S., R. 31 E. Along Bishop Creek road	5	Zircon	792	35	110
Lamarck Granodiorite	Lamarck	Mt. Goddard quad. NW¼ sec. 14, T. 9 S., R. 31 E. NE side of South Lake	4	Zircon	400	15	93 } 91
				Thorite	4670	205	88 }
Round Valley Peak Granodiorite	Round Valley Peak	Mt. Tom quad. ¼ mile NE of Rock Creek Lake	4	Zircon	396	12, 13, 14, 16 (13.8)	88
Granodiorite of McMurry Meadows		Big Pine quad. NE¼ sec. 9, T. 10 S., R. 33 E.	3	Monazite	4897	234, 238 (236)	100
Tinemaha Granodiorite		Big Pine quad. NW¼ sec. 14, T. 10 S., R. 33 E.	2	Zircon	331	15, 16 (15.5)	116
Inconsolable Granodiorite		Big Pine quad. SE cor. sec. 33, T. 9 S., R. 33 E. ¼ mile S. of Third Lake	1	Zircon	221	10	112

medium-grained hypidiomorphic-granular groundmass. The groundmass minerals commonly are 2–4 mm across, and the phenocrysts, many of which are tabular euhedral crystals, average about half an inch thick and 1 inch to several inches in apparent length. Fresh surfaces of the quartz monzonite are light gray, and the content of mafic minerals averages about 12 per cent but ranges from a little less than 5 per cent to 18 per cent. Porphyritic facies are distinctive in appearance and superficially resemble the porphyritic facies of quartz monzonite similar to the Cathedral Peak Granite, which, however, is much more felsic, and the Tinemaha Granodiorite, which is more mafic. By decrease in the size and abundance of phenocrysts the porphyritic rock grades into equigranular rock with a texture identical with that in the groundmass of porphyritic rock. The dark minerals, biotite and hornblende, are evenly scattered in small clusters through the rock and are concentrated along the margins of phenocrysts of K feldspar. Individual grains of hornblende and biotite are anhedral and small, generally less than 1 mm across. Near the north edge of the mapped area the quartz monzonite grades to lighter-colored rock that resembles the typical rock only slightly.

In most places the quartz monzonite has a primary foliation marked by planar orientation of ovoid clots of mafic minerals and by lenticular inclusions. Shearing is common, and mortar structure can be seen in most thin sections. In a few places a secondary gneissic foliation is shown by layers of hornblende and biotite along closely spaced shears.

The Wheeler Crest quartz monzonite is intruded by the Round Valley Peak Granodiorite, Tungsten Hills Quartz Monzonite, and alaskite similar to the Cathedral Peak Granite. It intrudes only diorite, quartz diorite, and hornblende gabbro.

Round Valley Peak Granodiorite

The Round Valley Peak Granodiorite (Cretaceous) forms a mass in the northwest corner of the Mt. Tom quadrangle and the adjoining three quadrangles (Fig. 1). It underlies a little more than 18 square miles within the Mt. Tom quadrangle, and its total area is about 40 square miles. Both sides of upper Rock Creek, the type locality, show good exposures. Rinehart and Ross (1957), mapped the intrusive mass in the Casa Diablo quadrangle as granodiorite of Rock Creek, and Sherlock and Hamilton (1958) followed this usage in the north half of the Mt. Abbot quadrangle. Since the name Rock Creek has long been pre-empted in formal stratigraphic nomenclature, the granodiorite is here named for Round Valley Peak, a high point along Wheeler Crest, which is composed of granodiorite of typical appearance.

The granodiorite is notably equigranular and medium-grained. Biotite and hornblende are evenly distributed in discrete euhedral crystals, which give the rock a distinctive "tidy" appearance. The grain size averages about 3 mm but is about 2 mm in the eastern part and 3–4 mm in the southwestern part. Both K feldspar and plagioclase (An_{35-40}) are white, quartz is light gray, and the rock has an over-all light-gray color. The average content of mafic minerals in 13 modally analyzed specimens is 12.7 per cent, but the finer-grained rock in the eastern part is darker than coarser-grained rock in the southwestern part.

Foliation parallel to contacts with older rocks is pronounced near the eastern and southern contacts and is progressively less conspicuous away from them. The foliation is shown best by mafic inclusions, which become progressively less tabular and less abundant with distance from contacts with older rocks. Near contacts with older rocks the foliation is also shown by orientation of the mafic minerals. Granodiorite more than a few hundred feet from these contacts appears structureless.

In thin section, the texture is hypidiomorphic-granular; no mortar structure or other evidence of cataclasis was observed as in the neighboring Wheeler Crest Quartz Monzonite.

The Round Valley Peak Granodiorite is clearly younger than the Wheeler Crest Quartz Monzonite and older than quartz monzonite similar to the Cathedral Peak Granite. Intrusive relations with the Tungsten Hills Quartz Monzonite are less certain, but the Tungsten Hills Quartz Monzonite is believed to be younger.

Lamarck Granodiorite

The Lamarck Granodiorite (Cretaceous) is here named after Mt. Lamarck. It is well exposed in the cirques east of Mt. Lamarck, which constitute the type locality. Two masses crop out along the west and southwest sides of the mapped area. The larger, the Lamarck mass, underlies about 54 square miles within the southwestern part of the mapped area; the smaller, called the Chickenfoot Lake mass following the usage of Sherlock and Hamilton (1958), who mapped it in the adjoining Mt.

Abbot quadrangle, underlies less than 3 square miles in the northwestern part of the map area. Both masses extend west of the map area. The Chickenfoot Lake mass is generally finer-grained and in the south part is darker than the Lamarck mass, and its assignment to the Lamarck Granodiorite may prove incorrect.

The rock in the Lamarck mass appears in the field remarkably homogeneous in both composition and texture, except in the thin southeastern part of the mass, which is more felsic and somewhat porphyritic. It is medium-grained and generally seriate, less commonly equigranular. The grain size averages 3–4 mm, but K feldspar is in grains up to 1 cm across. The seriate texture is especially prominent in the thin southeastern part, where the rock appears porphyritic in hand specimen. Biotite and hornblende generally are evenly distributed both in clusters and in discrete subhedral to euhedral crystals. The average content of mafic minerals in the Lamarck mass is 11.5 per cent but ranges from 4.4 per cent to 18.4 per cent. The mafic-mineral content of specimens from the southeastern part averages 6.5 per cent, from the northern part, 12.2 per cent.

Commonly the granodiorite has a conspicuous foliation, shown by numerous lenticular mafic inclusions and by the planar orientation of hornblende and biotite.

The Lamarck Granodiorite is younger than the Inconsolable and Tinemaha Granodiorites and older than the granodiorite of Cartridge Pass, Tungsten Hills Quartz monzonite, and quartz monzonite similar to the Cathedral Peak Granite.

Tungsten Hills Quartz Monzonite

The rock here named the Tungsten Hills Quartz Monzonite (Cretaceous) crops out discontinuously in a northwest-trending belt through the central part of the mapped area. A hill 2 miles N. 20° E. of Grouse Mountain in the southwestern part of the Tungsten Hills is designated the type locality because it is readily accessible and the exposed rock is representative of most of the formation. Fresher rock of similar appearance is exposed on Grouse Mountain and east of Bishop Creek below the junction of the South and Middle forks.

The formation crops out in about 120 square miles within the mapped area and continues westward into the Mt. Abbot and Blackcap Mountain quadrangles. Within the mapped area it includes six separate masses: the Morgan Creek, Basin Mountain, Pine Creek, Tungsten Hills, Bishop Creek, and Shannon Canyon masses. Some of these masses are separated from one another only by alluvial deposits and doubtless are continuous in bedrock, and others are separated by younger intrusive masses and probably were once continuous. Originally there were probably only two plutons, one on either side of a belt of metamorphic rock that extends from the Pine Creek pendant southward to Mt. Humphreys.

With a few notable exceptions the quartz monzonite is homogeneous in composition and in appearance. The typical quartz monzonite, away from the margins, is medium-grained and medium light gray on fresh surfaces. It consists of roughly equal amounts of quartz, plagioclase, and perthite. Generally 3–8 per cent of biotite is present. Hornblende is absent in most specimens and exceeds 2 per cent only in the western part of the Basin Mountain mass, which is granodioritic.

Commonly the quartz monzonite is porphyritic or subporphyritic with subhedral phenocrysts of perthite that are 1 cm across and up to 3 cm in the longest dimension, parallel with the composition plane of Carlsbad twins. The mafic minerals are in small irregular crystals and clusters of crystals distributed evenly through the rock. Peripheral concentrations of mafic minerals commonly provide frames for the K feldspar phenocrysts. Rock in the margins of the masses generally is finer-grained than rock from their interiors and contains fewer and smaller feldspar phenocrysts.

In most places the rock appears structureless, and planar foliation was mapped at only a few places such as the Morgan Creek mass along the west side of the Pine Creek pendant. Mafic inclusions are scarce, and most of those observed are ovoid rather than lenticular. Joints are widely spaced, and at many places weathering along two nearly vertical sets that intersect at very close to 90° has produced a conspicuous rectilinear pattern of troughs and slots. Bold, rounded forms produced by weathering along the joints are characteristic.

Rocks of abnormal appearance or composition occur at several places. Rock of finer grain makes up the Morgan Creek mass along the west side of the Pine Creek pendant and is present locally in the Pine Creek mass along the east side of the pendant. Light-colored albitized rock is present along the north and east margins of the Bishop Creek pendant in a discontinuous belt that in places is almost a

mile wide. Rock of granodiorite composition makes up the western part of the Basin Mountain mass.

The Tungsten Hills Quartz Monzonite intrudes the Wheeler Crest Quartz Monzonite, the granodiorite of Deep Canyon, the Lamarck Granodiorite, and the Round Valley Peak Granodiorite. It is intruded by quartz monzonite and alaskite similar to that in the Cathedral Peak Granite and the granodiorite of Coyote Flat, and probably by finer-grained quartz monzonite.

INFORMAL UNITS THAT INCLUDE THE ROCK IN SEVERAL PLUTONS

DIORITE, QUARTZ DIORITE, AND HORNBLENDE GABBRO: The small bodies of diorite, quartz diorite, and hornblende gabbro in the Sierra Nevada have been aptly referred to by Mayo (1941, p. 1010) as "basic forerunners," or simply as "forerunners." Their distribution is reminiscent of the metamorphic rocks; they occur as inclusions or small pendants within individual plutons of more silicic rock or as septa between plutons. Commonly they are associated with metamorphic rocks, and many are crowded with inclusions of metamorphic rock. Later granitic intrusive masses disrupted many of the original masses and recrystallized, granitized, and assimilated smaller fragments and the marginal parts of larger ones.

Partly as a result of original differences and partly as a result of subsequent modification the rocks grouped under diorite, quartz diorite, and hornblende gabbro are heterogeneous in composition and texture; very likely they include rocks of diverse origin.

The darker-appearing rocks (content of mafic minerals 40–60 per cent) generally contain plagioclase more calcic than An_{50} and hornblende or uralitic amphibole rather than augite and are therefore classed as hornblende gabbro. Most of the hornblende gabbro ranges between 1 and 5 mm in average grain size and is medium-grained, but these limits are so wide as to permit very great differences in the appearance of different rocks. Many plutons exhibit panidiomorphic-granular texture, strong zoning of plagioclase, layered facies, and dikes that cut metamorphic rocks, indicating that they crystallized from a magma and are truly igneous. Unusual and interesting fabrics are common, however. Locally coarse-grained, almost pegmatitic rock is found which contains euhedral prisms of hornblende an inch or more long and a quarter to half an inch across. In several places, hornblende gabbro contains almost equidimensional crystals of plagioclase. Rocks in which elongate hornblende crystals lie in a well-defined foliation plane, but are randomly oriented within that plane, occur in thin tabular masses that are bordered by younger silicic granitic rocks, suggesting that the fabric may be metamorphic.

Rocks of quartz dioritic or granodioritic composition are generally lighter-colored than the hornblende gabbro, although darker than the granodiorite of other cartographic units. In both texture and composition the quartz diorites and granodiorites are transitional between hornblende gabbro and granodiorite of the larger and younger plutons. The mafic-mineral content of quartz diorite ranges from 20 to 40 per cent, plagioclase is less calcic than An_{50} (and commonly less calcic than An_{40}), and the rock generally contains 10 per cent or more of quartz. The grain size is from 1 to 5 mm, but more quartz diorite than hornblende gabbro is in the lower part of this range. Most quartz diorite is hypidiomorphic-granular and probably crystallized directly from a magma.

Much of the dark granodiorite in this unit and some of the quartz diorite may be hybrids between more silicic granitic rock and diorite, hornblende gabbro, or mafic volcanic rock. The fabric is generally irregular; some rocks are very coarse-grained and in places contain poikilitic hornblende crystals an inch or more long.

ROCKS SIMILAR TO THE CATHEDRAL PEAK GRANITE: Alaskite and quartz monzonite similar in appearance to the Cathedral Peak Granite of Yosemite (F. Calkins, *in* Matthes, 1930, p. 126–127) occur in several discrete bodies within the mapped area. The total area of Cathedral Peak-type rocks is about 68 square miles, divided almost equally between quartz monzonite and alaskite. In a general way, masses of alaskite and quartz monzonite fall into geographically different areas. Alaskite is confined to the Sierra Nevada front from Big Pine Creek north to Wheeler Crest; quartz monzonite lies west of the alaskite in a belt that extends northwesterly from near the southeast corner of the mapped area to near the northwest corner. Quartz monzonite masses of this unit are the Mono Recesses, McGee Creek, Mt. Alice, Palisade Creek, and Red Mountain Creek masses; alaskite masses include a dike along Wheeler Crest and the Round Valley, Rawson

Creek, and Warren Bench masses. Overlapping mineral and textural characteristics and the absence of any evidence that rock of one composition intrudes the other support the view that the rocks are genetically and temporally closely related. Nevertheless, mineralogic differences probably reflect different temperature ranges of crystallization, and it is not likely that the two facies are precise temporal equivalents.

Quartz monzonite typical of the Cathedral Peak is medium- to coarse-grained, has an average content of mafic minerals of 3.5 per cent, and commonly is equigranular to seriate but locally is porphyritic. Conspicuously porphyritic rock megascopically identical with the Cathedral Peak Granite of the Yosemite region is present in the McGee Creek mass, just west of Mt. Humphreys, and in the Mono Recesses mass, two lobes of which extend into the west side of the mapped area. The Mono Recesses mass extends to the northwest more than 25 miles and is porphyritic in many places. Inclusions are few except in the immediate vicinity of intrusive contacts with metamorphic or mafic igneous rocks. Foliation is rarely discernible, probably because of the paucity of mafic inclusions or mafic minerals. Joints commonly are widely spaced and prominent.

Quartz, K feldspar, and oligoclase constitute more than 95 per cent of the average rock and are present in roughly equal amounts. The average biotite content is about 3 per cent; hornblende is scarce and where present probably reflects contamination of the magma by mafic igneous or metamorphic rocks.

Knopf (1918, p. 67–69) described the alaskite facies as orthoclase-albite granite. Megascopically it closely resembles the nonporphyritic facies of the quartz monzonite. The most obvious features that distinguish the alaskite from the quartz monzonite are a pinkish cast of the K feldspar and a very low biotite content—about 1.6 per cent on the average for uncontaminated alaskite, with many specimens containing less than 1.0 per cent. However, the most distinctive feature of the alaskite, plagioclase in the albite rather than the oligoclase compositional range, can be ascertained only through microscopic study or chemical analysis.

The grain size of the alaskite averages 3–4 mm but ranges from less than 2 mm in a dike along Wheeler Crest to more than 5 mm in the Rawson Creek mass, along the range front south of Bishop. The alaskite is megascopically equigranular but appears slightly seriate in thin section. The largest grains are of K feldspar. Foliation is prominent only in the dike along Wheeler Crest. Inclusions are scarce. Joints commonly are widely spaced and conspicuous.

Rocks similar to the Cathedral Peak Granite are among the youngest of the plutonic rocks, and only the granodiorites of Coyote Flat and Cartridge Pass and finer-grained quartz monzonite could have been emplaced later. None of these rocks was observed to intrude rocks of Cathedral Peak type; evidence of a younger age rests on the gross geometrical relations especially as shown by the map pattern (Fig. 1). The most southerly mass of quartz monzonite of Cathedral Peak type, unlike any other mass assigned to the Cathedral Peak, is cut by mafic dikes, which suggests that it is older than other masses of Cathedral Peak type and may be improperly assigned.

FINER-GRAINED QUARTZ MONZONITE: Six small masses with an aggregate outcrop area of only a little more than 6 square miles are grouped under "finer-grained quartz monzonite". Although most or perhaps all of these masses may have been emplaced at about the same time, evidence bearing on their relative ages is too meager for them to be considered a formational unit.

The rock in all the masses is generally similar in texture and mineral content, although minor differences exist. The typical rock is medium-grained, although finer-grained than any other intrusive mass, and is locally porphyritic. The grain size averages 1–2 mm; the size varies slightly from mass to mass but generally is nearly constant throughout a single mass. Phenocrysts of K feldspar ½ to 1½ cm across are present locally.

The rock ranges from very light gray to yellowish gray. Biotite, ordinarily the only dark mineral, is present in amounts ranging from 1.0 to 6.5 per cent, and most rocks have between 2.0 and 5.0 per cent. The rock contains few mafic inclusions, and much of it appears structureless, but locally oriented feldspar grains and biotite flakes and aggregates of biotite flakes in thin layers give the rock a planar foliation. Some of this foliation may reflect cataclasis rather than orientation by magmatic flow.

Much of the mass along Taboose Creek is composed of two similar-appearing rocks of about equal abundance, one of which intrudes the other in narrow irregularly branching

dikes. Because the two rocks are almost indistinguishable, I believe that they are closely related.

INFORMAL UNITS THAT INCLUDE THE ROCK IN SINGLE PLUTONS

GRANODIORITE OF MCMURRY MEADOWS: The granodiorite of McMurry Meadows constitutes a single pluton that intrudes and is enclosed by the Tinemaha Granodiorite. It has the greatest range in composition of any plutonic mass within the mapped area. The pluton is concentrically zoned; it grades from quartz monzonite in the core to granodiorite or quartz diorite in the margins. The southwest margin is more mafic than other parts and approaches quartz diorite in composition. Specific gravities of modally analyzed specimens range from 2.62 to 2.69 in the quartz monzonite core and from 2.69 to 2.82 in the granodiorite rim. Modal analyses show that the plagioclase content ranges from as little as 24 per cent in the core to as much as 64 per cent at the margins.

Hand specimens of rock of quartz monzonite composition usually can be distinguished readily from those of granodiorite or quartz diorite composition. Those of quartz monzonite composition commonly are porphyritic with conspicuous phenocrysts of perthite and contain not more than 1.5 per cent of hornblende. Specimens of granodiorite composition, on the other hand, are equigranular and contain as much as 10 per cent of hornblende. Furthermore, much of the hornblende in the granodiorite contains augite cores, whereas no augite was found in the hornblende of the quartz monzonite.

The general appearance of the rocks suggests that the presence or absence of perthite phenocrysts determines whether the rock is a quartz monzonite, but modal studies show that differences in the amount of plagioclase is more critical in classification.

The granodiorite of McMurry Meadows is in contact with only two intrusive masses other than older diorite, quartz diorite, and hornblende gabbro. It intrudes the Tinemaha Granodiorite and is intruded by dikes of quartz monzonite of Cathedral Peak type.

GRANODIORITE OF DEEP CANYON: The granodiorite of Deep Canyon includes two masses in the Deep Canyon area of the Tungsten Hills with a combined area of about a square mile and several smaller masses along the north edge of the Tungsten Hills enclosed in alaskite similar to that of the Cathedral Peak Granite. In hand specimen the rock appears equigranular with an average grain size of about 1 mm. The content of dark minerals ranges from about 10 to more than 20 per cent. The darkest rock is in the easternmost part of the larger and more easterly of the masses along Deep Canyon. Within this mass the rock is progressively lighter-colored and coarser-grained toward the west, and the western contact with the Tungsten Hills Quartz Monzonite appears gradational in places. Elsewhere, the rock is clearly older than the Tungsten Hills Quartz Monzonite. These relations suggest that the age difference between the granodiorite of Deep Canyon and the Tungsten Hills Quartz Monzonite may be small and that the granodiorite of Deep Canyon may be, in fact, an early phase of the Tungsten Hills Quartz Monzonite.

GRANODIORITE OF COYOTE FLAT: A more or less equidimensional pluton of granodiorite underlies about 13 square miles in the northeastern part of Coyote Flat and adjoining areas on the north and east. Most of the pluton is well exposed, but the west-central part is covered by alluvial fill in Coyote Flat.

Most of the granodiorite is light gray and medium-grained; it is equigranular, and the grain size averages 1–2 mm. A marginal zone a few hundred feet thick is generally present in which the rock is darker and finer-grained than the more abundant rock from the interior of the pluton. The marginal rock is conspicuously foliated parallel with the external contact. The rock contains few inclusions, and the foliation is shown by orientation of the constituent minerals.

The granodiorite of Coyote Flat sends dikes into and contains inclusions of the Tungsten Hills Quartz Monzonite and alaskite similar to the Cathedral Peak Granite and is clearly younger. Intrusive relations with finer-grained quartz monzonite were not established by field observations. The roundish form of the granodiorite in plan suggests that it may be a late stock and may intrude all the rocks with which it is in contact.

GRANODIORITE OF CARTRIDGE PASS: Light-gray equigranular granodiorite with an average grain size of 1–2 mm occupies a little less than 3½ square miles in the southeastern corner of the mapped area and extends into adjoining areas to the south and west. James G. Moore has made intensive studies of the pluton in the Mt. Pinchot quadrangle in the vicinity of Cartridge Pass and has found that it is concentrically zoned, like the granodiorite of

McMurry Meadows, and that the average composition is granodiorite very close to quartz monzonite (Moore, written communication, 1960). The pluton intrudes the Lamarck Granodiorite and according to Moore it also intrudes all the other granitic rocks with which it is in contact.

REFERENCES CITED

Bailey, E. H., and Stevens, R. E., 1960, Selective staining of K-feldspar and plagioclase on rock slabs and thin sections: Am. Mineralogist, v. 45, p. 1020–1025

Chayes, Felix, 1949, A simple point counter for thin-section analysis: Am. Mineralogist, v. 34, p. 1–11

Curtis, G. H., Evernden, J. F., and Lipson, J. I., 1958, Age determinations of some granitic rocks in California by the potassium-argon method: California Div. Mines Special Rept. 54, 16 p.

Evernden, J. F., Curtis, G. H., and Lipson, J. I., 1957, Potassium-argon dating of igneous rocks: Am. Assoc. Petroleum Geologists Bull., v. 41, p. 2120–2127

Holmes, Arthur, 1960, A revised geological time scale: Edinburgh Geol. Soc. Trans., v. 17, pt. 3, p. 183–216

Knopf, Adolph, 1918, A geologic reconnaissance of the Inyo Range and the eastern slope of the southern Sierra Nevada: U. S. Geol. Survey Prof. Paper 110, 130 p.

Larsen, E. S., Jr., Keevil, N. B., and Harrison, H. C., 1952, Method for determining the age of igneous rocks using the accessory minerals: Geol. Soc. America Bull., v. 63, p. 1045–1052

Larsen, E. S., Jr., Gottfried, David, Jaffe, H. W., and Waring, C. L., 1958, Lead-alpha ages of the Mesozoic batholiths of western North America: U. S. Geol. Survey Bull. 1070-B, p. 35–62

Matthes, F. E., 1930, Geologic history of the Yosemite Valley: U. S. Geol. Survey Prof. Paper 160, 137 p.

Mayo, E. B., 1941, Deformation in the interval Mt. Lyell-Mt. Whitney, California: Geol. Soc. America Bull., v. 52, p. 1001–1084

Rinehart, C. D., and Ross, D. C., 1957, Geologic map of the Casa Dieblo Mountain quadrangle, California: U. S. Geol. Survey Geol. Quad. Map GQ-99

Shapiro, Leonard, and Brannock, W. W., 1956, Rapid analysis of silicate rocks: U. S. Geol. Survey Bull. 1036-C, p. 19–56

Sherlock, D. G., and Hamilton, Warren, 1958, Geology of the north half of the Mt. Abbot quadrangle, Sierra Nevada, California: Geol. Soc. America Bull., v. 69, p. 1245–1268

Manuscript Received by the Secretary of the Society, June 20, 1960
Publication Authorized by the Director, U. S. Geological Survey

WALDEN P. PRATT *U. S. Geological Survey, Denver, Colo.*

Local Evidence of Pleistocene to Recent Orogeny in the Argentine Andes

Abstract: Deformed continental sedimentary rocks are exposed in the province of Salta, northwestern Argentina, in one of many intermontane basins of the Puna, a high desert region of subparallel north-trending block-fault ranges. These rocks, formerly thought to be Tertiary but recently dated by fossil diatoms as Pleistocene or younger, comprise several thousand feet of clastics and evaporites interpreted as having accumulated in a structural basin under geologic and climatic conditions much like those of today. They are overlain unconformably by sedimentary rocks and sediments of three distinct depositional periods. The stratigraphic section is as follows:

Fan gravels and playa deposits (Recent)
— *Disconformity* —
Flat-lying lacustrine sandstones and siltstones, minor salines
— *Angular unconformity* —
Gently folded conglomerates and sandstones
— *Angular unconformity* —
Folded and faulted conglomerate, sandstone, shale, evaporites, and tuffs

The basin rocks are folded along north-trending axes and are cut by northeast- to southeast-trending normal faults and by a north-trending reverse fault; the next younger conglomerates and sandstones are gently folded; the two youngest units are undisturbed. The three unconformities, the faults and folds in the older beds, and post-lake-bed faulting of an erosion surface on an adjacent block all indicate intermittent late Pleistocene to Recent local deformation.

Neither regional tension nor regional compression can explain both the Pleistocene to Recent movements on the regional block faults and the contemporaneous compressional structures within the basin. The mechanism of *horst-wedging*, suggested by a current explanation of the analogous ranges of the Great Basin, is proposed as a solution to the dilemma; the horst blocks, forced directly upward along Miocene normal faults, acted as wedges and compressed the sediments accumulating in the graben, creating the pattern of faults and folds now observed. If such structures are ever discovered in the North American Great Basin, as seems reasonable, they should offer new insight into the understanding of basin-and-range structure.

CONTENTS

Introduction 1540
Regional setting 1540
Geology of the Sijes trough 1542
Topography 1542
Stratigraphy 1544
Structure 1545
Regional structure 1545
Structures within the Sijes trough 1546
Sequence of structures 1547
Origin of structures 1548
Summary and conclusions 1549
References cited 1549

Figure
1. Regional geologic map of part of the province of Salta, Argentina 1541
2. Inferred prevolcanic structure of part of the province of Salta, Argentina 1542
3. Geologic sketch map of Sijes area, province of Salta, Argentina 1543
4. Block diagram of south-central Sijes trough . . 1548

Plate Facing
1. Panoramas, province of Salta, Argentina . . . 1544
2. Lake beds, hanging U-shaped valley, and structures in basin rocks, province of Salta, Argentina 1545

Table
1. Stratigraphy of the Sijes trough 1546

Geological Society of America Bulletin, v. 72, p. 1539–1550, 4 figs., 2 pls., October 1961

INTRODUCTION

In 1955, while on leave of absence from the U. S. Geological Survey, I was a member of a small geological party assigned to map some deformed sedimentary rocks in the Andes. These rocks formerly were thought to be Miocene and Pliocene, but the oldest exposed unit yielded fossil diatoms that have been identified as Pleistocene or younger. The fossils occur in consolidated playa sediments of a structural basin, similar to basin sediments accumulating today, that are folded and faulted and are overlain unconformably by other fan, playa, and lacustrine deposits of three distinct depositional periods. The several unconformities, the faults and folds in the sedimentary rocks, and a recently faulted erosion surface all indicate crustal instability in late Pleistocene or Recent time. This paper describes the local effects of this instability—compression of sediments within a structural basin—and shows how both the basin and the compression are thought to be related to differential vertical movements on a regional scale. The paper concludes with a suggestion of how the explanation proposed here might apply to interpretation of structures in the analogous ranges of the Great Basin.

The mapping on which this paper is largely based was done during April to August 1955 by Siegfried Muessig, Allen M. Bassett, and myself. The mapping, observations, and counsel of Muessig and Bassett have contributed much to this paper, and both have read it critically, but I am responsible for the conclusions. Kenneth E. Lohman of the U. S. Geological Survey identified the fossil diatoms. I am grateful to William R. Jones, Prof. Ernst Cloos, and Prof. William F. Jenks for reading and commenting upon the manuscript, and to Prof. Cloos for a very illuminating discussion of related scale-model experiments.

REGIONAL SETTING

LOCATION: The area mapped covers about 60 sq km in one of the intermontane basins of the Puna, in the province of Salta, Argentina, approximately at lat. 24°45′ to 25° S. and long. 66°45′ W.; it is about 75 km south-southwest of the supply center of San Antonio de los Cobres on the transandean General Belgrano railway and about 180 km east of the Chilean border (Fig. 3, inset). This basin is here designated the Sijes (sē′-hĕs) basin after a small native settlement near its north end. The nearest town, Santa Rosa de Pastos Grandes, is at the north end of the basin.

GEOLOGY: The Sijes basin lies near the southeast edge of the Puna, a high mountainous desert that extends across the Andes from northwestern Argentina into Chile, Bolivia, and Peru (Fig. 3, inset). Harrington (1956, p. 156) described the Puna as ". . . a region of basins occupied by dry salt lakes, [each basin] flanked by . . . subparallel ranges rising about 1000 m above the level of the depressions. . . ." In Argentina the ranges trend north to northeast, parallel to the structural grain of this part of the Andes. Harrington noted that

> "vast masses of rhyolitic and andesitic tuffs and flows of Upper Tertiary and Quaternary age mask the Precambrian and lower Paleozoic rocks in the basement, which are brought to light only in the low ranges just mentioned. The uplift of the Puna began in Pliocene time and continued during the Quaternary."

Many geologists have studied the southeastern Puna; this summary of the geology is drawn from reports by Catalano (1927; 1930a; 1930b) and Vilela (1953). The Sijes basin is the easternmost of three linear basins, each about 20 km wide and several hundred km long, that trend approximately north-northeast along the southeast boundary of the Puna (Fig. 1). The gross structure of the basin appears to be that of a graben lying between two horsts. ("Graben" and "horst" are used here to mean fault blocks that have been relatively depressed or uplifted, whether they have been tilted or not.) The western horst is a narrow range composed of lower Paleozoic and Precambrian metamorphic rocks; these are erroneously generalized as "Permian continental" on the Geologic Map of South America (Geol. Soc. America, 1950). The eastern horst, forming the lofty Cachi range, is composed of undifferentiated Precambrian rocks and attains a maximum altitude of 22,047 feet in the Nevado de Cachi. Within the graben, along its eastern side, is an irregular subsidiary horst or "step", probably composed of several fault blocks, that forms the foothills of the Cachi range. It is underlain by volcanic rocks classified as Tertiary by Catalano and listed as Pliocene in the explanation of the Geologic Map of Argentina (Argentine Republic, 1950).

Three similar terms will appear frequently throughout the rest of this paper, and I wish here to differentiate among them. The structural unit between the two major horsts will be referred to as the *Sijes graben*, and it includes

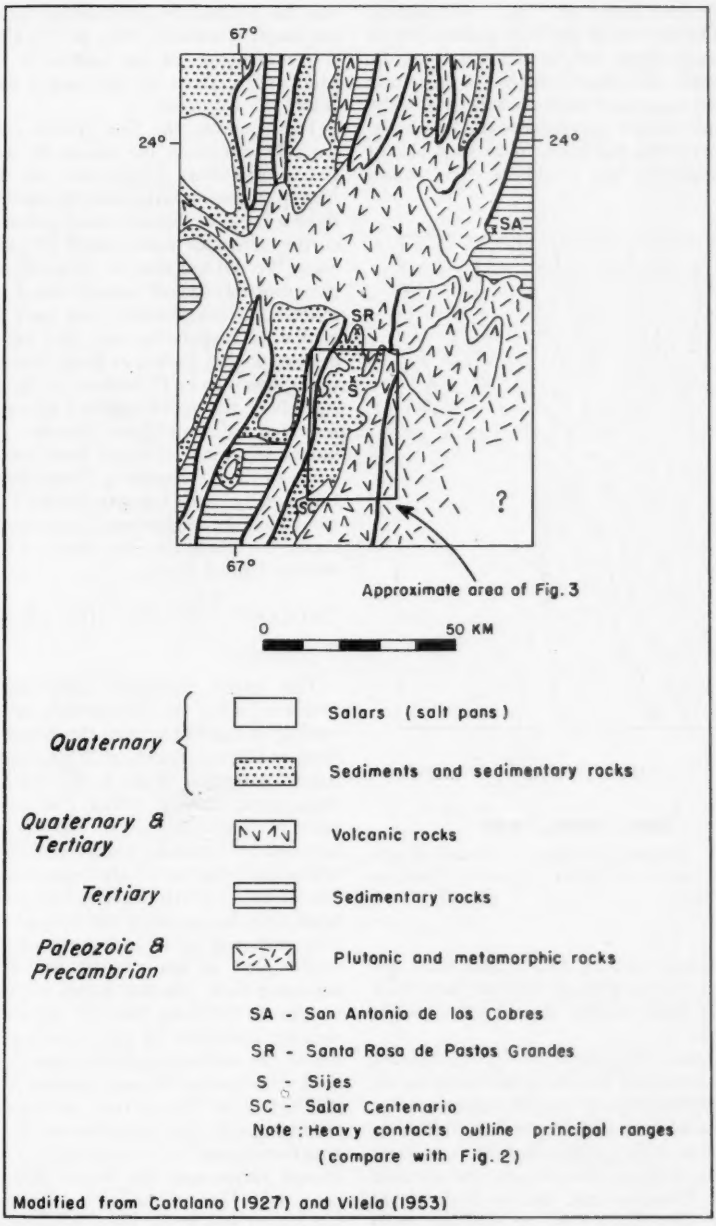

Figure 1. Regional geologic map of part of the province of Salta, Argentina

the subsidiary horst or "step" of volcanic rocks. The portion of the Sijes graben west of the volcanic block will be referred to as the *Sijes trough*. The Sijes trough is a structural entity but is approximately coincident with the topographic entity designated as the *Sijes basin;* these two terms will seem to be used almost interchangeably, but I will use *Sijes trough*

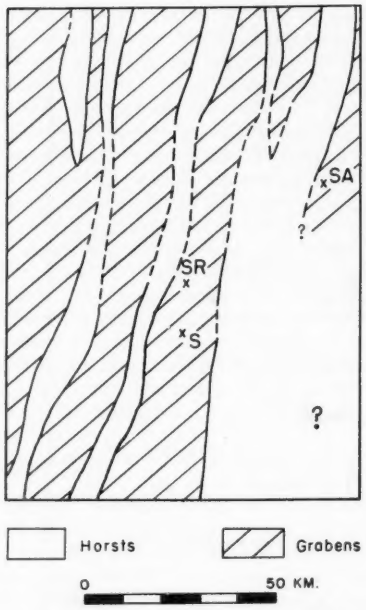

Figure 2. Inferred prevolcanic structure of part of the province of Salta, Argentina. Compare with Figure 1

mainly when referring to the structures, the sediments, or the general tectonic framework and *Sijes basin* mainly in reference to the topography.

The structural outlines of the Sijes graben continue for nearly 100 km to the north but are interrupted by a great mass of volcanic rocks, capped by a trio of peaks more than 18,000 feet high. Vilela (1953) subdivided these volcanic rocks into an upper Miocene unit and a middle or upper Pliocene unit; one or both of the units are continuous with the volcanic rocks along the east side of the graben. Such volcanic piles as this one, located along major transverse vents, subdivided the main valleys into "cells" and thus formed the gross outlines of the present basins (Catalano, 1927, p. 17). Figure 2 is a reconstruction of the pattern of the main valleys, or grabens, as they might have been before the volcanism.

To the south, the Sijes graben extends essentially unbroken for about 80 km. Both Catalano (1930a; 1930b) and the Geologic Map of Argentina (Argentine Republic, 1950b) show a band of Tertiary continental deposits cutting across the valley about 20 km south of Sijes. We did not observe these deposits, and they probably include some of the deposits described hereafter, which may have been regarded as Tertiary because they are severely deformed; they have now been shown by contained fossils to be Pleistocene or Recent.

In short, the Sijes trough is a structural basin receiving sediments from the two mountain blocks adjoining it, which have been eroded down to their Paleozoic or Precambrian cores. Structurally and topographically, the Sijes trough and its neighboring ranges appear to be similar to parts of the Great Basin of the southwestern United States.

GEOLOGY OF THE SIJES TROUGH

Topography

This paper considers approximately the northern half of the Sijes trough, or basin, extending about 40 km from the village of Santa Rosa de Pastos Grandes, at its northern end, to Salar Centenario (Figs. 1, 3). The principal topographic feature within this part of the basin is an irregular rib of hills about 30 km long and 1–3 km wide, which extends obliquely south-southwest across the basin from northeast of Sijes to west of Salar Centenario; this small range is here called the Sijes hills (Fig. 3). The hills rise to a maximum elevation of 14,000 feet, or about 1500 feet above the adjoining flats. The hill slopes are in general steeper on the west than on the east, where they are controlled by the prevailing eastward dip of the underlying sedimentary rocks; but both sides have gullies and canyons as much as 200 feet deep, characteristic of erosion in this desert region. The remainder of the basin is largely occupied by extensive alluvial flats with several playas and two major *salars*, or salt pans: Salar Pastos Grandes, northwest of Sijes, and Salar Centenario. These two elements, the Sijes hills and the flats, constitute the integral parts of the Sijes basin to be described in more detail.

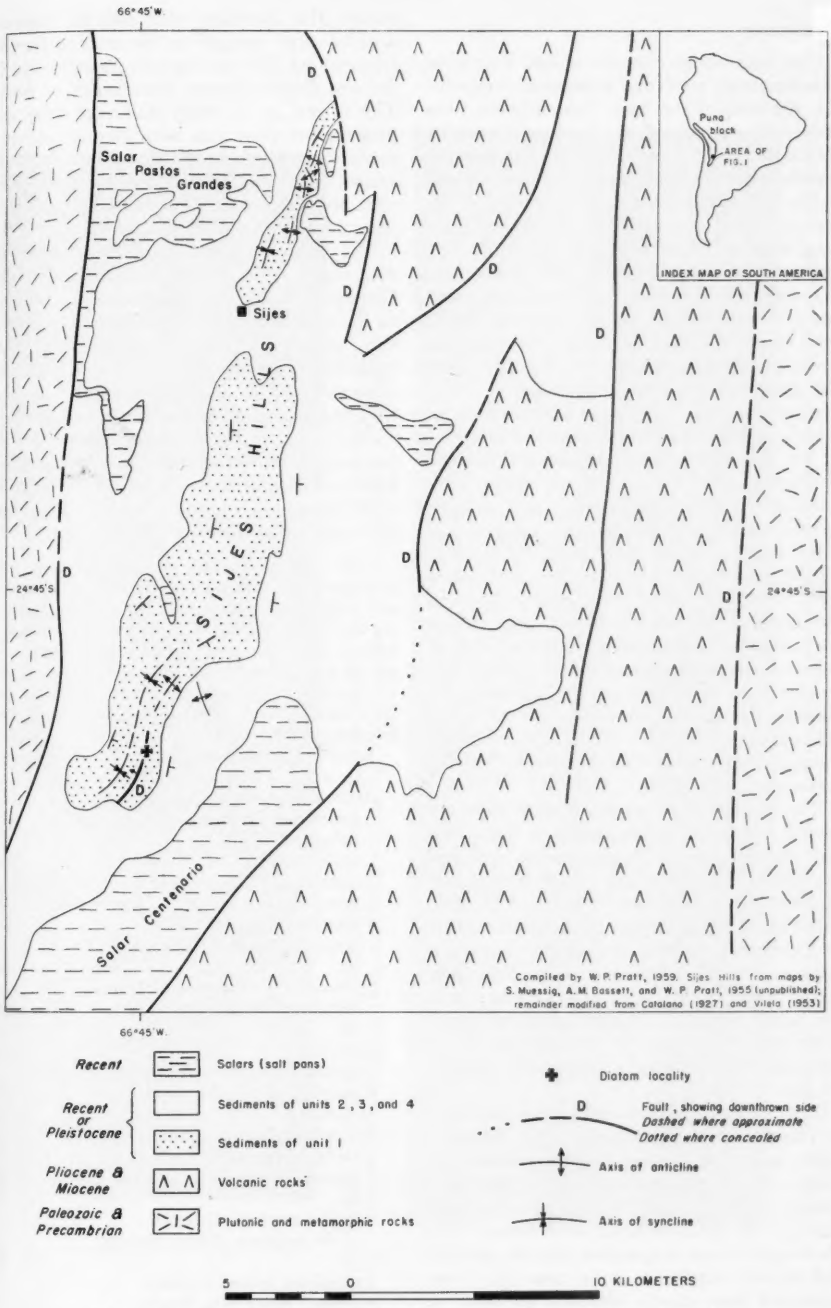

Figure 3. Geologic sketch map of Sijes area, province of Salta, Argentina

Stratigraphy

The Sijes trough contains at least four units of sedimentary rocks and sediments; except for the alluvium of the flats, these deposits were previously considered as Tertiary (Catalano, 1930a; Geol. Soc. America, 1950), but they are now known to be Pleistocene or younger. From oldest to youngest, the four units are: (1) intensely folded and faulted beds ranging from conglomerate to evaporites, and tuffs; (2) gently folded conglomerates and sandstones; (3) dissected flat-lying lacustrine sandstones and siltstones with minor gypsum and halite; and (4) fans and playa sediments of the present period of erosion and deposition. Figure 3 shows the general distribution of the units.

UNIT 1: Unit 1 comprises moderately to intensely folded and faulted beds that form most of the Sijes hills proper and are well exposed throughout the hills. They are fairly well-indurated clastic sedimentary rocks ranging from conglomerate to shale to gypsum and other evaporites, including borates (Catalano, 1930a), and they are interbedded with many tuffs. Near the base of the exposed section in the southern part of the hills is a conglomerate with abundant cobbles of argillite and schist in a green matrix of sand and clay, which evidently were derived from the metamorphic rocks in the range to the west. The best available estimated thickness of the exposed beds is more than 2500 feet (Allen M. Bassett, written communication, 1958).

The Pleistocene sediments in the trough may extend to great depths; unit 1 is the oldest unit exposed but does not necessarily represent the oldest sediments in the trough. Seismic and gravity surveys (Mabey, 1956, p. 852) indicate that the sedimentary fill in similar basins in southern California extends in places perhaps to as much as 5000 feet. The fill in these basins is not known to be deformed as it is in the Sijes trough, but because of the structural similarity of the basins it is reasonable to expect that the thickness of fill would be comparable.

This assemblage of clastics and evaporites is so characteristic of sediments being deposited today as fans and playa deposits in structural basins of arid regions—not only in the Sijes trough itself (*See* unit 4), but also in many places in the southwestern United States—that there seems to be no question that the geologic and climatic conditions at the time unit 1 was deposited were nearly identical to those of today. The abundant tuffs indicate volcanic activity close enough to the area to furnish frequent ash falls but far enough away that it did not furnish coarser pyroclastics or flows. This is perhaps the only difference from the present, for there has been Recent volcanic activity elsewhere in the Puna but the latest known volcanic deposits in this immediate area are "Holocene" basalt flows near San Antonio de los Cobres (Vilela, 1953).

The geologic age of the unit 1 beds has been determined by Kenneth E. Lohman of the Geological Survey as Pleistocene or Recent, on the basis of fossil diatoms that occurred with tiny gastropods (which unavoidably were mashed in transit to the U. S.) in a 1-inch bed of green mudstone included in hard, cinderlike tuffs near the south end of the Sijes hills (Fig. 3; Pl. 1, fig. 1). The fossil-bearing bed lies an estimated 1000 feet stratigraphically above the lowest exposed beds of unit 1, but the distance above the actual base of the unit is not known. Lohman's report reads in part as follows:

"The gastropods were so badly mashed that identification was impossible. Therefore the gastropod fragments together with the matrix, amounting to a total volume of about half a cubic centimeter, were processed for diatoms. Thirty-one species and varieties of diatoms were found, which are listed below, where their relative abundances are indicated by A—abundant, C—common, F—frequent, and R—rare.

Achnanthes conspicua A. Mayer	C
sp. aff. *A. conspicua* A. Mayer	F
Amphora coffaeformis Agardh	F
commutata Grunow	C
holsatica Hustedt	C
ovalis Kützing	F
Anomoeoneis polygramma (Ehrenberg) Pfitzer	F
Caloneis bacillum (Grunow) Mereschkowsky	R
formosa (Gregory) Cleve	C
permagna (Bailey) Cleve	F
sp.	F
Cymbella cf. *C. haucki* Van Heurck	R
hebridica (Gregory) Grunow	F
sp.	R
Denticula sp.	R
Fragilaria leptostauron (Ehrenberg) Hustedt	A
Mastogloia elliptica (Agardh) Cleve	C
Melosira sp.	R
Navicula cf. *N. amygdalina* Hustedt	F
cari var. *angusta* Grunow	R
pygmaea Kützing	R
sp.	R
Nitzschia amphibia Grunow	F
cf. *N. paradoxa* (Gmel) Grunow	F
sp.	R
Scoliopleura peisonis Grunow	F
Stauroneis salina Wm. Smith	R

Figure 1. Panorama of southern Sijes hills, showing diatom locality (marked by long arrow) in steeply dipping unit 1 beds overturned beneath reverse fault (marked by small arrows and dashed line). Note earthflow in foreground. View is southwest

Figure 2. Panorama, looking southeast; 1, unit 1 beds; 2, unit 2 gravels; 3, Salar Centenario (unit 4); 4, Miocene and Pliocene volcanic rocks surmounted by erosion surface; 5, Precambrian of the Cachi range

PANORAMAS, PROVINCE OF SALTA, ARGENTINA

Figure 1. Lake beds of unit 3 in foreground and middle ground; Salar Pastos Grandes in middle ground; Miocene and Pliocene volcanic rocks form high peaks. View is north

Figure 2. Hanging U-shaped valley in Miocene and Pliocene volcanic rocks; note northeasterly dip of layering. Nevado de Cachi (22,047 feet) in background. View is east. Photograph by Siegfried Muessig

Figure 3. Folded unit 1 beds in central Sijes hills. View is southeast

Figure 4. Gentle anticline in unit 2 beds, which overlie steeply dipping unit 1 beds along low hills at far right. View is south. Photograph by Siegfried Muessig

Surirella crumena Brebisson	C
cf. *S. striatula* Turpin	F
testudo Ehrenberg	C
Synedra affinis Kützing	R

"All of the diatoms in this assemblage are represented in living assemblages in many localities, and are characteristic of very saline lakes of moderate to cool temperatures. Species characteristic of lakes containing fresh water pure enough to be potable are rare or absent in this assemblage. Frenguelli (1939) has listed 118 species and varieties of diatoms from Lake Titicaca, of which only seven of those listed as rare also occur in the Sijes assemblage. Furthermore these seven species are members of a group that will tolerate a wide range in salinity. Judging solely from their diatom populations, the lake in which the Sijes assemblage lived was many times as saline as Lake Titicaca.

". . . The fact that no species known to be extinct occurred in this assemblage strongly suggests that the geologic age of the beds cannot be older than Pleistocene. Extinct species of diatoms occur in abundance in the Provo formation of Wisconsin age in Utah, as well as in other late Pleistocene beds. Their absence in the present assemblage implies that the Sijes material may be late Pleistocene in age."

In addition to indicating the geologic age of the beds, the diatoms offer further evidence that the climate was similar to that of today, for the waters in which the diatoms lived, like the present playa lakes, were highly saline.

UNIT 2: Unit 2 consists of poorly consolidated conglomerates and sandstones that are exposed chiefly in the central part of the Sijes hills and in foothills along the east side of the southern part (Pl. 1, fig. 2), and are deeply cut by the gullies now draining the hills. These beds, at least several hundred feet thick, are gently folded, dip generally east, and lie with angular unconformity above the more intensely folded beds of unit 1.

Gravel fans exposed across the flat west of the Sijes hills, which appear to be faulted down against the Paleozoic rocks of the western horst, may overlie the beds of unit 2 (Siegfried Muessig, written communication), but because of the uncertainty they are here included in unit 2.

UNIT 3: Unit 3 is composed of flat-lying lacustrine sandstones and siltstones, containing some gypsum and halite, exposed only in the northwest part of the trough as flat-topped mesas in and near the Salar Pastos Grandes (Pl. 2, fig. 1). These beds lie unconformably above the beds of unit 1. Their relationship to unit 2 is not clear, and they could represent the basin facies of the conglomerates, but because they have not been deformed they are thought to be younger. The exposed thickness of unit 3 is at least 100 feet, and the unit probably extends below the present salar surface and is therefore thicker.

UNIT 4: Unit 4, the youngest, comprises the alluvial fans and playa sediments of the present depositional period, which lie disconformably above (adjacent to) the lake beds of unit 3 and with angular unconformity above units 1 and 2. These deposits range from coarse, poorly sorted gravels to silts, clays, and salines; the salines form the broad white expanses of Salar Pastos Grandes and Salar Centenario (Pl. 1, fig. 2; Pl. 2, fig. 1) and according to Catalano (1930a, p. 299) consist of halite, gypsum, and borates—chiefly ulexite and borax—as well as sodium sulfate, magnesium sulfate, and sodium carbonate. Except for the degree of consolidation, the absence of tuffs, and the details of saline mineralogy, the sediments of unit 4 are much like those of unit 1. The thickness of unit 4 is unknown; pits on Salar Centenario have exposed the sediments to a depth of about 6 feet, but judging from the extensive erosion of the older units they are probably much thicker.

Table 1 summarizes the stratigraphy of the Sijes trough.

Catalano (1927, p. 16–20) describes folded beds southwest of Salar Pastos Grandes, probably corresponding to unit 1, as Tertiary, and considers them to have been deformed during the Tertiary. He also describes evidence involving the salt beds in and around Salar Pastos Grandes which he interprets to mean three periods of local uplift later than the Tertiary deformation. Unfortunately his rather unclear descriptions and his omission of a map make it impossible to evaluate this information or to relate it to the facts that have just been set forth.

STRUCTURE

Regional Structure

That the Sijes basin occupies a true graben is not merely a tacit assumption. The general topography of the basin and the adjoining ranges is similar to the North American Great Basin, and the similarity extends to the delineation of the ranges by abrupt lithologic discontinuities coincident with well-developed scarps. These features suggest that the similarity to the ranges of the Great Basin is structural as well as topographic, a suggestion substantiated

in the literature. Catalano (1927, p. 17) mentions ". . . great fault lines, which follow the same trend as the valleys, [and] are verified by the abrupt forms with which the delimiting mountains rise up," although he does not describe the faults or even show them on his reconnaissance map (1930a; 1930b). Picard (1948, p. 797–798), discussing structures on a more regional scale, refers specifically to block-mountains, horsts, and grabens in the Puna, and says ". . . these are, morphologically and structurally, 'basin-range structures'." Vilela (1953), on a more detailed map (1:294,000) of the region north of Sijes, shows reverse faults bounding some of the mountain ranges northwest of San Antonio de los Cobres (Fig. 1) but does not discuss them. Finally, Harrington (1956, p. 164), after a presumably thorough review of the literature and with a wealth of experience in Argentine geology, specifically mentions the basin-range structure of the Puna. I therefore consider it reasonably well established that the Sijes graben is a fault block relative to which the two adjacent blocks have been uplifted, even though I have not actually observed the boundary faults and do not know whether they are normal or reverse.

Harrington (1956, p. 164) states that the basin-and-range structure of the Puna was first outlined by orogenic movements between the middle and late Miocene, even though the uplift of the Puna block as a whole did not begin until the Pliocene. What Muessig, Bassett, and I have seen within the Sijes graben neither confirms nor refutes this, but does indicate that the trough, and therefore the graben, must have been established by the early or middle Pleistocene in order to have received the sediments described. Could the Pleistocene sediments—at least unit 1—have been deposited as a regional sedimentary blanket before the graben was formed? Very probably they were not, because the lithology of units 1 and 2 indicates basin deposition; moreover, if a uniform blanket as thick as unit 1 were deposited over areas later uplifted to produce the present mountain blocks, the uplifted areas almost certainly would still contain remnant patches of the sediments, and no such remnants are known.

BOUNDARY FAULTS: The west boundary of the Sijes trough is an inferred fault marked by a well-defined scarp developed on the Paleozoic and Precambrian rocks of the range to the west. The east boundary of the trough is the fault that separates it from the volcanic block. The scarp that marks this fault truncates a well-developed erosion surface on the tilted volcanic rocks and also truncates layering in the volcanic rocks; these truncations, and several hanging U-shaped valleys on the erosion surface (Pl. 2, fig. 2), are all good evidence that both the scarp and the present relief are a direct result of the faulting.

TABLE 1. STRATIGRAPHY OF THE SIJES TROUGH

Unit	Lithology	Estimated thickness	Origin
4	Gravels, silts, clays, salines	Unknown	Fans and playa deposits
	Disconformity		
3	Sandstones, siltstones, some gypsum and halite	100′+	Lacustrine deposits
	Unconformity		
2	Conglomerates and sandstones	Several hundred ft.	Fans
	Unconformity		
1	Conglomerate to shale, evaporites, tuffs; Pleistocene diatoms	2500′+	Fans and playa deposits

Structures Within the Sijes Trough

FAULTS: Faults within the Sijes trough comprise normal and strike-slip faults and one major reverse fault, all restricted to unit 1; no other faults are known. The normal and strike-slip faults occur near the north and south ends of the Sijes hills but are absent from the central part. Most of them strike in the quadrant between northeast and southeast, dip steeply, and have displacements of a few tens of feet. The reverse fault is near the south end of the hills (Pl. 1, fig. 1); it strikes approximately north and dips steeply west, and the displacement is estimated to be at least 900 feet.

FOLDS: Exposures of folds within the Sijes

trough are restricted to units 1 and 2 in the Sijes hills. The dominant structures in unit 1 throughout most of the Sijes hills are a general eastward dip and a few broad to moderately tight northerly-trending folds (Pl. 2, fig. 3), but at the north and south ends the dips are steep. The most intense deformation took place at the south end, where the steeply dipping beds are locally overturned and dip west beneath the reverse fault described above; west of the fault the beds are right-side up and dip west, forming the east limb of a syncline (Pl. 1, fig. 1). Unit 2, which overlies unit 1 unconformably, is much less intensely deformed than unit 1. In many places along the east side of the Sijes hills the unit 2 beds dip gently eastward, and at one place they are arched into a gentle anticline (Pl. 2, fig. 4). No other structures in unit 2 are known.

LANDSLIDES: A large, partly dissected mudflow caps unit 1 in the southern part of the Sijes hills. The mass has a relatively smooth base and surface, is 30–50 feet thick in most places, and covers an area of about two-thirds of a square kilometer. It seems clearly to have been a well-lubricated mudflow, probably an earthflow in the classification of Thornbury (1954, p. 91). (It is described here only because it is so clearly visible in Figure 1 of Plate 1.) Several small debris slides also occur in the southern part of the hills, but they are not pertinent to this discussion.

Sequence of Structures

Four distinct groups of structures must now be accounted for:

(1) the major boundary faults delineating the graben;
(2) the subsidiary faults of the volcanic block, especially the fault that separates it from the trough;
(3) the faults and folds in unit 1;
(4) the folds in unit 2.

The sequence and the origin of the structures are of course interrelated, but the discussion will become less involved if we first establish the sequence, as far as possible, and then consider the origin.

Parts of the structural sequence are clear almost at once and have already been stated or implied: the faults and folds in unit 1 must have preceded the deposition of unit 2 and therefore the folds in unit 2, because unit 2 truncates the structures in unit 1 and is much less intensely deformed. Moreover, the graben must have been established before unit 1 was deposited, and therefore the major boundary faults were the earliest structures. (That is, the original movement on them was earliest; there may have been later movement on them as well). Indeed, according to Harrington (1956, p. 164), the major faults originated during the Miocene.

The relative age of the subsidiary faults in the volcanic rocks is less apparent, and pertinent to this question are the following facts and inferences:

(1) A well-developed erosion surface is cut directly on the gently north- or northeast-dipping volcanic rocks and ends along the abrupt linear scarp on its west side (Pl. 1, fig. 2; Pl. 2, fig. 2). *Inferences:* The surface postdates tilting of the volcanic rocks; moreover, it once extended farther west but the west side—now occupied by the basin—was dropped down along a fault now marked by the scarp. The surface predates the initial movement on this fault.

(2) The erosion surface on the volcanic rocks appears to be free of any sediments of the type that fill the trough. *Inference:* Initial movement on the fault preceded the deposition of unit 1.

(3) The erosion surface on the volcanic rocks is indented by several broadly U-shaped hanging valleys. *Inferences:* A major uplift of the volcanic block—at least that producing the present relief above the basin—must have occurred quite late. There is no direct evidence as to the exact meaning of "quite late," but indirect evidence (the U shapes of the hanging valleys, notably the one just left of center in Figure 2 of Plate 2) suggests that the valleys have been glaciated, and the apparent absence of glacial deposits, from the valleys themselves and the basin, suggests further that if they *were* glaciated, it must have been prior to the uplift. This probable glaciation of the volcanic block and the glaciation of the volcanic peaks to the north indicate a more humid climate in the past than at present, because the peaks are not now being glaciated. The lacustrine lithology of unit 3 also calls for a more humid climate. It seems reasonable that the glaciation in both places and the deposition of unit 3 were contemporaneous, all resulting from a single period of increased humidity. If this inference is correct, then the major uplift of the volcanic block occurred after the deposition of unit 3, and was thus "quite late" indeed, even though the original separation of the block predated unit 1.

In summary, the sequence of the major late

Tertiary and Quaternary structural events, and of the intervening episodes of erosion and deposition, is inferred to be as follows:

Delineation of the graben during the Miocene.

Renewed movement on major faults, perhaps concomitant with tilting of volcanic rocks. Development of erosion surface on the volcanic rocks.

Faulting and initiation of the trough, in which unit 1 was then deposited.

Deformation of unit 1, probably with further faulting in the volcanic block. Deposition of unit 2.

Deformation of unit 2, and therefore of unit 1. Deposition of unit 3 with concurrent glaciation of volcanic block and peaks to north.

Second and major uplift of volcanic block. Present cycle—erosion of older units and deposition of unit 4.

Origin of Structures

The real nature of the faults that bound the graben and the trough—that is, whether they are normal or reverse—does not seem to be known, but from the several casual references in the literature to block faults, or horsts and grabens, or basin-and-range structure (*See* Regional Structure), and from a striking topographic resemblance to the ranges of the Great Basin, I think the safest inference is that the major faults here are the normal faults of typical horst and graben structure. Such structure is generally attributed to regional tension. The structures within the trough however—the easterly trending normal and strike-slip faults, the north-trending reverse fault, and the northerly trending folds—all indicate a relatively uncomplicated picture of surficial compression, along an east-west axis. The sequence of events deduced heretofore shows clearly that the structures within the trough were developed contemporaneously with renewed movements on the older (Miocene) regional faults—movements that occurred intermittently throughout the Quaternary. It follows that the origin of the local structures must be explained in terms of a mechanism that is compatible with normal movement on the regional faults. (If the regional faults are some day shown to be reverse faults, then there is no problem and the rest of this paper is erroneous. The succeeding paragraphs presuppose that the faults are normal).

PROPOSED EXPLANATION—HORST-WEDGING: I suggest that the local structures were formed by uplift of the horst blocks, which acted as wedges and compressed the graben between them. Gilluly, Waters, and Woodford (1959, p. 431) suggest this general mechanism for the fault-block structures of the ranges of the Great Basin; they refer to the mechanism as "differential vertical movements of adjacent crustal blocks along normal faults." A similar mechanism is implied by Harrington (1956, p. 164) for the basin-and-range structure of the Puna. Applying the mechanism to the Sijes area, and *assuming* that the Sijes trough is bounded by normal faults dipping inward, then either or both horst blocks, if uplifted, would act as wedges; the horizontal component of uplift

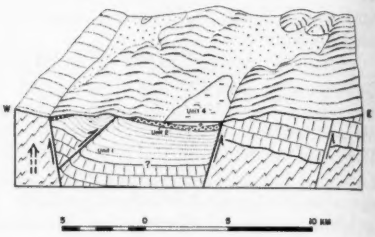

Figure 4. Block diagram of south-central Sijes trough and adjoining ranges, with cross section near south end of Sijes hills

would compress the graben block, with expectable results similar to the structures observed. This explanation, which for simplicity I would refer to as *horst-wedging*, is shown diagrammatically in Figure 4. It is perhaps a roundabout approach, but it seems the most reasonable interpretation of the meager field evidence available.[1]

ALTERNATE EXPLANATIONS AND OBJECTIONS TO THEM: The futility of lengthy speculations based on such a tentative assumption—that the regional faults are normal—is manifest, but I feel bound to point out briefly the objections to several other apparent explanations of the local structures.

Probably the most obvious alternate explanation is that the compressional features in the

[1] I would stress that this mechanism differs fundamentally from regional tension: briefly, in regional tension the horsts would move apart, whereas in the horst-wedging mechanism they are pushed upward. The one mechanism involves lengthening of the crust as a cause or at least a corollary; the other involves it, if at all, as a result.

trough are due simply to regional compression during the Pleistocene. This explanation, however, is incompatible with the (assumed) *normal* movement on the regional faults.

Another "obvious" explanation is that the compressional structures were created as a by-product of renewed regional tension, by squeezing or pinching of the graben (and the trough) as it dropped between the separating horst blocks. While this idea is appealing because of its apparent geometric simplicity, it is not supported by experimental evidence (H. Cloos, 1930, Figs. 6–8; 1931, Figs. 2, 3; 1939, Figs. 7, 15, 16; E. Cloos, 1955, p. 246–247; Fig. 3; Pl. 4, fig. 3).

Finally, several people have suggested to me that the structures within the trough might be due to simple gravity sliding—presumably, sliding of the entire Sijes hills mass into its present position. This explanation would require that the materials of at least unit 1 slid into their present locations from somewhere to the east or west, in order to account for their east–west compressional pattern. But it is hard to understand how, within a trough steadily filling up with sediments, relief could be developed sufficient to cause (and permit) gravity sliding of the very sediments filling the trough. Nor is it clear whether, according to this hypothesis, the deformation of unit 2 is also to be explained by gravity sliding. This hypothesis does not appear to satisfy, either structurally or topographically, the deduced regional picture of accumulation of sediments in a structural basin.

SUMMARY AND CONCLUSIONS

The existence of Pleistocene or Recent diatoms in steeply folded and faulted basin sediments, overlain by three distinctly younger sedimentary units, indicates that a great deal of deformation has taken place in the Puna in geologically very recent times. The structures described here are specific evidence of local movement that has gone on intermittently throughout the later Quaternary—or at least since the deposition of the diatom-bearing beds. Whatever may be the precise age of the beds within the Quaternary, this is real evidence of a late Pleistocene to Recent orogeny.

Simple compression or tension is inadequate to explain both the local compressive structures within the trough and the Quaternary movement on the regional block faults, since the two sets of structures were active contemporaneously. The mechanism of horst-wedging, a special case of the general theory of differential vertical movements of adjacent crustal blocks, seems to afford an acceptable explanation. Vertical forces, probably extending from the base of the crust, raised the horst blocks along the pre-existing normal faults. This uplift continued intermittently, and as the debris being shed off the rising horst blocks collected in the graben, the horst blocks acted as wedges and squeezed the graben sediments into their present pattern of faults and folds.

I have referred often in this paper to the ranges of the Great Basin, because I think their apparent analogy with the Puna provides a basis for understanding of some of the Puna structures. Conversely, this interpretation of the Puna structures may be applicable to the ranges of the Great Basin, because the principle of compatibility between contemporaneous regional and local structures ought to be just as valid in the Great Basin as it is in the Puna. I do not know of any structures in the sedimentary fill of the North American basins that are like those described here, but if such structures exist—and I think we should be on the lookout for them—they might give us a new insight into the structural interpretation of the region in which they lie.

REFERENCES CITED

Argentine Republic, 1950a, Explicación del mapa geologico de la República Argentina: Dir. Nac. de Minería, Bol. no. 73, 28 p.

—— 1950b, Mapa geológico de la República Argentina (1:2,500,000): Dir. Nac. de Minería

Catalano, L. R., 1927, Geología química de los boratos; formación de las cuencas y característicsa generales de la superficie de los salares, Puna de Atacama: Ministerio de Agr. de la Nación, Dir. Gen. de Minas, Geol. e Hidrología, Pub. no. 28, 101 p.

—— 1930a, Reseña geológica preliminar de la Puna de Atacama, Territorio Nacional de los Andes: Revista Minera, v. 2, p. 270–286, 289–305

—— 1930b, Puna de Atacama, Reseña geológica y geográfica: Univ. Nacional del Litoral, Pub. num. 8 del Departamento de extensión universitaria (Santa Fe, República Argentina), 106 p.

Cloos, Ernst, 1955, Experimental analysis of fracture patterns: Geol. Soc. America Bull., v. 66, p. 241–256

Cloos, Hans, 1930, Zur Experimentellen Tektonik. Methode und Beispiele: Die Naturwiss., v. 18, no. 34, p. 741–747

—— 1931, Zur Experimentellen Tektonik. Brüche und Falten: Die Naturwiss., v. 19, no. 11, p. 242–247

—— 1939, Hebung, Spaltung, Vulkanismus: Geol. Rundschau, v. 30, p. 405–527

Frenguelli, Joaquín, 1939, Diatomeas del Lago Titicaca: Notas del Museo La Plata, Tomo IV, Bot. No. 24, p. 175–196

Geological Society of America, 1950, Geologic map of South America

Gilluly, James, Waters, A. C., and Woodford, A. O., 1959, Principles of geology, 2d ed.: San Francisco, W. H. Freeman and Co., 534 p.

Harrington, H. J., 1956, Argentina, p. 129–165 *in* Jenks, W. F., *Editor*, Handbook of South American geology: Geol. Soc. America Mem. 65, 378 p.

Mabey, D. R., 1956, Geophysical studies in southern California basins: Geophysics, v. 21, p. 839–853

Picard, Leo, 1948, La structure du Nord-Ouest de l'Argentine avec quelques réflexions sur la structure des Andes: Soc. géol. France Bull., 5th ser., v. 18, p. 765–846

Thornbury, W. D., 1954, Principles of geomorphology: New York, John Wiley and Sons, Inc., 618 p.

Vilela, C. R., 1953, Los periodos eruptivos en la Puna de Atacama: Asoc. Geol. Argentina Rev., v. 8, p. 5–36

Manuscript Received by the Secretary of the Society, June 13, 1960
Publication Authorized by the Director, U. S. Geological Survey

CARLOS RUIZ
LUIS AGUIRRE
JOSÉ CORVALÁN
Instituto de Investigaciones Geológicas, Santiago, Chile

H. J. ROSE, JR.
KENNETH SEGERSTROM
T. W. STERN
U. S. Geological Survey, Santiago, Chile, and Washington, D. C.

Ages of Batholithic Intrusions of Northern and Central Chile

Abstract: Their stratigraphic setting demonstrates that three batholithic intrusions in northern and central Chile are respectively pre-Jurassic, Jurassic, and Cretaceous. Radiometric age determinations, by the lead-alpha (Larsen) method, indicate ages of 265 ± 30, 120 ± 15 to 125 ± 15, and 95 ± 10 to 130 ± 15 million years respectively for samples from the batholiths whose stratigraphic setting has been established or is inferred. With one exception, the radiometric ages are consistent with the stratigraphy. The exceptional determination of 130 ± 15 million years was for a sample of granite that intrudes Cretaceous rocks. Three other samples of Cretaceous granitic rocks were within the range of 95 ± 10 to 105 ± 10 million years.

Angular unconformities whose ages are correlative with the intrusions suggest that the three batholiths can be related respectively to Hercynian, Late Jurassic, and middle Cretaceous orogenies.

CONTENTS

Introduction 1551
Acknowledgments 1552
Ages of batholithic intrusions of northern and central Chile 1552
Pre-Jurassic intrusions 1552
Jurassic intrusions 1553
Cretaceous intrusions 1554
Lead-alpha age determinations 1555
Method 1555
Upper Paleozoic granite 1555
Upper Jurassic granitic rocks 1556
Middle Cretaceous granitic rocks 1556
Relationship of orogeny to intrusive activity . . 1557
Hercynian orogeny 1557
Late Jurassic orogeny 1557
Early Late Cretaceous orogeny 1558
Conclusions 1558
References cited 1559

Figure
1. Index map of northern Chile, showing localities of samples used in lead-alpha age determinations 1554

Table
1. Lead-alpha age determinations of zircon from Chilean rocks 1556

INTRODUCTION

Recent studies in northern and central Chile by geologists of the Instituto de Investigaciones Geológicas (I.I.G.) and the Empresa Nacional del Petroleo (E.N.A.P.) have fixed the boundaries of three batholithic intrusions and determined their ages. The ages were determined by the lead-alpha (Larsen) method and are correlated with orogenic epochs by stratigraphic evidence based on numerous fossil determinations.

Samples of intrusive rock collected by I.I.G. and E.N.A.P. geologists from nine localities in northern and central Chile were dated by the lead-alpha (Larsen) method at the Geochronology Laboratory of the U. S. Geological Survey in Washington. Two samples had small zircon yields, and insufficient material was available to obtain acceptable precision in the spectrochemical lead determination. No ages were calculated for these two samples. Age determinations of the other seven samples are in acceptable agreement with known stratigra-

Geological Society of America Bulletin, v. 72, p. 1551–1560, 1 fig., October 1961

phy using the time scale of Kulp (1959), although the upper or lower limits calculated for several of the ages must be used to relate the lead-alpha ages for the granites to the ages determined by stratigraphic studies of the three batholithic intrusions.

Orogenic epochs related to each of the three major intrusions can be established by stratigraphic evidence. The epochs seem to fall naturally within Hercynian, Late Jurassic, and mid-Cretaceous orogenic cycles.

Age determinations of granites from other parts of Chile will be made.

ACKNOWLEDGMENTS

Floreal García, a geologist of the Empresa Nacional del Petroleo, conducted those of the authors in Chile on a tour of Antofagasta and Tarapacá provinces, thereby greatly increasing their knowledge of the stratigraphy of northern Chile. Thanks are due Sr. García and the management of E.N.A.P. for permission to use some of García's unpublished data.

The authors are also grateful to J. M. Mangum and H. W. Worthing of the U. S. Geological Survey for aid in making the lead-alpha (Larsen) age determinations used in this paper. R. J. Dingman and G. E. Ericksen of the Instituto de Investigaciones Geológicas and the U. S. Geological Survey aided in the preparation of the present report. Mr. Dingman translated the first draft from Spanish to English, and Mr. Ericksen critically reviewed the manuscript. Pierre St. Amand, of the Naval Ordnance Test Station, China Lake, California, and C. R. Allen, of California Institute of Technology, made valuable suggestions which were followed in revising the manuscript. Ernesto Pérez, of the Instituto de Investigaciones Geologicas, assisted Corvalán in the identification and age determinations of the fossils.

AGES OF BATHOLITHIC INTRUSIONS OF NORTHERN AND CENTRAL CHILE

Pre-Jurassic Intrusions

Batholithic intrusions of three different ages can be distinguished in northern and central Chile.

Pre-Jurassic granite occurs in Atacama, Antofagasta, and Coquimbo provinces. Along the coast near the border between Atacama and Antofagasta provinces, granites are exposed for 120 km. The granites are light gray, medium- to coarse-grained, and consist principally of quartz, microperthite, plagioclase, and biotite. Fifteen km east of Chañaral they intrude quartzites, phyllites, and slates that are tentatively correlated with the El Toco formation, whose type locality is 10 km west of El Toco railroad station, on the east slope of Sierra Angostura, about 400 km north-northeast of Chañaral. Wetzel (1927) collected Permo-Carboniferous fossil plants in the El Toco formation.

In some localities the quartzites and phyllites are unconformably overlain by light-red arkosic conglomerate containing granite cobbles and by rhyolite or soda-trachyte flows and tuffs. Geologists of the Empresa Nacional del Petróleo who have found poorly preserved fossil plants in the conglomerate-rhyolite section have included these younger beds in the Cifuncho formation, which crops out 6 km east of Caleta Cifuncho, 25 km south of Taltal in the southern part of the province of Antofagasta. The Cifuncho formation is believed to be Triassic on the basis of its lithologic similarity to Triassic sedimentary and volcanic rocks in other parts of Chile.

The granite is cut by black diabase dikes that strike northeast. The dikes also intrude the quartzites and phyllites and the overlying Cifuncho formation. The granite, metamorphic rocks, Cifuncho formation, and black dikes are all unconformably overlain by the Pan de Azúcar formation, named by geologists of the Instituto de Investigaciones Geológicas for Quebrada Pan de Azúcar, 40 km northeast of Chañaral, in the northern part of the province of Atacama. The unconformity is well exposed on the north bank of Quebrada Pan de Azúcar, 4 km west of Bombas. The formation has a basal conglomerate containing pebbles of quartzite and phyllite. Higher in the Pan de Azúcar formation are marls and calcareous sandstones containing pelecypods and abundant ammonites of the genera *Psiloceras* (*Franziceras*), *Pseudaltomoceras*, and *Kammerkaroceras*, which are forms restricted to the Hettangian (Early Jurassic) (Ortiz *et al.*, written communication).

Pre-Jurassic granites also crop out on the lower slopes of the Andes in Antofagasta, Atacama, and Coquimbo provinces. On Cerro Mesa, east of Chuquicamata, in Antofagasta province, there is an extensive mass of light-gray, medium-grained granite composed principally of microcline, perthite, plagioclase, quartz, muscovite, and biotite. Floreal García (Oral communication) reports that geologists of the

Anaconda Company have named this intrusion "Mesa granite," and that Liassic (Early Jurassic) sedimentary rocks overlie the granite unconformably.

In Quebrada Asientos, 7.5 km northeast of Potrerillos, in the northeastern part of Atacama province, there is a granite that was first described by Bailey Willis (1929). The granite is gray, medium-grained, composed of plagioclase and orthoclase feldspars, quartz, biotite, and amphibole, and is disconformably overlain by a sedimentary sequence. The lowest part of the sequence is Early Jurassic (Lias) (unpub. section by Ernesto Pérez of the Instituto de Investigaciones Geológicas). The fossils collected from the sedimentary beds include *Oxynoticeras*, *Arieticeras*, *Lithotrochus humboldti* von Buch, and *Weyla alata* (von Buch) Bayle et Coquand.

Pinkish-gray, medium-grained granite crops out on the north and east sides of the junction of the Copiapó and Jorquera rivers at Juntas, 85 km southeast of Copiapó in Atacama province (Segerstrom, 1959). The granite, composed of quartz, orthoclase, microcline and biotite, is disconformably overlain by basal conglomerate of the Lautaro formation, containing boulders of the underlying granite. The Lautaro formation contains fossils of Liassic age. *Lithotrochus humboldti* von Buch, *Gryphaea darwini*, *Weyla alata* (von Buch) Bayle et Coquand, *Arieticeras* sp., and *Oxynoticeras* oxynotum (Quenstedt) were found in the lower beds of the formation and *Harpoceras falcifer* (Sowerby), *Peronoceras* sp. aff. *fibulatum* (Sowerby), and *Dactylioceras* sp. in the upper part.

Another extensive mass of pinkish-gray granite exposed 35 km west of Juntas is composed of quartz, orthoclase, microcline, and plagioclase. It is disconformably overlain by a formation of continental origin containing a thick lower sequence of conglomerates overlain by cross-bedded sandstones and by layers of volcanic rocks. The formation, which is unnamed, underlies the Lautaro formation, and it is probably Late Triassic.

Reddish sandstone and conglomerate, containing abundant boulders of granite, crop out in Quebrada Paipote, 4–15 km east of Puquios, or about 70 km east of Copiapó, in Atacama province. The granite boulders are pinkish gray and lithologically similar to the granite described in the two preceding paragraphs. The sandstone and conglomerate disconformably underlie the coal-bearing beds of La Ternera (Segerstrom, 1960). The coal beds contain a Late Triassic (Rhaetic) flora including *Copiapaea plicatella* Solms-Laubach, *Taeniopteris* (*Yabeiella*) cf. *mareysiaca* Gein, *Thinnfeldia* (*Dicroidium*) cf. *Lancifolia* Morr. et cf. *Incisa* Sap., *Pecopteria* (*Asterotheca ?*) *fuchsi* Schpr., and *Podozamites distans* (Presl), according to the determinations of Solms-Laubach and Steinmann (1899), as corrected by Steinmann (1920).

Another granite mass is exposed in the area of Rivadavia, 80 km east of La Serena, in Coquimbo province. This rock is yellowish gray, medium-grained, and composed of quartz, perthite, plagioclase, and biotite. It is disconformably overlain by the Early Liassic Tres Cruces formation (Pedro Dedios, oral communication). The Tres Cruces formation contains *Lithotrochus humboldti* von Buch, *Gryphaea darwini* Forbes, *Spiriferina rostrata* Schlotheim, and *Cardinia densestriata* Jaworski.

Thus stratigraphic evidence indicates that the granites described are definitely pre-Jurassic and possibly pre-Late Triassic. No direct stratigraphic evidence permits the assigning of a lower age limit to these intrusions, but if it is true that the quartzites and slates intruded by granite along the coast near the border between Atacama and Antofagasta provinces are equivalent to the El Toco formation, then the earliest age of the granite is Permian and Carboniferous.

According to our present knowledge, no metallization accompanied the emplacement of granite of pre-Jurassic age; moreover, the granite does not appear to be a favorable host for metalliferous deposits.

Jurassic Intrusions

Granitic rocks of Jurassic age occur in the provinces of Tarapacá and Antofagasta, in the Coast Range and in the Andes. Grayish-red augite granodiorite exposed in Quebrada Camarones, 70 km south-southeast of Arica (Fig. 1), intrudes the Chiza formation of Callovian (Jurassic) age (containing *Reineckeia* and *Macrocephalites*) and is disconformably overlain by beds of eastward-dipping reddish, fine-grained arkosic conglomerate. The granodiorite is composed of plagioclase, quartz, potassium feldspars, augite, and scarce amphibole. The conglomerate is overlain by tuffaceous breccia and andesitic lava. Cecioni and Garciá (1960, p. 18) assign the conglomerate to the Atajaña formation. At its type locality, 20 km south-southwest of Quebrada Cama-

rones, the Atajaña formation is of continental origin, and it consists of beds of reddish sandstone and conglomerate containing cobbles of fine-grained granodiorite. The overlying Blanco formation is of marine origin and contains the

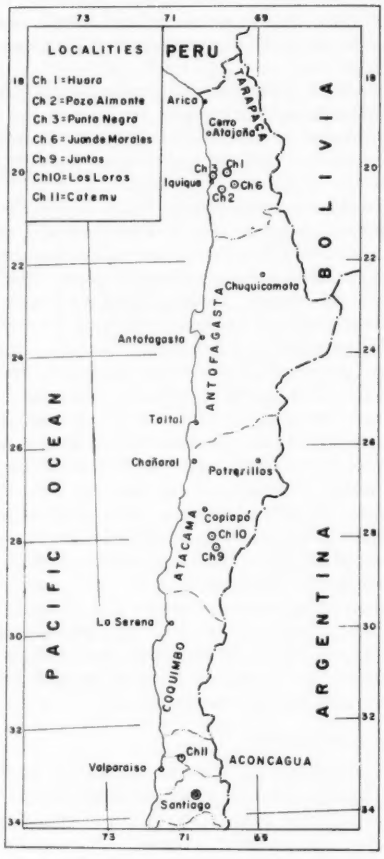

Figure 1. Index map of northern Chile showing localities of samples used in lead-alpha determinations

Neocomian (Early Cretaceous) fossils *Panopaea dupiniana* D'Orbigny, *Exogyra couloni* D'Orbigny, and *Argentiniceras*, of the Berriasian stage (Early Cretaceous).

Cobbles of plutonic rock in the Caleta Coloso formation in the Coast Range of Antofagasta province are also indicative of a pre-Cretaceous batholith. On the north side of Quebrada Way, 20 km south of Antofagasta, and about 3 km east of the mouth of the quebrada, the Caleta Coloso formation is composed mainly of conglomerate, of continental origin. The conglomerate contains cobbles of: (1) grayish-red, medium-grained granodiorite composed of plagioclase, quartz, and potassium feldspar; (2) grayish-red and gray, medium-grained granites composed of quartz, potassium feldspar (perthite), plagioclase, and augite; (3) porphyritic granites containing orthoclase, plagioclase, quartz, and a few altered ferromagnesian minerals; and (4) grayish-red aplites containing quartz, perthite, and orthoclase.

The Caleta Coloso formation is conformably overlain by the marine El Way formation. The calcareous beds of the lower part of this formation contain abundant pelecypods, and at a slightly higher level, the ammonite *Crioceras*. Certain species of pelecypods, hexacorals, and echinoids in the upper middle part of the formation indicate an age equivalent to the Hauterivian and Barremian stages of the Neocomian. Thus the granitic cobbles in the Caleta Coloso formation demonstrate the existence of a pre-Hauterivian batholith.

A marked unconformity between the Caleta Coloso formation and the underlying La Negra formation is exposed between high- and low-tide levels along the beach about halfway between Antofagasta and Quebrada Way. In northern Antofagasta province, the volcanic rocks that form the La Negra formation are intercalated farther to the north with marine sedimentary rocks whose ages correspond to the Bajocian and Callovian stages of Jurassic time. Granite cobbles like those in the Caleta Coloso formation are not known in the La Negra formation, so the pre-Cretaceous granite is believed to be post-Callovian.

North of Chuquicamata, in the El Abra area of Antofagasta province, granitic bodies intrude the previously mentioned Mesa granite and are themselves intruded by granodiorite. The "El Abra granite," so-called by Anaconda Company geologists, is light reddish gray, medium-grained, and composed principally of microperthite, quartz, plagioclase, and biotite. Possibly the El Abra granite is Jurassic and equivalent in age to the granite that crops out in Quebrada Camarones.

Cretaceous Intrusions

The best known exposures of Cretaceous or younger granites in Chile extend from the

Andean region of the Maule River to the northern extreme of the province of Atacama.

In central Chile and farther north, in Coquimbo and Atacama provinces, both in the Coast Range and in the Andes, massifs of granodiorite, granite, and tonalite intrude a series of sedimentary and volcanic rocks that correspond to the Abanicos (Coya-Machalí, Las Chilcas, and Cerrillos) and Farellones (Lo Valle and Hornitos) formations. The series unconformably overlies a sequence of marine sedimentary rocks mainly composed of impure limestone containing abundant ammonites of Neocomian age, such as *Spiticeras*, *Holcostephanus curacoensis* (Weaver), *Lissonia riveroi* (Lisson), and *Crioceras andinum* Gerth. Abundant pelecypods and hexacorals, of various stages of the Neocomian, are also present. In some areas the marine sedimentary rocks are intertongued with red sandstone, of continental origin, and with andesite.

Thus the intrusions are post-Neocomian; however fixing their minimum age presents the same difficulty as trying to determine the age of the unfossiliferous Abanicos and Farellones formations, also of post-Neocomian age. Both these and equivalent formations are completely of continental origin, and it has been impossible to date them more closely than as post-Neocomian. Brüggen (1915) reported that in the area of Algarrobo, 40 km south of Valparaiso, a transgressive conglomerate overlies the granites of the Coast Range. This conglomerate contains ammonites of the genus *Grossouvreites*, considered by the present authors to be late Campanian. Thus the pluton that intrudes the sedimentary rocks at that place cannot be younger than late Campanian.

A great part of the metalliferous deposits of Chile, including the well-known porphyry copper bodies of Chuquicamata, Salvador, Potrerillos, and El Teniente are associated with the granitic rocks of Cretaceous age. Tourmaline breccia deposits containing copper and gold are also related to these.

LEAD-ALPHA AGE DETERMINATIONS

Method

The lead-alpha ages of seven granitic rocks were determined on zircon by the method developed by Larsen (*See* Gottfried, Jaffe, and Senftle, 1959). In this method zircon is separated from about 25 kg of rock and purified by means of a concentrating table, magnetic separator, and heavy liquids. The final concentrate is carefully examined, and any remaining impurities are removed by hand picking. The zircon concentrate must be free of any foreign minerals that might introduce lead, uranium, or thorium into the zircon sample.

It is assumed that the zircon crystallized contemporaneously with the enclosing rock-forming minerals, that the lead in the zircon is all of radiogenic origin formed by the decay of uranium and thorium in the zircon, and that neither parent nor daughter products have been added or lost since crystallization except for the decay to lead of the uranium and thorium.

The uranium and thorium contents of the zircon were determined by thick-source alpha-counting techniques. The lead was determined by an emission spectrographic method (Rose and Stern, 1960) which uses a synthetic "zircon" as the standard.

The lead-alpha ages were calculated from the following equations:

$$t = \frac{C\,\mathrm{Pb}}{\alpha}, \qquad (1)$$

where t is the calculated age in millions of years, C is a constant based upon the Th-U ratio, Pb is the lead content in ppm, and α is the alpha counts per mg per hr;

$$T = t - 1/2\,kt^2, \qquad (2)$$

where T is the age in millions of years corrected for decay of uranium and thorium, and k is a decay constant based upon the Th-U ratio. The following constants were used:

Mineral	*Assumed Th-U ratio*	C	k
Zircon	1	2485	1.56×10^{-4}

The results are listed in Table 1.

Upper Paleozoic Granite

A sample of pre-Jurassic granite from the Juntas locality southeast of Copiapó in Atacama province was determined to have a calculated lead-alpha age of 265 ± 30 million years. This corresponds to early Permian on Kulp's scale (1959) and agrees with the geologic relationships, which indicate a pre-Jurassic age for the intrusion. Because of their stratigraphic position the pre-Jurassic granites of the Coast Range, in the border area between Atacama and Antofagasta provinces, are probably correlative with the granite from Juntas.

Upper Jurassic Granitic Rocks

A sample of quartz monzonite was taken from an elongated pluton just south of Pozo Almonte, approximately 40 km east-southeast of Iquique, in Tarapacá province. The pluton intrudes a series of volcanic rocks of Bajocian age. The zircon in this sample was calculated to have an age of 120 ± 15 million years. The quartz monzonite is light gray, medium-grained, and composed principally of orthoclase, plagioclase, quartz, and tourmaline.

A sample of granodiorite was taken from an intrusive body located at Punta Negra 3 km north of Iquique. This rock intrudes a sedimentary sequence of the Huantajaya formation of Callovian to Tithonian age. The lead-alpha age was determined to be 125 ± 15 million years. The rock is a light-gray, medium-grained granodiorite, composed of plagioclase, orthoclase, quartz, and biotite.

The maximum age represented by the two samples is Late Jurassic on Kulp's scale, an age that probably corresponds to that of the Jurassic intrusion in Quebrada Camarones. The minimum is middle Cretaceous, but in accordance with the minimum ages calculated for Cretaceous granites of the Iquique region (85 million years and 90 million years) it is probable that the intrusions at Pozo Alamonte and Punta Negra are old enough to be of pre-Cretaceous age. Unfortunately the intrusion in Quebrada Camarones had not been sampled at the time the determinations were made.

Middle Cretaceous Granitic Rocks

A sample of granite was taken from a small body that intrudes the Hornitos (= Farellones) formation immediately downstream from Los Loros on the Copiapó River and 60 km southeast of Copiapó, in Atacama province. The lead-alpha age determination for the sample is 105 ± 10 million years. The rock is a yellowish-gray, medium-grained granite composed of quartz, orthoclase, plagioclase, and amphibole.

Another sample of granite was taken from an intrusive mass near Huara, approximately 45 km east-northeast of Iquique, in the province of Tarapacá. This rock intrudes a formation consisting principally of volcanic rocks of Bajocian age. Stratigraphic relationships which would fix a minimum geologic age for this intrusive mass are unknown. The lead-alpha age was determined to be 100 ± 10 million years. The granite is pinkish gray, medium-grained, and composed of orthoclase, quartz, plagioclase, biotite, and amphibole.

A sample of porphyritic microgranite obtained on the west slope of Cerro Juan de Morales, 80 km east of Iquique, from a small intrusive mass that cuts sedimentary rocks of Carboniferous and Late Triassic(?) age showed

TABLE 1. LEAD-ALPHA AGE DETERMINATIONS OF ZIRCON FROM CHILEAN ROCKS*
Determinations made by the U. S. Geological Survey

Specimen		Rock type and locality	α/mg-hr†	Pb(ppm)**	Calculated age
Chile	1	Granite, Huara, Tarapacá, Chile	158	6.5 (6.5, 6.4)	100 ± 10 m.y.
	2	Quartz monzonite, Pozo Almonte, Tarapacá, Chile	453	21.5 (21, 22)	120 ± 15 m.y.
	3	Granodiorite, Iquique (Punta Negra), Tarapacá, Chile	128	6.4 (6.0, 6.8)	125 ± 15 m.y.
	6	Porphyritic microgranite, Cerro Juan de Morales, Tarapacá, Chile	755	29.5 (29, 30)	95 ± 10 m.y.
	9	Granite, Juntas, Río Copiapó, Atacama, Chile	372	40 (38, 42)	265 ± 30 m.y.
	10	Granite, Los Loros, Río Copiapó, Atacama, Chile	222	9.2 (9.0, 9.4)	105 ± 10 m.y.
	11	Granite, Catemu, Aconcagua, Chile	272	14.1 (13.3, 15.0)	130 ± 15 m.y.

* Zircon separated and purified by T. W. Stern and J. H. Mangum
† Alpha activity measured by T. W. Stern
** Lead analysis by H. J. Rose, Jr. and H. W. Worthing

a lead-alpha age of 95 ± 10 million years. The intrusive mass is light olive gray and is composed principally of orthoclase, quartz, plagioclase, and amphibole.

The lead-alpha age of the sample of granite from near Los Loros indicates that granites in the post-Neocomian formations are middle Cretaceous. Inasmuch as they intrude the Hornitos (= Farellones) formation and the equivalent Lo Valle formation, the formations are probably late Early Cretaceous (Albian or Aptian ?). Because of the great thickness of the two post-Neocomian formations, and because of the unconformities that form their limits, they were generally considered to be somewhat younger: a lower Senonian age had been tentatively assigned to the Farellones formation. It now seems likely that the post-orogenic sediments accumulated in a much shorter time than had previously been considered. The most interesting result of the age determination of the sample from near Los Loros is that it shows that the granites that penetrate the youngest formations of the so-called Andean geosyncline are Cretaceous.

The samples from near Huara and from 80 km east of Iquique, for which lead-alpha ages of 100 and 95 ± 10 million years were determined, are also related to the middle Cretaceous intrusive activity which took place in the Copiapó area and in central Chile.

A sample of granite from Catemu, 70 km east-northeast of Valparaíso, from an intrusive mass in the Las Chilcas (= Abanicos) formation, showed a lead-alpha age of 130 ± 15 million years. The rock is an olive-gray, medium-grained granite, composed of orthoclase, quartz, plagioclase, biotite, and amphibole. According to its stratigraphic setting this intrusion should have a maximum age of late Neocomian or Aptian (late Early Cretaceous).

RELATIONSHIP OF OROGENY TO INTRUSIVE ACTIVITY

Hercynian Orogeny

It is believed that each of the intrusions whose ages have been discussed were emplaced during or at the end of a major orogenic epoch. Major angular unconformities with ages correlative with those of the intrusions strengthen this belief.

In Quebrada Pan de Azúcar and near Posada de los Tres Hidalgos in the Coast Range near the boundary between Atacama and Antofagasta provinces, a large angular unconformity separates late Paleozoic (El Toco formation?) metamorphic rocks and Triassic(?) (Cifuncho formation) sedimentary-volcanic rocks. At those localities, granite of probable late Paleozoic age intrudes the rocks below the unconformity but is in turn cut by the unconformity. The orogeny that deformed the older rocks can logically be considered as corresponding to a phase of the Hercynian orogeny, which started in Late Mississippian time and was completed in late Permian time. The granite at these localities is certainly correlative with the orogeny.

Late Jurassic Orogeny

Investigations by geologists of E.N.A.P. have shown that orogeny terminated the Jurassic period in Tarapacá province. A pronounced angular unconformity separates Jurassic and Lower Cretaceous sedimentary rocks in Tarapacá province; it is well exposed in the area of Atajaña, 90 km south of Arica.

The granodiorite nearby in Quebrada Camarones, described under *Jurassic Intrusions*, must have been emplaced during a phase of the same orogenic epoch.

In Quebrada Asientos, in the northeastern part of Atacama province, a notable angular unconformity separates marine sediments of Callovian age, containing *Sphaeroceras*, *Macrocephalites*, and *Reineckeia*, and marine beds of Tithonian and Neocomian age, containing forms of *Berriasella* and *Spiticeras*. The lower part of the overlying formation is apparently of latest Tithonian age. The Late Jurassic orogeny thus took place a little earlier in Quebrada Asientos than farther north, in Tarapacá province.

H. Thomas (Oral communication) notes that north and south of Punta Colorada, near Incahuasi, in the northern part of Coquimbo province, a pronounced angular unconformity separates the La Negra formation, of probable Bajocian to Callovian age, and marine rocks containing fossils of Neocomian age. There are strong indications that the same unconformity is strongly angular at least as far south as Quebrada Potrerillos, about 20 km northeast of La Serena, in the west-central part of Coquimbo province.

In central Chile, it has not been possible as yet to establish the presence of an angular unconformity in the Upper Jurassic rocks. However, Thomas (1958) has recognized a hiatus in marine deposition of rocks of the Coast Range between Valparaíso and Acon-

cagua. In this area, the Melón formation of Bajocian age, containing abundant pelecypods and ammonites, such as *Emileia* cf. *singularis* Gottsche, *Lhytoceras rasile* Vacek, *Sonninia* cf. *fascicostata* Tornquist, and *Stephanoceras* sp., is disconformably overlain by the Lo Prado formation, of Neocomian age, characterized by the presence of *Holcoptychites neuquensis* Douvillé and *Thurmannites* sp.

Klohn (in press) has established that in the area now occupied by the Andes Mountains of O'Higgins, Colchagua, and Curicó provinces of central Chile, marine sedimentation was interrupted during Late Jurassic time. In that area, the Nacientes del Teno formation is composed of marine strata of Bajocian to Lusitanian (middle Late Jurassic) age. The formation is overlain, apparently conformably, by the continental Río Damas formation, of Kimmeridgian (Late Jurassic) age, which contains conglomerate, red sandstone, and lava. The Río Damas formation is in turn overlain by a series of marine strata of Tithonian-Neocomian age. In the Río Lenas area, in the Andean region of O'Higgins province, the marine series begins with beds of lowermost Tithonian age (Corvalán, 1959) as evidenced by the presence of abundant forms of *Virgatosphinctes* (*V. andesensis* Douvillé, *V. lenaensis* Corvalán). The nature of the Río Damas formation indicates that the Late Jurassic sea regressed, no doubt as a result of epeirogenic uplift.

In central Chile, granitic rocks that are disconformably overlain by sedimentary rocks of Tithonian or Neocomian age have not been observed.

In summary, there seems to have been an epoch of epeirogenic uplift in central Chile during Late Jurassic time, but without a corresponding intrusive phase in that area. Practically continuous earth movements—epeirogenic to the south, orogenic to the north—have been recognized from Curicó province northward to the frontier with Peru. These movements were not synchronous throughout the length of this vast area, however. In central Chile the epeirogenic uplift took place during the Kimmeridgian stage; in Atacama, during the early Tithonian stage; and in Tarapacá province, at the end of the Tithonian stage of Late Jurassic time. Only in Tarapacá province is there more or less conclusive evidence of intrusive activity that occurred during the Late Jurassic orogeny.

Early Late Cretaceous Orogeny

Orogenic movements that began at the end of Neocomian time apparently had three culminations. The first, which was probably the strongest, initiated a period of active erosion that resulted in the unconformable deposition of postorogenic clastic sediments (Molasse facies). In many localities, lower members are of coarse conglomerate, which was apparently deposited in deltas. Farther up in the sequence, the sedimentary rocks are finer-grained and include siltstone, shale, and freshwater limestone, as well as many intercalations of andesitic material. In the Andes Mountains of central Chile these rocks form a mappable unit designated as the Coya-Machalí formation (Klohn, in press). The sequence is also represented in the Coast Range of central Chile by the Las Chilcas formation (Thomas, 1958) and east of Copiapó by the Cerrillos formation (Segerstrom, 1959). The formations have a maximum thickness of 5000 or 6000 m. Their upper limits are marked by an unconformity that corresponds to the second phase of the middle Cretaceous orogeny.

Above the second unconformity is another sequence of sedimentary and volcanic rocks that are lithologically similar to the underlying formations. Overlying volcanic rocks are also andesitic, for the most part, but intercalations of ash flows, partly of welded tuff of dacitic or rhyolitic composition, also occur. The unconformity at the base is markedly angular at some localities, but at other localities there is a disconformity. The upper sedimentary-volcanic sequence is known as the Farellones formation in the Andes of central Chile, the Lo Valle formation in the Coast Range, and the Hornitos formation in Atacama province. The maximum thickness of these formations is 2000 or 2500 m.

The third phase of the orogeny occurred after the deposition of the Farellones and equivalent formations. During this phase, the sedimentary and volcanic rocks were slightly folded, so that they now show gentle flexures or are in slightly inclined positions. During or shortly after this orogenic phase, the middle Cretaceous granitic rocks were emplaced.

CONCLUSIONS

The foregoing discussion has shown that the granitic rocks in Chile are of at least three different ages.

The writers have shown that geosynclinal sedimentary and volcanic rocks of post-Neo-

comian age are at least as old as middle Cretaceous, rather than latest Cretaceous or Tertiary, as had been believed previously.

The Cretaceous granites, which probably make up the bulk of the "Andean batholith," were intruded during or shortly after a three-phase orogeny. The middle Cretaceous emplacements, the most important in the geologic history of Chile, occurred about 100 million years ago.

The oldest, or pre-Jurassic, granite seems to have been emplaced without accompanying metallization. The youngest, or Cretaceous, intrusions were accompanied by widespread metallization, including that of the major (porphyry copper) deposits in Chile. More age determinations of granites are needed to establish the relationship, if any, between Jurassic intrusions and metallization.

REFERENCES CITED

Brüggen, Joh., 1915, Die Kreide von Algarrobo in Chile: Centralblatt fur Mineralogie, Geologie und Paläontologie, no. 12, p. 406–409

Cecioni, Giovanni y, and García, Floreal, 1960, Observaciones geológicas en la Cordillera de la Costa de Tarapacá: Santiago, Inst. Inv. Geológicas Bol. 6, 28 p.

Corvalán, José, 1959, El Titoniano del Río Lenas (con una revisión del Titoniano y Neocomiano en la parte chilena del Geosinclinal Andino): Santiago, Inst. Inv. Geológicas Bol. 3

Gottfried, David, Jaffe, H. W., and Senftle, F. E., 1959, Evaluation of the lead-alpha (Larsen) method for determining ages of igneous rocks: U. S. Geol. Survey Bull. 1097-A, p. 41

Klohn, Carlos, in press, Geología de la Cordillera de los Andes entre el río Cachapoal y el río Teno: Santiago, Inst. Inv. Geológicas

Kulp, J. L., 1959, Geological time scale (Abstract): Geol. Soc. America Bull., v. 70, p. 1634

Rose, H. J., Jr., and Stern, T. W., 1960, Spectrochemical determination of lead in zircon for lead-alpha age measurements: Am. Mineralogist, v. 45, p. 1246–1256

Segerstrom, Kenneth, 1959, Geología del Cuadrangulo Los Loros: Santiago, Inst. Inv. Geológicas, Carta geológica de Chile, v. 1, no. 1

—— 1960, Structural geology of an area east of Copiapó, Atacama province, Chile: 21st Internat. Geol. Cong. (Copenhagen), Part XVIII, p. 14–20

Solms-Laubach, H., and Steinmann, G., 1899, Das Auftreten und die Flora der rhätischen Kohlenschichten von La Ternera (Chile): Neues Jahr. für Mineralogie, Geologie und Paläontologie, Beilage-Band 12, p. 581

Steinmann, G., 1920, Rhätische Floren und Landverbingunger auf der Südhalbkugel: Geol. Rundschau, v. 11, p. 350–354

Thomas, Hubert, 1958, Geología de la Cordillera de la Costa, entre el valle de La Ligua y la Cuesta de Barriga: Santiago, Inst. Inv. Geológicas, Bol. 2, p. 86

Wetzel, W., 1927, Zur Erdgeschichte der mittleren Atacama: Neues Jahr. für Mineralogie, Geologie und Paläontologie, Beilage-Band 58

Willis, Bailey, 1929, Earthquake conditions in Chile: Carnegie Inst. Washington, 178 p.

Manuscript Received by the Secretary of the Society, May 10, 1960
Publication Authorized by the Director, U. S. Geological Survey

Short Notes

L. P. TREMBLAY

WIND STRIATIONS IN NORTHERN ALBERTA AND SASKATCHEWAN, CANADA

Abstract: Striations on outcrops and erratics over a large area in northern Alberta and Saskatchewan trend mainly N. 35° W. and are believed to be the result of sandblasting rather than glacier action and to indicate a wind from the south-southeast.

During the summer of 1960, the writer mapped an area of Precambrian gneisses and granite in northern Saskatchewan and Alberta near the western boundary of the Canadian Shield (Fig. 1). The area is largely drift-covered and has an annual precipitation of about 15 inches. While mapping the bedrock the writer noted highly polished weathered surfaces and well-developed striae, grooves, and channels on rock outcrops and on a few erratics (Pl. 1). These features, particularly the striations, are briefly described here as they are believed to be due to wind action or sandblasting and not to glacial erosion as has been implied (Ells, 1932, p. 116; Glacial Map of Canada, Wilson *et al.*, 1958), probably on the assumption that all striations in the Canadian Shield are due to ice action.

These features were briefly examined in the field, a few measurements were made, and some of the results are shown on Figure 1.

The features were noted over an area extending from north and east of Frobisher Lake in Saskatchewan to as far north as the area northwest of the Marguerite River in Alberta and as far east as Patterson Lake in Clearwater River area, Saskatchewan. They may occur over a more extensive area but, as they were not recognized as such before from this area and as they seem to become fainter away from the Marguerite River in Alberta, the writer believes that the area of Figure 1 represents approximately their maximum extent. They are more spectacular and better developed on outcrops than on the erratics. In the Marguerite River area most of the outcrops show the features remarkably well, and it was there that they were recognized as different from the strikingly similar glacial erosional features.

The features are normally developed on outcrop surfaces facing and sloping south and southeast. They were also observed on top of outcrops and even on the undersurfaces of low ledges facing southeast but sloping northwest. Such undersurfaces negate a possible glacial origin. They are best developed also on rock outcrops made up of minerals of about the same hardness.

The polished surface exhibits a typically high gloss, a gloss much more accentuated than that on the polished surfaces commonly seen in the shield and due to glacial action. This feature alone is not sufficient to prove the phenomenon is the result of wind erosion, but the striations locally are very typical of wind erosion. They could be described as fine striae, grooves, channels, or funnel-shaped striations depending on the size, depth, and shape. The striae are generally so shallow that it is practically impossible to determine a direction on them except in the proper light. In the Marguerite River area where they are well developed and very closely spaced, they present an almost square outline in cross section. There the ridge separating two adjoining striae looks vertical and is almost a knife edge. The groove is somewhat larger and deeper than the striae, whereas the channel may be as much as 5 inches deep. None of these striations, particularly the fine striae, is more than 3–4 feet long; generally they are less than a foot. A fine striae may appear at first glance to cross a whole outcrop, but on careful study each is seen to be a succession of short scooplike depressions 1 inch to a few inches long and slightly deeper near the handle or the back of the scoop. The opening of the scoop faces the direction from which the wind came, and the scoop is opened upward.

Geological Society of America Bulletin, v. 72, p. 1561–1564, 1 fig., 1 pl., October 1961

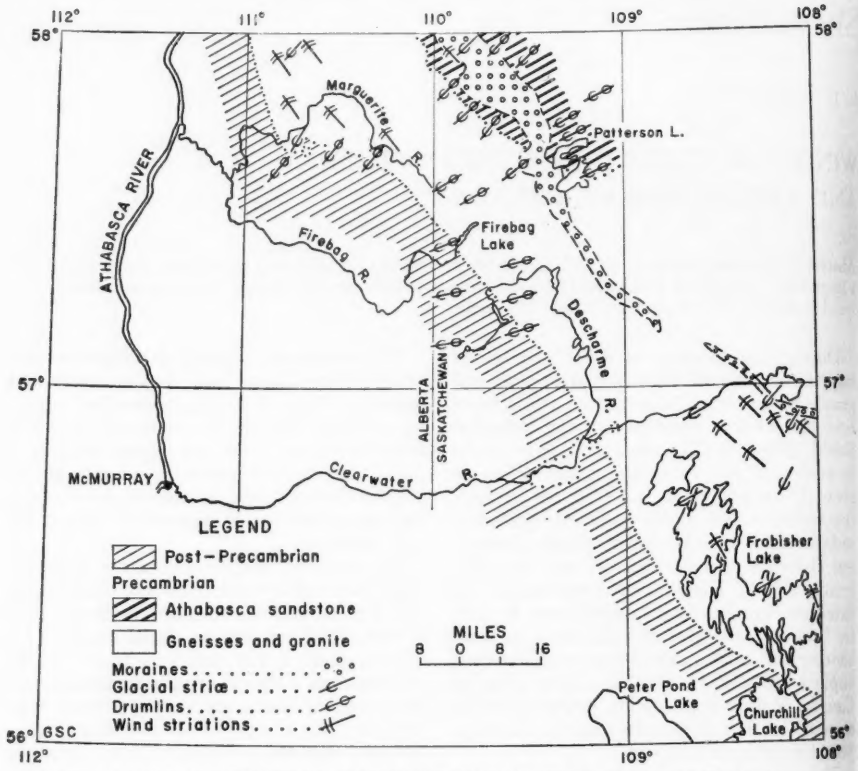

Figure 1. Map showing direction of the wind striations in relation to the main glacial features

This is very well shown where the striations seem to be discontinuous and not too closely developed, as in the Clearwater River area or the Frobisher Lake area. Locally near the edges of outcrops or here and there on the outcrop, where the surface of the outcrop is irregular, the fine striae become grooves, channels, or funnel-shaped striations as if in those spots the wind was stronger and more heavily loaded with sand.

The striations as seen on outcrops are commonly oriented N.35°W., and they are super-

PLATE 1. WIND STRIATIONS AND DREIKANTERS

The smallest division on all the scales represents 1 mm

Figure 1. Wind striae on a specimen of graphic granite from the Frobisher Lake area. The black line indicates the direction of the striae

Figure 2. Channel-like and scooplike grooves on an outcrop surface facing and sloping southeasterly. From a kodachrome slide from D. W. Scafe

Figure 3. Grooves on an erratic near Firebag Lake

Figure 4. Erratic showing one polished face facing and sloping south. The arrow indicates approximately the north direction

Figure 5. Erratic showing one polished face facing and sloping southeasterly. The arrow indicates approximately the north direction

Figure 6. A dreikanter

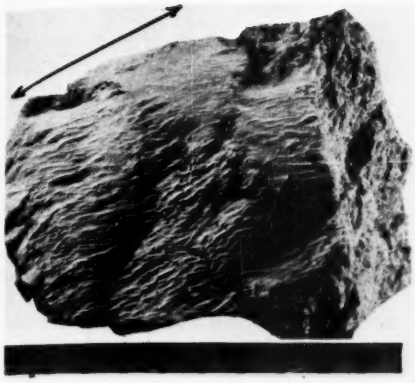

Figure 1

Figure 2

Figure 3

Figure 4

Figure 5

Figure 6

WIND STRIATIONS AND DREIKANTERS

TREMBLAY, PLATE 1
Geological Society of America Bulletin, volume 72

imposed on glacial striae trending southwesterly.

As most of the area is covered with a thick mantle of gravel and sand, there are surface erratics of various sizes. These erratics show in many instances the same erosional features as the outcrops. The buried portion of the erratics is not affected. The largest erratics have commonly a well-polished face sloping at about 45°S.–SE. and facing south–southeast. The remaining surface of the erratic has been very little eroded; it is still unpolished but locally may be faintly striated and pitted probably mainly as a result of recent erosion. The cobbles and pebbles have been eroded in the same fashion as the boulders, but in many instances they have developed a dreikanter shape, with the edge trending most commonly southeasterly. Other erratics show pits, striations, grooves, or channels just as the outcrops do. After these erosional features were recognized on a few erratics, particularly the polished surface, the dreikanter shape, and the deep groove, an amazingly large number were found. Naturally such erratics are most abundant in the area where the outcrops show most strikingly these erosional features.

North and northeast of the area studied, the Athabasca sandstone occurs as a thin, flat-lying mass overlying large areas of Precambrian gneisses. This sandstone could be a good source for the sand used in the sandblasting to produce the features. When the glacier passed over this large area of Athabasca sandstone, much sand was removed, carried south either by the glacier itself or by streams during or soon after the deglaciation, and much of it was deposited in the area studied or southeast of it. Large deposits of sand were observed in the area around and east of Firebag Lake near the Alberta–Saskatchewan boundary or about 40 miles southeast of the Marguerite River area. The great amount of sand there is believed to have been the primary source for the sandblasting that took place in the Marguerite River area in Alberta, and its abundance would explain why the erosional features are so well displayed there. Elsewhere, where these erosional features were recognized but are not so well developed, the amount of sand at the source was probably smaller. The sand or gravel deposits southeast of Frobisher Lake do not seem to be as extensive as those in the Clearwater River area. Possibly, also, there was a more extensive vegetation cover there at that time than in the Clearwater River area, and consequently only a limited amount of material could be obtained. The erosion effect would thus be in proportion to the amount of material that could be picked up and moved.

These erosional features and some of the sand deposits in the form of dunes, sheets, and ridges, not described here, suggest that the area was a huge desert during or soon after the deglaciation, that the sand could move readily under the action of wind, that the vegetation cover was practically nonexistent, and that during a fairly long period there were strong winds blowing predominantly from south–southeast to northwest (ca. N.35°W.). The slightest amount of vegetation would have checked in part the wind velocity, reduced the amount of sand available for transportation, and consequently reduced the effects of sandblasting on outcrops and erratics. This may have been the case for the areas where the features are not too well displayed or developed. The amount of material at the source probably varied from place to place and was responsible for the degree of development of these features. At present the predominant wind direction in the area is from the northwest.

The direction indicated by these striations is not that in which the ice moved. As indicated by glacial striae, eskers, and drumlins (Fig. 1), the ice moved S. to S.60°W. in this area. Two possible periods of glaciation were indicated by glacial striae, the later glacier moving about S.60°W., and the older advance about S.15°W. If there were other directions of glacial advances, no indications of them were recognized. If the striations described here were glacial features, it would be simple to explain the source of the erratics of Bituminous sand (Kupsch, 1954) found in the Peter Pond Lake area since a southeasterly direction would suggest the area of Bituminous sand in Alberta near McMurray as the probable source, but, since they are believed to be due to wind erosion, they cannot be used to explain the probable source of the Peter Pond Lake erratics. Other evidence must be gathered, or another source to the northeast suggested.

Acknowledgments

Thanks are extended to members of the Geological Survey of Canada who critically read this note.

References Cited

Ells, S. C., 1932, Exploration of bituminous sand areas in northern Alberta: Canadian Mines Branch Rept. no. 727, p. 116

Kupsch, W. O., 1954, Bituminous sands in till of the Peter Pond Lake area, Saskatchewan: Dept. Min. Res. Saskatchewan Rept. 12, p. 25–27

Wilson, J. T., *et al.*, 1958, Glacial map of Canada: Geological Association of Canada

Geological Survey of Canada, Ottawa, Ontario, Canada
Manuscript Received by the Secretary of the Society, January 24, 1961
Published by Permission of the Director, Geological Survey of Canada, Ottawa, Canada

T. P. THAYER
C. E. BROWN

IS THE TINAQUILLO, VENEZUELA, "PSEUDOGABBRO" METAMORPHIC OR MAGMATIC?

Abstract: The "pseudogabbro" associated with peridotite at Tinaquillo, Venezuela, is believed to be of magmatic rather than metamorphic origin principally because: (1) there are major mineralogic and compositional differences between the "pseudogabbro" and the most highly metamorphosed country rock; (2) rocks intermediate in compositional between peridotite and "pseudogabbro" are present; (3) augen of lamellar pyroxene which occur in the "pseudogabbro" but not in the country rock are of a kind found elsewhere rarely except in igneous rocks; (4) gabbroic rocks are associated with peridotite elsewhere in Venezuela and in the Caribbean region; (5) textural and structural features of the kind found in the Tinaquillo rocks are characteristic of alpine-type peridotite-gabbro complexes.

D. B. MacKenzie (1960) describes rocks of gabbroic composition ("pseudogabbros") that occur in dunite near Tinaquillo, Venezuela, as metamorphosed inclusions of country rock "... since positive criteria of a magmatic origin are absent and since the evidence points strongly to the peridotite as the cause of the metamorphism of the country rocks to rocks of gabbroic composition in the inner part of the contact aureole . . .". (p. 312). MacKenzie cites as his principal evidence: (1) similarities between the "pseudogabbros" and metamorphosed country rocks; (2) absence of rocks intermediate between dunite and "pseudogabbros"; (3) sharp contacts; (4) the composition of the "pseudogabbros"; (5) the absence of relict euhedral grains and interlocking textures in the "pseudogabbros". We believe that MacKenzie's data contain evidence that the gabbroic rocks more probably were of magmatic origin and that the "pseudogabbro"-peridotite textural, compositional, and mineralogical relations are typical of the alpine-type peridotite-gabbro clan (Thayer, 1960).

MacKenzie emphasizes similarities between the most highly metamorphosed rocks in the contact aureole and the "pseudogabbros", but he also points out (p. 312) that the two kinds of rocks are easily distinguished in the field, apparently even where both are enclosed in peridotite very close together (MacKenzie, Pl. 4). We believe that their comparative features, as listed in Table 1, set the two kinds of rocks apart as distinct types.

TABLE 1. COMPARATIVE FEATURES OF THE "PSEUDOGABBROS" AND ROCKS OF THE CONTACT AUREOLE

"Pseudogabbro"	Country rock
Lamellae-bearing pyroxenes	No lamellae-bearing pyroxenes
Pyroxene "porphyroblasts"	No pyroxene "porphyroblasts"
Orthopyroxene 5–15 per cent	Orthopyroxene absent or at most 2 per cent
Clinopyroxene about 15 per cent	Augite up to about 20 per cent
Brown hornblende 20–35 per cent	Green to brown hornblende abundant
Plagioclase: Range An_{50}–An_{70}, average An_{50-55}	Plagioclase range An_{10}–An_{50}
No quartz	Quartz-rich layers

Although MacKenzie says (p. 311) that the Tinaquillo mass contains no rocks intermediate between "pseudogabbro" and dunite, the pyroxene and amphibole layers he describes (p. 307) seem to be precisely that. "Layers have been found with the following compositions: (1) orthopyroxene with a very small amount of clinopyroxene or plagioclase; (2) augite; (3) equal amounts of augite and orthopyroxene (websterite); and (4) light-brown amphibole with or without a small amount of pyroxene. The first and last types are most abundant. . . . The layers range in thickness from a few millimeters to half a meter." He further says

Geological Society of America Bulletin, v. 72, p. 1565–1570, October 1961

that the amphibole-rich layers commonly contain "only a peculiar brown amorphous alteration mineral . . . in addition to the amphibole." Shagam (1960, p. 274) and Smith (1953, p. 55) describe similar minerals in Venezuelan peridotites as alteration products of feldspar; calcic feldspar in ultramafic rocks commonly alters in this fashion (Guild, 1947, p. 230; Hess, 1960, p. 58). Even if the amorphous alteration material were not derived from plagioclase, the pyroxene and amphibole rocks are intermediate chemically between gabbro and dunite. Websterite and augitite commonly contain 10–20 per cent CaO and 2–5 per cent Al_2O_3 (Johannsen, 1938, p. 457). The normative composition of the analyzed amphibole (MacKenzie, Table 1) is that of a nepheline-bearing troctolitic gabbro made up of about 40 per cent plagioclase, 7 per cent nepheline, 35 per cent olivine, 13 per cent wollastonite, and 5 per cent magnetite and ilmenite. Likewise, the amphibole which constitutes 20–35 per cent of the "pseudogabbro" must be chemically equivalent to a substantial amount of feldspar and olivine. The Mg content of the enstatite, according to MacKenzie, varies systematically as follows: in dunite, 90–92 per cent; in pyroxenite and amphibole layers, 85–90 per cent; in "pseudogabbro" 62–85 per cent, and averaging 70–78 per cent. The composition of the enstatite, therefore, is consistent with the variation in bulk composition of the rocks from dunite to "pseudogabbro" and true gabbro.

The outcrop relations between the gabbroic rocks and dunite shown in MacKenzie's detailed map (his Pl. 4) are typical of those found in many alpine-type peridotite-gabbro complexes (Thayer, 1960). The smaller, more tabular masses of "pseudogabbro" are interlayered in the peridotite, but the boundaries of the larger masses are irregular. Foliation and lineation in the gabbroic and ultramafic rocks commonly line up across, and at any angle to, contacts. Although in complexes of this kind many contacts are likely to be gradational, sharp contacts between very different kinds of rocks are equally common; the small proportion of mappable intermediate pyroxene-rich rocks is characteristic.

MacKenzie argues that the "pseudogabbros" contain less olivine and plagioclase of more sodic composition than do the gabbros associated with alpine-type peridotites. We believe that the normative composition of the "pseudogabbro" is that of an olivine-bearing gabbro, as are the amphibole-rich layers. Although troctolites and olivine-rich gabbros containing very calcic plagioclase commonly occur in alpine-type ultramafic complexes, the average composition of the gabbroic rocks is much less extreme. In eastern Oregon (Thayer, 1956) and in the Zambales Range in Luzon olivine-free noritic rocks in which the plagioclase ranges between An_{50} and An_{65} are interlayered in places with, or grade into, peridotite and are at least as abundant as olivine gabbro and troctolite. Compositionally, therefore, the "pseudogabbros" cannot be distinguished from truly magmatic rocks in the alpine-type ultramafic complexes.

Despite extraordinary flow textures in the dunite, granoblastic texture and lack of "igneous texture" are cited as one line of evidence for metamorphic origin of the "pseudogabbro". MacKenzie regards poikilitic texture as particularly diagnostic of igneous origin. The predominance of textures due to flowage in the gabbroic parts of alpine-type ultramafic complexes seems to have gone generally unrecognized (Thayer, 1960). The gabbroic rocks in eastern Oregon (Thayer, 1956) essentially are orthogneisses and have granular textures even where relatively fine-grained near intrusive contacts. Flow textures likewise characterize extensive gabbro and peridotite masses in the Zambales Range of Luzon (Rossman and others, 1959). Gabbroic rocks in eastern Cuba have gneissic structure and, in places, feldspar augen (Thayer, 1942, Pls. 1, 2) directly comparable to the pyroxene augen described as porphyroblasts by MacKenzie. Bartrum and Turner (1928, p. 123) describe strongly foliated noritic gabbro associated with peridotite in New Zealand as follows:

> "The rock is typically a fine-grained basic type . . . and . . . is strongly gneissic in structure (see Fig. 9). The foliation is believed to be due to piezo-crystallization; it is very regular in orientation. . . . Locally it is on a very fine scale, but more generally it is coarse and regular, exhibiting laminae about 1/8 in. in depth which are alternately rich in feldspar and ferromagnesian minerals. West of North Cape this gneissic rock is associated with lherzolite, but the mutual relations were not determined."

In these examples the field relations of the gabbroic rocks to the peridotite, and country rocks as well, leave little doubt as to their magmatic origin. Poikilitic texture would be preserved in such rocks only in parts which escaped granulation, but might be present

where recrystallization occurred after movement ceased.

The lamellae-bearing pyroxene augen have a critical bearing on the origin of the "pseudogabbro". According to MacKenzie's hypothesis both augite and hypersthene grew as porphyroblasts in a solid medium before the latest deformation, perforce at high temperature. In the absence of specific data, we assume that the pyroxenes in the augen lamellae are similar in composition to the hypersthene (En_{70-78}) and clinopyroxene (perhaps 80–90 per cent diopside) in the groundmass. If this is indeed so, MacKenzie is postulating mutual intergrowth of two pyroxenes in an environment in which they already occur separately as stable phases. We believe it much more likely that the lamellae-bearing augen are relics from a coarse-grained gabbro in which homogeneous augite and homogeneous hypersthene both crystallized at high temperature and that the lamellae and the groundmass pyroxenes were formed by exsolution at lower temperatures during granulation accompanying emplacement. In view of the variations in size and form of the "pseudogabbro" masses and their relations to the peridotite, why should relict augen be evenly distributed, as postulated by MacKenzie (p. 309)?

MacKenzie describes the pyroxene-, amphibole-, and plagioclase-bearing layers as having "a 0.5- to 1-mm even-grained cataclastic texture" and the enstatite in them as containing thin diopsidic lamellae. We agree that they must have formed at high temperatures before movement ceased. Bowen and Tuttle (1949, p. 460) in discussing the system MgO-SiO_2-H_2O suggested formation of "dikes" richer in either olivine or enstatite than the country-rock peridotite by gas transfer of SiO_2 and iron oxide. Because they were concerned with a non-feldspathic system, however, we do not believe the context of their discussion justifies extension of their theory to form layered rocks of gabbroic composition as MacKenzie proposes (p. 308).

Intimate association of gabbro with peridotite in the Caribbean region on a large scale has been shown in eastern Cuba (Flint, DeAlbear, and Guild, 1948), and a similar association, although perhaps on a smaller scale, is strongly suggested in Venezuela. In Loma de Hierro, about 85 miles east of Tinaquillo, Smith (1953, p. 55) described the central exposures of peridotite as containing "an appreciable amount of isotropic, white, fine-grained interstitial material [which] probably represents altered plagioclase." Adjoining Smith's map area on the west and 50 to 75 miles from Tinaquillo, Shagam describes the peridotite as feldspar bearing (1960, p. 274) and maps three masses of gabbro very near or in contact with serpentine. The largest mass, about 5 miles long and one-third of a mile wide, lies along the southern edge of the Loma de Hierro peridotite mass. MacLachlan, Shagam, and Hess (1960, p. 247) regard the gabbroic intrusives as part of the Tiara volcanic sequence, of which Shagam (1960, p. 278) says "the amount of albite present suggests a spilitic composition." Shagam observes (p. 278), however, that "with one exception all specimens of the intrusive facies contain saussuritized plagioclase only, to the exclusion of albite." The differences between the gabbro and volcanic rocks, and the close areal association between gabbro and feldspar-bearing peridotite, seem more than fortuitous.

We agree completely with MacKenzie that the structural relations between the gabbroic rocks and peridotite (and, we would add, of the peridotite to the country rock) at Tinaquillo are in effect those of metamorphic rocks. Whether of true magmatic origin or formed by gabbroization, the "pseudogabbros" must have been deformed as semisolid rocks at the same time as, and apparently in equilibrium with, the peridotite. In both rocks the last deformation occurred at temperatures at which pyroxene solid solutions are unstable and exsolution takes place. The substantial amount of amphibole in the "pseudogabbro" and pyroxene-plagioclase layers in the peridotite bespeaks a significant content of volatiles which also would account for the garnets in the "pseudogabbro" (Yoder and Chinner, 1960). Gabbroization of the country rocks would be much more expectable around a composite magma containing a major proportion of gabbro and some volatiles than around a dry magma consisting of peridotite alone. Enrichment of country rocks in CaO was described by C. H. Smith (1958) at the contacts with peridotite in the Bay of Islands complex, which consists largely of gabbro. We would point out that at Mt. Albert, to which MacKenzie refers in his reply, Smith and MacGregor (1960) found no significant changes in bulk composition of contact rocks around the peridotite. The scarcity of pyroxenitic facies at Tinaquillo argues against separation of the various rocks by differentiation in place (Aguerrevere, Zuloaga,

and Tello, 1937), leaving as the only alternative their emplacement together as separate semisolid phases. The granulitic texture shown by the pyroxene and amphibole in the "pseudogabbro" seems entirely consonant with the intense deformation of enstatite in the peridotite.

We believe that the crystal-mush theory advocated by Bowen and Tuttle (1949), extended to include rocks of gabbroic composition (Thayer, 1960), explains the relations at Tinaquillo most reasonably. According to the theory the ultramafic rocks and gabbro were originally differentiated at depth by a mechanism of crystal settling similar to that indicated by the stratiform complexes (Hess, 1960). The rocks we now see in the alpine-type complexes are believed to have been emplaced by remobilization of stratiform-type layered rocks during unusually strong deformation along eugeosynclinal belts. By analogy with the stratiform complexes, peridotites moving from lower levels would have to pass gabbroic rocks at higher levels, and, depending upon local conditions, mixtures of various kinds might result. Several lines of evidence indicate that the peridotitic and gabbroic rocks were emplaced together as semisolid mushes in which fragments of chromitite layers behaved as solid bodies while limited differentiation during flowage formed new layering locally in parts of the silicate rocks. The rarity of interlocking and poikilitic textures in alpine-type ultramafic rocks, in contrast to their predominance in stratiform complexes, must be regarded as evidence that the two types of complexes were emplaced and consolidated under fundamentally different conditions.

More specific comparative data on the composition of the pyroxenes and garnets in the contact aureole and gabbroic rocks, combined with the calibration of the two-pyroxene geothermometer, should help resolve the question.

References Cited

Aguerrevere, S. E., Zuloaga, G., and Tello, M., 1937, Informe geológico sobre la región amiantífera de Tinaquillo, Estado Cojedes: Venezuela Bol. de Geol. y Min., Tomo 1, no. 1, p. 5–36

Bartrum, J. A., and Turner, F. J., 1928, Pillow-lavas, peridotites and associated rocks of northernmost New Zealand: Royal Soc. New Zealand Trans., v. 59, p. 98–138

Bowen, N. L., and Tuttle, O. F., 1949, The system MgO-SiO_2-H_2O: Geol. Soc. America Bull., v. 60, p. 439–460

Flint, D. E., Albear, J. F. de, and Guild, P. W., 1948, Geology and chromite deposits of the Camagüey district, Camagüey Province, Cuba: U. S. Geol. Survey Bull. 954-B, p. 39–63

Guild, P. W., 1947, Petrology and structure of the Moa chromite district, Oriente Province, Cuba: Am. Geophys. Union Trans., v. 28, p. 218–246

Hess, H. H., 1960, Stillwater igneous complex, Montana: Geol. Soc. America Mem. 80, 230 p.

Johannsen, A., 1938, A descriptive petrography of the igneous rocks: Univ. Chicago Press, Chicago, Ill., 4, 523 p.

MacKenzie, D. B., 1960, High-temperature alpine-type peridotite from Venezuela: Geol. Soc. America Bull., v. 71, p. 303–318

MacLachlan, J. C., Shagam, R., and Hess, H. H., 1960, Geology of the La Victoria area, Aragua, Venezuela: Geol. Soc. America Bull., v. 71, p. 241–248

Rossman, D. L., Fernandez, N. S., Fontanos, C. A., and Zepeda, Z. C., 1959, Chromite deposits on Insular Chromite Reservation No. 1, Zambales, Philippines: Philippine Bur. Mines, Special Projects Series pub. no. 19, 12 p.

Shagam, R., 1960, Geology of central Aragua, Venezuela: Geol. Soc. America Bull., v. 71, p. 249–302

Smith, C. H., 1958, Bay of Islands igneous complex, western Newfoundland: Canada Geol. Survey Mem. 290, 132 p.

Smith, C. H., and MacGregor, I. D., 1960, Ultrabasic intrusive conditions illustrated by the Mount Albert ultrabasic pluton, Gaspe, Quebec (Abstract): Geol. Soc. America Bull., v. 71, p. 1978

Smith, R. J., 1953, Geology of Los Teques-Cua region, Venezuela: Geol. Soc. America Bull., v. 64, p. 41–64

Thayer, T. P., 1942, Chrome resources of Cuba: U. S. Geol. Survey Bull. 935-A, p. 1–74

—— 1956, Preliminary geologic map of the John Day quadrangle, Oregon: U. S. Geol. Survey Mineral Inv. Field Studies Map MF 51

Thayer, T. P., 1960, Some critical differences between alpine-type and stratiform peridotite-gabbro complexes: 21st Internat. Geol. Cong., Rept. pt. XIII, p. 247–259

Yoder, H. S., Jr., and Chinner, G. A., 1960, Almandite-pyrope-water system at 10,000 bars: Carnegie Inst. Washington Year Book 59, p. 81–84

U. S. Geological Survey, Washington, D. C.
Manuscript Received by the Secretary of the Society, August 2, 1960
Publication Authorized by the Director, U. S. Geological Survey

D. B. MacKENZIE

IS THE TINAQUILLO, VENEZUELA, "PSEUDOGABBRO" METAMORPHIC OR MAGMATIC?—A REPLY

Large masses of hypersthene gabbro composition ("pseudogabbro") within the Tinaquillo peridotite, Venezuela (MacKenzie, 1960), were interpreted as large inclusions of contact-metamorphosed country rock. This interpretation was based principally upon similarity of the pseudogabbros to the rock of the inner part of the contact aureole and the absence of positive criteria of magmatic origin, such as ophitic or interlocking texture and intrusive igneous contacts. Secondary lines of argument were based on the absence of rocks intermediate in composition between gabbro and peridotite and the spatial relationship of the gabbro and peridotite.

As an alternative hypothesis, Thayer and Brown (1961) contend that the gabbroic masses at Tinaquillo, as well as many gabbroic masses associated with alpine-type peridotites elsewhere, were intruded with the peridotite as composite, semisolid, crystal mushes. The gabbro and peridotite are regarded as having been differentiated at depth by the mechanism of crystal settling. Thayer (1960, p. 257) has suggested that the gabbroic rocks in such complexes were "squeezed up or torn off" by peridotites moving upward from lower levels during strong deformation.

In reply to Thayer and Brown, there can be little argument that igneous gabbros are spatially and genetically associated with some peridotites intruded along axes of strong deformation. Where poikilitic textures are present (Flint, de Albear, and Guild, 1948), or where gabbros grade into troctolites or pyroxenites, the magmatic origin of the gabbro is particularly clear. However, the demonstration that gabbros in this association *can have* a magmatic origin is no basis for concluding that all or even a majority of such gabbroic rocks are magmatic. Furthermore, the observation by Thayer and Brown that strongly foliated gabbroic rocks are not uncommonly associated with peridotites elsewhere is not pertinent, unless the magmatic origin of the gabbroic rocks at each locality can be demonstrated. Although the field relationships may leave little doubt in the minds of Thayer and Brown that the gabbroic rocks to which they refer are of igneous origin, satisfactory evidence is not given in the papers cited [with the possible exception of the paper by Rossman and others (1959) which I have not seen]. If definite criteria of magmatic origin are absent, the possibility should be considered that many of these gabbroic rocks, as well as the "pseudogabbros" at Tinaquillo, are metamorphic rather than magmatic.

Around gabbro intrusions of all kinds, including stratiform complexes, high-temperature contact aureoles are commonly present. Such aureoles, although much less common, are also present around some alpine-type peridotites (MacKenzie, 1960). Where the composition of the country rocks is appropriate, the inner parts of these aureoles may be pyroxene hornfelses of gabbroic composition (Smith and MacGregor, 1960; Schwartz, 1943; Harry, 1952; MacKenzie, 1960; T. N. Irvine, 1959, unpub. Ph.D. Thesis, California Institute of Technology). Consequently, the gabbroic rocks "torn off" (in Thayer's hypothesis) need not be derived from igneous differentiates. They could also be derived from country rocks reconstituted to gabbro at the site of differentiation, along the path of intrusion, or at the site of final emplacement.

Turning now to one of several specific points made in the criticism by Thayer and Brown, I concede that I erred in stating that rocks intermediate in composition between gabbro and peridotite do not exist. They do indeed exist, but they differ in form and probably in origin from the gabbroic masses. The "intermediate rocks" consist of layers, commonly only 1–2 cm thick, composed predominately of amphibole and orthopyroxene (plagioclase is uncommon). Although they may have resulted in part from mixture of phases during intrusion, it seems more probable that they resulted from hydrothermal action (Bowen and Tuttle, 1949; MacKenzie, 1960, p. 308). Thus it is not evi-

Geological Society of America Bulletin, v. 72, p. 1571–1574, October 1961

dent that their presence demonstrates a continuous magmatic series between gabbro and peridotite. Furthermore, the "intermediate" phases are volumetrically insignificant. Although Thayer and Brown say that a small proportion of intermediate rock types is characteristic of many such complexes, it is not satisfactorily established, as pointed out earlier, that the gabbros in the examples to which they refer are, themselves, of igneous origin.

In discussing the significance of the lamellae-bearing pyroxene augen, Thayer and Brown state that my hypothesis calls for a mutual intergrowth of two pyroxenes in an environment in which they already occur as separate stable phases. In the original discussion, however, I suggested (MacKenzie, 1960, p. 312) that the augen grew, in the solid state, at a temperature in which each pyroxene took small amounts of the other into solid solution. Thus, the "mutual intergrowth" mentioned by Thayer and Brown developed only after exsolution during cooling. Thayer and Brown propose essentially the same mechanism except that, in their hypothesis, the augen are relict from a coarse-grained igneous gabbro rather than porphyroblasts.

In the first part of their criticism, Thayer and Brown present a table (Thayer and Brown, 1961, Table 1) with the objective of pointing up the differences rather than the similarity between the gabbroic masses and the rocks in the inner part of the contact aureole. This table may be misleading because the characteristics of the "pseudogabbro" are compared not with the particular characteristics of the inner, most highly metamorphosed part of the aureole, as implied in the text, but with the characteristics of the entire contact aureole. For a more accurate comparison, the table should be amended to show that the inner part of the aureole has a range in plagioclase composition of An_{45}–An_{50} (not An_{10}–An_{50}, as in the cited table), contains only brown hornblende (not brown and green hornblende), and contains garnets in amounts up to 20 per cent. In addition the quartzose layers in the country rocks are largely obliterated in the inner part of the contact aureole (MacKenzie, 1960, p. 310).

In my opinion, there is a strong resemblance rather than a marked difference between the gabbroic masses and the rocks in the inner part of the contact aureole; furthermore, those differences that do exist are consistent with the hypothesis that the gabbroic masses were metamorphosed at a higher temperature.

With respect to the evidence bearing on the origin of the gabbroic masses at Tinaquillo, a point that is not stressed in the criticism is that garnets, although uncommon, are present in the gabbroic masses (MacKenzie, 1960, p. 309). They occur, for example, along the northwestern part of the intrusion between El Tigre and La Montañita. If the gabbroic masses originated as magmatic members of a peridotite-gabbro complex at depth, the presence of garnet is anomalous for the following reasons: (1) Garnets are absent in the gabbroic and noritic phases of the classical stratiform complexes (Hall, 1932; Wager and Deer, 1939; Hess, 1960). (2) In the area south of the contact aureole, garnets were not observed in country rocks of appropriate composition subjected only to regional metamorphism. Although it is possible to invoke contamination as an explanation for the presence of garnets, contamination by country rock of pockets of gabbro enclosed within peridotite seems unlikely.

On the other hand, if the gabbroic masses are incorporated blocks of garnet-bearing rocks of the contact aureole, the presence of a few relict garnets is to be anticipated, in spite of the tendency of garnet to disappear in the direction of increasing temperature of metamorphism (Yoder, 1952).

In summary, some gabbros associated with peridotites are of igneous origin; others are demonstrably of contact-metamorphic origin. In the majority of peridotite-gabbro complexes, however, valid criteria for determining the origin of the gabbro are lacking. Consequently, arguments based on relationships in these complexes are not particularly relevant in determining the origin of the gabbro in any specific complex.

As originally recognized, and as the preceding exchange has emphasized, the presently known characteristics and relationships of the gabbroic masses at Tinaquillo are interpretable in more than one way. Although I still favor the belief that they are of contact-metamorphic origin, for reasons cited above and in the original paper, I agree with Thayer and Brown that a satisfactory resolution of the question of origin would require additional data.

References Cited

Bowen, N. L., and Tuttle, O. F., 1949, The system MgO-SiO_2-H_2O: Geol. Soc. America Bull., v. 60, p. 439–460

Flint, D. E., Albear, J. F. de, and Guild, P. W., 1948, Geology and chromite deposits of the Camagüey district, Camagüey Province, Cuba: U. S. Geol. Survey Bull. 954-B, p. 39–63

Hall, A. L., 1932, The Bushveld igneous complex of the Central Transvaal: Geol. Survey S. Africa Mem. 28, 560 p.

Harry, W. T., 1952, Basic hornfels at a gabbro contact near Carlingford, Eire; Geol. Mag., v. 89, p. 411–416

Hess, H. H., 1960, Stillwater igneous complex, Montana: Geol. Soc. America Mem. 80, 230 p.

MacKenzie, D. B., 1960, High-temperature alpine-type peridotite from Venezuela: Geol. Soc. America Bull., v. 71, p. 303–318

Rossman, D. L., Fernandez, N. S., Fontanos, C. A., and Zepeda, Z. C., 1959, Chromite deposits on Insular Chromite Reservation No. 1, Zambales, Philippines: Philippines Bur. Mines, Special Projects Series pub. no. 19

Schwartz, George M., 1943, Metamorphism of extrusives by basic intrusives in the Keweenawan of Minnesota: Geol. Soc. America Bull., v. 54, p. 1211–1226

Smith, Charles H., and MacGregor, I. D., 1960, Ultrabasic intrusive conditions illustrated by the Mount Albert ultrabasic pluton, Gaspe, Quebec (Abstract): Geol. Soc. America Bull., v. 71, p. 1978

Thayer, T. P., 1960, Some critical differences between alpine-type and stratiform peridotite-gabbro complexes: 21st Internat. Geol. Cong., Rept. pt. XIII, p. 247–259

Thayer, T. P., and Brown, C. E., 1961, Is the Tinaquillo, Venezuela "pseudogabbro" metamorphic or magmatic?: Geol. Soc. America Bull., v. 72, p. 1565-1570

Wager, L. R., and Deer, W. A., 1939, Geological investigations in east Greenland. Pt. III, Petrology of the Skaergaard intrusion, Kangerdluzssuaq, East Greenland: Med. om Grønland, Bd. 105, no. 4, 335 p.

Yoder, H. S., 1952, The MgO-Al_2O_3-SiO_2-H_2O system and related metamorphic facies: Am. Jour. Sci., Bowen volume, p. 569–627

The Ohio Oil Company, Denver Research Center, Box 269, Littleton, Colo.
Manuscript Received by the Secretary of the Society, April 28, 1961

E. PENNER

ICE-GRAIN STRUCTURE AND CRYSTAL ORIENTATION IN AN ICE LENS FROM LEDA CLAY

Abstract: The long axes of ice grains were oriented parallel to the direction of heat flow. A random *c*-axis orientation, determined by an etching technique, appeared to exist. In some adjacent crystals the *c*-axes were as much as 45° apart. This disorder seems to be consistent with the disorderly distribution of clay particles in the ice lens.

Marked differences have frequently been observed in the character of frozen soil and the disposition of ice and soil resulting from the ice-segregation process in different soil types (Czeratzki and Frese, 1958). The soil structure and the related features that consistently occur when remolded Leda clay is frozen (Pl. 1) are in sharp contrast to the regular soil strata, well-ordered ice lenses, and flat freezing fronts so common in coarser frost-susceptible soils.

The main purpose of this preliminary investigation was to determine whether there is some well-defined regularity in the ice structure both with respect to the crystal orientation and the form and orientation of the ice grains despite the apparently random occlusions of clay in the ice and the undulating soil–ice interface. Such regularity is common for ice produced from bulk water in a container by one-dimensional cooling.

A block sample of Leda clay was obtained from a depth of 20 feet in a freshly dug excavation. It was thoroughly remolded at its natural moisture content of about 60 per cent and consolidated in a 6-inch-diameter mold to a dry density of 1.58 gm/cm³ (101 lb/ft³). The resultant moisture content of this saturated specimen was about 26 per cent. Grain size was determined using the hydrometer method. The clay content (<0.002 mm) and silt content (0.002 to 0.2 mm) were 69 and 25 per cent respectively. Some details on the origin and geotechnical properties of this soil are given by Eden and Crawford (1957).

A cylindrical specimen 6 inches in diameter and 2 inches high was frozen unidirectionally in the frost-cell apparatus described by Penner (1960). The pre-freezing temperature gradient was 1.16°F/inch with the cold side of the specimen close to 32°F. After a constant heat flow was achieved the cold end was supercooled to about 31°F, and crystallization of the soil water was easily induced by rubbing the top of the soil with a previously inserted steel wire. The cold-side temperature of the conditioning plate was set, and freezing was allowed to proceed without any changes in the temperature of the conditioning plates. A moderate rate of heat removal from the specimen insured that only a part of the specimen would be frozen in a period of a week. At the same time a slowly penetrating frost line was needed to build up an ice lens with some soil inclusions. A heave of 0.59 inch was achieved over a period of 174 hours giving an average heave of about 0.08 inch/day. The rate of heaving at the beginning was nearly 0.1 inch/day and after 7 days slowed down to 0.0605 inch/day.

After the freezing period the specimen was removed from the frost cell and taken into a cold (15°F) room. Half of the sample was cut in about 1/8-inch slices with a band saw to permit examination of the vertical section of the ice lens. The other half was cut horizontally for examination of the horizontal section.

The etching procedure used to determine the *c*-axes orientation was essentially that described by Higuchi (1958) and was carried out at a cold-room temperature of 15°F. Samples were prepared by polishing the surface of the ice lens in the cut slices. A 1 per cent solution of polyvinyl formal in ethylene dichloride was applied to the surface of the ice lens directly after polishing. After evaporation of the solvent the surface was examined microscopically (mag. 40 ×) under transmitted light for the appearance of etch pits. It took up to 30 minutes for mature pits to develop.

A vertical slice of the specimen is shown in Plate 1. The heat flow during freezing was unidirectional from the bottom to the top. All the soil below the ice lens was unfrozen when removed from the frost cell. To preserve the sample it was rapidly frozen and kept at a

Geological Society of America Bulletin, v. 72, p. 1575–1578, 1 fig., 4 pls., October 1961

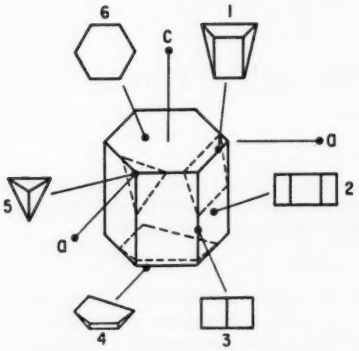

Figure 1. Schematic diagram of possible types of etch pits on an ice crystal (after Higuchi, 1958)

regular boundaries. The orientation of the long axes of the ice grains seems to be the same as that reported by Gold (1960) when water in a tank is frozen by one-dimensional cooling in the direction normal to the water surface.

The etch pits developed on the surface of horizontal and vertical sections of the ice lens are shown in Plates 3 and 4. The diagram by Higuchi (1958) showing the *c*-axis orientation of an ice crystal in relation to the type of etch pit is reproduced in Figure 1. A résumé of all these results is given in Table 1.

The disorder in the optic axes of the ice grains appears to be consistent with the disorderly nature of the clay and ice distribution in the frozen layer and the uneven character of the ice-soil interface at the freezing front. How

TABLE 1. ETCH PITS OF ICE LENS FROM LEDA CLAY

Illustration	Plane of ice surface with reference to direction of heat flow	Type of etch pit*	Orientation of *c*-axes with reference to direction of heat flow
Pl. 3, fig. 1	Parallel	Between type 1 and type 2	Nearly perpendicular
Pl. 3, fig. 2	Parallel	Between type 1 and type 2	Nearly perpendicular
Pl. 4, fig. 1 lower half	Perpendicular	Type 6	Parallel
Pl. 4, fig. 1 upper half	Perpendicular	Type 1	About 45°
Pl. 4, fig. 2 lower half	Perpendicular	Type 1	About 45°
Pl. 4, fig. 2 upper half	Perpendicular	Between type 4 and type 6	Nearly parallel

*Type of etch pit refers to the various types shown in Figure 1.

room temperature of 15°F. The random fissures visible in the soil below the ice lens developed as a result of the quick freeze.

Plate 1 clearly shows the concoidal shape of the soil fragments, the undulating or uneven soil–ice interface, and the discontinuous ice-lens formation. Some soil fragments have been rotated during the ice lensing.

Vertical sections (+1 mm. thick) of the same specimen, placed between crossed polaroids and viewed in transmitted light, show that the long axes of most ice grains are in the direction of the heat flow (Pl. 1, fig. 2b). Not all ice-grain boundaries, however, are exactly vertical. In many cases the grains extend the full distance across the ice lens and terminate in soil at both ends.

Horizontal sections show the short-axes ice-grain pattern which is normal to the heat flow (Pl. 2). The grains range in size and have ir-

much the two are related is still a matter for conjecture.

The disorderly nature of the clay distribution may be related to nonlinear heat flow and uneven moisture supply at local sites at the freezing front where the ice is formed. Uneven shrinkage at the interface is almost certainly involved in breaking away the clay fragments at the freezing front.

The rotation of the soil particles could be caused by the differential rates of growth of two adjacent ice crystals with different optical orientations since the rate of crystal growth depends on its orientation (Hillig, 1958). The random orientation in the c-axes of ice crystals found in the ice lens studied may result from random nucleation. In ice produced from bulk water the orientation changed with depth (Perey and Pounder, 1958). In these studies the ice lens was too thin to permit study of the

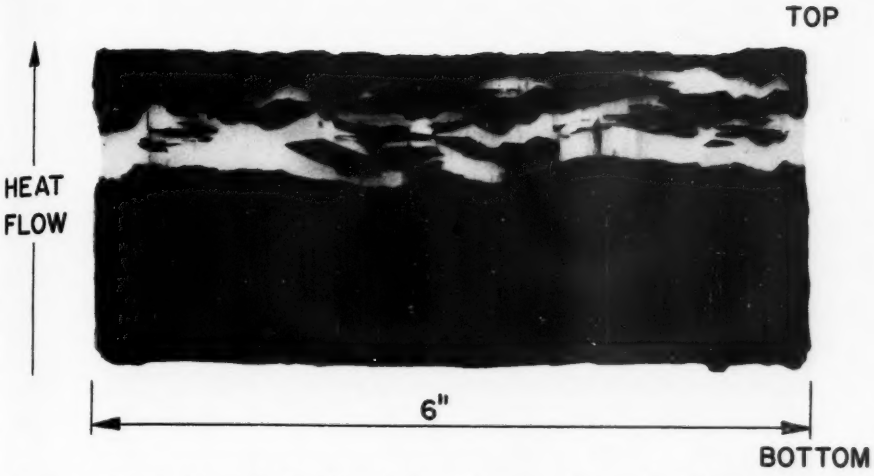

Figure 1. Normal photograph of specimen showing soil structure, ice lens, shape of freezing front, and occluded clay. Note rotation of large soil fragment to left of center and near bottom of ice lens.

Figure 2. Ice lens showing ice-grain boundaries in vertical section. (a) Normal photograph of specimen; (b) specimen photographed from same location as in (a) but with transmitted light between crossed polaroids. Note grain boundaries are not exactly vertical and mostly extend full distance between soil particles.

VERTICAL SLICE OF SPECIMEN AFTER FREEZING

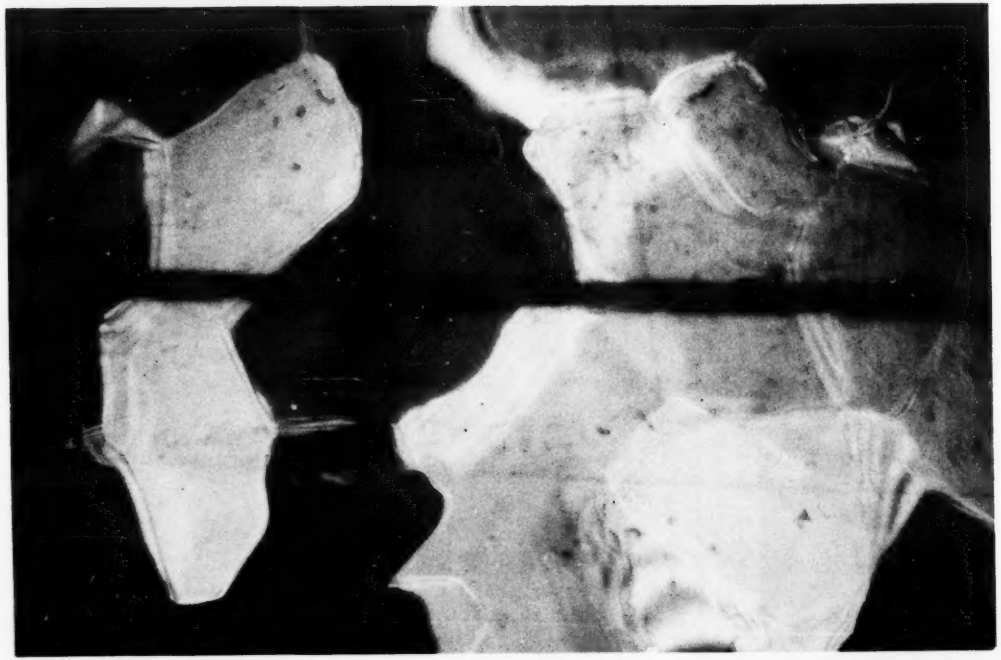

ENLARGED VIEW OF HORIZONTAL SECTION OF ICE LENS (MAG. 10 ×)

Heat flow normal to plane of photograph. Note irregular grain boundaries and uneven grain sizes.

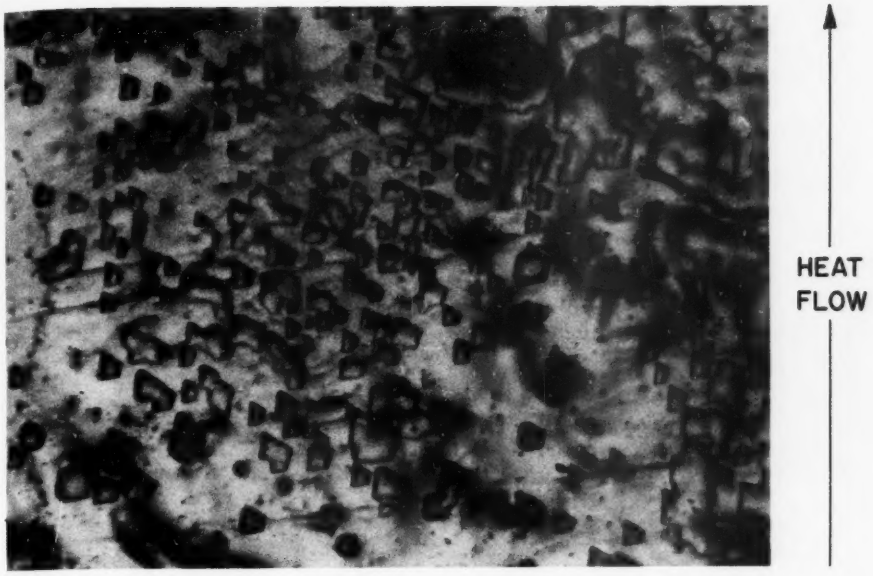

Figure 1

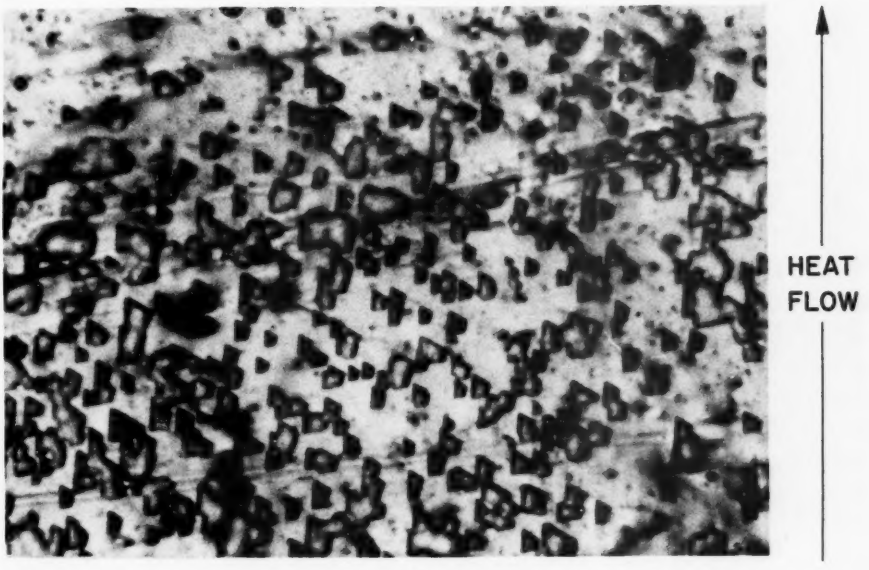

Figure 2

ETCH PITS DEVELOPED ON VERTICAL FACE OF ICE LENS IN TWO LOCATIONS (MAG. 180 ×)

Shape of pits are between type 1 and 2 (Fig. 1 in text), *i.e.*, the *c*-axis is nearly perpendicular to direction of heat flow; consequently, growth direction of crystals was normal to *c*-axes.

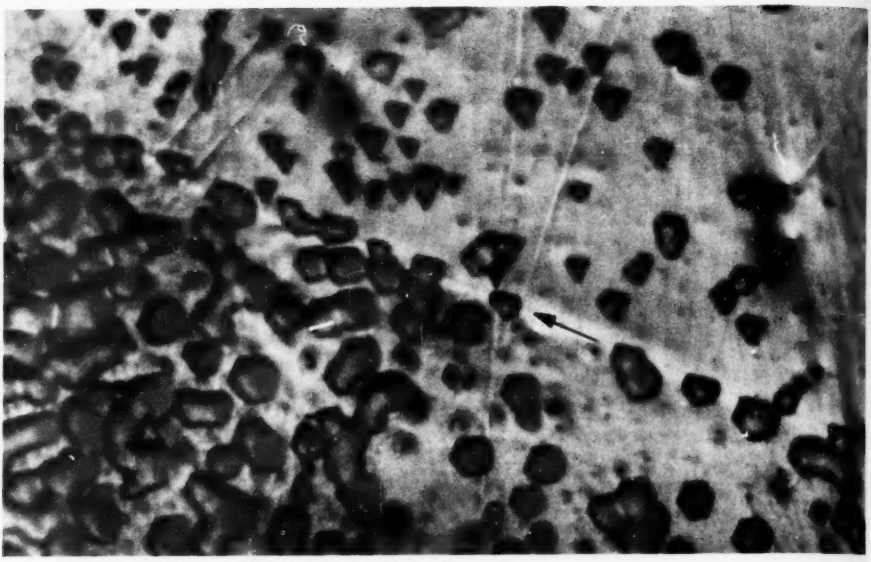

Figure 1. Note crystal boundary running diagonally from bottom right to top left. In lower crystal *c*-axis nearly parallel to heat flow, and is type 6 (Fig. 1 in text). Upper crystal is oriented at about 45° to lower crystal and is type 1.

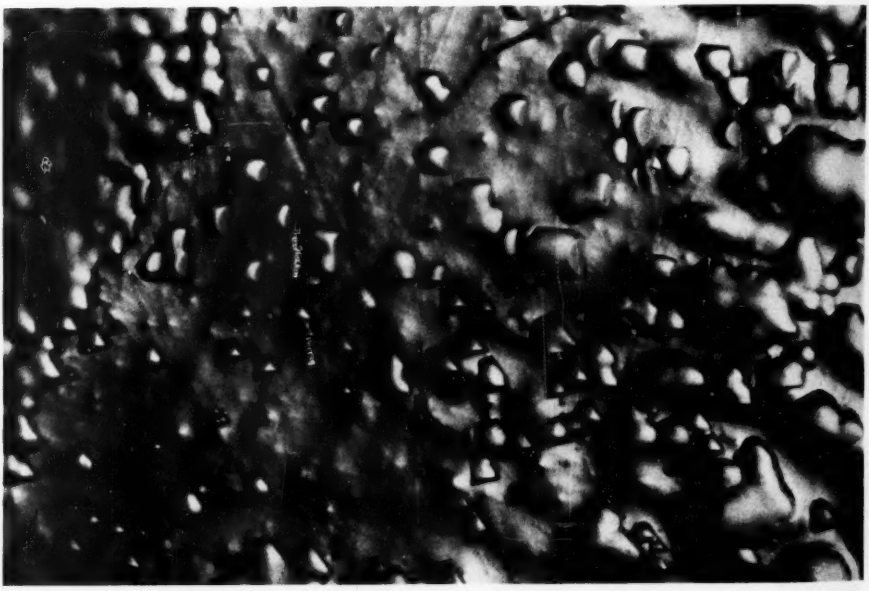

Figure 2. Crystal in bottom half belonging to type 1 indicating *c*-axes at about 45° to direction of heat flow. Crystal upper half is oriented between types 4 and 6; thus *c*-axes nearly parallel to heat flow.

ETCH PITS DEVELOPED ON HORIZONTAL FACE OF ICE LENS
Heat flow and long axes of grains normal to plane of paper

change of orientation with depth; this should be checked in future studies.

Acknowledgments

The author is indebted to L. W. Gold for his assistance and suggestions. This paper is a contribution from the Division of Building Research, National Research Council, Canada, and is published with the approval of the Director of the Division.

References Cited

Czeratzki, W., and Frese, H., 1958, Importance of water in formation of soil structure: Highway Research Bd. Special Rept. 40, p. 200–212

Eden, W. J., and Crawford, C. B., 1957, Geotechnical properties of Leda clay in the Ottawa area: 4th Conf. Internat. Soc. Soil Mechanics and Foundation Engineering Proc., v. 1, Div. 1, p. 22–27

Gold, L. W., 1960, The cracking activity in ice during creep: Canad. Jour. Physics, v. 38, p. 1137–1148

Higuchi, K., 1958, The etching of ice crystals: Acta Metallurgica, v. 6, p. 636–642

Penner, E., 1960, The importance of freezing rate on frost action in soils: Am. Soc. Testing Materials Proc., v. 60, p. 1151–1165

Perey, F. G. J., and Pounder, E. R., 1958, Crystal orientation in ice sheets: Canad. Jour. Physics, v. 36, p. 494–502

Soil Mechanics Section, Division of Building Research, National Research Council, Ottawa, Canada

Manuscript Received by the Secretary of the Society, January 31, 1961

VAL LaMARCHE

RATE OF SLOPE EROSION IN THE WHITE MOUNTAINS, CALIFORNIA

Attention is called to a means of directly establishing rates of erosion of certain dolomite areas in the White Mountains of California. Here, Schulman (1958) has found Bristlecone pines (*Pinus aristata*) more than 4500 years old. Growing along with limber pines (*Pinus flexilis*) and a sparse ground cover at elevations of over 10,000 feet, stands of bristlecone pines are virtually restricted to outcrops of Reed dolomite of late Precambrian age (Knopf, 1918).

The White Mountains border the eastern side of Owens Valley in southeastern California. Rising to elevations of more than 14,000 feet, the range presents a bold western face. A dissected, probably compound fault scarp, the face rises nearly 10,000 feet above the valley floor. The gentler eastern slope of the range exhibits remnants of a rolling mature topography, faulted and tilted eastward, which is deeply incised by modern canyons. This old surface, with a maximum relief of 1000 feet and a maximum slope angle of about 20°, probably represents an erosional surface developed prior to Basin and Range faulting. On this surface, and in the steep-walled canyons that cut into it, the bristlecone pines are found.

The climate at elevations above 10,000 feet in the White Mountains is cool and semiarid. Temperatures as recorded at the University of California High Altitude Station seldom go above 70° F in the summer or below −20° in the winter. Summer thunderstorms bring 2 to 3 inches of rain, and 3 or 4 feet of snow falls during the winter.

The bristlecone pines seem to thrive under these rigorous conditions and attain their greatest ages where survival appears most difficult—on the drier, steeper slopes. As emphasized by Schulman, the oldest individuals are not the largest, healthiest-appearing trees, but those that are short, squat, and three-fourths dead. Often only a narrow strip of bark leads to the two or three branches that make up the living part of the tree. The remainder of the tree, bleached white and deeply eroded, may have been dead for more than 1000 years. So resistant is the wood to weathering and decay that dead trees often stand until the support is literally eroded out from around their roots. On living trees the stubs of ancient side roots may project into the air 3 or 4 feet above the present ground surface.

There are no data now available as to the ages of these exposed side roots, but these data could be obtained by ring counting and correlation or by C^{14} dating of cores. The unique longevity of the bristlecone pines of this area, their suitability for accurate age determinations, and the testimony offered by their exposed roots make possible direct, accurate measurements of slope erosion in this area during the past 5000 years.

References Cited

Knopf, A., 1918, A geologic reconnaissance of the Inyo Range and the eastern slope of the Sierra Nevada: U.S. Geol. Survey Prof. Paper 110, 130 p.

Schulman, E., 1958, Bristlecone pine, oldest known living thing: Nat. Geog. Mag., v. CXIII, p. 355–372

2321 Howe Street, Berkeley, Calif.

Manuscript Received by the Secretary of the Society, August 10, 1960

Geological Society of America Bulletin, v. 72, p. 1579–1580, October 1961

WALTER L. MOORE

ROLE OF FLUID PRESSURE IN OVERTHRUST FAULTING: A DISCUSSION

The paper on the role of fluid pressure in overthrust-faulting (Hubbert and Rubey, 1959) presents some interesting concepts regarding buoyant forces on solid and porous bodies. The concept of buoyancy, as commonly developed, is considered to apply to an entire submerged solid body or to the entire submerged part of a floating body. The authors state (below Fig. 10b) that "the principle of Archimedes does not require for its validity that the body acted upon by the fluid pressure be completely enclosed by an exterior surface". This is an unusual concept that requires careful consideration if it is to be applied to a completely submerged body.

Solid Bodies

The crux of the problem lies in the assumption by the authors that

$$\frac{\partial p}{\partial z} = -\rho_1 g$$

inside of a submerged solid body as used in the development of Equations (29) and (30). The authors do not identify this as an arbitrary assumption, and one's first reaction is to reject the whole concept as fallacious. Since the fluid is excluded from the interior of a solid body, surely the physical existence of the fluid pressure inside the body cannot be taken for granted.

It is of interest, however, to see the results of making the *arbitrary assumption* that the fluid-pressure field extends throughout the region occupied by the solid. The total stress S within the solid may arbitrarily be divided into two parts, p and σ, where p is a fictitious hydrostatic stress in the solid equal to that in the liquid at the same elevation and σ is simply the remaining stress to satisfy the equation

$$S = p + \sigma . \qquad (1)$$

By this division, p is the hydrostatic portion including no shear stress, while σ is nonhydrostatic and includes shear stress. This division of stress is the same as that assumed by the authors.

Based on this arbitrary division of stress, a straightforward analysis of the forces on any part of a submerged solid may be made. The results closely resemble those of Hubbert and Rubey, but the analysis contained herein clarifies the fictitious and arbitrary nature of the stresses p and σ within the region occupied by the solid. In the following development, an effort is made to present the concepts in the simplest possible manner. A combination of words and symbols is used which will convey

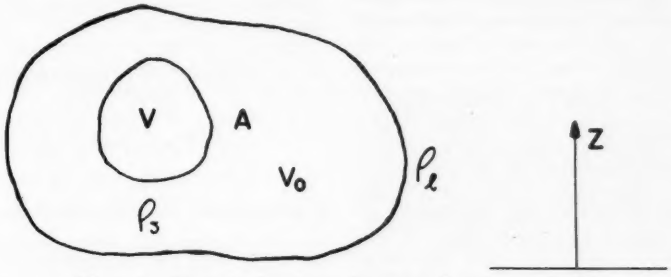

Figure 1. Diagram of an internal portion of a submerged solid

Geological Society of America Bulletin, v. 72, p. 1581–1586, 3 figs., October 1961

the concepts with no ambiguity to anyone familiar with fundamental stress concepts. Of course, a more rigorous and impressive presentation can be made in terms of tensor notation, but that seems unnecessary in this case.

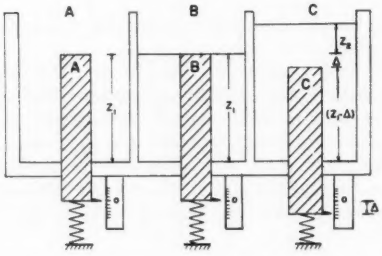

Figure 2. Apparatus showing the fictitious nature of "buoyant forces" on a portion of a submerged body

Consider the volume V as shown in Figure 1, which is a part of the larger volume V_0 of a solid with density ρ_s immersed in a liquid of density ρ_l and bounded by the surface A which is internal to the volume of V_0. Let S be the stress, including both normal and shear components, acting on the surface A. Let

$$\iint_A S dA$$

represent the vector summation of all stress components over the surface A and let

$$\iiint_V \nabla W dV$$

represent the summation of all body forces acting on the volume V. In the last integral W, the body-force potential due to gravity, is equal to $\rho_s gz$ where z is an elevation coordinate measured positive upward, and ∇ is a vector operator; that is, ∇W is grad W. The equilibrium of forces may be expressed as

$$-\iint_A S dA - \iiint_V \nabla(\rho_s gz) dV = 0 . \quad (2)$$

If it is arbitrarily assumed that the hydrostatic pressure p exists inside the solid, the total stress S may be expressed as

$$S = p + \sigma \quad (1)$$

where σ is the residual nonhydrostatic portion of the total stress. If, in Equation (2), $p + \sigma$ is substituted for S, and the identity

$$\rho_s = \rho_l + (\rho_s - \rho_l) \quad (3)$$

is used to replace ρ_s, the equation assumes the following form:

$$-\iint_A \sigma dA - \iint_A p dA - \iiint_V \nabla(\rho_l gz) dV$$
$$-\iiint_V \nabla(\rho_s - \rho_l)\, gz dV = 0 . \quad (4)$$

Now by Gauss's Theorem

$$\iint_A p dA = \iiint_V \nabla p dV \quad (5)$$

since p and ∇p as arbitrarily defined are continuous in the region V. Equation (4) may then be rewritten as

$$-\iint_A \sigma dA - \iiint_V \nabla(p + \rho_l gz) dV$$
$$-\iiint_V \nabla(\rho_s - \rho_l) gz dV = 0 . \quad (6)$$

For hydrostatic conditions the integral

$$-\iiint_V \nabla(p + \rho_l gz) dV = 0 \quad (7)$$

because the x and y components of the gradient are zero and

$$\frac{\partial p}{\partial z} = -\rho_l g . \quad (8)$$

This leads to the equation

$$-\iint_A \sigma dA - \iiint_V \Delta(\rho_s - \rho_l) gz dV = 0 . \quad (9)$$

which says that the summation of the *nonhydrostatic portion* of the total stress over the bounding surface A is equal to the weight of the solid minus the weight of the liquid displaced or the weight of the solid minus a "buoyant force" as used by Hubbert and Rubey.

It is important to realize that for the submerged solid it is the total stress S that is significant and not the nonhydrostatic portion σ. This may be illustrated by considering the equilibrium of the three cylinders shown in Figure 2. Each cylinder has a density ρ_s and is identical in every respect to the others. Each

one passes through a hole in the bottom of its individual tank. It is assumed that there will be no leakage where the cylinders pass through the bottoms of the tanks and that there is no resistance to movement of the cylinders through the holes. Each cylinder is supported on a spring at its base with a pointer attached to indicate the position of the cylinder. When tanks A, B, and C are all empty the pointers all read zero. The stress in cylinder A at the distance z_l below its top is clearly compressive amounting to $gz_l\rho_s$.

Now consider that tank B is filled to the top of the cylinder, that is to a depth z_1, with a liquid of density $\rho_l = 2\rho_s$. The nonhydrostatic portion of the stress σ in the cylinder at the depth z_1 may be computed from Equation (9) as $\sigma = gz_1(\rho_s - \rho_l) = gz_1(\rho_s - 2\rho_s) = -gz_1\rho_s$. This is a tension stress of magnitude $gz_l\rho_s$. If this stress were significant—that is, if buoyancy were really effective on the upper portion of this cylinder—the load on the spring supporting the cylinder would be reduced, and the cylinder would rise. The total stress in cylinder B at depth z_1 is

$$S_B = \sigma + p = -gz_1\rho_s + gz_1\rho_l = -gz_1\rho_s + 2gz_1\rho_s = gz_1\rho_s \qquad (10)$$

or a compressive stress of magnitude $z_1\rho_s$ the same as in tank A which is empty. Since the stress at depth z_1 is the same for cylinders A and B the load on the springs would be the same in each instance, and there would be no movement of cylinder B due to filling the tank. This demonstrates that the buoyancy concept as applied to cylinder B is arbitrary and fictitious.

If the tank is filled above the top of the cylinder as in tank C, the cylinder will move downward an amount Δ. The stress in the cylinder at the bottom of the tank may be computed directly from the free-body principle, as

$$S_c = g(z_2 + \Delta)\rho_l + g(z_1 - \Delta)\rho_s = g(z_2 + \Delta)2\rho_s + g(z_1 - \Delta)\rho_s = g\rho_s(z_1 + 2z_2 + \Delta) \qquad (11)$$

or as the sum of the hydrostatic and nonhydrostatic portions (Equations (1) and (9)) as

$$\begin{aligned} S_c &= \sigma + p = g(z_1 - \Delta)(\rho_s - \rho_l) + g(z_2 + z_1)\rho_l \\ &= gz_1\rho_s - gz_1\rho_l - g\Delta(\rho_s - \rho_l) + gz_2\rho_l + gz_1\rho_l \\ &= gz_1\rho_s + gz_2\rho_l + g\Delta(\rho_l - \rho_s) \\ &= g\rho_s(z_1 + 2z_2 + \Delta). \end{aligned} \qquad (12)$$

Either method gives the same result. This shows that the compressive stress in the cylinder at the bottom of tank C is greater than the corresponding stress for cylinder A by the amount

$$gz_2\rho_l + g\Delta(\rho_l - \rho_s) = g\rho_s(2z_2 + \Delta)$$

and that cylinder C will in fact move downward as assumed. If a buoyant force were active in the commonly accepted sense, cylinder C would move upward since $\rho_l > \rho_s$. Again the buoyancy concept is shown to be arbitrary and fictitious.

This example has shown that an analysis based on the arbitrary assumption on a hydrostatic pressure field extending inside a submerged solid results in an arbitrary and fictitious concept of buoyancy. However, if carefully applied to obtain the *total stress*, the concept will yield true results for the equilibrium of submerged bodies or sections of such bodies. The writer believes that for solid bodies the concept has no advantage over a direct computation of total stresses by the free-body principle. In fact the artificial concept is apt to lead to confusion and errors. One easily can be led to think of a fictitious buoyancy acting on a portion of a body and forget to account properly for the hydrostatic stress field which must be added. For solid bodies the artificial concept of dividing the total stress into a hydrostatic and nonhydrostatic component is more apt to lead to confusion than to clarification.

Porous Bodies

When dealing with forces on a porous body, the concept has a closer resemblance to reality and seems to serve a useful purpose. In a porous body the liquid actually penetrates into the region partially occupied by solid particles, and thus on a macroscopic scale the liquid pressure is actually transmitted into the interior of the body.

Before attempting to analyze the forces within a porous body let us examine the detailed stress picture in such a body and some of the simplications that may be made to deal with an extremely complex system. Figure 3 represents a plane section A-A cut through a granular material with its pores filled with a liquid. Below the section line is a hypothetical diagram of the true distribution of stress normal to section A-A. Where the section cuts the liquid-filled regions the stress is constant and equal to the hydrostatic pressure in the liquid. Where the section cuts the solid grains the stress has an irregular value starting at the

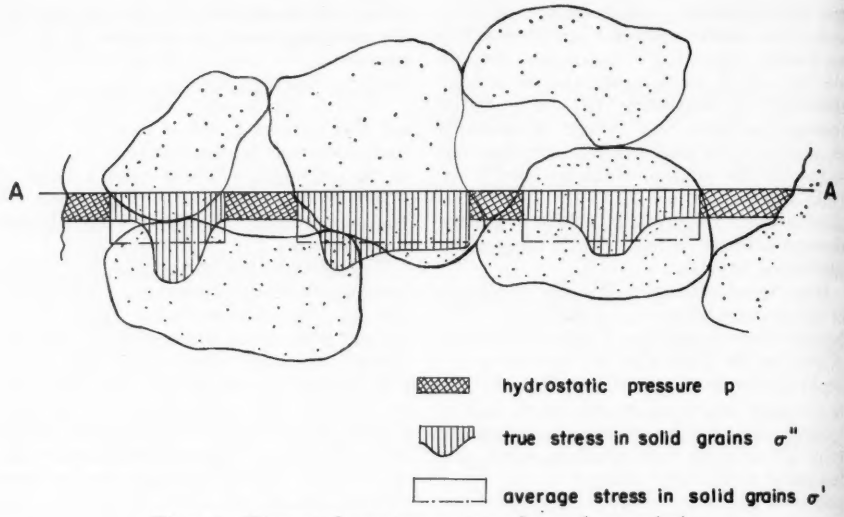

Figure 3. Diagram of stress patterns in a submerged porous body

hydrostatic pressure on the surface and increasing toward the interior of the grain. The stress values within the grain would be exceedingly complex depending on the shape and area of the contact points and the distance from the contact point to the section.

Now let us consider some possible ways of representing the stress, on a macroscopic scale, across the section A-A. This stress is defined as $S = \frac{\Delta F}{\Delta A}$ where ΔF is the force transmitted across the area ΔA, and ΔA is large enough to average out the local variation in stress but small in relation to the macroscopic dimensions. If A_l represents the area of the liquid cut by section A-A, and A_s represents the area of the solid grains cut by section A-A, the stress S may be stated as

$$S = \frac{1}{A_s + A_l}\left[pA_l + \iint_{A_s} \sigma'' dA\right] \qquad (13)$$

where p is the hydrostatic pressure and σ'' is the true stress in the solid. Because it is obviously impractical to evaluate the integral of the true stress over the solid area it may be helpful to define an average stress in the solid grains as

$$\sigma' = \frac{1}{A_s}\iint_{A_s} \sigma'' dA\,. \qquad (14)$$

The total stress S may then be expressed as

$$S = \frac{1}{A_s + A_l}\left[pA_l + \sigma' A_s\right] \qquad (15)$$

$$S = f_b\, p + (1 - f_b)\,\sigma' \qquad (16)$$

where f_b is the boundary porosity $f_b = \frac{A_l}{A_s + A_l}$.

Another possible way to represent the stress S would be to follow the concept of a hydrostatic stress field extending through the solid grains as assumed by Hubbert and Rubey. The total stress S may then be expressed as

$$S = p + \sigma \qquad (1)$$

where both p and σ are assumed to act over the entire area $(A_s + A_l)$. If this were written in form to compare with Equation (15) it would be

$$S = \frac{1}{A_s + A_l}\left[pA_l + pA_s + \sigma' A_s - pA_s\right] \qquad (17)$$

$$S = \frac{1}{A_s + A_l}\left[p(A_s + A_l) + (\sigma' - p)A_s\right]. \qquad (18)$$

But since

$$A_s = (1 - f_b)\,(A_s + A_l) \qquad (19)$$

this may be written as

$$S = \frac{1}{(A_s + A_l)} [p(A_s + A_l) + (\sigma' - p)(1 - f_b)(A_s + A_l)] \quad (20)$$

or

$$S = p + (\sigma' - p)(1 - f_b). \quad (21)$$

By comparing Equations (1) and (21) it is apparent that

$$\sigma = (\sigma' - p)(1 - f_b) \quad (22a)$$

or that

$$\sigma' = p + \frac{\sigma}{(1 - f_b)}. \quad (22b)$$

By means of Equations (22a) and (22b) it may be shown that Equations (1) and (16) are identical.

Hubbert and Rubey imply that there is something wrong with the term $f_b p$ which appears as their Equation (60) and as the first term of our Equation (16). The writer is convinced that the breakdown of total stress represented by Equation (16) is as valid as that represented by Equation (1). It is, of course, important to recognize that σ' is not equal to σ. Equation (1) based on Hubbert and Rubey's concept of a continuous hydrostatic stress field has the advantage that the terms can be easily evaluated. The stress S can be determined from equilibrium of a free body, the stress p can be calculated for the hydrostatic pressure field, and σ calculated from Equation (1). In Equation (16), S and p can be determined as before, and, if f_b is known, σ' can be calculated from the equation. However, the writer knows of no practical way to measure σ' and use it to calculate f_b. If the value of f_b is taken as equal to the volumetric porosity f_v the arbitrary stress σ' can be calculated, which probably is as significant as the arbitrary stress σ.

With the simpler division of stresses represented by Equation (1), the analysis of forces previously described for a solid body may be modified easily to apply to a body of porosity f. This will bring out the significance of the seepage forces on a porous body in a non-hydrostatic pressure field. The seepage forces are frequently important in causing earth movements and land slides.

In this case the ρ of the body will be the sum of $f\rho_l$ and $(1 - f)\rho_s$ where f is the volume porosity. Thus Equation (2) becomes

$$-\iint_A S dA - \iiint_V \nabla [(f\rho_l + (1 - f)\rho_s)gz] dV = 0. \quad (23)$$

But as before

$$\rho_s = \rho_l + (\rho_s - \rho_l) \quad (3)$$

so

$$[f\rho_l + (1 - f)\rho_s] = f\rho_l + (1 - f)[\rho_l + (\rho_s - \rho_l)] = [\rho_l + (1 - f)(\rho_s - \rho_l)] \quad (24)$$

By the same development as for the solid,

$$-\iint_A \sigma dA - \iiint_V \nabla(p + \rho_l gz) dV - \iiint_V \nabla(\rho_s - \rho_l)(1 - f) gz dV = 0. \quad (25)$$

The quantity $(p + \rho_l gz)$ in the second integral may be replaced by $\gamma_l h$ where h is the piezometric head or the elevation to which the liquid will rise in a piezometer open to the atmosphere, and γ_l is the specific weight of the liquid which is considered constant. Equation (25) would then read

$$-\iint_A \sigma dA - \iiint_V \nabla(\gamma_l h) dV - \iiint_V \nabla(1 - f)(\rho_s - \rho_l) gz dV = 0. \quad (26)$$

For hydrostatic conditions h = constant so $\nabla(\gamma_l h) = 0$, and the second integral drops out leaving

$$-\iint_A \sigma dA - \iiint_V \nabla(1 - f)(\rho_s - \rho_l) gz dV = 0. \quad (27)$$

This says that the stress σ (acting over the entire area) is due to the effective submerged weight of the solid portion of the porous body.

If there is seepage of liquid through the porous body, h is not constant, and by Darcy's Law

$$\nabla h = \frac{Q}{AP} = \frac{v}{P}$$

where v is the vector of nominal seepage velocity, and P is the permeability coefficient. Thus, in very tight materials with a low perme-

ability, very high values of piezometric gradient ∇h may occur. Under these conditions the second integral in Equation 26

$$\iiint_V \nabla(\gamma_l h)\,dV$$

may represent a very large force. It may also represent a very large force if the piezometric gradient ∇h is moderate but acts essentially in the same direction over a large volume. This integral may be thought of as an evaluation of the seepage forces, and the quantity $\nabla\gamma_l h$ as the force per unit volume due to seepage. It represents the force transmitted to the volume by the fluid moving through the pores. Thus for a region in which a fluid is moving through a porous solid, the nonhydrostatic stress σ is the summation of the effective submerged weight of the solid portions of the porous body and the seepage forces. For many instances of earth movements and landslides, the seepage forces are an important factor tending to cause movement.

Reference Cited

Hubbert, M. King, and Rubey, William W., 1959, Role of fluid pressure in mechanics of overthrust faulting, I: Mechanics of fluid-filled porous solids and its application to overthrust faulting: Geol. Soc. America Bull., v. 70, p. 115–116

Dept. Civil Engineering, The University of Texas, Austin, Texas
Manuscript Received by the Secretary of the Society, August 7, 1959

M. KING HUBBERT AND WILLIAM W. RUBEY

ROLE OF FLUID PRESSURE IN MECHANICS OF OVERTHRUST FAULTING: A REPLY TO DISCUSSION BY WALTER L. MOORE

In the foregoing discussion the critic admits to an initial doubt concerning the validity of the authors' stress resolution into a partial stress equal to the pressure of the ambient fluid and a residual effective stress which is the difference between the total stress and the fluid pressure. He then demonstrates that the resolution is indeed valid but contends that it is "arbitrary," implying that any other resolution would have served equally well. He next argues that while the resolution used may have some justification on physical grounds when dealing with a fluid-filled porous solid, and is formally valid when applied to a nonporous solid, it is of no practical use in the latter instance since only the total stresses there need to be considered. Finally, in dealing with a fluid-filled porous solid, the critic, by means of a lengthy analysis, derives what he calls the "seepage force" for the case when the associated liquid is not static, apparently under the impression that this force had not been taken into account in the original paper.

The critic's principal method of procedure is to write the equation of equilibrium for a finite portion of a three-dimensional distribution of matter having a volume V and exterior surface A, which may be either a nonporous solid or a fluid-filled porous solid. For such a system the equation of equilibrium is the following:

$$\begin{pmatrix}\text{Surface forces acting}\\ \text{on area } A\end{pmatrix} + \begin{pmatrix}\text{Body forces acting}\\ \text{on the volume } V\end{pmatrix} = 0 .$$

This is, of course, a fundamental equation, and, by a proper statement of what the various surface and body forces are, any desired component can be evaluated in terms of the others.

Regrettably some confusion has been introduced into the critic's analysis by using symbols in a different sense from their definition either in the original paper or in the generally accepted literature of the subject. For example, in the original paper, the symbol S was defined as the normal component across any given plane surface of the tensor of total stress Σ; T was defined to be the shear component of this stress (Hubbert and Rubey, 1959, p. 138, Eq. 67 and 68). The critic, on the other hand, writes

$$\iint_A S dA$$

for the surface force due to the total stress, where S is said to be the stress, "including both normal and shear components, acting on the surface A." This integral is used throughout the subsequent analysis. While the critic's intentions are clear, this integral, as written, is mathematically ambiguous. It is a scalar integral and, as such, valid only for scalar quantities; whereas, by the critic's usage, the quantity S is a tensor, and the equating of the surface integral of S to a force is a vector operation which requires either the use of vector notation or else the expansion of S and its associated forces into their respective scalar Cartesian components.

Again, the critic defines ∇W to be the body force per unit volume due to gravity, where

$$W = \rho_s g z$$

is said to be the body-force potential. This is not in accordance with the definition of gravitational potential which has been in standard use for nearly two centuries. Since its original definition by Lagrange, gravitational potential has represented an energy per unit mass, and its gradient is simply $\mathbf{g}$, the intensity of the field, or the force it would exert per unit of mass on an elementary particle placed at the point considered. The equation for W as used by the critic not only is not the accepted gravitational potential, but it is ambiguous for matter of variable density.

Hence, to rectify the confusion that may have been introduced by the critic's re-definition of terms, and by his disregard of the conventions of mathematics, the authors wish

Geological Society of America Bulletin, v. 72, p. 1587–1594, October 1961

briefly to restate their thesis in terms of the complete equation of equilibrium.

As was defined in equations (67) and (68) of the original paper, the tensor of total macroscopic stress at any given point in a solid body, which may or may not be porous, is the following:

$$\Sigma \equiv \begin{vmatrix} S_{xx} & T_{xy} & T_{xz} \\ T_{yx} & S_{yy} & T_{yz} \\ T_{zx} & T_{zy} & S_{zz} \end{vmatrix}, \tag{1}$$

in which the first subscript signifies the axis to which the plane considered is normal, and the second the axis to which the stress component is parallel. Also

$$T_{ij} = T_{ji}, \tag{2}$$

where $i = x$, y, or z, and $j = y$ or z, z or x, or x or y, respectively.

In present usage, contrary to the customary practice, compressive stresses will be considered positive, and positive shear stresses on positive surfaces will be in the negative direction of the respective axes.

If a surface A encloses a finite volume V of a solid, which may or may not be porous, the equation of equilibrium is a statement that the sum of the surface forces and body forces must be zero. For the problem under consideration the body force is the weight of the body in the earth's gravitational field, or

$$\mathbf{F}_V = \iiint_V \rho_b \mathbf{g}\, dV, \tag{3}$$

where ρ_b is the bulk density of the matter contained within the volume V, and $\mathbf{g}$ the force per unit mass exerted by gravity. The body force can also be resolved into the following x-, y-, and z components:

$$\left.\begin{aligned} F_{Vx} &= \iiint \rho_b g_x\, dV, \\ F_{Vy} &= \iiint \rho_b g_y\, dV, \\ F_{Vz} &= \iiint \rho_b g_z\, dV. \end{aligned}\right\} \tag{4}$$

The surface force, which must be derived from the components of the tensor of equation (1), can best be written in terms of its x-, y-, and z-components. Thus, the stresses acting upon an element dA of the external surface A, whose external normal makes the angles α, β, and γ with the x-, y-, and z-axes, respectively, will produce the following components of force (Love, 1944, p. 75–76; Macelwane, 1936, p. 15):

$$\left.\begin{aligned} dF_{Ax} &= -(S_{xx}\cos\alpha + T_{yx}\cos\beta \\ &\quad + T_{zx}\cos\gamma)\, dA, \\ dF_{Ay} &= -(T_{xy}\cos\alpha + S_{yy}\cos\beta \\ &\quad + T_{zy}\cos\gamma)\, dA, \\ dF_{Az} &= -(T_{xz}\cos\alpha + T_{yz}\cos\beta \\ &\quad + S_{zz}\cos\gamma)\, dA. \end{aligned}\right\} \tag{5}$$

The terms in parentheses in equations (5) can be represented, respectively, by Σ_{nx}, Σ_{ny}, and Σ_{nz}. Then, with this substitution, we obtain upon integration of equations (5)

$$\left.\begin{aligned} F_{Ax} &= -\iint_A \Sigma_{nx}\, dA, \\ F_{Ay} &= -\iint_A \Sigma_{ny}\, dA, \\ F_{Az} &= -\iint_A \Sigma_{nz}\, dA. \end{aligned}\right\} \tag{6}$$

Then, if we combine the components of the surface force from equations (6) with the respective components for the body forces from equations (4), we obtain the three equations for translational equilibrium:

$$\left.\begin{aligned} -\iint \Sigma_{nx}\, dA + \iiint \rho_b g_x\, dV &= 0, \\ -\iint \Sigma_{ny}\, dA + \iiint \rho_b g_y\, dV &= 0, \\ -\iint \Sigma_{nz}\, dA + \iiint \rho_b g_z\, dV &= 0. \end{aligned}\right\} \tag{7}$$

Further, if the axes are chosen with the z-axis vertical and positive downward (as in the original paper),

$$\left.\begin{aligned} g_x = g_y &= 0, \\ g_z &= g, \end{aligned}\right\} \tag{8}$$

where g is the total intensity of gravity.

By virtue of equations (8), equations (7) simplify to

$$\left.\begin{aligned} -\iint \Sigma_{nx}\, dA &= 0, \\ -\iint \Sigma_{ny}\, dA &= 0, \\ -\iint \Sigma_{nz}\, dA + \iiint \rho_b g\, dV &= 0. \end{aligned}\right\} \tag{9}$$

Now let us resolve the tensor of total stress Σ into the two partial stresses Ω and Π, such that

$$\Omega + \Pi = \Sigma, \tag{10}$$

where

$$\Omega \equiv \begin{vmatrix} \sigma_{xx} & \tau_{xy} & \tau_{xz} \\ \tau_{yx} & \sigma_{yy} & \tau_{yz} \\ \tau_{zx} & \tau_{zy} & \sigma_{zz} \end{vmatrix}, \tag{11}$$

and

$$\Pi \equiv \begin{vmatrix} p & 0 & 0 \\ 0 & p & 0 \\ 0 & 0 & p \end{vmatrix}, \tag{12}$$

as defined in equations (72), (73), and (74) of the original paper. Then, in terms of these partial stresses,

$$\left.\begin{aligned} \Sigma_{nx} &= \Omega_{nx} + \Pi_{nx}, \\ \Sigma_{ny} &= \Omega_{ny} + \Pi_{ny}, \\ \Sigma_{nz} &= \Omega_{nz} + \Pi_{nz}, \end{aligned}\right\} \tag{13}$$

where Ω_{nj} and Π_{nj} ($j = x$, y, or z) are defined in the same manner as Σ_{nj}.

With these substitutions, equations (9) become

$$\left.\begin{aligned} -\iint \Omega_{nx}\, dA - \iint \Pi_{nx}\, dA &= 0, \\ -\iint \Omega_{ny}\, dA - \iint \Pi_{ny}\, dA &= 0, \\ -\iint \Omega_{nz}\, dA - \iint \Pi_{nz}\, dA + \iiint \rho_b g\, dV &= 0. \end{aligned}\right\} \tag{14}$$

But from equations analogous to (5), and from equation (12),

$$\left.\begin{aligned} \Pi_{nx} &= p \cos\alpha\, dA = p dA_x, \\ \Pi_{ny} &= p \cos\beta\, dA = p dA_y, \\ \Pi_{nz} &= p \cos\gamma\, dA = p dA_z; \end{aligned}\right\} \tag{15}$$

and, as was shown in equations (27) to (32) of the original paper,

$$\left.\begin{aligned} \iint p dA_x &= \iiint \frac{\partial p}{\partial x}\, dV, \\ \iint p dA_y &= \iiint \frac{\partial p}{\partial y}\, dV, \\ \iint p dA_z &= \iiint \frac{\partial p}{\partial z}\, dV. \end{aligned}\right\} \tag{16}$$

Thus, by means of equations (15) and (16) we can convert equations (14) to the form

$$\left.\begin{aligned} -\iint \Omega_{nx}\, dA - \iiint \frac{\partial p}{\partial x}\, dV &= 0, \\ -\iint \Omega_{ny}\, dA - \iiint \frac{\partial p}{\partial y}\, dV &= 0, \\ -\iint \Omega_{nz}\, dA + \iiint \left(\rho_b g - \frac{\partial p}{\partial z}\right) dV &= 0. \end{aligned}\right\} \tag{17}$$

These are the general equations of translational equilibrium for the body in terms of the forces produced by the fluid pressure p, the effective stress Ω, and the weight of the body in the gravitational field. If the body is small enough that gravity may with negligible error be assumed to be constant in magnitude and direction, and if the pressure corresponds to that of a liquid of the constant density ρ_l in hydrostatic equilibrium, then the pressure field will be given by

$$p = p_o + \rho_l g z. \tag{18}$$

Consequently

$$\left.\begin{aligned} \frac{\partial p}{\partial x} &= 0, \\ \frac{\partial p}{\partial y} &= 0, \\ \frac{\partial p}{\partial z} &= \rho_l g. \end{aligned}\right\} \tag{19}$$

Then, in this special case, equations (17) reduce to

$$\left.\begin{aligned} \iint \Omega_{nx}\, dA &= 0, \\ \iint \Omega_{ny}\, dA &= 0, \\ \iint \Omega_{nz}\, dA &= \iiint \rho_b g\, dV - \iiint \rho_l g\, dV. \end{aligned}\right\} \tag{20}$$

In the third of equations (20) the surface integral is the fraction of the weight of the enclosed body supported by the effective stress Ω. The first volume integral to the right is the total weight of the mass contained within the volume V, and the second is the weight of an equal volume of liquid of density ρ_l. The equation, therefore, shows that, for the case of a pressure field equivalent to that of a hydrostatic liquid, the load which must be supported by the effective stress Ω is simply the weight of the body less the weight of the displaced (or an equivalent volume of) liquid.

This, as was stated in the original paper, is in precise agreement with the principle of Archimedes. Since neither the volume porosity nor the surface porosity occurs in any of the foregoing equations, the validity of the latter evidently must not depend upon the magnitudes of those quantities.

Equations (20) are true only for the case where the pressure field is that of a hydrostatic liquid; equations (17), which are more general, are true for any continuous pressure field whatever. Again, considering only the third equation of (17), that for the vertical component, we have, by transposition,

$$\iint \Omega_{nz}\, dA = \iiint \rho_b g\, dV - \iiint \frac{\partial p}{\partial z}\, dV. \tag{21}$$

In this case, the second integral to the right represents the buoyant force exerted upon the body by the stress field Π of normal components p. If this should become equal to the negative of the weight of the body given by the first integral to the right then the load supported by the effective stress—the integral to the left—would be zero, and the body would be in a state of flotation. If it should be greater than the total weight, then the effective stress would have to become tensile in order to maintain equilibrium and prevent the body from rising. As rocks in large masses may be considered to have essentially zero tensile strength, it follows that the maximum value which the pressure integral—the force of buoyancy—is likely to have will be a force sufficient to float the overburden, with the support by the effective stress reduced to zero.

The general equations (17) are also pertinent with respect to the critic's "seepage force." The critic went to some trouble for the case where the liquid is not in hydrostatic equilibrium to introduce Darcy's law and in this manner to derive a supplemental force which he called the "seepage force." However, it may be seen from equations (17) that this is unnecessary and in fact irrelevant to the problem under consideration here. Everything that is essential to the problem is contained in equations (17), or equivalent equations in which the volume integral of pressure is replaced by the equivalent surface integral

$$\iiint \frac{\partial p}{\partial z}\, dV = \iint p \cos \gamma\, dA, \tag{22}$$

in accordance with equations (27) and (29) of the original paper.

Case of Nonporous Solid

In the original paper (Hubbert and Rubey, 1959, p. 133–135), and in the reply to an earlier discussion (Hubbert and Rubey, 1960, p. 623–627), the case of the force of buoyancy on a nonporous solid was introduced merely to show that this buoyant effect does not depend in any manner upon the so-called "surface porosity." To demonstrate this the authors (Hubbert and Rubey, 1960, Fig. 3) devised a submerged spring balance by means of which it would be possible to measure directly the force of buoyancy on a submerged nonporous cylinder, the surface porosity of whose base could be varied arbitrarily between the limits zero and unity. It was shown in this manner that in all cases the force of buoyancy exerted upon the cylindrical segment is equal to the negative of the weight of the displaced liquid and is quite independent of the surface porosity.

The critic has devised a superficially similar but fundamentally different experiment. The apparatus consists of three identical systems, A, B, and C, each comprising a vessel through the base of which a vertical cylinder protrudes, supported from below by a spring. Instead of using these systems to determine the force of buoyancy on a detachable cylindrical segment inside the vessels, as the authors have done, the critic's experiment consists in leaving vessel

A empty, filling vessel B to the top of the cylinder with a liquid of density ρ_l, and filling vessel C somewhat beyond the top of the cylinder. He concludes that the cylinder in vessel B will show no deflection, and that in vessel C will be deflected downward. This demonstrates, he asserts, the "arbitrary and fictitious" nature of the authors' buoyancy concept when applied to a nonporous solid.

It should be pointed out, however, that the system devised by the critic fails to satisfy the conditions specified by the authors in their original analysis, namely that, in the macroscopic space considered, all space not occupied by the solid be interconnected and filled with liquid so as to produce a pressure field which is continuous in such space. In the experiments described, which produce an effect that apparently violates the authors' conclusions, the critic has devised a system in which the nonsolid space consists of two separate chambers which are isolated from one another and so permit the simultaneous application on the solid piston of two independent pressure fields. It is a simple matter to show, however, that even in this case the results obtained, instead of contradicting the authors' conclusions, are in fact completely confirmatory.

The object whose equilibrium is to be investigated is in each instance the total solid cylinder. The complete equations of equilibrium applicable are equations (14) or (17) herein. However, since in all three cases the pressure fields specified are either $p=0$ (taking atmospheric pressure to be zero), or the hydrostatic pressure $p = p_0 + \rho_l gz$, where z is positive downward, $\partial p/\partial x = \partial p/\partial y = 0$, so that the x- and y- components of force in equations (14) or (17) vanish, leaving only the vertical component.

For the vertical component the only factor that is varied independently in the three cases is the pressure p which induces whatever force of buoyancy may exist. Therefore consideration needs to be given only to the force of buoyancy acting on the cylinder in each of the cases. According to equation (36) in the original paper (Hubbert and Rubey, 1959, p. 131), to equation (20) in the previous discussion (Hubbert and Rubey, 1960, p. 622), or to equations (16) and (22) herein, the vertical component of this force is given by

$$F_b = -\iint_A p \cos\gamma \, dA = -\iiint_V \frac{\partial p}{\partial z} \, dV. \quad (23)$$

In the problem specified by the critic the pressure p is given at all points on the exterior surfaces of the three cylinders. In system A

$$p = 0$$

throughout; therefore for this system

$$F_b = -\iint p \cos\gamma \, dA = 0. \quad (24)$$

In system B, p is zero at the top of the piston and increases linearly from the top to the bottom of the tank according to the hydrostatic equation

$$p = \rho_l gz.$$

Below the bottom of the tank $p = 0$.

In this system also

$$F_b = -\iint_A p \cos\gamma \, dA = 0, \quad (25)$$

and no deflection should occur.

In system C, if we let the vertical co-ordinate be measured downward from the free surface of the liquid, the pressure in the tank is given by $p = \rho_l gz$, and below the bottom of the tank $p = 0$. In this case if we let z_1 be the depth of the top of the cylinder, then the pressure on the top of the cylinder will be

$$p_1 = \rho_l gz_1,$$

and

$$F_b = -\iint_A p \cos\gamma \, dA = p_1 A_z = \rho_l gz_1 A_z, \quad (26)$$

where A_z is the horizontal area of cross section of the cylinder. This is a positive or downward force since $\cos\gamma$ on the top surface of the cylinder has the value -1. Therefore, in this case the cylinder should be deflected downward.

These results, using the surface integral, are obvious by inspection. The same results are also obtainable by the volume integral, although in this case they are not so obvious because of the mathematical discontinuity in p introduced at the bottom of the vessel.

To see more clearly the meaning of the volume integral we may note that

$$\iiint_V \frac{\partial p}{\partial z} \, dV = A_z \int_z \frac{\partial p}{\partial z} \, dz, \quad (27)$$

where A_z is the constant area of cross section of the cylinder and is regarded as a positive

quantity. Equation (27) has meaning only when p varies continuously from the top to the base of the cylinder. If p (z) has one or more finite discontinuities then both the volume integral and the linear integral of equation (27) can be evaluated only in the subdomains in which p is continuous. To these results the finite values of Δp across the surfaces of discontinuity must be added. In the problem given, no pressure discontinuity occurs inside the cylinder in case A, but in both cases B and C such a discontinuity has been introduced across the horizontal surface coincident with the bottom of the tank.

In this case let p_1 be the pressure at the top of the cylinder at depth z_1 and p_2 that at depth z_2 of the bottom of the tank, according to the hydrostatic equation

$$p = \rho_1 g z.$$

Then from z_2 to the base of the cylinder at z_3, let the pressure be zero.

The force of buoyancy given by the volume integral of equation (23) will then be

$$F_b = -\iiint_V \frac{\partial p}{\partial z}\, dV$$

$$= -A_z \left\{ \int_{z_1}^{z_2} \frac{\partial p}{\partial z}\, dz + \Delta p + \int_{z_2}^{z_3} \frac{\partial p}{\partial z}\, dz \right\}. \quad (28)$$

For the interval z_1 to z_2

$$\frac{\partial p}{\partial z} = \rho_1 g, \quad (29)$$

and from z_2 to z_3

$$\frac{\partial p}{\partial z} = 0. \quad (30)$$

However, at z_2 a discontinuous pressure drop occurs for which

$$\Delta p = -[p_1 + \rho_1 g\,(z_2 - z_1)]. \quad (31)$$

Introducing these quantities into equation (28) then gives

$$F_b = -\iiint \frac{\partial p}{\partial z}\, dV$$

$$= -\left\{ \rho_1 g\,(z_2 - z_1) - [p_1 + \rho_1 g\,(z_2 - z_1)] \right\} A_z$$

$$= +\, p_1 A_z, \quad (32)$$

which, as it should be, is the same result as was obtained by means of the surface integral in equation (26).

The physical effect of applying to the midsection of a solid cylinder a fluid pressure greater than that at its ends is to create opposite forces tending to expel the end sections away from the middle. If the pressures on the two ends of such a cylinder are equal, the net propulsive force on the cylinder as a whole is zero. Opposing these oppositely directed propulsive forces is a cohesive force resulting from the tensile strength of the material. If the end pressures on the cylinder are zero and if p is the pressure on the midsection, then the propulsive force on each half will be of magnitude pA_z. Opposing this will be a tensile force of magnitude $\sigma_{zz}A_z$. Then, since the sum of these two forces must be zero it follows that

$$(p + \sigma_{zz})\, A_z = 0$$

or

$$\sigma_{zz} = -p. \quad (33)$$

Consequently, if the pressure p on the midsection of the cylinder is increased until it becomes equal to the negative of the tensile strength of the material, the cylinder must be parted in a tensionlike failure.

This phenomenon, in fact, has been demonstrated in the well-known paradoxical experiments of P. W. Bridgman (1912; 1931, p. 91-92; 1952, p. 108, 125). By letting rods of metals and of glass extend completely through a pressure chamber, and emerge on either end through packing boxes, Bridgman was able to apply a high pressure to the midsections of the cylinders while keeping the end sections at atmospheric pressure. In each instance, when the applied pressure was increased until it slightly exceeded the tensile strength of the material, the cylinder parted as if in tension, and the two ends were expelled violently in opposite directions, often with the velocity of a rifle bullet.

The pressure application in the Bridgman experiment, and in the critic's case B, are similar in that in each instance the pressure is applied only to the exterior cylindrical surface. Since the force induced by such a pressure has no axial component, it is quite impossible to account for the results of Bridgman's experiments by means of a surface integration of this pressure over the external surface only—hence the paradox. The behavior is readily understood, however, by means of either the surface

or the volume integral of equation (23) if these are evaluated over one of the longitudinal halves of the cylinder regarded as being contained in a completely closed surface A.

The total stress Σ in this problem, if we neglect the friction of the packing boxes, consists solely of radial pressures with the axial stress equal to zero. However, when the neutral stress Π of components p is subtracted from Σ we obtain the effective stress Ω which consists of a pure axial tension $-\sigma_{zz}$ which increases in absolute magnitude from zero at each end of the cylinder to a maximum in its midsection. In response to this tension the cylinder fails in the same manner and at the same stress as in a conventional tensile test.

The Drillpipe Fallacy

In his discussion of the "arbitrary and fictitious concept of buoyancy" as applied to nonporous solids the critic concludes:

> "For solid bodies the artificial concept of dividing the total stress into a hydrostatic and nonhydrostatic component is more apt to lead to confusion than to clarification."

That in at least some cases this is not true may be seen by considering one of the classical fallacies that has plagued engineers in the petroleum industry for several decades. The problem is this: A string of drillpipe of length l, uniform cross-sectional area A_z, and density ρ_s is suspended in a vertical well filled with drilling mud of density ρ_m, where $\rho_m < \rho_s$. The forces, both horizontal and vertical, exerted upon the pipe by the mud pressure acting on its vertical surface are zero. Hence the only vertical force exerted on the pipe by the mud is that of the mud pressure on its base, namely

$$F_m = -\rho_m g l A_z. \tag{34}$$

The pipe is supported jointly by this mud pressure on its base and by a force of tension at its upper end. The total axial stress in the pipe, therefore, must grade from tension at the top to compression at the bottom, with a neutral point somewhere between. The question is: Will not the lower section, between the neutral point and the bottom, which comprises a slender tube under axial compression, buckle? From the total-stress analysis many engineers have concluded that it will.

A quite different conclusion may be arrived at by inspection if we resolve the total stress into the neutral and effective partial stresses Π and Ω. The partial-stress Π has no shear components. Its normal components at any point are equal to the pressure p which the mud would exert at that point if the pipe were not present. This stress supports in hydrostatic equilibrium the fractional weight of the pipe having the partial density ρ_m.

The effective stress Ω then is that stress required to support the remainder of the pipe of partial density $(\rho_s - \rho_m)$ as if it were suspended in a vacuum. The horizontal components of this stress will be zero, and its vertical component σ_{zz} at any depth z will be obtainable from the equation of equilibrium of that section of the pipe suspended below depth z. This equation is

$$\sigma_{zz} A_z + (\rho_s - \rho_m)\, g A_z\, (l - z) = 0.$$

Eliminating A_z and solving for the vertical component of effective stress σ_{zz} then gives

$$\sigma_{zz} = -(\rho_s - \rho_m)\, g\, (l - z), \tag{35}$$

which shows that σ_{zz} is negative, or tensile, throughout the length of the pipe, and varies linearly from a maximum tensile stress $[-(\rho_s - \rho_m)\, gl]$ at the top to zero at the bottom.

The pipe is thus subjected simultaneously to a neutral stress, which tends to produce no deformation, and an effective stress which is tensile throughout. Hence, no buckling can occur.

Arbitrariness of Stress Resolution

Although the critic has apparently convinced himself of the validity of the authors' resolution of the total stress into the partial stresses Ω and Π, he several times remarks upon the arbitrariness of the resolution. This, of course, implies that any other resolution would serve equally well. While it is true that a given stress field can be regarded as being the sum of any number of superposed partial stress fields, the question of whether any particular resolution should be made is entirely a matter of convenience. If the problem can be simplified and its solution made easier by some particular resolution, then the use of that resolution not only is justified, but its choice is dictated by the problem itself.

In the original paper (p. 140–142) it was shown that the experimental data of McHenry on concrete and of Handin on a natural sand stone with a wide range of internal pore pressures become consistent with the jacketed or "dry-rock" tests on the same materials only

when the total stress is corrected for the internal fluid pressure. The choice of this resolution, therefore, instead of being arbitrary, is dictated by the physical behavior of the materials. Similarly, in the drillpipe problem, while an infinite number of arbitrary stress resolutions is mathematically possible, only the one actually used is relevant to the physical data being considered and leads to the desired simplification.

Thus, despite the critic's repeated implications to the contrary, the resolution actually employed, instead of being an arbitrary choice, is the one demanded by the phenomena being considered.

Conclusion

The critic's discussion has contributed no new results that were not implicit in the equations derived in the original paper. His contention that the resolution of the total stress into neutral and effective partial stresses is without usefulness when applied to nonporous solids immersed in liquids has been shown not to be valid. Finally, his resolution of the total buoyant force exerted by a fluid not in hydrostatic equilibrium into hydrostatic and "seepage-force" fractions, while a permissible procedure, serves no useful purpose here because the only quantity of significance in the problem under consideration is the total buoyant force, and this has already been expressed by either of the equivalent integrals

$$\mathbf{F} = -\iint_A p d\mathbf{A} = -\iiint_V \text{grad}\, p dV \quad (36)$$

in the original paper.

Acknowledgment

The authors are indebted to Mr. Henry Rainbow, Consultant, Mathematics, Shell Development Company, for a critical review of the manuscript.

References Cited

Bridgman, P. W., 1912, Breaking tests under hydrostatic pressure and conditions of rupture: Philos. Mag., v. 24, p. 63–80

—— 1931, The physics of high pressure: New York, Macmillan, 393 p.

—— 1952, Studies in large plastic flow and fracture: New York, McGraw-Hill, 362 p.

Hubbert, M. King, and Rubey, William W., 1959, Role of fluid pressure in mechanics of overthrust faulting, I. Mechanics of fluid-filled porous solids and its application to overthrust faulting: Geol. Soc. America Bull., v. 70, p. 115–166

—— 1960, Role of fluid pressure in mechanics of overthrust faulting: Reply to discussion by Hans P. Laubscher: Geol. Soc. America Bull., v. 71, p. 617–628

Love, A. E. H., 1944, A treatise on the mathematical theory of elasticity: New York, Dover Publications, 632 p.

Macelwane, J. B., 1936, Introduction to theoretical seismology, Part I, Geodynamics: New York, John Wiley and Sons, Inc., 339 p.

Shell Development Company, Exploration and Production Research Division, Houston, Texas; University of California, Los Angeles, California

Manuscript Received by the Secretary of the Society, February 16, 1961

Announcements

Register of Scientists Interested in Overseas Assignments

American participation in the educational and economic development of other countries is likely to continue on an increasing scale during the next few years. In anticipation of the growing need for personnel under international programs in which it co-operates, the National Academy of Sciences-National Research Council is compiling a register of American scientists and other specialists who are interested in the possibilities of assignments abroad for periods ranging from several weeks to 2 years.

Assignments become available irregularly throughout the year, and they vary greatly with respect to location, duration, stipends, and responsibilities. Some programs sponsored by private foundations require scientists of high competence and reputation for short-term lecturing and consultative duties in a single country or in several countries. A number of government-sponsored projects call for specialists who are available for 2-year periods, have had previous experience in certain geographical areas, and are fluent in Spanish or French. Also, under the exchange program authorized by the Fulbright and Smith-Mundt acts, younger as well as established science educators are welcomed as lecturers at many African, Asian, and Latin American colleges and universities.

Persons who wish to be considered for any of such assignments are asked to fill out a special form, available upon request from the *Committee on International Exchange of Persons*, 2101 Constitution Avenue, N.W., Washington 25, D.C. Completion and return of the form does not constitute an application, but it would ensure a person's consideration for openings in his field.

The Register is intended specifically for specialists in the biological and physical sciences and related technologies. However, the Committee will be happy to receive inquiries from persons in other fields.

Mexican Association of Petroleum Geologists Meets

The Mexican Association of Petroleum Geologists has extended an invitation to geologists to attend its third convention in Mexico City in the last week of November 1961.

Further information on this meeting can be obtained from the Mexican Association (Tacuba 5, Apartado Postal 1884, Mexico 1, D. F.).

UN

Back Stock of GSA Bulletin

Arrangements were recently completed whereby The Geological Society of America appointed the firm of Walter J. Johnson, Incorporated, international dealers of scientific periodicals, as distributors for the remaining back stock of Volumes 37–65 of the Bulletin.

Orders for this back stock should be directed to Walter J. Johnson, Inc., 111 Fifth Avenue, New York 3, New York. The prices for back volumes of the Bulletin are $25 per volume and $2.50 per single issue.

Orders for back stock may also be placed with the distributor's branch offices: California Office, 1901 West Eighth Street, Los Angeles 57; British Office, 17 Old Queen Street, London S. W. 1; German Agency, Minerva, G.m.b.H., Holbeinstrasse 25–27, Frankfurt am Main; Italian Office, Periodici Scientifici, Via Gran Sasso 24, Milano.